Cranfield University

A Smith

Some Effects Of Transpiration On The Boundary Layer At The Leading Edge Of A Swept Wing

College Of Aeronautics

PhD Thesis

Cranfield University

College Of Aeronautics

PhD Thesis

Academic Year 1999-2000

A Smith

Some Effects Of Transpiration On The Boundary Layer At The Leading Edge Of A Swept Wing

Supervisor: D I A Poll

March 2000

Abstract

The effect of transpiration on the boundary layer near the leading edge of a swept wing has been investigated using a large swept cylinder model with a laser-drilled titanium leading edge to model the leading edge of a swept wing.

In the region near the leading edge, boundary layer transition due to crossflow instability has been examined. Natural transition on a porous surface was compared with that on a non-porous surface, and it was found that transition occurred at lower $\overline{R}$'s on the porous surface (ie there was a performance penalty due to the porous surface). The effect of suction on transition due to crossflow instability was then studied. It was found that only moderate amounts of suction were required to delay the onset of crossflow-induced transition and a simple algebraic model has been derived, in terms of $\overline{R}$, Re_x, and C_q, to describe transition on the porous surface with or without suction. It was also found that two-dimensional trip wires had a negligible effect on crossflow transition, except where they caused attachment-line contamination.

On the attachment-line, several subjects were addressed. The effect of attachment-line blowing was considered, and good agreement was obtained with previous work. The effect of spanwise blowing length was also addressed, and a simple algebraic model was derived, in terms of $\overline{R}$, s/η, and C_q, to describe attachment-line transition due to blowing. A comparison has also been made with linear stability theory.

The effect of suction at the wing-fuselage junction was examined as an alternative to suction on the attachment-line. However, it was found that applying suction on the attachment-line when the boundary layer had attained infinite swept conditions was much more efficient than applying suction in the junction region.

Suction was successfully used to relaminarise a turbulent attachment-line at $\overline{R}$ values between 600 and 950, the magnitude predicted for the next generation of large transport aircraft. During the experiments, no sign of critical oversuction was found.

Finally, the behaviour of a relaminarised attachment-line flowing onto a non-porous surface was studied. The conditions for natural transition on the non-porous surface were measured, and it was found that they were the same as those predicted by previous work on an entirely non-porous attachment-line.

Acknowledgements

I would like to thank my supervisor, Professor Poll, for his guidance throughout his work. I would also like to thank NASA and DERA for providing the funding. Thanks must go to Malcolm Goodridge and the workshop staff for sensible designs in the face of odd requirements. Support from the College technicians throughout the wind tunnel testing was particularly appreciated, especially Linton Banks-Davies for sitting in the corner with his feet up for long hours.

Most of all I would like to thank Sarah for being there, and for badgering me to write my thesis. Thanks also to Saul, for waking me up in the middle of the night and generally being a new-born baby, making it very difficult to get anything done.

Contents

ABSTRACT I
ACKNOWLEDGEMENTS II
CONTENTS III
LIST OF FIGURES VI
LIST OF TABLES VIII
NOTATION IX
1. INTRODUCTION 1
2. LITERATURE REVIEW 4
3. THE SWEPT WING BOUNDARY LAYER 12
3.1 The Swept Wing 12
3.2 The Attachment-Line 12
3.3 Cross-Flow Instability 12
3.4 Intermittency 13
3.5 Receptivity 13
3.6 Parameters Used for the Study of Leading Edge Flows 13
3.7 Experimental Simplifications 14
4. EXPERIMENTAL ARRANGEMENT 18
4.1 The Model 18
4.1.1 Model Description 18
4.1.2 Static Testing 19
4.1.3 Checking For Leaks 19
4.1.4 Model Alignment 20
4.2 Verification of Infinite Swept Conditions 20
4.3 The Experimental Determination of Flow Parameters 21
4.3.1 Kinematic Viscosity 21
4.3.2 Freestream Dynamic Pressure 22
4.3.3 Length Scale 22
4.3.4 Spanwise Leading-Edge Reynolds Number 24
4.3.5 Transpiration Coefficient 25
4.4 Potential Flow 28
4.4.1 Divergence Coefficient 30
4.5 Calculation of the Attachment-Line Position 32
4.6 Data Acquisition And Manipulation 33
4.7 Hot-Wire Anemometry 34
4.8 Transition Criterion 35
5. CROSS-FLOW TRANSITION 36
5.1 Introduction 36
5.2 Natural Transition 36
5.2.1 Introduction 36
5.2.2 Previous Work 36
5.2.3 Experimental Method 38
5.2.4 Results and Discussion 39
5.2.4.1 Non-Porous Surface 39
5.2.4.2 Porous Surface 39
5.2.5 Conclusions 42
5.3 The Control of Cross-Flow Instability By Surface Suction 43

5.3.1 Introduction 43
5.3.2 Previous Work 43
5.3.3 Experimental Method 43
5.3.4 Results and Discussion 44
5.3.5 Conclusions 47
5.4 The Effect of Two-Dimensional Disturbances on Cross-Flow Induced Transition 47
5.4.1 Introduction 47
5.4.2 Previous Work 48
5.4.3 Experimental Method 48
5.4.4 Results and Discussion 49
5.4.4.1 Non-Porous Surface 49
5.4.4.2 Porous Surface 50
5.4.5 Conclusions 50
6. THE EFFECT OF BLOWING ON THE ATTACHMENT-LINE BOUNDARY LAYER 51
6.1 Introduction 51
6.2 Previous Work 51
6.3 Blowing At Large s/η 52
6.3.1 Experimental Method 52
6.3.2 Results and Discussion 52
6.3.3 Comparison With Linear Stability Theory 53
6.4 Effect of Spanwise Blowing Length 55
6.4.1 Introduction 55
6.4.2 Experimental Method 55
6.4.3 Results and Discussion 56
6.5 Conclusions 57
7. A STUDY OF THE EFFECT OF ATTACHMENT-LINE SUCTION ON THE SPANWISE PROPAGATION OF GROSS DISTURBANCES IN THE WING-FUSELAGE JUNCTION 59
7.1 Introduction 59
7.2 Previous Work 59
7.3 Experimental Method 60
7.4 Results and Discussion 61
7.5 Conclusions 62
8. ATTACHMENT-LINE BOUNDARY LAYER RELAMINARISATION BY SUCTION 63
8.1 Relaminarisation Of A Turbulent Attachment-Line Boundary Layer When the Attachment-Line Reynolds Number Exceeds 600 63
8.1.1 Introduction 63
8.1.2 Previous Work 63
8.1.3 Experimental Method 64
8.1.4 Results and Discussion 65
8.1.5 Conclusions 66
8.2 The Effects of Large Suction Levels on Transition in the Attachment-Line Boundary Layer 67
8.2.1 Introduction 67
8.2.2 Previous Work 67
8.2.3 Experimental Method 68
8.2.4 Results and Discussion 68
8.2.5 Conclusions 70

9. AN INVESTIGATION OF THE TRANSITION THAT OCCURS WHEN A RELAMINARISED ATTACHMENT-LINE ENCOUNTERS A NON-POROUS SURFACE **71**
9.1 Introduction 71
9.2 Previous Work 71
9.3 Experimental Method 72
9.4 Results and Discussion 73
9.5 Conclusions 74
CONCLUSIONS **76**
RECOMMENDATIONS FOR FURTHER WORK **77**
REFERENCES **79**
APPENDIX A. WORK PROPOSAL FOR NASA RESEARCH CONTRACT **86**
APPENDIX B. WORK PROPOSAL FOR DERA RESEARCH CONTRACT **90**
APPENDIX C. CALCULATION OF FREESTREAM TURBULENCE **105**
APPENDIX D. WIND TUNNEL CALIBRATION **109**
APPENDIX E. EXPERIMENTAL DATA FOR THE EFFECT OF SUCTION ON CROSSFLOW TRANSITION **112**
APPENDIX F. RELATION OF PARAMETERS USED BY PFENNINGER TO THOSE USED CURRENTLY **119**

List of Figures

Figure 1. The Variation of Crude Oil Prices And The Correlation With World Events, from WTRG Economics 1998
Figure 2. The Flow Near The Leading Edge of a Swept Wing
Figure 3. Typical Velocity Profile for a Three-Dimensional Boundary Layer, from Yardley63
Figure 4. Leading Edge Perforation Pattern, From Danks21
Figure 5. Distribution of Perforated Areas on Titanium Leading Edge, From Danks21
Figure 6. Distribution of Suction Chambers Within the Perforated Titanium Leading Edge Surface, From Danks21
Figure 7. Arrangement of Model in 8'x6' Wind Tunnel
Figure 8. Example Static Pressure Coefficient Distribution Around Cylinder Leading Edge
Figure 9. Chordwise Velocity Distribution and Comparison With Potential Flow Solution
Figure 10. Diagram Showing The Addition Of A Uniform Flow And A Doublet To Represent The Potential Flow Over A Cylinder, From Anderson65
Figure 11. Typical Non-Dimensionalised Chordwise Velocity Distribution
Figure 12. Comparison of Divergence Coefficients Obtained During Experimental Work and Potential Flow Solution
Figure 13. An Example of the Effect of Operator Experience When Using Hot-Wire Anemometry
Figure 14. Typical Output from Hot-Wire For Laminar Boundary Layer
Figure 15. Power Spectrum of Laminar Boundary Layer Shown in Figure 14
Figure 16. Typical Output from Hot-Wire For Laminar Boundary Layer With Laminar Disturbance
Figure 17. Power Spectrum of Laminar Boundary Layer With Laminar Disturbance Shown in Figure 16
Figure 18. Typical Output from Hot-Wire For The Onset of Transition: Laminar Boundary Layer With Laminar Disturbance And Turbulent Bursts
Figure 19. Power Spectrum of Laminar Boundary Layer With Laminar Disturbance and Turbulent Bursts Shown in Figure 18
Figure 20. Typical Output From Hot-Wire For Turbulent Boundary Layer
Figure 21. Power Spectrum of Turbulent Boundary Layer Shown in Figure 20
Figure 22. The Onset and End of Transition, Caused by Cross-Flow Instability, from Danks21
Figure 23. Natural Transition on a Non-Porous Surface and Comparison with Previous Work By Poll4 and Danks5
Figure 24. Transition Characteristics In The Absence Of A Trip-Wire, From Poll62
Figure 25. Comparison of the Onset of Transition on Porous and Non-Porous Surfaces, With Data From Poll *et al52* and Danks5
Figure 26. Comparison of Power Law Approximations with Experimental Data, With Data From Danks5
Figure 27. The Magnitude Of The Reduction Due to the Porous Surface
Figure 28. Percentage Reduction of Due to the Porous Surface
Figure 29. Example Suction Distribution, From Danks5

Figure 30. The Effect of Uniform, Distributed Suction on Cross-Flow Instability - The Onset of Transition
Figure 31. Comparison of Power Law Curve Fits with Experimental Data
Figure 32. Variation of Empirical Relation Coefficient n With Cq and Linear Approximation
Figure 33. Variation of Empirical Relation Coefficient B with Cq and Linear Approximation
Figure 34. Curve Fits Calculated from Empirical Relation and Comparison with Experimental Data
Figure 35. The Suction Required To Offset The Porous Surface Penalty
Figure 36. The Variation Of With d/h And s/h For The Appearance Of First Bursts Of Turbulence, From Poll4
Figure 37. Transition Characteristics, On Non-Porous Surface, with Two-Dimensional Trip-Wires, And Comparison With Natural Transition Data From Danks5
Figure 38. Transition Characteristics, On A Porous Surface, with Two-Dimensional Trip-Wires
Figure 39. Schematic Diagram of Flow Pattern Leading To Attachment-Line Blowing
Figure 40. Attachment-Line Transition Characteristics Caused by Blowing, With s/h Values
Figure 41. Comparison of Attachment-Line Transition Characteristics Caused by Blowing with Data from Danks65 and Arnal47
Figure 42. Attachment-Line Blowing Results Plotted on a Logarithmic Scale
Figure 43. Comparison of Empirical Function with Experimental Blowing Results
Figure 44. Linear Stability Envelope For =350, From Theofilis48
Figure 45. Comparison of Experimental and Numerical Blowing Results
Figure 46. Difference Between Experimental and Theoretical Blowing Results
Figure 47. Example of Laminar Disturbance in an Attachment-Line With Blowing; =372, Cq=0.000349, s/h=1900
Figure 48. Amplitude Spectrum of Laminar Disturbance with Key Frequencies Marked; =372, Cq=0.000349, s/h=1900
Figure 49. Effect of Spanwise Transpiration Length on Blowing Characteristics for a Sweep Angle of 55°
Figure 50. Effect of Non-Dimensional Spanwise Length on Blowing Characteristics at Constant
Figure 51. Comparison of Empirical Asymptotic Blowing Coefficients with Previous Experimental Results
Figure 52. Collapsed Blowing Data and Comparison with Empirical Function
Figure 53. Schematic Representation Of The Likely Flow Characteristics In The Root Region, From Bergin44
Figure 54. Variation of in the Wing-Fuselage Junction, From Bergin51
Figure 55. Arrangement of the Model in the Wind Tunnel during the Wing-Fuselage Junction Experiments
Figure 56(a). Hot-Wire Signal of Attachment-Line Downstream of Wing-Fuselage Junction - =518, s/h=2492, s/D=2.2, Cq=0, G=1
Figure 57. Variation of Intermittency With Suction Coefficient In The Wing-Fuselage Junction, =518, s/h=2492, s/D=2.2
Figure 58. Results for the End of Attachment-Line Relaminarisation, From Danks21

Figure 59. Critical Suction Rate For The End Of Relaminarisation (At Constant Values Between 600 and 750)
Figure 60. Critical Suction Rate For The End Of Relaminarisation (At Constant Values Between 800 and 950)
Figure 61. Comparison of Asymptotic Suction Coefficient Results with Danks51 and Reneaux49
Figure 62. Normalised Suction Rate as A Function of Streamwise Distance (At Constant)
Figure 63. Revised Curve Fit For Normalised Suction Rate as A Function of Streamwise Distance (At Constant) And Comparison With Danks51
Figure 64. The Beginning Of Transition On A 45° Swept Blunt-Nosed Wing For Different Spanwise Length Reynolds Numbers, From Pfenninger7
Figure 65. The Beginning of Transition at the Leading Edge of a 45° Swept Blunt-Nosed Wing for Different Spanwise Lengths, From Pfenninger26
Figure 66. The Beginning of Transition at the Leading Edge of a 45° Swept Blunt-Nosed Wing for Different Spanwise Reynolds Numbers, From Pfenninger26
Figure 67. Comparison Of The Two-Dimensional Ellis Criterion Values For The Pfenninger26 and The Current Data
Figure 68. Variation of Transition Location With Chordwise Extent of Suction, From Bobbitt et al77
Figure 69. Transition Data For A Relaminarised Attachment-Line Flowing Onto A Non-Porous Surface, From Reneaux48
Figure 70. Schematic of Attachment-Line Arrangement During Non-Porous Surface Experiments
Figure 71. Transition Characteristics of A Relaminarised Attachment-Line Boundary Layer Flowing Onto A Non-Porous Surface
Figure 72. The Effect of Spanwise Distance on the Transition Characteristics of A Relaminarised Attachment-Line Boundary Layer That Flows Onto A Non-Porous Surface

List of Tables

Table 1. The Variation of Suction Coefficient Percentage Uncertainty With Percentage of Full Scale Reading
Table 2. Asymptotic Blowing Coefficients at Large s/η
Table 3. Values of Suction Coefficient Required For Relaminarisation in the Limit as $s/\eta \rightarrow \infty$

Notation

α_i	Spatial amplification ratio
δ	Boundary layer thickness (m)
δ^*	Displacement thickness (m)
γ	Ratio of specific heats
κ	Strength of doublet ($m^3\ s^{-1}$)
η	Viscous length scale (m)
Δ	The height above the surface at which the crossflow velocity drops to 1% of its maximum value, from Poll[62]
θ	Angle of arc of segment of circle (radians); polar co-ordinate
θ_L	Laminar momentum thickness (m)
χ	Cross-flow Reynolds number
Λ	Geometric (measured) sweep angle (degrees)
ψ	Stream function
ν	Kinematic viscosity (m^2 /s)
ρ	Fluid density (kg/m^3)
Γ	Intermittency
τ	Shear stress ($kg\ m^{-1}\ s^{-2}$)
μ	Viscosity coefficient ($kg\ m^{-1}\ s^{-1}$)
A	Oversuction parameter, from Ellis[84]
AC	Alternating current (Volts)
ACEE	Aircraft Energy Efficiency Programme
ASU	Arizona State University
ATTAS	Advanced Technologies Testing Aircraft System
C	Model chord (m)
C^*	Attachment-line similarity parameter from Cumpsty and Head[63]
CFD	Computational fluid dynamics
C_p	Pressure coefficient
C_q	Suction coefficient
C_{div}	Divergence coefficient – see Section 4.3
d	Two-dimensional trip-wire diameter (m)
d_h	Porous surface hole diameter (m)
D	Model diameter (m)
DC	Direct current (Volts)
DLR	German aerospace research centre
DOC	Direct Operating Cost
ELFIN	European Laminar Flow Investigation
f	Boundary layer disturbance frequency (Hz)
F	Non-dimensional frequency
FFT	Fast Fourier transform
HLFC	Hybrid Laminar Flow Control
ISA	International standard atmosphere
LEFT	Leading Edge Flight Test programme
LFC	Laminar Flow Control
M	Mach number

$\dot{M}$	Mass flow rate (kg s^{-1})
NLF	Natural Laminar Flow
NPL	National Physical Laboratory
ONERA	Office National d'Études et de Rescherches Aerospatiales
OPEC	Organisation of Petroleum Exporting Countries
p	Static pressure (N/m^2)
psi	Pounds per square inch (lb/in^2)
p_T	Total pressure (N/m^2)
Pr	Prandtl number
PSE	Parabolised stability equations
q	Dynamic pressure (N/m^2)
Q_∞	Freestream velocity with model present (m/s)
$\overline{Q}_\infty$	Empty tunnel freestream velocity (m/s)
r	Leading edge radius (m); polar co-ordinate
RMS	Root mean square
R	Potential flow cylinder radius
$\overline{R}$	Leading-edge Reynolds number
Re_x	Chordwise Reynolds number
R_{δ^*}	Displacement thickness Reynolds number
R_{Θ_L}	Laminar momentum thickness Reynolds number
s	Distance measured along span (m)
s_{TT}	Spanwise distance from the start of the suction surface to the measuring station (mm)
S	Suction chamber surface area (m^2)
S&C	Stability and control
T	Temperature (Kelvin)
Tu	Turbulence level
u'	Chordwise freestream turbulence component (%)
u_β	Crossflow velocity, from Owen and Randall[14]
U	Chordwise velocity – see Figure 2 (m/s)
$\overline{v}$	Crossflow velocity, from Poll[4]
v'	Spanwise freestream turbulence component (%)
v_o*	Suction parameter, from Pfenninger[26]
V	Spanwise velocity – see Figure 2 (m/s)
w'	Scaling parameter, from Danks[5] ; vertical freestream turbulence component (%)
W	Vertical velocity within the boundary layer
w(0)	Wall transpiration velocity at attachment-line (m/s)
x	Chordwise distance (m)
z	Distance perpendicular to the attachment-line and perpendicular to the chordwise direction (m)

Subscripts

a	Attachment-line
asymptotic	Asymptotic value

∞	Freestream conditions
calib	Calibration value
e	At the boundary layer edge
max	Maximum
M	With the model present
outlet	Conditions at the outlet of a rotameter
porous	On the porous surface
non-porous	On the non-porous surface
h	Value at a specific hole on the porous surface
w	At the wall
x	At some position on the chord

1. Introduction

Advances in aviation during and following the Second World War led to an enormous improvement in the performance of aircraft. The jet engine and the push for enhanced efficiency increased cruising altitudes and brought cruise speeds into the transonic range. Shock waves appeared in the locally sonic flow, producing a sharp increase in drag that limited the performance. Wing sweep was adopted to reduce the local Mach number and therefore delay the onset of this drag rise. However, introducing sweep created several unforeseen problems with the boundary layer near the leading edge of the wing.

The boundary layer on a swept wing is complex with a mixture of three-dimensional and quasi two-dimensional regions. In particular, the boundary layer near the leading edge is three-dimensional (see Section 3 for a more detailed description of the boundary layer near the leading edge). The attachment-line is the flow along the leading edge of the wing with zero chordwise velocity and is the direct result of sweep, since without sweep the attachment-line would be the locus of stagnation on the leading edge. The state of the attachment-line boundary layer, whether laminar, turbulent or transitional is important because, for a large number of cases, it will determine the boundary layer state of the rest of the wing, the so-called attachment-line contamination transition mechanism. Moving onto the wing chord, a laminar boundary layer will be subject to crossflow instability, caused by the combination of the root-to-tip pressure gradient imposed by the external flow field and the viscosity of the air. The velocity profile will contain an inflection which is a source of instability. Further onto the chord the laminar boundary layer, assuming it has made it this far in a laminar state, becomes subject to two-dimensional transition mechanisms, such as Görtler vortices if the surface is concave, Tollmein-Schlichting (T-S) waves or the effects of adverse pressure or temperature gradients.

The state of the wing boundary layer is not just an academic curiosity – it has important practical implications. The skin friction of a turbulent boundary layer can be as much as ten times that of a laminar boundary layer and the total friction drag can be as much as 40%-50% of the total aircraft drag[1, 2] for a typical transport aircraft, such as the Airbus A320 or Boeing 747, with turbulent boundary layers in the cruise configuration.

Propulsive, structural and aerodynamic development has now reached a point where additional increases in aircraft efficiency are both difficult and expensive to achieve. Consequently, manufacturers are looking elsewhere for ways to reduce Direct Operating Costs (DOC) or to increase performance (range, endurance, payload, etc). Industry has been focusing attention on Hybrid Laminar Flow Control (HLFC) as a possible method of reducing DOC for civil aircraft for a number of years. HLFC is a combination of Natural Laminar Flow (NLF) and Laminar Flow Control (LFC). NLF involves shaping the aerofoil to maintain a favourable pressure gradient as near to the rear as possible, reducing the amplification of the crossflow and T-S instabilities. LFC uses an active method (often surface suction) to reduce the amplification of the crossflow, T-S and attachment-line instabilities. The aim of LFC is to delay the transition of the wing boundary layer and therefore maintain the laminar boundary layer state at Reynolds numbers greater than those that would be associated with the transitional or turbulent

states. The combination of the two produces an aerofoil with active control around the leading edge to delay attachment-line and crossflow transition with a favourable pressure gradient profile. Additional active control can be applied on the chord if the aerofoil profile can not prevent transition alone. This HLFC combination could produce laminar flow over 50-60% of the upper surface of a wing, leading to a possible reduction in total aircraft drag of up to 15%[3]. In terms of DOC, this translates to a reduction of up to 5%[2]. Employing flow control on the fin, tailplane, and engine nacelles as well could increase this reduction to as much as 10%.

The LFC system can also be used to relaminarise a turbulent boundary layer. Relaminarisation is the opposite of the normal boundary layer transition process, so the boundary layer goes from turbulent to laminar, usually because the Reynolds number reduces below the critical value or suction is applied. In certain cases, relaminarisation can also occur if the flow accelerates. Relaminarisation is not the purpose of the LFC system and the suction required can be as much as an order of magnitude larger than that needed for LFC. However, for the majority of typical civil transport aircraft during the cruise, the turbulent fuselage boundary layer will cause the attachment-line boundary layer to be turbulent, so relaminarisation will be required[4]. In addition, particles on the wing surface (eg insect debris, ice accretion or steps and gaps) can cause local transition and require relaminarisation of the boundary layer immediately downstream of the disturbance source.

The work contained here is concerned with the use of transpiration at the leading edge of swept wings and addresses its effect on both crossflow and attachment-line instabilities. The emphasis has been to measure what happens when transpiration is applied and then to use the data to formulate simple design criteria that can be applied during the design stage. There has only been a limited attempt to fathom the fundamental physics of the transition process. The work reported in this thesis covers the following areas:

Crossflow Instability
A systematic study has been made of the natural transition due to crossflow instability that occurs on a porous and non-porous surface for a range of sweep angles and chordwise measuring locations. This was to see if there was a significant drag penalty to pay for having a porous surface. The effect of distributed uniform suction on crossflow transition has also been investigated to quantify the amount of suction required to delay transition onset. The effect of two-dimensional, circular cross-section, trip wires wrapped around the leading edge on crossflow transition was also briefly studied.

Attachment-Line Transition
Previous work[5] addressed the relaminarisation of a turbulent attachment-line boundary layer for values of the characteristic leading edge Reynolds number up to 600. This was sufficient for current transport aircraft but future, larger, transports like the Airbus A380 will have characteristic leading edge Reynolds numbers as high as 1000. To cover this increased Reynolds number range the relaminarisation of a turbulent attachment-line boundary layer has been investigated here up to a value of 1000 to find the suction required. At the same time the effect of very high suction levels, so called critical oversuction, was assessed to see if too much suction could cause premature transition.

Having relaminarised the attachment-line, the behaviour of the relaminarised attachment-line flowing onto a non-porous surface was examined. This was to see whether suction could just be applied locally to remove a disturbance or whether suction would be needed along the entire leading edge. The effect of suction at the wing-fuselage junction on the spanwise propagation of gross disturbances emanating from the wing-fuselage junction was also studied. This was to see whether it would be more efficient to prevent the attachment-line being contaminated by the fuselage's turbulent boundary layer rather than relaminarising the boundary layer downstream of the junction. Finally, the stability of the attachment-line to blowing was checked and a quantitative study of the effect of blowing length was made.

The two transition mechanisms have been studied independently so, for example, the suction used to control the crossflow instability did not include any on the attachment-line. This is an artificial situation since a practical system would use attachment-line control and crossflow control together rather than one or the other. Studying them independently is relevant because on the one hand it is necessary to understand how each control method affects transition before trying to understand how the combination works. From a practical viewpoint, there is also always the possibility that one part of the system will malfunction.

The work was sponsored by NASA and DERA and the research proposals are given as Appendices A and B respectively and reported separately in references 6 and 7.

2. Literature Review

Early theoretical work[8,9] assumed that the boundary layer transition characteristics on a swept wing would be subject to the independence principle, so the chordwise transition position could be predicted from two-dimensional data. However, during flight tests on an Armstrong Whitworth 52 by Gray[10], little or no laminar flow was observed, rather than the 60% upper surface chord expected. Further flight tests were scheduled using various swept wings (eg Armstrong Whitworth 52, Meteor fin, etc) and were reported by Gray[11,12]. Using sublimation and china-clay flow visualisation techniques, striations were observed in the laminar boundary layer prior to transition and Gray noted the similarity between the striation patterns observed in his tests and those caused by Görtler vortices during experiments on a cusped, unswept, aileron at NPL[13]. He also found that as the sweep angle increased beyond 20° the transition front moved swiftly towards the leading edge and, at larger sweep angles, transition occurred at the leading edge itself. He suggested the presence of a 'cross flow' within the boundary layer, perpendicular to the external streamline, as the source of the instability (see Section 3.3). Attachment-line contamination was also observed, but was not identified as an independent transition mechanism. Subsequently, cross-flow instability was demonstrated theoretically by Owen and Randall[14,15] and Stuart *et al*[16], who found that, at the leading edge of a swept wing, the boundary layer velocity profile normal to the external streamline contained a point of inflexion and was, therefore, dynamically unstable[17] at infinite Reynolds number. This instability took the form of stationary vortices appearing within the laminar boundary layer roughly aligned with the external flow direction which gave rise to the striation pattern which had been observed in flow visualisation. Owen and Randall proposed a cross-flow Reynolds number, χ, which depended on the characteristics of the cross-flow velocity profile, and suggested that transition would occur when this Reynolds number exceeded a critical value. They estimated a value of 125 for the appearance of striations and 175 for the transition front to have moved very close to the leading edge. Stuart[16] investigated the stability problem in three-dimensional incompressible flows, neglecting curvature effects, including a comparison between the three-dimensional cross-flow instability and Görtler type vortices. He showed that, although the two conditions appeared visually similar, they were different instability mechanisms. At the same time cross-flow instability was investigated experimentally on a swept wing in the wind tunnel by Anscombe and Illingworth[18] and by Gregory and Walker[16] on a swept wing and a rotating disc. Both groups noted striations in the laminar boundary layer prior to transition and that increasing sweep caused the transition front to move towards the leading edge until transition occurred very close to the leading edge.

In the UK, Head *et al*[19] had realised the importance of the crossflow instability and performed flight trials using LFC to control it. One wing of a Vampire III was covered with a sleeve of porous Monel Metal cloth. The wing was swept at 11.5° and the sleeve covered from 6% to 98% of the chord. Early trials, with and without suction, showed transition close to the leading edge, which was attributed to the rough surface of the Monel Metal cloth. The problem was solved by covering the surface with a nylon parachute fabric and further trials gave full chord laminar flow up to Mach 0.7 and chord Reynolds numbers of 26×10^7. This showed that suction could be used to delay the onset of transition and gave a reduction in profile drag, accounting for the suction

penalties, of 70 to 80%. In the US, Northrop conducted LFC flight trials using an F-94A. Suction was provided by slots, rather than the porous surface used by Head[19]. Pfenninger[20] reported that full chord laminar flow was recorded for chord Reynolds numbers from 12×10^6 to 30×10^6 and Mach numbers from 0.6 to 0.65. On two of the flights transition occurred close to the leading edge and Pfenninger noted that this was due to insect debris on the leading edge (attachment-line contamination). Pfenninger also noted that laminar flow was lost when the aircraft flew through a cloud but was regained less than one minute after leaving the cloud (as soon as the moisture had evaporated).

Further laboratory experimental work by Allen and Burrows[21] and Burrows[22] produced results that were in qualitative agreement with Owen and Randall's constant χ theory[15], and work by Boltz *et al* [23] gave approximate values of χ between 190 and 260. Although these were substantially higher than the value of 175 suggested by Owen and Randall, the discrepancy was blamed on the measuring techniques used and the boundary layer calculation methods employed, which were approximate integral methods. In 1961, Brown[24] extended Stuart's analytical work by using a numerical method developed at Northrop that enabled the eigenvalue approach of Lin[25] to be used. Results for several three-dimensional boundary layers were presented, but of particular interest is the result for the boundary layer on a swept wing with surface suction. Although no quantitative data on the suction type or distribution is given the use of suction greatly increases the critical Reynolds number for transition. In addition, he showed that the greater the suction the greater the Reynolds number difference between the first appearance of the cross-flow instability and transition onset.

Pfenninger and others[26,27,28] at Northrop worked on the X-21A project from 1960 to approximately 1965. The two X-21A aircraft were much-modified Douglas WB-66D Destroyer swept wing jets (eg the wings were completely changed and the original under-wing engines were moved to the aft) with wing sweep of 30°. The flight test envelope was from Mach 0.3 to Mach 0.8 and from 5000ft to 44 000ft. The programme was supported by a substantial series of high and low speed wind tunnel tests to validate the wing design. Chordwise suction was provided by slots from 1% to 100% chord and the X-21A team were aware of the dangers of attachment-line contamination because they used a boundary layer fence and suction slot combination to prevent it. The trials achieved almost 100% chord laminar flow over the upper surface up to mean aerodynamic chord (MAC) Reynolds numbers of approximately 20×10^6 and 60% chord laminar flow was achieved at MAC Reynolds numbers of approximately 40×10^6. Trials were also conducted to assess the effect of acoustic disturbances on transition with little evidence found. Companion wind tunnel tests investigated the stability and control (S&C) effects of a sudden loss of LFC and found that although there were some S&C problems these were sufficiently long period that they shouldn't be flight safety critical.

Gaster[29] performed flight trials using the Handley Page suction wing attached to the top of the fuselage of a Lancaster and then a Lincoln aircraft. The suction wing was a 10ft semi-span symmetrical 12.5% RAE 103 aerofoil section with a number of laminarisation slits intended to control the crossflow instability. Gaster found that for a variety of altitudes and speeds transition occurred at approximately constant leading edge radius Reynolds number. He then undertook wind tunnel tests to investigate the

basic physics behind the leading edge transition mechanism. Using circular cross-section wires wrapped around the leading edge to act as disturbance sources Gaster found that the larger the tripwire diameter the lower the transition Reynolds number. He also found that as the distance between the tripwire and the measuring station increased the transition Reynolds number increased, but that at large distances the transition Reynolds number reached an asymptotic value. This implied that there was a Reynolds number above which any turbulence would not decay but would propagate along the attachment-line instead, leading to a turbulent attachment-line and therefore a turbulent wing boundary layer. He used this data to define a critical roughness height for round cross-section tripwires. Having established that any disturbances introduced into the attachment-line from the wing-fuselage junction at flight-representative Reynolds numbers would probably cause a turbulent attachment-line, Gaster developed a passive device, a Gaster bump, to prevent this. The Gaster bump was a protuberance on the leading edge that caused a local stagnation point so that the boundary downstream of it would be laminar.

So, by the end of the 1960s crossflow and attachment-line transition had been identified as independent mechanisms particular to swept wing flows and several ideas had been proposed for their control. Flight trials had successfully implemented these ideas and significant regions of laminar flow had been obtained at practical Mach number/altitude conditions. However, by that time commercial interest in laminar flow had waned and funding for the research was stopped.

The oil crisis in 1973 caused crude oil prices in the West to double. OPEC imposed an oil embargo against the West following the West's support for Israel during the Yom Kippur war and the Iranian revolution followed by the Iran/Iraq war caused crude oil prices to more than double again by 1982. Figure 1 shows crude oil prices from 1947 to 1998 and is marked with the major events in the Middle East. The increase in oil prices caused interest in laminar flow to return as airline Direct Operating Costs increased, and methods were sought to reduce overheads. NASA resumed laminar flow research in 1976 with the Laminar Flow Control project, part of the Aircraft Energy Efficiency Program (ACEE), and later as the NASA Research and Technology Base Program. In 1975 the Eurovisc Working Party on Transition in Boundary Layers made swept wing research its primary recommendation and a national research program was set up in Germany on transonic wing technology 1985.

In 1978 Poll[4] conducted a thorough investigation of the effect of sweep on cross-flow instability. Using a swept-cylinder model, he examined the stability of the chordwise flow in the vicinity of the attachment-line at sweep angles between 52.5° and 72° using three measurement techniques: oil flow visualisation, hot-wire anemometry and surface Pitot tubes. He found that the conditions at which cross-flow vortices first appeared (calculated at the position the characteristic streaks started in oil flow) could be correlated by a constant value of the cross-flow Reynolds number, χ, and that the value was approximately 220, which agreed with previous data. This was defined differently to Owen and Randall[15], although it was still dependent on the characteristics of the cross-flow velocity profile. He noted that when a sublimation flow visualisation technique had been used by previous researchers a lower value of χ was obtained for the first appearance of striations. However, when correlating the data for the onset of

transition, Poll showed that χ varied with chordwise position and, therefore, that the constant χ hypothesis was of limited value.

During the early to mid 1980s NASA sponsored a flight-test program using a modified Lockheed C-140 Jetstar aircraft [30,31,32] as part of the Leading Edge Flight Test (LEFT) part of the ACEE. The main aim of the LEFT programme was to investigate the practicality of integrating an LFC system and then to operate a system in simulated airline service. Suction gloves were made for both wings, one designed by Lockheed and the other by the Douglas Aircraft Company. The Lockheed design used 27 slots to provide suction up to 12% chord, the position of the front spar. The Douglas design used a porous titanium sheet drilled using an electron beam. Again, suction was applied up to 12% chord. Each wing had a leading edge sweep of 30° and a super-critical aerofoil design up to 65% chord. The design point was Mach 0.75 at an altitude of 38000ft but the trials covered a range of conditions from Mach 0.7 to 0.8 and 29000ft to 40000ft. In the first flights the amount of laminar flow on the porous titanium surface varied from 97% to 7% chord, with 83% chord laminar at the design condition. The amount of laminar flow increased as the chord Reynolds number decreased and vice versa. The designers had not considered attachment-line contamination so a combined notch/Gaster bump was introduced. With this in place 96% of the chord was laminar at the design condition. The slotted surface was, in general, less effective than the porous surface with laminar flow covering between 80% and 94% at the design condition. The aircraft was operated in a way designed to simulate normal airline service. 62 flights were made to 33 different airports over a period of two years through all weather conditions and with no special treatment paid to the suction surface. The aircraft was operated in the same way as commercial aircraft, including queuing to takeoff, air traffic control of vector, altitude and speed and parking outside during the night. Importantly, NASA found no appreciable degradation of the suction systems over the two years.

As the Jetstar trials were finishing, a HLFC flight trial on a Dassault Falcon 50 was beginning in Europe[33]. The aim of the trial was to prove the concept of HLFC applied to a business jet size aircraft and to gather data to validate design tools. Suction was provided by a perforated stainless steel wing glove up to 10% chord and attachment-line contamination was controlled by a Gaster bump, with the target for the tests laminar flow up to 30% chord. The programme was successful with laminar flow over most of the test region and this success led to the European Laminar Flow Investigation (ELFIN) programme. One interesting series of tests during the Falcon 50 trials involved placing the Gaster bump at various distances from the wing-fuselage junction. It was found that with suction but without the bump the wing was fully turbulent. With the bump but without suction the wing was also fully turbulent. With the bump placed 150mm from the wing root and the suction on the wing boundary layer was mostly intermittent while with the bump 300mm from the wing root and the suction on most of the test region was laminar. It seemed that the vortex formed in the wing root area prevented a stagnation point forming on the Gaster bump if it was too close to the wing root.

The success of the Jetstar trials led NASA to try the HLFC concept on a large commercial transport aircraft. In collaboration with the Boeing Aircraft Company, a

Boeing 757 was flown to gather data at higher Reynolds numbers[34]. A perforated titanium surface was used to give suction from the leading edge to the position of the front spar. Laminar flow beyond 65% chord was obtained with suction rates one-third of those predicted and the overall drag reduction was projected as approximately 6%[35]. However, although the HLFC concept had been proven doubt had been thrown on the prediction methods used because only one third of the predicted suction had been required.

Two types of vortices occur in three-dimensional boundary layers due to cross-flow instability: stationary vortices and travelling vortices. The type that dominates crossflow transition has been linked to the receptivity mechanism of the boundary layer in work by Bippes and Müller[36] and Bippes[37], using wind tunnels with different freestream turbulence intensities. In the high turbulence conditions, they found that travelling cross-flow vortices were observed whereas, in the low turbulence environment, stationary vortices were dominant. Linear stability theory predicts that travelling cross-flow disturbance would be amplified more rapidly than stationary ones, but work by Kohama *et al*[38] showed that the transition process is dominated by a high frequency, secondary instability rather than the primary, low frequency instability. This secondary instability, with a frequency an order of magnitude larger than the primary instability, is caused by the parallel co-rotating stationary vortices near the edge of the boundary layer. High momentum fluid is bordered by low momentum fluid which leads to multiple inflection points high in the streamwise velocity profiles (Poll[4] noted a high frequency instability during his work which may have been the first published observation of the secondary instability). This process is highly non-linear. Saric *et al*[39] showed that the intermittency of stationary cross-flow vortices is strongly influenced by streamwise vorticity and that, even in the Stokes-flow limit, a small three-dimensional roughness is a source of vorticity. Further work on the effect of micron-sized roughness elements[40] showed that the effect of isolated 6μm roughness elements was confined to a small chordwise zone close to the attachment-line where the cross-flow disturbances were first amplified, and that transition was caused by the stationary vortex which passed close to the location of the roughness element.

Computational work by Malik *et al*[41] attempted to demonstrate the dominance of the stationary cross-flow vortex and the appearance of a high frequency secondary disturbance. The swept Heimenz flow that forms near an attachment-line was used and both linear and non-linear PSE calculations were performed. Good correlation was obtained with previous experimental results. The calculated wall vorticity distribution showed the streaks (or striations) associated with the onset of cross-flow instability and multiple inflection points in the streamwise velocity profiles of the stationary cross-flow vortices were found. The high frequency secondary instability was also found and had a frequency an order of magnitude larger than the most amplified travelling mode, in agreement with the findings of Kohama[38] and Poll[4].

Radeztsky[42] compared linear stability results from previous investigations with detailed measurements taken for the growth of low amplitude stationary cross-flow vortices. Linear theory correctly predicted the mode shapes and the wavelengths of the cross-flow vortex, including the most amplified wavelength. However, the growth rates were not correctly predicted, and in many cases theory predicted strong growth when the

amplitude was actually decaying. Taken in conjunction with results from Bippes[37] and Dagenhart[43] it can be seen that linear theory fails to predict the correct growth of cross-flow vortices, even when curvature and non-parallel effects are included. Reibert *et al*[44] reported a comparison with nonlinear PSE calculations and showed good correlation for the growth rate of the cross-flow vortex.

During the early 1990s interest in HLFC widened from wings alone to encompass other parts of the airframe. Wind tunnel tests at the University of Manchester[45, 46] on a two-dimensional engine nacelle model showed that suction could be used to delay transition on an engine nacelle. A collaboration between Rolls Royce, DLR and MTU Aeroengines resulted in a 93 hour flight trials programme on a VFW 614 ATTAS (Advanced Technologies Testing Aircraft System) that showed laminar flow was possible over 60% of the nacelle length. It also showed that the noise and vibration near the engines did not affect the capability of an LFC system to deliver laminar flow on the nacelle. Another good candidate for HLFC is the tail fin. Collaboration between Airbus, ONERA and DLR led to a wind tunnel and flight trial programme using an Airbus A320 fin[47]. The fin was chosen because no de-icing system would be needed, the installation would be straightforward and flight Reynolds numbers could be replicated in the ONERA S1MA wind tunnel at Modane. Robert[47] showed that a 1% fuel burn saving for an A320 could save as much as 25 200 tonnes of fuel for a fleet of 20 aircraft over 15 years. Modelling predicted approximately 50% chord laminar flow, which would give a reduction in overall aircraft drag of 1 to 1.5%.

French work at ONERA on swept wing transition began in the early 1980's and continues today. The work has, to a large extent, paralleled that of Gaster and Poll in the UK and has been in general agreement with it. The ONERA work has been particularly focused on predictive methods and the attachment-line. Arnal and Juillen[48] looked at transition near the leading edge of a swept wing in the ONERA F1 and F2 wind tunnels. They found that the onset of transition due to crossflow instability along a strong negative pressure gradient could be modelled well by the linear stability e^n method. They also found that strongly accelerating chordwise flow near the leading edge could prevent turbulence from a turbulent attachment-line contaminating the chord boundary layer at various Reynolds numbers. Reneaux *et al*[49] looked at methods to prevent attachment-line contamination. Firstly they looked at a passive Gaster bump device, showing that contamination could be prevented over a range of Reynolds number and angles of attack. They also showed that investigations using their CFD code produced good designs for Gaster bumps. Reneaux also looked at the effect of suction on the leading edge and demonstrated that suction was effective for relaminarising a turbulent attachment-line and that the boundary layer profiles following relaminarisation had characteristics typical of laminar boundary layers. Interestingly, the suction coefficients presented by Reneaux were higher than those given by Danks[5] for $\overline{R}$ values greater than 400. Arnal *et al*[50] presented a comparison between leading edge transpiration wind tunnel results (both suction and blowing) and a numerical study using non-linear parabolised stability equations (PSE). This gave data in broad agreement with the experimental results, although the numerically predicted transpiration coefficients were slightly lower than their experimental equivalents. Importantly, the numerical results showed a smooth trend through the zero suction case, suggesting that the same basic physics was at work for both relaminarisation by suction and destabilisation by blowing.

Danks[5] studied the effect of suction on transition at, and near, a swept attachment-line using the same swept-cylinder model as was used in this thesis at the University of Manchester. On the attachment-line, he found that suction could be used to relaminarise a fully turbulent boundary layer and that the longer the spanwise suction length the higher the transition Reynolds number[51]. Additionally, at large spanwise distances the suction required approaches an asymptotic value, so there was a suction coefficient at which turbulent flow would not be possible and it was approximately C_q=-0.0035. Experiments with blowing on the attachment-line showed that small blowing coefficients ($C_q \approx 0.0002$ at flight scale Reynolds numbers) had a large destabilising effect. Danks also looked at the use of suction for controlling the crossflow instability[52]. He found that modest amounts of suction could be used to delay the onset of cross-flow instability at least until the minimum pressure location on his model, provided transition was caused by cross-flow instability and not attachment-line contamination. The porous surface of the model was divided into eight plenum chambers so that different distributions of suction could be used. He found that there was no single, ideal, suction distribution, but that a number of successful distributions had approximately the same average suction coefficient. It was also found that suction was not required through all of the plenum chambers round to the monitoring station, with suction most effective when applied upstream of the position transition would have occurred at without suction. Danks noted that suction applied off the attachment-line could be used to relaminarise a chordwise boundary layer which had been contaminated by a turbulent attachment-line. Again, various suction distributions were used and it was found that, for transition at the minimum pressure location, the average suction coefficient required was an order of magnitude larger than had been required for the condition with no attachment-line contamination (suction coefficient of approximately C_q=–0.0025 with a turbulent attachment-line and C_q=–0.0003 with a laminar attachment-line). A combination of attachment-line and chordwise suction was then used to control an originally turbulent attachment-line. Danks found that using suction on the attachment-line reduced the suction coefficient from C_q=-0.0025 to C_q=-0.0015 to give laminar flow at the minimum pressure location. Also at Manchester, Yardley[53] developed a turbulence model that could predict relaminarisation for a variety of low Reynolds number flows, including the attachment-line and a zero pressure gradient flat plate. The model incorporated the effects of suction and convective acceleration, and Yardley showed that relaminarisation on a swept wing could not be caused by a pressure gradient but was caused either by the low Reynolds number or a combination of the low Reynolds number and suction and/or convective acceleration. His model also predicted that the minimum momentum thickness Reynolds number, R_θ, for self sustaining turbulent flow was 130.

Although the Boeing 757 flight trials[34] had shown substantial amounts of laminar flow, the suction required had been much less than predicted and this had thrown doubt on the prediction tools used. To recover the situation, NASA and Boeing conducted wind tunnel tests in the NASA Langley 8ft transonic pressurised tunnel[54]. Laminar flow was apparently obtained back to the minimum pressure location, but results have not been officially published yet.

Bippes and Lerche[55] investigated the effect of suction on travelling and stationary cross-flow vortices on a swept flat plate with a pressure gradient imposed by a shaped tunnel liner. The flow on the plate was stable to T-S instabilities so it was ideal for the study of the crossflow instability on its own. The experiments were designed to study the evolution of the crossflow instability rather than measure the effect of suction on the transition location so, at the Reynolds numbers used, the onset of transition did not occur on the model. On a porous surface, without suction, the amplitudes of both travelling and stationary disturbances were more than double those on a polished non-porous surface at the same conditions. When suction was applied the amplitudes of travelling disturbances were damped, but the amplitudes of stationary disturbances were unaffected or even slightly increased. This was in contrast to Danks' results, but the authors considered that it was due to the considerable non-uniformity of the suction velocity across the plate due to manufacturing quality. However, no details of the suction used (distribution or magnitude) were given so firm conclusions can not be drawn.

3. The Swept Wing Boundary Layer

3.1 The Swept Wing

As an aircraft's speed increases the freestream Mach number increases and eventually, at some point on the wing surface, the local flow speed reaches Mach one. At still higher speeds a small region of supersonic flow is established which is terminated by a shock wave. The interaction of this shock wave with the wing boundary layer causes an increase in drag and may produce shock-stall if the adverse pressure gradient associated with the shock wave causes boundary layer separation. The onset of this drag rise can be delayed to higher flight speeds by sweeping the wing which reduces the local chordwise velocity by the cosine of the sweep angle. This is the technique currently employed.

3.2 The Attachment-Line

An important consequence of wing sweep is the creation of a flow along the leading edge, which has an associated boundary layer. Figure 2 shows the potential flow streamlines near the leading edge of a swept wing and it can be seen that sweeping a wing splits the freestream into two components, a chordwise flow and a spanwise flow. The spanwise flow naturally has a boundary layer and this is termed the attachment-line boundary layer. The attachment-line is defined as the line along the leading edge that separates the flow passing over the upper surface from that passing over the lower surface (equivalent to the locus of stagnation along the leading edge of an unswept wing) and is indicated by the line A-A in Figure 2. This boundary layer has great importance for the state of the wing boundary layer as a whole because fluid particles do not travel the entire length of the leading edge. Instead, fluid elements in the attachment-line boundary layer flow onto the wing chord and are replaced by fluid elements entrained from the freestream. This is fundamentally different to two-dimensional flat plate boundary layers where the fluid elements record the 'history' of the boundary layer following events upstream (eg the momentum defect introduced by a trip-wire). This means that a turbulent attachment-line boundary layer will, in general, result in turbulent upper and lower surface chordwise boundary layers with the associated increase in skin friction over laminar chordwise boundary layers.

3.3 Cross-Flow Instability

All three-dimensional boundary layers are characterised by streamline curvature[56]. Outside the viscous layer this curvature is maintained by pressure gradients that act in a direction perpendicular to the external streamline direction, in planes drawn parallel to the surface. As the surface is approached fluid is slowed by viscosity and moves in the direction of these gradients to create a 'cross-flow' velocity component within the boundary layer. Figure 3 is a schematic diagram of such a boundary layer. For the cross-flow component of the profile, the boundary conditions are no slip at the surface and zero velocity at the edge of the boundary layer. It follows that such a profile contains at least one point of inflection and, consequently, as demonstrated by Gregory *et al*[56], these profiles become unstable at low characteristic Reynolds numbers.

3.4 Intermittency

When a boundary layer is transitional flow parameters at a fixed measuring station are found to switch almost instantaneously between the laminar and turbulent states, and the size of the turbulent 'patches' and the time between them seems random. This characteristic was recognised by Emmons[57] who introduced the concept of the intermittency, Γ. Intermittency at the leading edge of a swept wing was investigated by Gaster[29] and Poll[4], amongst others. Emmons defined the intermittency as the probability that, at a particular time, t, the flow at a given location is turbulent. Therefore, for purely laminar flow the intermittency is zero and for fully turbulent flow the intermittency is unity. It should be recognised that just as the leading edge boundary layer is three-dimensional so intermittency is a three-dimensional concept.

Poll[4] investigated the intermittency of the attachment-line for incompressible conditions and then extended this to the compressible regime[58]. Poll found from his experimental results that, for the incompressible case, the intermittency could be approximated as

$$\Gamma = 1 - e^{-0.411 \cdot \frac{\overline{R} - \overline{R}_b}{\overline{R}_{\Gamma=0.75} - \overline{R}_{\Gamma=0.25}}}$$

where $\overline{R}_b$ is the $\overline{R}$ at the onset of transition.

3.5 Receptivity

Receptivity[59,60,61] is the mechanism by which environmental disturbances enter a laminar boundary layer and interact with the flow to produce instability waves. The normal transition process occurs due to the amplification of these instability waves through linear and non-linear phases until a turbulent flow is established. Bypass transition describes the process where large, finite amplitude disturbances (for example from a large roughness element) amplify non-linearly and cause transition, 'bypassing' the linear amplification phase.

3.6 Parameters Used for th e Study of Leading Edge Flows

The flow field at the leading edge of a wing is governed by many parameters and restrictions need to be applied to the experimental system to reduce the problem to manageable proportions. A simple approach is the use of a model with constant spanwise section to give infinite swept conditions (see Section 3.7).

Dimensional analysis of the infinite-swept attachment-line, using Buckingham's pi theorem, shows that the boundary layer can be characterised by the freestream turbulence level, Tu, the Mach number, M, the Prandtl number, Pr, the ratio of specific heats, γ, the ratio of wall temperature to boundary layer edge temperature, T_w/T_e and a leading edge Reynolds number.

3.7 Experimental Simplifications

To simplify study of the physics of leading edge flows it is convenient to reduce the number of independent variables by aiming for infinite swept conditions. A model with constant spanwise geometry can be used to produce an attachment-line boundary layer with spanwise independent properties (e.g. boundary layer thickness, skin friction, the rate of divergence, etc.) provided that the boundary layer is either fully laminar or fully turbulent, but not transitional[62]. The spanwise independence is achieved by a balance between the transfer of fluid from the attachment-line into the chordwise boundary layer and the entrainment of fluid from the freestream into the attachment-line boundary layer.

In the case of low speed wind tunnel experiments near the attachment-line of a swept cylinder, several of these may be neglected. Mach numbers are less than 0.2, so the effects of Mach number (ie compressibility) may be ignored and the properties of the air may be regarded as constant, so the Prandtl number and the ratio of specific heats may also be ignored. Freestream turbulence may be ignored if the turbulence level is less than 0.8%, and the longitudinal turbulence component in the wind tunnel used was approximately 0.1% (See Appendix C). Assuming that the cylinder surface is not heated or cooled (ie adiabatic conditions) the ratio of wall temperature to boundary layer temperature can also be neglected.

With these simplifications, steady, incompressible flow without heat transfer, along an infinite-swept attachment-line is completely determined by the magnitude of the characteristic leading edge Reynolds number. Poll[62] defined a characteristic spanwise leading edge Reynolds number as $\overline{R}$ and this has been used in the current work. A description of Poll's derivation and its relationship to other characteristic Reynolds numbers is given below for completeness.

The characteristic spanwise leading edge Reynolds number, $\overline{R}$, is defined as

$$\overline{R} \equiv \frac{V_e \eta}{\nu}$$

where $\mathbf{V_e}$ is the spanwise velocity at the edge of the attachment-line boundary layer, η is a length scale and ν is the kinematic viscosity.

By analogy with the Blasius length scale the viscous length scale, η, is

$$\eta \equiv \left[\frac{\nu}{dU_e / dx} \right]_{x=0}^{0.5}$$

where $\mathbf{U_e}$ is the chordwise velocity at the edge of the boundary layer and $\mathbf{x}$ is the chordwise position measured along the surface, perpendicular to the leading edge, with the origin at the attachment-line – see Figure 1.

Poll showed that this could be related to the laminar momentum thickness, θ_L, by

$$\theta_L = 0.404\eta$$

and the laminar displacement thickness, δ^*, by

$$\delta^* = 0.404\eta$$

It follows that the Reynolds numbers are related as

$$R_{\theta_L} = 0.404\overline{R}$$

$$R_{\delta^*} = 1.026\overline{R}$$

See Gaster[29] and Pfenninger[20] for descriptions of the laminar momentum thickness and laminar displacement thickness Reynolds numbers applied to leading edge flows. Cumpsty and Head[63] proposed a different similarity parameter for the attachment-line, C*, defined as

$$C^* = \frac{V_e^2}{\nu\left(\frac{dU_e}{dx}\right)_{x=0}}$$

It can be seen that C* can be related to $\overline{R}$ as

$$C^* = \overline{R}^2$$

It follows that the length scale used for C* is

$$\frac{V_e}{\left(\frac{dU_e}{dx}\right)_{x=0}}$$

However, Poll argued that the length scale used was not physically representative of the boundary layer thickness and would make direct comparison with other work difficult (the magnitude of η is 10^{-3}m while the magnitude of the C* length scale is 10^{1}m).

As described above, a transitional attachment-line boundary layer cannot be spanwise independent so the spanwise position is important. When the attachment-line behaviour is investigated at different spanwise positions a length parameter, s, is introduced. The length, s, is the spanwise distance under consideration (eg the spanwise length between the position of a trip wire and the measuring station or the spanwise length between the end of the suction surface and the measuring station). The associated non-dimensional group is then,

$$\frac{s}{\eta}$$

Danks[5] showed that for chordwise flows close to the leading edge the chordwise Reynolds number to be used is

$$Re_x \equiv \frac{U_e x}{\nu_e}$$

where Re_x is zero at the attachment-line.

When surface transpiration is used a further parameter is required and this takes the form of a transpiration coefficient, C_q,

$$C_q \equiv \frac{w(0)}{Q_e}$$

where w(0) is the suction velocity perpendicular to the surface. Note that a positive value represents blowing and a negative value suction. However, it is difficult to measure the suction velocity so this definition of C_q is of limited practical use. A more useful definition for the suction coefficient is

$$C_q \equiv \frac{\dot{M}}{\rho_\infty S Q_e}$$

where $\dot{M}$ is the mass flow rate, S is the surface area across which transpiration is applied and Q_e is the freestream velocity at the edge of the boundary layer and can be calculated from

$$Q_e = \sqrt{V_e^2 + U_e^2}$$

Note that at the attachment-line the chordwise velocity is zero, so the suction coefficient is

$$C_q = \frac{\dot{M}}{\rho_\infty S V_e}$$

Since the surface is a nominally circular cylinder (see Section 4.1 for a description of the model) the surface area can be calculated as a segment of a cylinder from

$$S = Lr\theta$$

where L is the length of the transpiration surface, r is the radius of the cylinder and θ is the angular extent of the transpiration surface.

From the above discussion it follows that low speed measurements, made near the leading edge of an infinite swept circular cylinder at any spanwise and chordwise position, under any combination of freestream unit Reynolds number and sweep angle can be compared provided that the four non-dimensional parameters $\overline{R}$, s/η, Re_x, and C_q are duplicated.

It must be noted that although the low speed wind tunnel and swept cylinder environment may seem very different to a swept aircraft wing this is actually not the case. For a subsonic aircraft such as the Boeing 777 and Airbus A320 the flow in the leading edge region is a low Mach number, nominally incompressible flow regime since the flow decelerates to zero chordwise velocity at the attachment-line. The leading edge and chordwise Reynolds numbers are defined such that no scaling is required between wind tunnel and flight scale, therefore avoiding the most common wind tunnel/flight scale matching problem. The main difference between the flight scale and wind tunnel is the pressure distribution at the leading edge. The deceleration of the freestream flow at the leading edge and subsequent acceleration over the wing produces a 'peaked' pressure distribution and a strong positive pressure gradient. This cannot be reproduced in a conventional low speed wind tunnel and would require a tunnel with adjustable working section shape so that the required pressure distribution could be imposed. However, would be a costly business and the circular cylinder provides a good approximation.

4. Experimental Arrangement

4.1 The Model

4.1.1 Model Description

Tests have been conducted on a large swept cylinder model, previously used by Danks at the University of Manchester[5]. The model is composed of a wooden frame, faired to a "tear drop" section to prevent early boundary layer separation and the formation of an oscillating wake. The spanwise chord is 0.813m and the leading edge radius is 0.203m. The leading edge is formed from a perforated surface made from 1.2mm thick titanium sheet, laser drilled prior to model construction with holes of 50μm diameter and a hole-to-hole and row-to-row spacing of 400μm, as shown in Figure 4. The entire drilling pattern is skewed relative to the axis of symmetry by 14°, leading to a streamwise hole separation of not less than 1600μm and, in general, an irregular pattern of holes along any flow streamline. The leading edge was manufactured by Aerospace Systems and Technologies (AS&T) of Durham.

The titanium surface is divided into perforated and non-perforated areas to enable a range of suction conditions and distributions to be considered and a plan of the perforated areas is given as Figure 5. The layout of the perforated areas can be split into two distinct areas: at the top of the model there is no porosity on the attachment-line but instead there is continuous porosity from 10° to 90°; at the bottom the porosity is provided in strips 20° wide, except at the edge of the model where the strip is only 5°, separated by strips 5° wide. For this bottom section one of the strips covers ±5° either side of the geometric centreline of the model (the nominal attachment-line position). The top section porosity distribution was designed for the ELFIN project while the bottom section porosity distribution was intended to simulate the porosity distribution on the NASA Jetstar aircraft[31]. The regions of perforated surface are further divided into areas supplied by independent plenum chambers, shown in Figure 6, which allow different suction levels to be used around the chord if necessary. Figure 6 also shows the numbering system used for the chambers, with 14 independent chambers in the main part of the surface and one at the top of the model. Note that chambers 1 to 13 were approximately 355mm (10°) wide but chamber 14 (the attachment-line chamber) was approximately 709mm wide (±10° either side of the geometric centreline). All of the chambers were 900mm long and each plenum chamber had two outlets to the suction system and three static pressure tappings, as shown in Figure 6. Two outlets to the suction system were used to distribute the suction in the plenum chamber and avoid the large sink effects that would occur around a single pipe. The mass flow rate through the porous surface depends on the difference between the external static pressure and the plenum internal pressure, which is further modified by the pressure loss across the surface itself (see Poll *et al*[64] for a discussion of the aerodynamic performance of laser drilled sheets). The pressure drop across the particular surface on this model is quite large (see Section 4.1.2) which is designed to insulate the internal plenum pressure from the external pressure field. A constant pressure within the plenum chamber is necessary to ensure that the suction is constant across the surface area sourced by the plenum

chamber. The three static pressure tappings in each plenum chamber were used to monitor the pressure distribution along the plenum chamber.

Each plenum chamber was connected, via a valve and a flowmeter, to a vacuum tank, which had a maximum suction capacity of approximately 3000 litres/minute with the model connected. There were three sets of static tappings on the model, 440mm, 1360mm, and 2260mm from the upstream tip (see Figure 5). The top and bottom sets each extended to 85° either side of the line of geometric symmetry in steps of 5° while the middle set extended from 15° to 85° on one side of the model, also in steps of 5°. The model was mounted in the Cranfield College of Aeronautics low-speed, closed-return, wind tunnel as shown in Figure 7. This wind tunnel has a 2.44m x 1.83m working section and a maximum freestream velocity of $55ms^{-1}$. To prevent contamination of the model boundary layer by the turbulent boundary layer on the wind tunnel ceiling the distance between the upstream tip of the model and the ceiling was never less than 0.3m.

4.1.2 Static Testing

Danks[5] conducted a static calibration (ie in still air) of the plenum chambers, intending to use the results while in the wind tunnel to calculate the mass flow rate from the internal plenum pressure and the surface pressure distribution. Dynamic calibration checks showed this was not possible, so Danks used flowmeters to measure the mass flow rate. However, Danks' static calibration is a useful benchmark for the condition of the porous surface when it was first fitted to the model. It was compared to a static calibration at the start of the current work to see whether there has been any degradation in the efficiency of the surface. The performance of the surface could reduce for a number of reasons, mainly relating to dirt accumulation. Although wind tunnels are, in general, fairly clean environments there will be dust in the air. Also, Danks used tape to hold down the hot-wire probe and this would have left a residue on the surface, possibly blocking some of the laser drilled holes. Chambers 0 and 14 (see Figure 6 for the numbering scheme), the upstream tip and attachment-line chambers respectively, were checked because they covered the range of surface wear and tear - Danks used chamber 14 extensively, but used chamber 0 very little. The static calibrations were similar, with the recent calibration giving approximately 5% less pressure drop across the surface for the mass flow rate. The reasons for this are unknown, but the calibrations were sufficiently similar that it can be assumed that the performance of the surface has not degraded since it was fitted.

4.1.3 Checking For Leaks

The transpiration system was, by necessity, a series of different pipes connecting the plenum chambers to the valves and flow meters and then on to the evacuation tank. Each connection had the potential to leak, as did the plenum chamber itself. After any model change that could have disturbed the pipework, for example changing the sweep angle, the model was checked for leaks. Cling film was placed over the porous surface and suction was applied, with any leakage giving a reading on the flow meters.

4.1.4 Model Alignment

Alignment of the model in the wind tunnel was very important. Poor alignment of the model made it difficult to reliably identify the attachment-line (and therefore difficult to place the hot-wire in the correct position) and in extreme cases could lead to excessive model vibration and premature transition. There were two aspects to aligning the model: yaw and twist. Yaw related to aligning the model longitudinally with the flow direction while twist could occur if the block under the back of the model was not placed correctly.

The arrangement of the model in the working section is shown in Figure 7. The model was attached to the ceiling by a solid steel 'U' piece which ensured that the top of the model was horizontal. The back of the model was then supported by a wooden block. To provide stability steel wires were attached to a steel crosspiece at the back of the model and passed through the floor. Heavy weights were attached to these wires, pulling the back of the model down onto the supporting wooden block. These also helped to damp any vibrations.
The model was aligned with the freestream flow by using the static pressure distribution around the leading edge of the model as a yaw meter. When the model was correctly aligned the static pressure distribution at any spanwise point was symmetric about the attachment-line. Figure 8 shows a typical aligned and untwisted distribution. The x/C values in Figure 8 are actually geometric measurements with x/C=0 being the plane of symmetry on the leading edge. The alignment process is aimed at getting the attachment-line to align with the geometric x/C. By comparing the pressure distributions around the top, middle, and bottom of the leading edge any yawing or twisting of the model is apparent. At each sweep angle, the alignment of the model was checked throughout the freestream dynamic pressure range of the wind tunnel.

4.2 Verification of Infinite Swept Conditions

The static pressure distribution can also be used to determine whether conditions are infinite-swept. Figure 8 shows the static pressure distribution around the model and it can be seen that the pressure distributions at the middle and bottom tappings are in good agreement (within ±2%). The pressure distribution at the top location is larger by approximately 17% at the attachment-line (x/C=0), and this indicates that infinite swept conditions were reached at some point between the top and middle tappings. The section of the porous surface used for the attachment-line investigation was between the middle and bottom pressure tappings, so comparing the pressure distributions will show whether conditions were infinite swept. The crossflow experiments were conducted at the middle tappings location, so the pressure distribution comparison was sufficient to tell whether conditions were infinite swept at the measuring location. Additionally, the experimental chordwise velocity distribution was compared with the velocity distribution predicted by a potential flow approximation (see Section 4.4 for details). This again showed that conditions were infinite swept between the bottom and middle tappings.

4.3 The Experimental Determination of Flow Parameters

From Section 3.7 above, for the simplified experimental conditions used here, only four non-dimensional parameters are needed to characterise the flow near the leading edge of a swept circular cylinder with transpiration: $\overline{R}$, Re_x, s/η, and C_q. The experimental methods used to measure the dimensional components of these and so calculate the non-dimensional values are described below. Measurement uncertainties have been calculated for the various parameters measured during the experiments. These uncertainties were calculated using a Monte Carlo approach rather than a statistically rigorous student-t or Gaussian method and, as such, represent engineering judgement. Additionally, the uncertainties are not always independent; the attachment-line boundary layer length scale η, for example, is a function of the kinematic viscosity and the chordwise velocity. Both of these are functions of the density so they should not be regarded as independent sources of uncertainty in an error analysis. However, as discussed above the uncertainties have not been analysed in a statistically rigorous way so this has been ignored.

4.3.1 Kinematic Viscosity

The kinematic viscosity, ν, is defined as

$$\nu \equiv \frac{\mu}{\rho}$$

where μ is the viscosity coefficient and ρ is the fluid density. The viscosity coefficient is the constant of proportionality relating the shear stress, τ, and the vertical velocity gradient through the boundary layer – eg

$$\tau = \mu \frac{\partial V}{\partial z}$$

Given the assumptions that have been made about the flow regime (see Section 3.7) it can reasonably be assumed that μ is a function of temperature only so Sutherland's Law may be used[65]:

$$\frac{\mu_\infty}{\mu_0} = \left(\frac{T_\infty}{T_0}\right)^{1.5} \left(\frac{T_0 + 110}{T_\infty + 110}\right)$$

Using ISA conditions for the reference values,

$$T_0 = 288.16\text{K}$$
$$\mu_0 = 1.7894\text{x}10^{-5}\,\text{kg}\,\text{m}^{-1}\text{s}^{-1}$$

Similarly from the assumptions in Section 3.7, the freestream density, ρ_∞, can be calculated from Boyle's Perfect Gas Law,

$$\rho_\infty = \frac{p_\infty}{RT_\infty}$$

where R is the gas constant and R=287 J $kg^{-1}K^{-1}$ for air.

The temperature was measured using a thermocouple built into the wind tunnel. The reading could be taken electronically or could be read from the digital display in the control room. Accuracy was better than ±0.1°, which gave an uncertainty on the kinematic viscosity of ±0.06% and an uncertainty on the density of ±0.03%. The ambient pressure was measured using a Setra barometric pressure gauge with readings taken manually from the digital display. Accuracy was ±0.05% full scale (ie ±5.5mbar), which gave an uncertainty on the kinematic viscosity of ±0.6% and an uncertainty on the density of ±0.55%. Combining the two sources of uncertainty, the uncertainty on the kinematic viscosity was ±0.66% and the uncertainty on the density was ±0.6%.

4.3.2 Freestream Dynamic Pressure

The freestream dynamic pressure, q_∞, was calculated by measuring the static pressure change across the wind tunnel contraction cone and using the wind tunnel calibration. The method used to calibrate the wind tunnel is described in Appendix D. The static pressure change was measured using a Furness M0177 pressure gauge. Readings could be recorded electronically or manually from a digital display in the control room. The manufacturer's quoted accuracy was ±0.5% of full scale (ie ±7 N m^{-2}). Because the accuracy was a percentage of the full scale value the accuracy of the measured value depended on what percentage of the full scale value it was, so the test point dynamic pressure was always at least 20% of the full scale value. Using this technique, the uncertainty on the dynamic pressure was always less than ±2.5%.

The empty tunnel freestream velocity, $\overline{Q}_\infty$, was calculated from

$$\overline{Q}_\infty = \sqrt{\frac{2q_\infty}{\rho}}$$

From Section 4.3.2 above, the uncertainty on the density was ±0.6%. Combining this with the uncertainty on the dynamic pressure gives an uncertainty on the empty tunnel freestream velocity of approximately ±2.8%.

4.3.3 Length Scale

As discussed in Section 3.7 above, the viscous length scale, η, is defined as

$$\eta \equiv \left[\frac{\nu_\infty}{dU_e/dx}\right]^{0.5}_{x=0}$$

The kinematic viscosity can be calculated from the ambient conditions and the chordwise velocity gradient at the attachment-line, $(dU_e/dx)_{x=0}$, can be calculated from the static pressure distribution around the leading edge, as follows. Using Bernoulli again, the static and dynamic pressures at some point on the chord, p_x and q_x respectively, are related to the total pressure as

$$p_T = p_x + q_x = p_x + \frac{\rho Q_e^2}{2}$$

Equating this to the total pressure on the attachment-line,

$$p_x + \frac{\rho Q_e^2}{2} = p_a + \frac{\rho V_e^2}{2}$$

Rearranging,

$$p_a - p_x = \frac{\rho}{2}\left(Q_e^2 - V_e^2\right)$$

Now, because the co-ordinate system used is Cartesian (see Figure 2)

$$Q_e^2 - V_e^2 = U_e^2$$

So,

$$U_e = \sqrt{\frac{2\left(p_a - p_x\right)}{\rho}}$$

From this, the chordwise velocity distribution around the leading edge of the model can be calculated using experimentally measured quantities and Figure 9 shows an example of the chordwise velocity distributions, on one side of the model, at the top and bottom static pressure tappings positions. The velocity gradient, (dU_e/dx), is linear up to $\pm 0.15x/C$ and this can be used when calculating the experimental U_e for a test point. The gradient in the linear region can be determined by a simple least-squares method and the chordwise velocity can be calculated from

$$U_e = x.\left(\frac{dU_e}{dx}\right)_{x=0}$$

This can save time during the experiments, which is always useful. However, this is only valid for approximately ± 0.15 x/C (approximately $\pm 35°$). At larger chordwise distances U_e must be calculated from the static pressure distribution.

The uncertainty in the calculation of η comes from the kinematic viscosity, the density, the empty tunnel freestream velocity, the attachment-line static pressure and the static

pressure at the various chordwise positions. From Section 4.3.1, the uncertainty on the kinematic viscosity is ±0.66% and the uncertainty on the density was ±0.6% and from Section 4.3.2 the uncertainty on the freestream velocity was ±2.8%. The attachment-line and chordwise static pressures were measured using Setra 239 differential pressure transducers. The uncertainty on each measurement was ±0.14% full scale reading, which was approximately ±2.5% on average. Combining these, the uncertainty in the calculation of η was approximately ±3%.

4.3.4 Spanwise Leading-Edge Reynolds Number

The accurate determination of the characteristic spanwise leading-edge Reynolds number, $\overline{R}$, is of critical importance. From Section 3.7,

$$\overline{R} \equiv \frac{V_e \eta}{\nu}$$

Poll[4] showed that the potential flow solution for a swept circular cylinder could be used to derive an expression for $\overline{R}$ in terms of simple to measure parameters rather than the difficult to measure V_e and η:

$$\overline{R} = \left(\frac{Q_\infty r}{\nu} . \frac{\sin \Lambda \tan \Lambda}{2} \right)^{0.5}$$

where r is the leading edge radius, Q_∞ is the freestream velocity and Λ is the geometric sweep angle. A more detailed discussion of the potential flow solution is given in Section 4.4 below.

However, this method introduces two sources of inaccuracy:

(i) The effect of the model on the empty tunnel freestream velocity, usually accounted for with an empirical blockage correction
(ii) Use of the geometric (measured) sweep angle rather than the actual sweep angle which assumes the freestream flow approaching the model is perfectly horizontal and is not affected by the model

At Manchester, Danks[5] developed a method that allowed the calculation of V_e and η and, therefore, did not require these inaccuracies. Danks' method has been used in this work so it is described below.

At low freestream Mach numbers, the effects of compressibility can be neglected (see Section 3.7 above) and Bernoulli's equation is applicable outside the boundary layer. Knowing the empty tunnel calibration (ie the relation between the static pressure difference across the contraction cone and the working section dynamic pressure with no model in place) and the static pressure at the start of the working section, the empty tunnel freestream total pressure, p_T, can be calculated. The working section of the wind tunnel was open to the atmosphere at each end (via slots in the walls) and the model

frontal area was small compared to the working section area (less than 10%), so it can reasonably be assumed that the total pressure would be the same with or without the model present. Formalising this with Bernoulli's equation,

$$p_T = p_\infty + q_\infty = p_a + q_a$$

where p_T is the total pressure, p is the static pressure and q is the dynamic pressure, with the subscript ∞ denoting freestream conditions and the subscript *a* attachment-line conditions. Now, the static freestream pressure can be measured directly and the freestream dynamic pressure can be calculated from the empty tunnel calibration. The attachment-line dynamic pressure is defined as

$$q_a \equiv \frac{\rho_\infty V_e^{\,2}}{2}$$

Substituting this into the Bernoulli expression above and re-arranging gives

$$V_e = \left[\frac{p_T - p_a}{0.5\rho_\infty}\right]^{0.5}$$

and substituting for the total pressure gives

$$V_e = \left[\frac{(q_\infty + p_\infty) - p_a}{0.5\rho_\infty}\right]^{0.5}$$

Therefore, the spanwise attachment-line edge velocity, V_e, can be calculated by measuring the static pressure on the attachment-line, the wind tunnel static pressure, ambient conditions and the dynamic pressure.

The uncertainty on the calculation of $\overline{R}$ is a function of the uncertainties on η, ν, the freestream dynamic pressure, the freestream static pressure, the density, the attachment-line static pressure and the kinematic viscosity. Combining these (see the Sections above for the individual values) the uncertainty on the calculation of $\overline{R}$ is approximately ±3.5%.

4.3.5 Transpiration Coefficien t

From Section 3.7, the definition of the suction coefficient, C_q, was

$$C_q \equiv \frac{\dot{M}}{\rho_\infty S Q_\infty}$$

with the surface area, S, calculated from

$$S = Lr\theta$$

where L is the length of the suction chamber, r is the radius of the cylinder and θ is the segment of the surface arc, in radians. For the attachment-line work chamber 14 was used, but for the crossflow work chambers 1 to 8 were used to provide approximately uniform distributed suction. In this case the average suction coefficient was calculated such that

$$C_q \equiv \frac{\Sigma \dot{M}}{\rho_\infty (\Sigma S) Q_\infty}$$

Uniform distributed suction is not possible in practice because the pressure in the plenum chamber is affected by the external pressure gradient caused by the external flow field. To alleviate this, the suction surface was designed to have a large pressure drop across the surface[5]. This insulates the internal plenum pressure distribution from the external flow field and helps reduce the effects of varying external velocity. In addition, splitting the suction surface into discrete chambers reduces this effect, since the velocity change across each chamber is smaller than that across a single plenum. However, this introduces regions of zero porosity since the walls of the plenum chambers have a finite thickness, so the theoretically continuous suction surface actually consists of regions of porosity separated by thin non-porous regions. In practice, these non-porous regions are neglected, as are the chordwise variations in suction rate across each chamber.

Figure 6 shows that each plenum chamber had two outlets to the suction system. Having more than one suction connection reduces the localised effects around the suction pipe. One of the main reasons for using plenum chambers is to give nominally uniform suction rates across the surface. There is a possibility that the flow field within the plenum chamber may cause a pressure gradient along the chamber. This was monitored using the three static pressure tappings in each plenum chamber. In all cases, the static pressure variation along the plenum chambers was negligible.

Suction and blowing rates were measured using rotameter flow meters connected between the model and the suction system. Different sized flow meters were used depending on the experiment, with the indicated volumetric flow rate ranges varying from 200-4000 litres/minute, in graduations of 400 litres/minute, to 0-5 litres/minute, in graduations of 0.5 litres/minute. The rotameters had been calibrated by the manufacturer at ISA sea level conditions so the values read during the experiments had to be adjusted to account for the actual static pressure at the rotameter outlet and actual ambient temperature. The method given by the manufacturer was

$$\text{actual volumetric flowrate} = \sqrt{\left(\frac{p_{calib}}{p_{outlet}} * \frac{T}{T_{calib}}\right)} * \text{measured volumetric flowrate}$$

where the calibration outlet static pressure, p_{calib}, was 1013mbar and the calibration temperature, T_{calib}, was 288K. The maximum and minimum ambient temperatures during the tests were 35°C and 18°C, although most of the tests were conducted at temperatures between 20°C and 30°C. The maximum and minimum outlet static pressures during the tests were 990mbar and 940mbar, distributed fairly evenly across the range. These gave average adjustments of between 4 and 6%.

The temperature was measured using a thermocouple built into the wind tunnel. The reading could be taken electronically or could be read from the digital display in the control room. Accuracy was better than ±0.1°, which gave an uncertainty on the transpiration coefficient of less than ±0.02%. The static pressure was taken from a Setra 239 pressure transducer which was read electronically. The manufacturer's quoted accuracy was ±0.5% at full scale, giving an uncertainty of approximately ±0.25% on the transpiration coefficient.

The accuracy of the flowmeters, according to the manufacturer, was ±1% at the maximum scale reading (ie ±40 litres/min for the rotameters with a range of 200-4000 litres/min) and the maximum scale reading was the worst case. However, no details were available about how the accuracy varied at readings below full scale so it has been assumed, for simplicity, that the worst case applied throughout the scale range.

The flowmeters were read manually, which introduced a measure of uncertainty. The graduations on each rotameter were in steps of 10% of full scale reading (eg for a full scale reading of 4000l/min the graduations were each 400l/min). The value could comfortably be read to within a quarter of a graduation (ie within 2.5% of full scale deflection) when the float was between graduations.

So how does this affect the accuracy/uncertainty of the transpiration coefficients? As an example, take a test at 25°C and 980mbar, giving a freestream fluid density of 1.144kgm^{-3}. If chamber 14 was used the suction surface area would be 0.158 m^2. Using the 200-4000 litres/min flowmeters, if the freestream velocity was 45 ms^{-1} and the suction required gave a value, by manual reading, of 2000 litres/min, the corrected flowmeter reading would give a mass flow of approximately 2370 kg s^{-1}. The nominal suction coefficient would be –0.00485. The combined uncertainty would be 40 litres/min (manufacturer's quoted inaccuracy) and 100 litres/min from the manual reading, giving ±140 litre/min. This gives an uncertainty on the suction coefficient of ±7%. From this, it can be seen that the magnitude of the uncertainty is directly dependent on the maximum scale reading of the flow meters used. However, because the uncertainties can be expressed as factors of the full scale value, the percentage uncertainty does not vary for different flowmeters. What does affect the uncertainty is what percentage of the full scale value the actual value is. The example above uses a reading that is 50% of the full scale. Table 1, below, tabulates the effect of different percentages of the full scale value (column 2). It is clear from this that test conditions with low scale readings introduce large uncertainties into the results.

Percentage of Full Scale (%)	Percentage Uncertainty For Experiments (%)	Percentage Uncertainty With No Reader Error (%)	Percentage Uncertainty With Perfect Rotameter Accuracy (%)
10	35	10	25
20	17.5	5	12.5
30	11.7	3.3	8.3
40	8.8	2.5	6.3
50	7	2	5
60	5.8	1.7	4.2
70	5	1.4	3.6
80	4.4	1.3	3.1
90	3.9	1.1	2.8
100	3.5	1	2.5

Table 1. The Variation of Suction Coefficient Percentage Uncertainty With Percentage of Full Scale Reading

Columns 3 and 4 of Table 1 break this overall uncertainty into the effects of the quoted manufacturer's inaccuracy and the manual reading error. Column 3 assumes there was no manual reader error, so the uncertainty only comes from the 1% inaccuracy at full scale. Column 4 assumes that the rotameters are 100% accurate and the only uncertainty comes from the manual reading. The manual reading has the largest effect, as expected, but the rotameter inaccuracy alone can still give a 10% uncertainty in the transpiration coefficient at low scale readings. The rotameter inaccuracy could have been reduced to 0.1% at the full scale reading by using considerably more expensive flowmeters. This could have reduced the uncertainty at 10% scale reading to 1% but would have reduced the number of flowmeters available because of the penalising effect on the budget. The strategy actually used was to limit the test conditions to cases where the scale reading was at least 50% of full scale. This reduced the uncertainty due to rotameter inaccuracy to between 1 and 2% at each test point. Several methods were considered to reduce the manual reading uncertainty including, very briefly, an expensive optical reader. In practice, it was simple to set the flow meter rate first and then adjust the wind tunnel speed until transition occurred. This meant that there were no readings between graduations and the float could be lined up with the graduation line accurately, effectively reducing the manual reading error to less than 1% of the full scale value.

For the above reasons, care was taken to use the most appropriate flow meter range and to use volumetric flow rates of at least 50% full scale deflection. This kept the suction coefficient uncertainty to less than ±4%.

4.4 Potential Flow

The potential flow around an infinite swept cylinder gives a good approximation to the actual flow around an infinite swept wing. It has been used previously to develop a model for the turbulent boundary layer development[63] and to confirm the validity of experimental results[4, 5]. It will be used in the current work as a sanity check on the chordwise velocity distributions measured during the experiments and as a measure for the success of attaining infinite swept conditions. The following discussion is available

in other publications [4, 5, 65] but is included here for completeness. The derivation uses polar co-ordinates since these are more suitable for a general discussion on cylinders than Cartesian co-ordinates. However, the co-ordinate system used for the experiments was Cartesian so the results are converted from polar to Cartesian co-ordinates at the end.

The inviscid, irrotational, incompressible flow around a two-dimensional non-lifting cylinder can be derived as a combination of a uniform flow and a doublet. The stream function for a uniform flow is

$$\psi = Q_\infty r \sin\theta$$

while the stream function for a doublet of strength κ is

$$\psi = -\frac{\kappa}{2\pi}\frac{\sin\theta}{r}$$

Combining these two forms a two-dimensional cylinder arranged perpendicular to the uniform flow, so

$$\psi = Q_\infty r \sin\theta - \frac{\kappa}{2\pi}\frac{\sin\theta}{r}$$

A diagram showing this combination is given in Figure 10. The radius of the cylinder, R, is defined as

$$R \equiv \frac{\kappa}{2\theta Q_\infty}$$

Substituting,

$$\psi = (Q_\infty r \sin\theta)\left(1 - \frac{R^2}{r^2}\right)$$

The radius of the cylinder, R, is actually a streamline corresponding to the surface of the cylinder and is the streamline when ψ=0. The velocity distribution on the surface of the cylinder can be found by differentiating the stream function, so that

$$Q_r = \frac{1}{r}\frac{\partial\psi}{\partial\theta} = \frac{1}{r}(Q_\infty r\cos\theta)\left(1 - \frac{R^2}{r^2}\right) = \left(1 - \frac{R^2}{r^2}\right)Q_\infty \cos\theta$$

$$Q_\theta = -\frac{\partial\psi}{\partial r} = -\left[(Q_\infty r\sin\theta)\frac{2R^2}{r^3} + \left(1 - \frac{R^2}{r^2}\right)(Q_\infty \sin\theta)\right] = \left(1 + \frac{R^2}{r^2}\right)Q_\infty \sin\theta$$

At the cylinder surface, r = R, so

$Q_r = 0$, which satisfies the solid surface condition, and

$$Q_\theta = -2Q_\infty \sin\theta$$

To allow comparisons with the current work this can be converted from polar co-ordinates to the Cartesian terminology used in Section 4.3,

$$\theta = \frac{x}{r}\ ,\ -Q_\theta = U_e\ ,\ \text{and}\ Q_\infty = U_\infty$$

Therefore,

$$U_e = 2U_\infty \sin\left(\frac{x}{r}\right)$$

Differentiating to get the chordwise velocity gradient at the attachment-line,

$$\left(\frac{dU_e}{dx}\right)_{x=0} = \frac{2U_\infty}{r}\cos\left(\frac{x}{r}\right)_{x=0} = \frac{2U_\infty}{r}$$

In the particular case of the cylinder used for the current experiments, r=C/4 so

$$U_e = 2U_\infty \sin\left(\frac{4x}{C}\right)$$

and

$$\left(\frac{dU_e}{dx}\right)_{x=0} = \frac{8U_\infty}{C}$$

4.4.1 Divergence Coefficient

In the course of their work Cumpsty and Head[63] attempted to derive a calculation method for the development of a turbulent boundary layer on an infinite swept wing. They defined a parameter, k, as an attempt to capture a general characteristic of infinite swept wing flows. They defined the velocity gradient of the potential flow perpendicular to the span (along the x co-ordinate, see Figure 2), k, such that

$$k \equiv \frac{U_e}{U_\infty x}$$

Re-arranging and differentiating with respect to the chordwise distance, x,

$$\frac{dU_e}{dx} = kU_\infty$$

Noting that

$$U_\infty = Q_\infty \cos\Lambda$$

then

$$\frac{dU_e}{dx} = k.[Q_\infty \cos\Lambda]$$

The potential flow solution, as derived in Section 4.4, calculates the chordwise velocity gradient from

$$\frac{dU_e}{dx} = \frac{2U_\infty}{r}$$

which explicitly includes a parameter for the model geometry. Note that both of these should be independent of the sweep angle.

The current work has avoided the use of empirical blockage corrections and the geometric sweep angle so a different form was used. This was done by non-dimensionalising the chordwise velocity using the empty tunnel freestream velocity, $\overline{Q}_\infty$. Using $\overline{Q}_\infty$ was entirely arbitrary but this was used because it could be determined simply and accurately from the empty tunnel calibration. An example of this method applied to the top pressure tappings is shown in Figure 11. Note that in the region near to the attachment-line the relationship between $U_e/\overline{Q}_\infty$ and x/C is linear, so the gradient in the linear region was determined using a simple least-squares method.

This gradient will be called the divergence coefficient, C_{div}, here and can be expressed as

$$C_{div} = \left[\frac{d\left(U_e/\overline{Q}_\infty\right)}{d\left(x/C\right)}\right]_{x=0} = \left[\frac{dU_e}{dx}\right]_{x=0}.\left[\frac{C}{\overline{Q}_\infty}\right]$$

Note that C_{div} is dependent on the empty tunnel freestream velocity, and the model geometry. Therefore, for a given model, the divergence coefficient is a characteristic of the freestream velocity alone. The chordwise velocity gradient is, therefore,

$$\left[\frac{dU_e}{dx}\right]_{x=0} = \left[\frac{d\left(U_e/\overline{Q}_\infty\right)}{d\left(x/C\right)}\right]_{x=0} \cdot \frac{\overline{Q}_\infty}{C} = C_{div} \cdot \left[\frac{\overline{Q}_\infty}{C}\right]$$

Note that C_{div} varies with sweep angle where Cumpsty and Head's parameter, k, should not.

A similar coefficient, C_{potdiv}, can be derived from the potential flow:

$$C_{potdiv} = \left(\frac{2U_\infty}{r}\right)\left(\frac{C}{Q_\infty}\right) = \cos\Lambda\frac{2C}{r}$$

The difference here is that the 'blocked' freestream velocity, Q_∞, has been used rather than the empty tunnel freestream velocity, $\overline{Q}_\infty$. This cancels with the chordwise velocity to leave the sweep angle.

A wide range of sweep angles was used during the experimental work and, at each sweep angle, the divergence coefficient was calculated. Coefficients from the top and bottom pressure tappings are compared with the potential flow solution in Figure 12. The potential flow results agree well with the divergence coefficients obtained from the bottom pressure tappings throughout the sweep angle range, and the divergence coefficients from the top tappings are significantly different from the potential flow values. Data for the bottom tappings are not available at sweep angles below 55° because at these low angles the model was swept through the wind tunnel floor so the bottom tappings were not in the working section. For these cases, given the good agreement between the experimental results and theory, the divergence coefficient derived from the potential flow was used.

4.5 Calculation of the Attachment-Line Position

On an unswept wing the attachment-line is the locus of stagnation along the leading edge and can be defined such that

$$V_e = U_e = 0$$

When the wing is swept a spanwise flow is created so V_e is no longer zero, but the chordwise flow component is still zero. Therefore, the attachment-line can be defined as the locus of points near the leading edge where the chordwise velocity is zero. This fact can be used with the chordwise velocity distribution discussed in Section 4.3.3. After the model has been aligned (see Section 4.1.4) the chordwise velocity distribution can

be non-dimensionalised using the freestream velocity and presented as in Figure 11. This shows ($U_e/\overline{Q}_\infty$) plotted against (x/C), so where ($U_e/\overline{Q}_\infty$)=0 is the x/C position of the attachment-line. Because the region -0.15<x/C<+0.15 is linear, a least-squares trend can be fitted to the data which allows the calculation of the position of the attachment-line to be automated.

For each test point the seven static pressure tappings about the geometric centre-line of the model from the top and bottom sets of tappings were sampled (±0.152 x/C or ±35°). Considerable time and effort was spent aligning the model, so the differences between the geometric centre-line and the calculated attachment-line position were always less than ±0.007m (±0.0087 x/C or ±1.88°).

4.6 Data Acquisition And Manipulation

For each test point the wind tunnel working section static pressure, measured at the end of the contraction cone, the static pressure across the contraction cone (to calculate the dynamic pressure), the ambient atmospheric pressure and the working section temperature were recorded. Static pressure readings were taken, from each of the sets of tappings on the model, around the attachment-line so that the exact position of the attachment-line could be calculated for each test point. When measurements were taken on a porous surface the plenum chamber internal static pressures were also recorded. When transpiration was used the flowmeter readings was recorded, along with the static pressure at the flowmeter outlet. Zero readings (ie with no wind) were taken before and after each run to provide the transducer offset values. The static pressure ports were connected to Setra differential pressure transducers, with ranges ±0.1psi, ±0.5psi, or ±1psi depending on the configuration. The static ports were connected to the transducers via 48 port Scanivalves, one for each set of static tappings and one pressure transducer for each Scanivalve. The Scanivalves were controlled electronically by a custom-written data acquisition program. Each transducer was calibrated before each wind tunnel session using a Druck calibrating rig.

All readings apart from the flowmeter flow rates were taken digitally using a custom written Microsoft Windows data acquisition software program. This program controlled the Scanivalves connected to the static pressure tappings and controlled a CIL analogue-to-digital converter. The outputs from the transducers were connected to the CIL, along with tunnel dynamic pressure and tunnel temperature outputs. The pressure data from the Setra transducers, the tunnel dynamic pressure, and the tunnel temperature were then read from the CIL, sampled at 200Hz, with the average of 50 samples recorded for each data point. The program displayed the data graphically, in real time, so the output from the pressure transducers could be monitored and any problems spotted and also saved the data to disk.

All data manipulation was done in Microsoft Excel, with the raw experimental data (voltages, pressures, etc) being entered into Excel worksheets. Any calibrations (eg pressure transducers) were applied and the relevant experimental parameters (eg $\overline{R}$, Re_x) were calculated. These were then plotted using Excel's built-in graphic functions.

This allowed a 'template' Excel workbook to be created that could be checked once and then used for all experiments.

4.7 Hot-Wire Anemometry

The state of the boundary layer was monitored by constant temperature hot-wire anemometry. Using this system a thin filament is connected in a Wheatstone Bridge arrangement and the system sets the current in the circuit so that the filament maintains a constant temperature. As air moves past the filament it cools it and the voltage increases to maintain the temperature of the filament. The voltage required can then be monitored and if required the hot-wire can be calibrated so that the flow speed can be calculated from the voltage. This method was used because the hot-wire element was sufficiently small that it could be set very close to the model surface, which enabled thin, laminar boundary layers (where $\delta \approx 1$mm) to be monitored. Because of the shiny titanium leading edge on the model the hot-wire element could be set using the reflection as a reference, allowing hot-wire element to model separations of less than 1mm relatively easily (the method previously used by Danks[5]).

Two different hot-wire systems were used during this work, depending on equipment availability. The first was a Dantec Streamware system, an integrated hardware/software hot-wire anemometry system which could monitor the output from up to three hot-wires simultaneously. The hot-wire outputs could be displayed on a computer monitor or routed to an external oscilloscope. The output from each hot-wire could also be sampled independently and stored for further analysis. The other system was a pair of Dantec 55M modules. Each 55M module was a stand-alone hot-wire setup. The 55M was purely hardware and provided no calculation or sampling facilities. The hot-wire signal was provided as an AC voltage output which was then displayed on a separate oscilloscope. The 55M modules were easier to set up than the Streamware system and were, on average, more reliable because of problems with the Streamware software. However, sampling the output from the 55M units was more complex than sampling using the Streamware system, so all sampling was done via the Streamware system. The output from the hot-wire was sampled at 60kHz, which provided ample resolution over the range of interest, 0-30kHz. Power spectra were obtained by Fast Fourier Transform using the Matlab© software package.

Hot-wire anemometry is, by the nature of the technique used in this context, subjective. However, repeatable and reliable results can be obtained provided the user has experience of hot-wire systems, the technique being used and the flow regime being monitored. In a way, the user needs to be calibrated. Figure 13 shows the results from a series of seven attachment-line relaminarisation tests (for the same conditions) conducted by the author at the beginning of the test programme (see Section 7 for a description of the experimental arrangement. The tests were at a sweep angle of 60° with the hot wire at the downstream end of the suction surface, s_{TT}=900mm). It can be seen that, as the author's familiarity with the hot-wire technique increased (ie his ability to recognise the transition criterion improved), the suction required decreased until it reached a minimum. There is a certain amount of scatter due to the subjectivity of the technique, as mentioned above.

4.8 Transition Criterion

Hot-wire anemometry converts the fluid velocity to a voltage, and when this is displayed on an oscilloscope a time history of the fluid velocity at the hot-wire position can be seen. This is of limited value without a quantitative method for identifying key events in that time history. It must be a quantitative method because it will not only need to be repeatable for the individual doing the tests but also for others who wish to repeat the test or compare the results with tests of their own. Conditions such as 'fully laminar' or 'fully turbulent' are easy to define, for example as $\Gamma=0$ and $\Gamma=1$ respectively, but are difficult to repeat experimentally, as Poll found[4]. The transition criterion used here is defined in terms of the number of turbulent bursts over a set period of time. Specifying the number of bursts and the period of time is a good quantitative definition, and the only subjective part is what defines a turbulent burst. However, turbulent bursts are fairly easy to spot in the leading edge boundary layer with the main difficulty being in differentiating between turbulent bursts and large amplitude laminar disturbances. Examples of the hot-wire signals and power spectra for the stable laminar boundary layer are shown in Figures 14 and 15, the unstable laminar layer in Figures 16 and 17, the intermittent boundary layer in Figures 18 and 19 and for fully turbulent flow in Figures 20 and 21. It can be seen from these that the turbulent bursts are fairly obvious. In general, the amplitude of the laminar disturbance increased with chordwise position, so it was small on the attachment-line and largest at chordwise positions between 70° and 80° ($x/C>0.3$). Great care was taken when the laminar disturbance amplitude was large.

The onset of transition (ie from laminar to turbulent) and the end of relaminarisation (ie from turbulent to laminar) criteria have been chosen to be the same, so the boundary layer is in the same state. The transition criterion was chosen as, at constant working section dynamic pressure, between one and three turbulent bursts passing the hot-wire location every two seconds, for a period of not less than two minutes.

This criterion is applicable for all of the tests described in this work, except where specifically mentioned in individual sections.

5. Cross-Flow Transition

5.1 Introduction

If the attachment-line boundary layer is laminar, transition can be caused near the leading edge of a swept wing by the crossflow instability. This instability is caused by an inflection in the boundary layer velocity profile, see Figure 3 for a diagram of a crossflow velocity profile, and is amplified in the negative pressure gradient region near the wing leading edge. Provided the attachment-line remains laminar, crossflow instability is the primary transition mechanism on swept wings so it is of great practical importance to know the conditions that will cause transition. The work in this section examines three elements of crossflow transition: the transition that occurs without surface suction, including any effect due to the porous surface; the effect of surface suction on the crossflow instability; the effect of two-dimensional trip wires on crossflow transition. The object was to derive an empirical mathematical description of the conditions at the onset of transition due to crossflow.

5.2 Natural Transition

5.2.1 Introduction

The natural transition that occurs due to cross-flow instability on a non-porous surface will be studied and compared with Poll's[4] and Danks'[5] work, both as a bench-mark exercise and to confirm the validity of the experimental method. Natural transition on a porous surface without suction will then be examined, to determine the effect of porosity on the cross-flow instability.

5.2.2 Previous Work

Owen and Randall[14, 15] suggested a theoretical basis for the crossflow instability and compared this theory with wind tunnel experiments at RAE[18] and NPL[13]. Their theoretical work suggested that a Reynolds number for the study of cross-flow instability, χ, could be defined as

$$\chi \equiv \frac{\left|u_\beta\right|_{max}\,\delta}{\nu}$$

where $\left|u_\beta\right|_{max}$ is the magnitude of the maximum value of the cross-flow velocity and δ is the cross-flow velocity boundary-layer thickness. They also suggested that the onset of transition due to crossflow could be correlated by a constant value of χ of approximately 100. Results from flight tests by Allen and Burrows[21] and Burrows[22] were in qualitative agreement with Owen and Randall but suggested that the critical crossflow Reynolds number would be higher than 100. Boltz *et al*[23] conducted a wind tunnel campaign to assess the effects of yaw on transition on a swept wing. Unfortunately, the approximate Polhausen method used for the boundary layer computations cast doubt on the quantitative results, but the qualitative results were in

agreement with Owen and Randall. As with the flight trials data, though, the wind tunnel results suggested the critical crossflow Reynolds number would be larger than 100, possibly as large as 260.

Poll[66] re-examined the above work in the light of his results concerning attachment-line contamination[67] and concluded that the majority, if not all, of the experimental data had reflected attachment-line contamination rather than crossflow. He redefined the cross-flow Reynolds number as

$$\chi = -\frac{\bar{v}_{max}\,\Delta}{\nu}$$

where $\bar{v}_{max}$ is the maximum value of the cross-flow velocity and Δ is the height above the surface at which the cross-flow velocity drops to 1% of its maximum value. This was easy to calculate using computational boundary layer methods and provided an unambiguous method for calculating χ. He showed that, for the onset of transition, the constant χ hypothesis was incorrect and that χ varied with chordwise position, x/C, as well.

The crossflow region is often characterised by stationary corotating vortices, commonly known as crossflow vortices, as well as travelling vortices. The stationary vortices are responsible for the characteristic striation patterns noted by Gray[11] and Anscombe and Illingworth[18] amongst others when using surface sublimation techniques. Müller and Bippes[68], studying the effect of freestream turbulence levels on crossflow transition, found that although in certain cases the stationary vortices amplified to large amplitudes this did not necessarily cause premature transition and they concluded that it was the travelling disturbances that caused transition. Sometimes a secondary instability with a frequency an order of magnitude higher than that of the stationary vortices is present, and several groups have observed this during experiments, including Poll[66] and Kohama *et al*[38]. Based on their results, Kohama *et al* suggested that the stationary vortices and the secondary high frequency instability dominated the transition process.

Assuming incompressible flow and an adiabatic surface, the flow in the vicinity of a swept attachment-line can be determined from five parameters: the chordwise velocity, U_e, the spanwise velocity, V_e, the chordwise position x, the freestream density, ρ, and the freestream viscosity ν. Dimensional analysis can be used to predict how these parameters can be combined to form characteristic non-dimensional groups, based on the number of physical variable types in the parameters. For the leading edge case, the variable types are length, time and mass and, according to Buckingham's π theorem, five physical variables described by three fundamental dimensions can be re-expressed as two non-dimensional π products, and it is convenient to choose these as the leading edge Reynolds number, $\overline{R}$, and the chordwise Reynolds number, Re_x. Danks[5], using Poll's data[4] along with his own, showed that these two parameters collapsed the data for the onset of transition onto a single curve, and the data for the end of transition onto another curve, shown in Figure 22. This was an important result because Poll and Danks' experimental arrangements differed on several counts. Although both used constant-radius swept cylinders, they were of different diameters, with Poll's 0.23m and

Danks' 0.406m. The wind tunnels used were also different, with Poll using the Cranfield 8'x6' and Danks the Manchester 9'x7'. Several measurement techniques were used as well; Poll used hot-wire anemometry and Danks used surface pitot probes and hot-wire anemometry. Given the quality of the data collapse, it can be seen that the conditions for transition near the leading edge can be specified by $\overline{R}$ and Re_x and it is not necessary to calculate the cross-flow Reynolds number,χ. This simplifies the experimental arrangement since boundary layer profiles no longer need to be measured and boundary layer computations are also not needed.

5.2.3 Experimental Method

The model was mounted in the wind tunnel, swept back, as shown in Figure 7. For these tests the top half of the model, between the top and middle static pressure tappings, was used and the distribution of porous and non-porous regions on this part of the model is shown in Figure 5. Measurements were taken with sweep angles ranging from 40° to 68° and chordwise positions between x/C=0.142 (40°) and x/C=0.231 (65°) were used at each sweep angle. The state of the boundary layer was monitored by a hot-wire anemometer placed 1300mm from the upstream tip of the model which, on the porous side of the model, was equivalent to the downstream end of the porosity.

For the experiments on the porous surface, the suction system was shut off and sealed to minimise the passive blowing effect. Passive blowing with the suction system open to the atmosphere would occur because of the pressure difference between the inside of the plenum chamber, at nominally atmospheric pressure, and the external surface of the plenum chamber, with the pressure imposed by the velocity distribution. However, this does not remove the possibility of passive blowing because there will still be a pressure gradient in the chordwise direction across the external surface of each plenum chamber and if the external pressure is lower than the internal pressure then blowing will occur (see Section 6 for a more detailed discussion of this). The magnitude of this gradient can be seen in Figure 8, noting that each plenum chamber covers 10° of the surface, which is equivalent to three data points on the graph. There were two factors working to reduce the passive blowing effect: the plenum chambers were not very large in the chordwise direction, so the external pressure gradient across a plenum chamber was not that large. Additionally, and most importantly, the porous surface was designed to have a large pressure drop across it. This was expressly for the purpose of insulating the plenum chamber internal pressure from the external pressure gradient and preventing the formation of circulating flows within the plenum chambers. Additionally, as described in Section 6, the amount of blowing required to destabilise a boundary layer is small. Given the good consistency of the data, as will be described below, it seems unlikely that passive blowing was the dominant source of instability. For each test point, the plenum chamber pressures were also allowed to stabilise before the transition criterion was applied so that transient effects did not affect the results. However, it is possible that blowing did occur.

It should be noted that the porous surface began at x/C=0.044 (10°) and not at x/C=0 (0°). This was unavoidable because the porous surface had been fabricated to Danks[5] specification so that the attachment-line and cross-flow transition mechanisms could be studied entirely separately. However, if future experiments provide results with suction

starting at the attachment-line it should be easy to quantify the effectiveness of the additional suction in the first 10°.

At each test condition the freestream velocity was increased until the onset of transition occurred and the conditions were noted. The first indication of cross-flow instability was usually, although not always, a harmonic laminar disturbance visually similar to a T-S wave when viewed on an oscilloscope. In general, the amplitude of the laminar disturbance increased with increasing chordwise position and at times was of the same order of magnitude as the turbulent bursts. In these cases great care was taken, but at all times it was possible to differentiate between the laminar disturbance and a turbulent burst.

5.2.4 Results and Discussion

5.2.4.1 Non-Porous Surface

The results for transition on the non-porous surface are shown in Figure 23, with the data from Poll[62] and Danks[5] for comparison. For clarity, the data from Poll and Danks has been reduced to a best-fit line with error bars to show the scatter of their data. The agreement is excellent, and this justifies the use of $\overline{R}$ and Re_x to describe cross-flow transition in the region near the attachment-line. At high $\overline{R}$, attachment-line contamination becomes the dominant transition mechanism and this can be seen on Figure 23 as an upper limit on $\overline{R}$. The difference between the current work and that of Poll was the value of $\overline{R}$ at which this occurred. From Poll, this was approximately 700, compared with 750 here. This was due to the smaller s/η values during the current tests and the result is consistent with Poll's work on transition at the attachment-line in the absence of a trip wire[62]. The s/η values for attachment-line contamination in the current tests were approximately 3000, with an $\overline{R}$ value of just under 750. Poll's data for natural attachment-line transition has been included as Figure 24 and referring to this transition on the attachment-line is predicted at an $\overline{R}$ of approximately 740.

These results remove any remaining doubts about the use of $\overline{R}$ and Re_x. Although Poll and Danks used different models in different wind tunnels, there was a remote possibility that the change of wind tunnel environment had some-how offset the change in model leading edge diameter. These tests have used the model Danks used in the wind tunnel Poll used. Historical data[69] shows that the turbulence levels and wind tunnel calibration of the Cranfield 8'x6' wind tunnel have not changed appreciably since Poll conducted his tests, so the current results remove any doubt about the applicability of the $\overline{R}$ and Re_x combination.

5.2.4.2 Porous Surface

The effect of a porous surface was examined by comparing results on the two sides of the model at the same chordwise positions relative to the attachment-line. The results from the porous surface are shown in Figure 25 along with the results for the non-porous surface. It is immediately apparent that the porous surface causes a reduction in the Reynolds number required for the onset of transition. Also shown on Figure 25 are

results from Poll, Danks and Davies[52] for the natural transition on a porous surface. These data were measured using the same model as was used for the current tests and although they show a reduction due to the porous surface it is much smaller than was found here. The reason for the difference is unknown, although the tone of the Poll, Danks and Davies paper seems to suggest that the authors were surprised that the effect was so small. However, the general result of a reduction in transition Reynolds number with a porous surface agrees with a qualitative result from Bippes and Lerche[55]. They found that the effect of a porous surface, on a swept flat-plate model, was to increase the amplitude of both travelling and stationary disturbances compared with equivalent conditions on a polished, non-porous surface.

It would be useful to examine the magnitude of the porous surface effect but the scatter of the data could hide any trends. Therefore, curve fits were applied to the data from the porous and non-porous surfaces and it was found that both sets of data could be represented by power laws. These are given below and are shown in Figure 26, together with the experimental data for comparison.

Onset of transition on a non-porous surface: $\overline{R} = 29400\,Re_x^{-0.31}$

Onset of transition on a porous surface: $\overline{R} = 73000\,Re_x^{-0.39}$

for $100x10^3<Re_x<1000x10^3$.

The data from the non-porous surface have a scatter of less than ±5% on $\overline{R}$, so the power law is a good fit for the data. On the porous surface, the data has a significant amount of scatter in places, as much as ±10% on $\overline{R}$, but in general the scatter is less than ±5% on $\overline{R}$ so the power law can be considered a satisfactory approximation.

With these power law approximations the magnitude of the porous surface effect can easily be calculated and Figure 27 shows the effect of the porous surface on $\overline{R}$, plotted against Re_x. This can be expressed as a percentage of the $\overline{R}$ for transition onset on a non-porous surface, ie

$$\% \text{ reduction} = \left(\frac{\overline{R}_{porous} - \overline{R}_{non-porous}}{\overline{R}_{non-porous}} \right) x100$$

and this is shown in Figure 28. From Figure 27, the magnitude of the $\overline{R}$ penalty increases rapidly between Re_x=200 000 and Re_x=450 000 from –43 to -65. At larger Re_x the $\overline{R}$ drop does not increase as quickly, from –65 to –72 between Re_x=450 000 and Re_x=950 000. On the other hand, the percentage reduction increases smoothly with Re_x, from 7% at an Re_x of $2x10^5$ to 17% when Re_x reaches $9x10^5$. The overall result, though, is that the $\overline{R}$ penalty of the porous surface increases as Re_x increases.

There are a number of possible causes for this. The possibility of small amounts of blowing was discussed earlier in this chapter, and it may be that as Re_x increases the boundary layer becomes more sensitive to the effects of blowing. However, Chapter 6

discusses the effect of blowing on the laminar attachment-line boundary layer and reducing the $\overline{R}$ increases the boundary layer stability, so it is probably not blowing that is driving this effect. Another possibility is that because the porous surface is not as smooth as the non-porous surface it is acting as distributed roughness elements. For this to be the cause the $\overline{R}$ would need to reduce as the chordwise measuring position increased, since the greater chordwise distance would affect transition more. At a particular sweep angle this is what happens, but this is not enough to explain the increase in the $\overline{R}$ penalty at large Re_x. The same chordwise positions have been used at different sweep angles, so the physical length of the roughness will be approximately the same for both cases but the $\overline{R}$ penalty will be larger for the small sweep angle case. This is because, assuming the dynamic viscosity was the same for both, although the physical length of the roughness is the same in both cases the chordwise velocity, U_e, at that chordwise location is smaller for the larger sweep angle case. To take a more extreme case, we can compare data taken at 70.8° and 40.1° sweep. The 70.8° data used an 80° chordwise position, while the 40.1° sweep data used 55° and 60° chordwise positions. The physical length of the roughness is greatest for the 70.8° sweep case, but the $\overline{R}$ penalty is almost 50% larger for the 40.1° sweep data. From this, it would seem that the physical length of the roughness can not fully explain why the $\overline{R}$ penalty increases as Re_x increases. However, work at the Arizona State University (ASU) by Saric and his team[40, 44, 42] has shown that distributed roughness elements with heights of the order of microns do affect crossflow transition so it is probable that the surface roughness is playing a part. Further experiments with different combinations of hole size and drilling pattern are really required to clearly identify the part the roughness plays, but in the meantime it should be stressed that the quantitative results obtained here are only applicable to this particular model with this particular hole size and drilling pattern.

An alternative may be that the fundamental cause of the transition process is changing and Re_x is simply a useful measure for this change. There is still some doubt whether it is the stationary vortices or travelling disturbances that actually cause transition, and the presence of the secondary high frequency disturbance further muddies the waters. Bippes and Lerche[55] and Malik *et al*[41] have suggested that the actual transition mechanism depends on the relative amplitudes of the stationary and travelling modes, showing that unless the amplitudes of the stationary vortices are the largest at the start of the transition process then it will be the travelling modes that dominate due to their greater amplification rates. It may be that the dominant cause of transition changes from stationary to travelling, or vice versa, across the Re_x range and the effect of the porosity roughness changes as well. It would be useful to conduct experiments on the swept cylinder model used here to look at which disturbance mode dominates. The ASU experiments have used a swept flat plate with a pressure gradient imposed by a displacement body above the model. This pressure gradient has been chosen, in general, to create a boundary layer unstable to crossflow but subcritical to the T-S instability, allowing crossflow to be studied in isolation. Additionally, transition did not occur on the models as they were concentrating on amplification characteristics. The leading edge of a swept cylinder can be a melting pot of different instabilities, with T-S and attachment-line contamination playing their part alongside the crossflow.

5.2.5 Conclusions

To implement Hybrid Laminar Flow Control (HLFC) a surface through which air can be drawn is required. This can be slotted, drilled, or naturally porous. Using modern manufacturing methods surfaces with small waviness and roughness can be produced relatively easily and the laser or electron-beam drilling processes can produce porous surfaces with very small holes, distributed as required. Assuming that a laser drilled surface is used, it appears that surface porosity causes the onset of transition to occur at a lower value of the characteristic Reynolds number, Re_x, than would be the case for a smooth, non-porous, surface. Additionally, the magnitude of the penalty seems to increase as Re_x increases.

The reason for this has not been found, but it is expected that the porosity, acting as distributed roughness, has a part to play. It has been suggested that different amplitudes and amplification rates for the stationary and travelling crossflow disturbances may be of fundamental importance and that experiments to identify which is actually responsible for transition on a swept cylinder are performed. Because of the uncertainty of the physical source of the Reynolds number penalty it should be stressed that the quantitative results obtained are only applicable to the model used with the particular combination of hole size and drilling pattern.

How might this affect an aircraft during cruise segment of the flight? That depends on the size of the aircraft. If the aircraft is small enough so that attachment-line transition does not occur then the dominant transition mechanism will be crossflow. This assumes that attachment-line contamination has been controlled using a Gaster bump or similar method. A porous surface suction system could then be employed to control the crossflow and this surface, if it was identical to the one used in these experiments, would incur a Reynolds number penalty. This penalty would then need to be offset by a finite suction amount just to regain the performance without the porous surface. However, the system would be employed to control the crossflow and generate some quantified benefit, such as DOC reduction or payload increase. A cost benefit analysis would then be needed to identify whether the suction needed to offset the porosity penalty affected the basic profitability of the system.

For a large aircraft, the situation is entirely different. From Poll[4], for a Boeing 727 in the cruise, the $\overline{R}$ is approximately 560. From Poll's work on attachment-line transition with trip wires[70], this would make the attachment-line sensitive to disturbances from small disturbance sources, so the attachment-line would probably be turbulent. This will cause transition to occur very close to the leading edge, typically 1% chord or less. In this case, the porosity penalty is irrelevant, since transition would occur at the same place with or without the porous surface.

Assuming that the attachment-line is laminar, the next question is: what is the effect of suction and is this porous surface penalty important? The next Section will answer this question.

5.3 The Control of Cross-Flow Instability By Surface Suction

5.3.1 Introduction

Laminar flow control and hybrid laminar flow control systems are designed to delay the onset of transition, often using suction near the leading edge of the wing. This Section describes a quantitative study on the capability of uniform distributed suction, applied in the region just off the attachment-line, to suppress the crossflow instability and delay the onset of transition. The results will be compared with the natural transition characteristics, on both a porous and non-porous surface, and the practical cost of the porosity penalty identified in Section 5.2.4.2 will be assessed. Also, an empirical mathematical description of the conditions at the onset of transition due to crossflow while using suction will be derived.

5.3.2 Previous Work

Little experimental work has been done on the effect of suction on the cross-flow instability. Bippes and Lerche[55] investigated the effect of suction on travelling and stationary waves individually. They found that suction damped travelling waves but had little effect on stationary waves, although no details of the suction amount or distribution were given. Danks[5] studied the effect of the suction distribution qualitatively because he did not have enough flowmeters to perform a quantitative study. Although no parametric trends were identified, he found that suction applied just upstream of the transition location for non-transpired flow was more effective than that applied at larger chordwise positions and for transition at the minimum pressure location (x/C=0.349), Danks found that the most efficient average suction coefficient was approximately -0.00034. Figure 29 shows an example of one of Danks' suction distributions.

5.3.3 Experimental Method

The arrangement of the model in the wind tunnel is shown in Figure 7. As with the natural transition experiments described in Section 5.2, the top half of the model was used. One side of the model had a porous surface that was used to provide suction (see Figure 5 for the distribution of porosity on the model leading edge). The porous surface was supplied by eight plenum chambers, extending from 10° to 90° (x/C=0.044 to x/C=0.393), with each plenum chamber supplying a 10° segment of the surface, as shown in Figure 6. The leading edge was originally designed and manufactured for Danks' PhD work[5] and at that time it was decided that the top half of the model should only have porosity off the attachment-line, so that attachment-line transition and cross-flow instability could be studied entirely separately. Therefore, porosity was not available around the attachment-line (0° to 10°). With this arrangement the flow around the chord would not be affected by any roughness effects of porosity on the attachment-line or by any damping effect caused by suction at the attachment-line. Therefore, conditions are probably not of a typical HLFC wing in service, where attachment-line suction would probably be used to control contamination from the turbulent fuselage boundary layer and/or transition due to roughness effects (eg inset impact, steps and gaps, waviness, etc.) or the amplification of freestream disturbances. However, uniform,

distributed suction is a very useful benchmark, with the reduced number of variables allowing a thorough investigation.

Suction was applied by connecting the plenum chambers, via a set of rotameter flowmeters and valves, to a pair of large capacity evacuation tanks, as described in Section 4.1. The size of the tanks, combined with evacuation pumps which were run during the experiments, meant that the overall suction pressure (the pressure difference between the vacuum tanks and the plenum chambers) during any test was essentially constant throughout that test. The flowmeters measured the volumetric flow-rate and were calibrated using the flowmeter outlet static pressure. Each flowmeter was equipped with a valve, so the volumetric flow-rate through each plenum chamber could be set accurately. In addition, each plenum chamber had three static pressure ports, distributed in the spanwise direction, so the internal plenum static pressure and pressure distribution could be monitored. The plenum static pressure could not be used to calculate the mass flow-rate accurately, for reasons described by Danks[5], but it could be used to give an approximate value for the flow-rate which could be checked against the value calculated from the flowmeter. This was a good method for spotting, and checking for, leaks in the suction system. Additionally, cling film was used to check for leaks whenever the suction system had been disturbed (see Section 4.1.3). The plenum static pressures were also used to check the internal static pressure distribution of each chamber to ensure that a constant mass flow rate was obtained along the spanwise length.

Sweep angles ranging from 33° to 70° were used during the tests, and at each sweep angle chordwise positions from 0.153 x/C (35°) to 0.349 x/C (80°) were used depending on conditions. For example, with large sweep angles the chordwise velocity was small so large chordwise positions were needed and the potential test conditions were limited by the maximum chordwise position available and the wind tunnel maximum speed. Conversely, at small sweep angles the chordwise velocities were larger so smaller chordwise positions were needed and the test conditions were limited by the minimum steady wind tunnel speed. The state of the boundary layer was monitored using a constant temperature hot-wire anemometer placed 1300mm from the upstream tip of the model, the position corresponding to the maximum spanwise length of the porous surface. The hot-wire filament was set as close to the surface of the model as possible, always less than 1mm away, using the reflections from the shiny titanium surface (Section 4.7). Another constant temperature hot-wire was used to monitor the attachment-line to make sure that it remained laminar at all times.

At each test point, the suction rate was set and then the freestream dynamic pressure was increased until the onset of transition. The static pressures within the plenum chambers were allowed to stabilise before the transition criterion was applied (Section 4.8).

5.3.4 Results and Discussion

The results are plotted in Figure 30 along with data for the onset of transition on a non-porous surface from Danks[5]. In order to produce readily interpretable information, the raw data were interpolated to give results at specific suction coefficient values. The data

for zero suction (C_q=0) were discussed previously in Section 5.2.4.2. The dimensional data underlying this Figure are given in Appendix E to allow for further analysis (eg for comparison with computation).

As expected, suction can be used to control the onset of transition due to cross-flow instability. The data form a series of 'stacked' curves of similar shape and the results for each suction coefficient can be described by a simple power law, as with the natural transition results discussed previously. Note that the scatter of the data increases as the suction coefficient increases, so it was decided to fit power laws to the data for C_q=0, -0.00006, and -0.00012 first because the scatter was smallest for these. These power laws would then be used to develop an empirical model for the conditions at the onset of transition and this model would be checked by extrapolating to cover the higher suction coefficient data. The scatter also increases as Re_x increases and $\overline{R}$ decreases. It is important to note that the curves are not parallel. As Re_x increases, at constant Re_x a specific increase in suction coefficient produces a smaller increase in the $\overline{R}$ at the onset of transition. In other words, the constant C_q curves are closer to each other at large Re_x.

The power law used for the natural transition on the porous surface had the form

$$\overline{R} = A\,Re_x^{\,n}$$

where **A** and **n** were constants. This has been changed to

$$\overline{R} = A\,Re_x^{\,n} - \left(BC_q\,Re_x\right)$$

where **B** is another constant. In this way increasing Re_x leads to a reduction of $\overline{R}$ for transition onset. For simplicity, and entirely arbitrarily, the constant A was set to 73 000, the same value as for the natural transition on the porous surface (ie C_q=0).

Empirical curve fits were then found for C_q's of-0.00006, -0.00012, -0.00018, since these data sets had the least scatter. These are shown in Figure 31, together with the experimental data and the agreement is good, although the scatter for C_q=-0.00018 at large Re_x is substantial. The variation of **n** and **B** with suction coefficient was then examined. Both varied linearly with C_q (to a good approximation), as shown in Figures 32 and 33 respectively. From these, a relation can be determined which describes the variation of $\overline{R}$ and Re_x with C_q, ie:

$$\overline{R} = 73000\,Re_x^{\,-(95C_q+0.39)} + \left[0.14\,Re_x\,C_q\right]$$

for $200\times10^3 < Re_x < 1000\times10^3$ and $-0.00018 < C_q < 0$

Curve fits were then generated for C_q=-0.00024, C_q=-0.0003 and C_q=-0.00036, the datasets which were not used to develop the relation. A comparison between these experimental data and the approximations is shown in Figure 34. At Re_x below 400×10^3 the approximations give good agreement with the experimental data, with average scatter of less than ±3%. However, at Re_x larger than this the agreement is poor with

scatter as large as ±10% on $\overline{R}$. Part of the difficulty lies in the lack of data at Re_x values greater than $400x10^3$, making it difficult to derive curve fits, but the main problem is probably the low $\overline{R}$ values which means that uncertainties in the data can produce a large percentage scatter. Therefore, the empirical relation above should only be applied at Re_x values smaller than $400x10^3$ for suction coefficients larger than 0.00018. Therefore, the range of applicability of the empirical relation above is:

$200x10^3<Re_x<1000x10^3$ and $0<C_q<-0.00018$
$200x10^3<Re_x<400x10^3$ and $-0.00018<C_q<-0.00036$

Having quantified the effect of suction we can now answer the question asked at the end of Section 5.2: how much suction is required to offset the porous surface penalty? The answer is shown in Figure 35, as the suction coefficient required for transition to occur at the same $\overline{R}$ as on the non-porous surface, as a function of Re_x. The suction required is not large, although it is by no means negligible. For the worst case measured here, $Re_x=1000x10^3$, a C_q of –0.0002 is required, which at an Re_x of $500x10^3$ would increase the transition $\overline{R}$ by 150, using Figure 30. This is a significant $\overline{R}$ but the fallacy of this result must be stressed: for most large civil aircraft in service today and in the foreseeable future this is just not relevant. Transition will occur close to the leading edge because of attachment-line contamination so there will be no porosity penalty.

The form of the equation derived to model the effect of suction on crossflow raises an interesting point. Looking at the effect of suction at constant Re_x, increasing the suction coefficient increases the $\overline{R}$ at the onset of transition. However, the experimental data shows that this $\overline{R}$ increase for a given suction coefficient increase is not constant across the Re_x range – it decreases as Re_x increases, and this has been incorporated into the empirical relation by adding an extra term to the power law. But what could be causing this? A wide range of sweep angles and chordwise positions were used during the experiments but the data seems to have collapsed into lines of constant suction coefficient in good order, so it seems unlikely that the principles behind using $\overline{R}$ and Re_x to characterise crossflow transition should be inapplicable for suction. No trend is visible in the data relating to the experimental geometry, whether sweep angle or chordwise position. Neglecting the influence of the dynamic viscosity, large Re_x values can be obtained in two ways: the sweep can be moderate (55° for example), which reduces the chordwise velocity, so a large Re_x value requires the hot-wire to be positioned at large chordwise distances. The Re_x values available this way are limited by the maximum chordwise position available and by the natural transition conditions for the attachment-line. Alternatively, a low sweep angle can be used (30° for example) to give high chordwise velocities. The maximum Re_x value is once again limited by the maximum chordwise position available but is also limited by the minimum steady speed the wind tunnel can support. In general, though, large Re_x values require large chordwise positions which introduces the possibility that crossflow was not the only transition mechanism at work. As the chordwise position increases, the pressure distribution changes and conditions become more conducive to T-S waves. Now, T-S waves are not controllable by surface suction but are rather controlled by careful aerofoil design to reduce the magnitude of the adverse pressure gradient. If transition is occurring due to T-S waves it should be fairly simple to test: two different sweep angles

could be used to produce the same Re_x. Two different chordwise positions would be required to account for the change in chordwise velocity, so the experiment would be set up such that the smaller chordwise position was firmly inside the positive pressure gradient area of the model so that it could be assumed transition was not due to the T-S instability. The current data does not allow such a comparison to be made because the combination of model and wind tunnel geometries severely restricted the low sweep angles that could be used, which is why there is so little large Re_x data. Alternatively, a frequency analysis of the hot-wire output would show the T-S instability, but that isn't available either, so no conclusive statement can be made. It is recommended that additional low sweep angle testing is done and that the frequency spetra of the hot-wire outputs are analysed.

5.3.5 Conclusions

Experiments have been conducted to quantitatively assess the effectiveness of uniform distributed porous surface suction for controlling the crossflow instability and it has been found that small suction coefficients are capable of delaying the $\overline{R}$ for the onset of transition, in agreement with Danks[5] qualitative result.

It has been shown that the conditions for the onset of transition for a given suction coefficient can be represented by a simple power law, so an empirical power law expression has been developed relating $\overline{R}$, Re_x and C_q.

The results suggest that, at large Re_x values, suction was not as effective for delaying the onset of transition as at small Re_x values. It is possible that this was because transition was not purely due to crossflow in this region and that T-S instability was playing a part. T-S instability is not controllable with suction, so this would explain the results. It is recommended that further low sweep angle testing is done and that the frequency spectra of the hot-wire signal is analysed to see which transition mechanism is dominating.

5.4 The Effect of Two-Dimensional Disturbances on Cross-Flow Induced Transition

5.4.1 Introduction

Two-dimensional trip-wires are commonly used in boundary layer studies as a simple method of introducing 'controlled' disturbances. The nature of the attachment-line is such that discrete fluid elements do not travel a large spanwise distance along the span. Instead, fluid is constantly diverging onto the chord and being replaced by new fluid elements entrained from the freestream. Therefore, 'turbulence' must be propagated along the attachment-line by a mechanism that is independent of the fluid elements themselves and is probably a system of pressure waves. For disturbance sources (eg two-dimensional trips) on the attachment-line this means that, while the perturbation introduced may be convected indefinitely along the attachment-line, the fluid whose momentum has been modified will be swept away in the chordwise direction – forming a turbulent wedge attached to the source.

Downstream of the trip-wire is a separation bubble (provided transition is not occurring at the trip location). Disturbances are introduced into the laminar boundary layer in the form of two-dimensional wave perturbations. These are similar to T-S waves and interact with them to increase the amplification of the two-dimensional disturbances. This causes transition to occur earlier than would have been the case without the trip-wire. Three-dimensional trips cause transition by introducing vorticity into the laminar boundary layer, which is entirely different.

The experiments described here were a limited number of tests designed to find out whether the disturbances introduced into a swept leading-edge flow by a two-dimensional trip-wire would interact with the crossflow instability and, if they did, to quantify this effect. In the light of the natural transition results discussed in Section 5.2.4.2, the behaviour of the boundary layer was investigated on both the porous and non-porous surfaces, to see if the porous surface made a difference.

5.4.2 Previous Work

For two-dimensional boundary layers, the effect of two-dimensional trip-wires on flat-plate boundary layers has been investigated thoroughly, in particular Gibbings[71,72], and Hall[73]. For the more complex three-dimensional boundary layer case, the effect of two-dimensional trip-wires on a swept wing was first studied by Gaster[29]. Using a tapered swept cylinder model he investigated the decay of turbulence, on the attachment-line, behind several different diameter two-dimensional trip wires. He found that as the distance between the trip-wire and the measurement position increased the wind tunnel speed for the onset of transition also increased. Also, for each trip-wire, at large distances away from the trip-wire the wind tunnel speed approached an asymptotic value, and Gaster used this to develop a critical roughness criterion. Poll[4] conducted a thorough investigation into the effect of two-dimensional trip-wires on the attachment-line of an un-tapered swept cylinder. He investigated the effect of varying the trip-wire diameter and of varying the distance between the trip-wire and the measuring station on the attachment-line. Poll found that, for an attachment-line boundary layer without transpiration, the onset of transition could be described by three non-dimensional groups: $\overline{R}$, s/η and d/η, where s was the distance between the trip-wire and the measuring station and d was the trip-wire diameter. His results for the appearance of first bursts of turbulence are shown in Figure 36 for reference.

5.4.3 Experimental Method

The arrangement of the model in the wind tunnel is shown in Figure 7 and, as with the other crossflow experiments described above, the top half of the model was used. The sweep angle used in this case was 60.4°. The state of the boundary layer was monitored at various chordwise positions, from 40° to 80°, on both the non-porous and porous surfaces. One side of the model had a porous surface (see Figure 5 for the distribution of porosity on the model leading edge) while the other was a smooth, non-porous surface. The symmetry of the flow about the attachment-line allowed the boundary layer state on the porous and non-porous surfaces to be monitored simultaneously. Three hot-wires were used during these tests; one was on the porous surface, one on the non-porous

surface and one was on the attachment-line to check that attachment-line contamination had not occurred. All three hot-wire anemometers were positioned 1350mm from the upstream tip, which corresponded to the end of the porous surface on one side of the model. This position was used to allow a comparison with the natural transition on a porous surface data described in Section 5.2.4.2 which also used this position.

Several different diameter trip-wires were used for the tests to give a range of d/η. For each series of tests the trip-wire was wrapped around the leading edge, perpendicular to the spanwise flow, approximately 790mm from the upstream tip. Care was taken to ensure the wire was perpendicular to the spanwise flow, was in contact with the surface all around the leading edge, and was sufficiently tight to prevent any vibration. When a new wire was attached the $\overline{R}$ at the onset of transition on the attachment-line was measured and compared with Poll's results[4], to check that the wire was attached correctly. This test was repeated periodically to ensure the trip-wire had not become loose.

The non-porous surface was tested with trip-wires of diameter 0.21mm and 0.32mm and the porous surface was tested with trip-wires of diameter 0.21mm and 0.268mm.

During the tests on the porous surface all of the suction system hoses were closed and sufficient time was left for the pressures inside and outside the plenum chambers to equalise before measurements were taken. This equalisation was monitored using the three static pressure tappings in each plenum chamber, as discussed in Section 5.2.3.

5.4.4 Results and Discussion

5.4.4.1 Non-Porous Surface

The results for two-dimensional trip-wires on the non-porous surface are shown in Figure 37 and have been plotted as $\overline{R}$ against Re_x to allow comparison with Danks' natural transition data[5]. It can be seen that the data for the onset of transition with a two-dimensional trip are in good agreement with the natural transition data until transition at the attachment-line bypasses the cross-flow transition process. Transition then occurs at a constant value of $\overline{R}$ (and therefore s/η). For the 0.21mm diameter trip the $\overline{R}$ was 675 with an s/η of approximately 2240 and d/η of 0.68. For the 0.32mm trip the $\overline{R}$ was 580 with an s/η of approximately 1920 and d/η of 0.87. These values are consistent with Poll's results for the onset of transition at the attachment-line, which are shown in Figure 35. Therefore, in the absence of attachment-line contamination, the disturbances produced by the two-dimensional trip-wires used here did not interact with the crossflow instability. These results agree with work by Radeztsky *et al*[40] who looked at the amplification of the stationary and travelling crossflow disturbances using a two-dimensional trip-wire on a swept aerofoil. They found that the cross-flow instability was only affected locally by the stationary cross-flow vortices which originated near the ends of the trip wire. In this case the interaction was actually between the crossflow instability and the vorticity introduced by the ends of the trip-wire acting as three-dimensional disturbance sources, not the two-dimensional disturbance.

5.4.4.2 Porous Surface

A similar result was obtained on the porous surface. Natural transition characteristics (ie with no suction) on the porous surface, with a two-dimensional trip, are shown in Figure 38. Also shown is the curve fit for natural transition on a porous surface without a trip-wire derived during the natural transition work discussed in Section 5.2.4.2 (the equation for this line is $\overline{R} = 73000\,Re_x^{-0.39}$). Although there is more scatter than for the non-porous surface, which was also a feature of the natural transition results, it appears that the onset of transition on a porous surface with a two-dimensional trip agrees with the data for the onset of transition on a porous surface without a trip. Therefore, it seems that on the porous surface as well the cross-flow instability was not affected by the disturbances produced by two-dimensional trip-wires.

5.4.5 Conclusions

Experiments have been conducted to quantify the interaction between two-dimensional trip-wires and the crossflow instability. For the s/η and d/η ranges studied it was found that the onset of transition measured off the attachment-line was not affected by the trip-wire unless the trip-wire caused transition on the attachment-line which contaminated of the chord.

The investigation was limited by a number of factors: limited wind tunnel time, a restricted number of trip wire diameters and a short spanwise length of porous surface. These in turn limited the s/η range to between 800 and 2000 and the d/η range to between 0.5 and 0.87. Poll's attachment-line data[4] covered an s/η range up to 8000 and a d/η range up to 4.5, so these findings can not be taken as a general result - further work to expand the experimental ranges would be required to confirm this as a general result. Several non-porous models exist that could be used to confirm a general result on a non-porous, particularly the models used by Poll[4] and Flynn[86]. Construction of a model with a sufficiently long porous surface would be expensive and would provide limited practical return for the investment. Assuming that confirmation of a general result for a non-porous surface could successfully be obtained then the current results could probably be read across to provide a general result for a porous surface. Therefore, it is recommended that further tests on an entirely non-porous model are made to provide this confirmation.

6. The Effect of Blowing on the Attachment-Line Boundary Layer

6.1 Introduction

As discussed in Section 3.2, the attachment-line is the line along the wing leading edge of zero chordwise velocity, and as such is a line of high pressure. This means that a porous attachment-line will always have suction at the attachment-line. Off the attachment-line, the flow accelerates so the chordwise velocity increases sharply and the pressure decreases. To be efficient, plenum chambers should have a large volume and an approximately constant internal static pressure, which in practical terms means being large in both the spanwise and chordwise directions. The large chordwise size means that the external pressure gradient, caused by the accelerating chordwise flow, between the attachment-line and the edge of the plenum chamber could be large. This could lead to the local pressure on the external surface being lower then the internal plenum pressure, which would lead to fluid flowing from the plenum out onto the external surface of the wing, ie blowing. See Figure 39 for a schematic diagram of this situation. Therefore, it is important to quantify the effect of blowing on the attachment-line so that plenum chambers may be sized correctly. The work described here is aimed at quantifying the effect of blowing and providing a mathematical tool that will aid the design and sizing of plenum chambers.

6.2 Previous Work

Attachment-line blowing tests have previously been conducted, on the model used here, by Danks [5, 74]. With a laminar boundary layer at the start of the porous surface Danks slowly increased the blowing rate until the onset of transition. Measuring the state of the boundary layer on the porous surface by hot-wire anemometry, he sampled the output of the hot-wire at several blowing conditions and found that at a certain blowing rate a single frequency peak appeared in the frequency spectrum of the sampled hot-wire output. As the blowing rate increased harmonics of this frequency also appeared, but the dominant frequency was unaffected by the blowing rate. It was, however, affected by $\overline{R}$, and Danks plotted $\overline{R}$ against a non-dimensional frequency, fitting a linear trend to the data.

It had been planned to conduct two series of blowing tests: firstly, a series of tests to investigate the effect of blowing on a laminar attachment-line boundary layer at $\overline{R}$'s less than 300 to give additional data at the low end of Danks' measurement range and then to extend the data range down to $\overline{R}$'s of approximately 100. Unfortunately, a slightly smaller wind tunnel had to be used instead of the one proposed originally so the low sweep angles required were not possible. Nevertheless, data was collected at $\overline{R}$'s between 300 and 600 to confirm Danks' results. The second series of tests investigated the effect of spanwise blowing length on the stability of a laminar attachment-line.

6.3 Blowing At Large s/η

6.3.1 Experimental Method

The model was set at a sweep angle of 55° and arranged as in Figure 7. Chamber 14 was used for these tests, with a hot-wire anemometer was placed 739mm downstream of the start of the porous surface to monitor the state of the attachment-line boundary layer. This position gave s/η values between 1538 and 2915 for $\overline{R}$ values between 313 and 566 respectively, where s in this case was the length of the blowing surface (ie 739mm). Blowing was applied using a small compressor and the flow rate was monitored using flow-rate rotameters. For each test point the blowing rate was set and the freestream dynamic pressure increased until the onset of transition at the hot-wire location. The conditions were then noted. The hot-wire output was also sampled using the Dantec Streamware system, as described in Section 4.7.

6.3.2 Results and Discussion

The blowing results for the onset of transition are given in Figure 40, with the s/η value beside each data point. It can be seen that, as the transpiration coefficient increases, the value of $\overline{R}$ required for transition onset decreases. Extrapolating the trend to the zero blowing case gives an $\overline{R}$ of approximately 650 (at s/η≈10000, where s in this case is the distance from the tip of the model to the measuring station). Referring to Poll's work on transition in the absence of a trip wire[4], at s/η≈10000 the required $\overline{R}$ for the onset of natural transition is between 600 and 650, so the results are in good agreement with this. Previous experimental work by Danks[74] and Arnal, Reneaux and Casalis[50] is compared with the current work in Figure 41 and there is excellent agreement between the three sets of data.

Although the current experiments did not reach the low values of $\overline{R}$ originally planned or obtained by Danks it is still worthwhile examining all the data together. One of the aims of this thesis was to provide simple expressions that could be used for prediction, rather than graphs or data tables. The relationship between $\overline{R}$ and C_q appears to be logarithmic and replotting all of the data with a logarithmic C_q scale confirms this, as shown in Figure 42. Fitting a logarithmic function to the data gives

$$\overline{R} = -122\ln(C_q) - 580$$

for $1\times10^{-4}<C_q<1.8\times10^{-3}$

This is compared with the experimental data on Figure 43, with linear scales this time, and the agreement is good. Unfortunately, being a logarithmic scale the empirical curve fit will not predict the correct behaviour as C_q tends to zero.

Note that, as $\overline{R}$ decreases, the rate of change of the blowing coefficient increases. Put another way, larger and larger blowing rates are needed to get smaller and smaller reductions in the $\overline{R}$ at the onset of transition, suggesting that there may be an asymptotic value of $\overline{R}$ below which blowing can not cause transition. This is not

entirely surprising, since Poll[4] showed that on a non-porous surface the attachment-line would be laminar at large s/η for $\overline{R}$'s less than 245. Hall *et al*[75] showed theoretically that blowing would have a strong destabilising influence on the attachment-line and Danks' lowest datum $\overline{R}$ of 190 demonstrates this. The blowing is, therefore, acting either as a source of disturbance itself or is amplifying the instabilities already in the boundary layer, or a combination of the two. If it is acting as the source of the disturbance, it should be possible to treat the blowing as a two-dimensional disturbance source such as a trip wire. This is because the hot-wire is thin and sits on the attachment-line, while the blowing surface extends 10° (35mm) either side of the attachment-line. Poll's work on the decay of turbulence behind two-dimensional trip wires can be used, because he gave data for non-dimensionalised trip-wire diameter, d/η, as a function of $\overline{R}$ and s/η. This data is shown in Figure 35, for reference. The difficulty here lies in deciding the value of s. The s/η values on Figure 39 use the blowing length, 739mm, giving values between 1500 and 3000. From Poll's data, the $\overline{R}$ at the onset of transition for these s/η values should be asymptotic at approximately 190 (ie the onset of transition should not be possible for $\overline{R}$ values smaller than 190). This clearly isn't the case, since Danks had an $\overline{R}$ =190 case and it isn't an asymptotic datum. At the other extreme we could take the distance to be zero, since the hot-wire is on the porous surface. Poll predicted that the asymptotic $\overline{R}$ for zero s/η would be approximately 65 as d/η tended to infinity. However, linear stability theory indicates that blowing does act as an amplification mechanism (see Section 6.3.3) so the situation is by no means clear cut.

No data exists for the $\overline{R}$ =65 case, so additional testing would be required to show whether the blowing is acting as a two-dimensional disturbance. Unfortunately, the wind tunnel and model combination used here would not be suitable. The model would need to have a smaller leading edge radius to reduce the $\overline{R}$ value for a given sweep angle, to be swept at a smaller angle or a combination of the two. $\overline{R}$ is a function of $\sqrt{r}$, so the radius would have to be reduced by a factor of 25, at the same sweep angle. This is impractical, since it would give a model with a leading edge radius of 8mm. Alternatively, $\overline{R}$ is a function of $\sqrt{\sin(\Lambda).\tan(\Lambda)}$ keeping the same leading edge radius, so the sweep angle would have to be reduced to approximately 12°, keeping the same leading edge radius. Clearly this is also impractical given the vertical height of the model in this configuration (approximately 2.9m) so a new shorter model with a smaller leading edge radius would be needed. However, even halving the leading edge radius would still need the model swept at approximately 15° and there would be practical difficulties involved in fitting a porous surface and suction system to a small cylinder. Additionally, the practical benefits of the test are minimal, since any aircraft operating at such low $\overline{R}$ values would not need a suction system in the first place. It is therefore suggested that further blowing tests of the type described above are unnecessary.

6.3.3 Comparison With Linear Stability Theory

A linear stability analysis on the effect of blowing on the attachment-line boundary layer has been performed by Theofilis[76]. Calculations were made for a range of blowing coefficients and from these the stability envelope of the boundary layer could be found.

For a given blowing coefficient, the boundary layer can be in one of three states:

- Stable, where the amplitude of a small disturbance decreases with increasing spanwise location (ie the boundary layer would always be laminar for large spanwise distances)
- Unstable, where the amplitude of the disturbance increases with increasing spanwise location and the boundary layer will always be turbulent at large spanwise distances
- Neutrally stable, where the amplitude of the disturbance neither increases nor decreases.

From Theofilis, the linear stability envelope for $\overline{R}$ =350 is given in Figure 44. The spatial amplification rate, α_i , is a measure of the stability of the boundary layer where for $\alpha_i > 0$, the flow is stable, for $\alpha_i < 0$ the flow is unstable, and $\alpha_i = 0$ is the special case of neutral stability. The frequency used in the stability analysis, F, was a non-dimensional term, and was related to the actual frequency by

$$F = \left(10^6 .2\pi . \frac{\nu}{V_e^2} \right) f$$

Theofilis' results for neutral stability were compared with all of the experimental results and with other theoretical results from Arnal *et al*[50] in Figure 45. The two sets of theoretical data agree well with each other but are offset from the experimental data. The magnitude of this offset was found by ratioing the experimental data and the theoretical data for a range of blowing coefficients. The results are shown in Figure 46 and it can be seen that the experimental results are approximately 17% larger than the theoretical results across the blowing coefficient range.

The frequency of the most amplified disturbance, for a given blowing coefficient, can be found from plots, such as Figure 43, as the frequency at which α_i is a minimum. Also, it can be seen that as the blowing coefficient increases the range of frequencies that are amplified increases. As the blowing coefficient increases and the magnitude of the amplification rate increases, disturbances at frequencies associated with harmonics of the fundamental most amplified frequency may appear as well[74]. During the experiments the most amplified disturbance was clearly visible in the hot-wire signal and an example is shown in Figure 47. To assess the correspondence between linear stability theory and experiment the output signal of the hot-wire was digitally sampled when a laminar disturbance was visible. The experimental conditions were: $\overline{R}$ =372, C_q=0.000349, and $s/\eta \approx 1900$ (where s was the distance between the hot-wire and the start of the porous surface). The signal was then manipulated using a Fast Fourier Transform (FFT) algorithm to obtain the amplitude spectrum. This spectrum, low passed to a frequency of 5kHz, is shown in Figure 48. It can be seen that the peak disturbance frequency occurs at approximately 750Hz, with a second, smaller, peak at approximately 1500Hz (ie twice the frequency of the main peak) and a third, smaller, peak at 380Hz (half the frequency of the main peak). From Theofilis' analysis, the frequency of the most amplified disturbance under these conditions would be approximately 730Hz, which is very close to the frequency of the observed disturbance (a 3% difference). From Figure 48, the bandwidth of the main peak was approximately 400Hz while the bandwidth predicted by stability theory was approximately 200Hz. The

most likely reason for this difference is the $\overline{R}$ values. In the experimental case no disturbances are visible without the blowing, so the blowing is either introducing the disturbances or is amplifying disturbances already in the laminar boundary layer. Assuming some amplification is present this would make the boundary layer unstable, using the definitions given at the start of this Section. The theoretical results are for the neutrally stable case, which would actually have been at a slightly lower blowing coefficient, and as discussed above, increasing the blowing coefficient in the stability analysis would increase the bandwidth.

Danks[74] plotted a non-dimensional disturbance frequency against $\overline{R}$ and obtained a linear trend. He defined the ono-dimensional frequency as

$$\frac{V_e^2 f}{\nu}$$

where f is the central frequency of the dominant spectral peak. For the example above, the non-dimensional frequency is approximately 18 500, which agrees well with Danks' results.

6.4 Effect of Spanwise Blowing Length

6.4.1 Introduction

From linear stability theory, for constant $\overline{R}$ and C_q the amplification rate, α_i, at each frequency is also constant. It follows from this that the greater the spanwise blowing length the more an instability is amplified, so the spanwise blowing length should be an important parameter. The transpiration length is also important when using suction to relaminarise a turbulent attachment-line, as shown by Danks[5] and by the current work in Section 8.1, so even without the stability theory reasoning one would intuitively expect the blowing length to play a critical role.

6.4.2 Experimental Method

Tests were conducted to investigate the effect, on the onset of transition for a laminar attachment-line boundary layer, of the spanwise length of blowing. Three sweep angles were used (42.8°, 55.1° and 61.2°), with the model arranged in the wind tunnel as in Figure 7, giving an $\overline{R}$ range from 300 to 600. Chamber 14 was used again, with the state of the attachment-line boundary layer monitored by a hot-wire placed at various spanwise positions on the porous surface. The blowing length, s, was the distance between the start of the porous surface and the measuring station and varied from 270mm to 890mm, giving an approximate s/η range from 600 to 3500. For each test point the blowing rate was set and the freestream dynamic pressure was increased until the onset of transition. The conditions were then noted.

6.4.3 Results and Discussion

Results are shown for a sweep angle of 55.1° in Figure 49 for different spanwise blowing lengths and it is immediately obvious that, as the blowing length decreases, the $\overline{R}$ at the onset of transition increases for a given blowing coefficient (ie the effect of the blowing reduces). Non-dimensionalising the blowing length, with η, and plotting the results for all three sweep angles at constant $\overline{R}$, reveals a set of curves with similar trends, as shown in Figure 50. Note that the experimental data has been interpolated to get results at specific $\overline{R}$ values. At each $\overline{R}$ the blowing coefficient tends to an asymptotic value at s/η values greater than approximately 2500, and as $\overline{R}$ increases the blowing coefficient required to cause the onset of transition decreases. These asymptotic blowing coefficients are given in Table 2 below.

$\overline{R}$	Asymptotic Blowing Coefficient ($x10^3$)
350	0.48
400	0.32
450	0.22
500	0.16
550	0.1

Table 2. Asymptotic Blowing Coefficients at Large s/η

The asymptotic s/η value of 2500 is approximately the same as for the relaminarisation of the attachment-line using suction case (see Danks[5] and Section 8.1 of this thesis), suggesting that the same basic physics is at work in both cases and that the transpiration, whether suction or blowing, damps or amplifies the boundary layer instabilities in the same fundamental way. This is confirmed by the success of linear stability theory to predict the effect of suction and blowing. Arnal *et al*[50], for example, calculated the effect of transpiration on the laminar attachment-line and there was no discontinuity between suction and blowing on the resulting curve . A comparison between the asymptotic blowing coefficients in Table 2 and the blowing coefficients from previous blowing experiments (see Section 6.3.2) is shown in Figure 51. The agreement is good, as would be expected since the experimental data down to $\overline{R}$=350 were at s/η values of approximately 2500 or greater. At $\overline{R}$ values below 350, though, Danks' data was taken at s/η values of less than 2500, with the $\overline{R}$=190 datum taken at $s/\eta \approx 1300$. This means that these are probably not the asymptotic blowing coefficient values, which would be smaller.

Rather than the set of curves shown in Figure 50 it would be useful to collapse the data to a characteristic curve that was a function of $\overline{R}$ and s/η. Using the asymptotic blowing coefficients shown in Table 2 the difference between the experimental blowing coefficient and the asymptotic blowing coefficient for each datum was calculated, ie

$$C_q - C_{q(\text{asymptotic})}$$

Figure 52 shows the modified results, and the data collapses reasonably well to a single characteristic curve. A simple function to model this characteristic curve was calculated to be

$$C_q - C_{q(\text{asymptotic})} = 25(s/\eta)^{-1.8}$$

This function describes the trend of the data reasonably well, although there is considerable scatter. The scatter is small at small s/η (approximately ±5%) but is large (approximately ±20%) at large s/η values. This is a consequence of subtracting the two $\overline{R}$ values, since as the differences become smaller (as s/η increases) the percentage scatter of a small value relative to another small value becomes large. The empirical function is also shown on Figure 52 so that the scatter can be seen. From Danks[5] and Section 6.3.2 the $\overline{R}$ at the onset of transition, at large s/η, was a function of the blowing coefficient. As discussed above, we can say that each of these test points, for $\overline{R}$ values of 350 and greater, represents an asymptotic blowing coefficient. Therefore, from Section 6.3.2, the asymptotic blowing coefficient, $C_{q(\text{asymptotic})}$, can be expressed as

$$C_{q(\text{asymptotic})} = e^{-[\overline{R}+580]/122}$$

Substituting for $C_{q(\text{asymptotic})}$ in the equation describing the effect of blowing length we can solve for the blowing coefficient at the onset of transition gives

$$C_q = 25(s/\eta)^{-1.8} + e^{-[\overline{R}+580]/122}$$

for $350<\overline{R}<600$ and $500<s/\eta<3000$.

This equation can be used as a first order design tool for estimating the maximum chordwise size of the attachment-line plenum chamber at given flight conditions. Given the wing leading edge radius and sweep angle the potential flow solution can be used to calculate the chordwise velocity distribution. The approximate allowable blowing coefficient at the given flight condition can be calculated from the above formula, and therefore the critical pressure difference between the surface pressure and the internal plenum pressure can be found. It should be possible to calculate the internal plenum pressure given the flight conditions and this will allow the chordwise position at which the critical blowing coefficient occurs to be calculated.

6.5 Conclusions

The effect of blowing on a laminar attachment-line boundary layer has been studied and excellent agreement with previous experimental data was achieved. Using all of the available experimental data a simple empirical function relating $\overline{R}$ and C_q has been derived.

Comparisons with linear stability theory show a good correlation between the predicted and experimental frequencies of the most amplified disturbance. The predicted bandwidth of the most amplified disturbance was only 50% of the experimental

bandwidth but this has been explained in terms of the difference between the neutral stability condition used in the prediction and the onset of transition condition used in the experiments. The predicted $\overline{R}$ for neutral stability was, on average, 17% lower than the measured $\overline{R}$ at the onset of transition for a range of blowing coefficients. This result could be used to calibrate the predictions from neutral stability calculations for use in predicting the onset of transition.

The effect of varying the spanwise length over which blowing occurs has been examined and it was found that it has a large effect on the $\overline{R}$ at the onset of transition. At a constant $\overline{R}$, as the non-dimensionalised spanwise length increased the destabilising effect of the blowing increased and the blowing coefficient required to cause the onset of transition decreased. For s/η values greater than 2500 the blowing coefficient approached an asymptotic value. Based on this, a single empirical function for the onset of transition has been derived relating $\overline{R}$, C_q and s/η.

7. A Study of the Effect of Attachment-Line Suction on the Spanwise Propagation of Gross Disturbances in the Wing-Fuselage Junction

7.1 Introduction

Previous work by Danks[5, 51], Reneaux[49], and Smith[6, 7], amongst others, has shown that surface suction on the attachment-line can be used to control attachment-line contamination by relaminarising a turbulent attachment-line boundary layer. In these experiments care was always taken that the flow conditions were infinite swept and the boundary layer was fully developed at the start of the suction surface. However, the turbulence that contaminates the attachment-line originates in the wing-fuselage junction, so could suction be applied there to suppress the turbulence at the source?

In the wing-fuselage junction area, the turbulent boundary layer from the fuselage surface wraps around the wing root and a complex flow field develops, shown schematically in Figure 53. A 'horse-shoe' vortex may form in the junction, with one branch on the upper surface of the wing and the other on the lower surface, and there may also be a separated region at the root of the wing caused by the large, local pressure gradients. The boundary layer that forms on the leading edge of the wing after the flow has reattached is generally turbulent and this turbulence may propagate in the spanwise direction, contaminating the attachment-line flow.

The experiments described in this chapter investigated the effectiveness of surface suction for suppressing the turbulence in the immediate vicinity of the wing-fuselage junction before it contaminated the outboard attachment-line. The results were then compared to the suction required to relaminarise a turbulent attachment-line when the flow conditions were infinite swept (ie outboard of the wing-fuselage junction region).

7.2 Previous Work

In the past, three main methods have been proposed for preventing attachment-line contamination: a Gaster 'bump'[77], a boundary layer fence combined with suction through a slot[28] and suction through a porous surface[5]. The Gaster bump is a specially shaped lump on the wing leading edge that creates a local stagnation point on the attachment-line, allowing a new laminar boundary layer to form and thereby removing the turbulence. Results from the Dassault Falcon 50 flight trials showed that the spanwise position of the bump was very important[33] and that placing the bump too close to the fuselage failed to produce a laminar attachment-line boundary layer. The boundary layer fence stops the spanwise flow and then uses strong suction to prevent flow separation outboard of the fence. As with the Gaster bump, a new laminar boundary layer forms on the other side of the fence. Porous surface suction removes mass and energy from the boundary layer, causing thinning of the boundary layer and relaminarisation, rather than causing a stagnation point.

The flow field in the wing-fuselage junction region has been studied by Bergin[78] using a swept cylinder model and a streamwise endplate to simulate the fuselage. He investigated the variation of $\overline{R}$ along the leading edge in the region of the wing-

fuselage junction and his results are given in Figure 54. These show that near to the junction the $\overline{R}$ reduced to zero, so there was a stagnation point, and that the distance away from the junction of this stagnation point was a function of sweep angle and the boundary layer thickness on the fuselage. The implication of these results is that turbulence does not simply flow from the fuselage onto the wing, causing contamination. The $\overline{R}$ will fall to zero in the junction region and there will, therefore, be a finite spanwise region where the $\overline{R}$ is low enough to damp disturbances being introduced by the vortices at the wing root. The outboard span will only be contaminated if the disturbances are sufficiently large that they are not damped in this region. This leads to the situation where the fuselage boundary layer may be turbulent and the $\overline{R}$ on the outboard span may be larger than 245, the value identified by Poll[4] as the minimum required for the amplification of turbulence along the attachment-line, but no contamination occurs because the lower $\overline{R}$ values near the root damp the disturbances. Conversely, the opposite is possible – a laminar fuselage boundary layer could lead to contamination if the sweep was sufficiently large that the region of low $\overline{R}$ was not sufficient to damp the disturbances produced by the wing root vortices and the outboard $\overline{R}$ was larger than 245, as it probably would be for large sweep angles.

Phillips *et al*[79] used suction on the fuselage to reduce the size of the wing root vortex using an unswept aerofoil model attached to the wind tunnel wall. Suction was applied through a porous patch just upstream of the aerofoil leading edge and vorticity was monitored using a five-hole probe. The results showed that, at the highest suction rates, the vorticity could almost entirely be suppressed. Applying this to the swept wing environment in the light of Bergin's results, this would mean that the spanwise extent of low $\overline{R}$ would not need to be as large so the sweep angle could be increased while still preventing attachment-line contamination. The drawback of this approach was the magnitude of the suction required: a suction coefficient of at least -1 was required to have any significant effect on the vorticity and to damp the vorticity almost completely a suction coefficient of approximately -2 was required. This was almost one thousand times larger than the suction coefficient required to relaminarise a turbulent attachment-line using porous surface suction outboard of the wing-fuselage junction, approximately –0.0033, so suction on the fuselage was not a viable alternative to the three currently accepted methods.

7.3 Experimental Method

The model was swept forward at 60°, so that the non-porous section of the attachment-line was downstream of the porous region, giving an $\overline{R}$ range of approximately 400 to 835. The plenum chamber used was chamber 14, which extended to ±10° either side of the attachment-line. For these tests a horizontal, streamwise endplate was attached to the leading edge, parallel to the wind tunnel floor, to simulate a wing-fuselage junction, and the arrangement of the model in the wind tunnel is shown in Figure 55. The endplate extended from 0.3m in front of the leading edge to beyond the trailing edge of the model, and spanned the entire working section. A 4mm diameter two-dimensional trip wire was attached to the plate, 10mm downstream of the leading edge. This ensured the boundary layer on the plate approaching the plate/wing junction was fully turbulent. Although, as discussed above, the fuselage boundary layer does not necessarily need to

be turbulent to cause attachment-line contamination, the probability is increased if the sweep angle is large and the fuselage boundary layer is thick. For this reason a sweep of 60° was used and the fuselage boundary layer was deliberately tripped. The total suction surface length on the attachment-line was 900mm and the state of the attachment-line was monitored on the suction surface at various locations using a hot-wire anemometer.

Tests were conducted at fixed freestream dynamic pressure and the suction rate was increased until relaminarisation had occurred.

7.4 Results and Discussion

The first test was to check that the attachment-line was turbulent throughout the $\overline{R}$ range and at all stations along the suction surface, and it was. Next, suction was applied to relaminarise the turbulent attachment-line. After several attempts, it became clear that, with this configuration, relaminarisation of the attachment-line was impossible. Using the entire available suction length (900mm) complete relaminarisation could not be achieved at the highest suction levels available (C_q=-0.0339). Figure 56, parts (a) to (e), show sampled signals from the hot-wire, for increasing suction, at $\overline{R} \approx 518$ and $s/\eta \approx 2490$. Each part of Figure 56 covers 0.5 seconds, which is only part of the actual sample. Each hot-wire sample covered two minutes, but these have not been shown in full because this compresses the data and hides the laminar drop-out in places. From work on relaminarising turbulent attachment-line flows (see Section 8) this value of s/η is approximately the value required for asymptotic suction, but Figure 56(e) shows that, even at a suction coefficient of -0.0339 (which is over ten times the suction coefficient required to relaminarise a fully turbulent, infinite swept, attachment-line at this $\overline{R}$), the intermittency had only been reduced to approximately 0.3. Although the intermittency could not be reduced to zero during the experiments the suction coefficient required to eliminate all attachment-line turbulence, at $\overline{R} \approx 518$ and $s/\eta \approx 2490$, can be estimated from this data. The intermittency, Γ, was estimated from each part of Figure 56 and the variation of intermittency with suction coefficient is plotted in Figure 57. The intermittencies were calculated simply by measuring the amount of time the boundary layer was laminar and ratioing this time with the total sample time of 120 seconds, so that

$$\Gamma = 1 - \left(\frac{\text{time}_{\text{laminar}}}{\text{time}_{\text{samplet}}} \right)$$

The data show a smoothly reducing trend that can be approximated well by a quadratic polynomial, fitting the data with a scatter of less than ±2.5%. Extrapolating this trend to the zero intermittency case, ie laminar flow, gives a required suction coefficient of approximately -0.06. Comparing this with the suction coefficient required to relaminarise a turbulent attachment-line measured by Danks[51] of approximately –0.003, the suction needed in the junction region is twenty times larger.

Why was suction so ineffective? The reason probably lies in the effective suction length. The vortex in the junction root would have had a finite spanwise extent and

would have acted as a disturbance source. According to Barber[80], the larger the fuselage boundary layer thickness the larger the region of influence of the wing-fuselage vortex, although no quantitative measure of the effect is given. The surface suction was, therefore, performing two tasks: reducing the vortex strength and attempting to relaminarise the turbulent attachment-line outboard of the vortex. Philip's work[79] showed that significantly larger suction rates are required to reduce the vortex strength than were used here, so the spanwise length covered by the vortex can probably ignored, leaving a reduced effective suction length. Additionally, Bergin[78] defined the root region as s/D less than 2, where s=0 is the actual wing-fuselage junction, and outside this region infinite swept conditions would be found. For the current model, this would give a spanwise distance of 0.81m, so infinite swept conditions were only attained approximately 90mm from the end of the suction surface. This would probably mean that the effective s/η was smaller than the measured value. Although a quantitative comparison cannot be made with Danks[51] attachment-line relaminarisation data because the conditions in the fuselage junction were, in the main, not infinite swept, the qualitative effect of reducing s/η is likely to be still valid. Danks[51] results are shown in Figure 58 for reference, and it can be seen that, for constant $\overline{R}$, as the s/η decreases the suction coefficient required increases rapidly.

Although extrapolating Danks' results is not valid, it is useful as an example. The effective infinite swept s/η that would require a suction coefficient of –0.06, the extrapolated suction coefficient value of –0.06 for relaminarisation found from the current results, would be approximately 1000. This would mean that the effective suction length would need to be approximately 375mm for infinite swept conditions, rather than the 900mm physically available. Taking into account the spanwise suction length neglected because of the vortex spanwise extent and including the effect of non-infinite swept conditions, it does not seem too improbable that the effective s/η is indeed quite small and may be as small as 375mm.

7.5 Conclusions

Wind tunnel experiments have been conducted to assess the effectiveness of attachment-line porous surface suction at the junction of a flat plate and swept cylinder. For the experimental arrangement used, the attachment-line could not be fully relaminarised, even using suction coefficients as large as –0.06, which is twenty times larger than the suction coefficient required to relaminarise a turbulent attachment-line with infinite swept conditions. A comparison with previous work has been attempted, although several differences prevent a direct comparison, and it is suggested that the large suction requirement is due to a combination of two effects: the effective suction length is smaller than the physical suction length because of the presence of the vortex in the junction root. Additionally, infinite swept conditions were not obtained over 90% of the suction surface. The combination of these meant that the effective s/η was significantly reduced and the suction coefficient required for relaminarisation was conversely increased significantly.

However, the important result is that attachment-line porous surface suction is much more effective under infinite swept conditions, so suction on the fully developed attachment-line should be used rather than suction in the wing-fuselage junction.

8. Attachment-Line Boundary Layer Relaminarisation by Suction

8.1 Relaminarisation Of A Turbulent Attachment-Line Boundary Layer When the Attachment-Line Reynolds Number Exceeds 600

8.1.1 Introduction

The state of the attachment-line boundary layer can have a profound effect on the drag of the wing. If the attachment-line is turbulent then the chordwise boundary layer will, in general, be turbulent as well leading to higher wing drag since the turbulent skin friction drag can be as much as 10 times the laminar drag. However, at the cruise conditions of modern civil airliners the attachment-line will itself, in general, be contaminated by the turbulent fuselage boundary layer. Additionally, imperfections in the wing surface, for example insect debris, can cause attachment-line transition on the outboard span, again leading to contamination of the chordwise boundary layer. The relaminarisation of a turbulent attachment-line is, therefore, of great practical importance.

Previous work by Danks[5, 51] explored attachment-line relaminarisation up to $\overline{R}$ values of 600, which is sufficient for current aircraft. Future civil and military aircraft will be larger, carrying greater payloads and, therefore, will require more lift. It is expected that the wings of these aircraft will have greater leading edge Reynolds numbers, so the previous work needed to be extended.

The wind tunnel tests described in this section investigated the use of porous surface suction to relaminarise a turbulent attachment-line at $\overline{R}$ values up to 950.

8.1.2 Previous Work

The main sources for data on attachment-line relaminarisation are the University of Manchester in the UK and ONERA in France.

Work performed previously by Danks[5], [51, 52] was conducted using the same model as used here but mounted in the 9' x 7' low-speed wind-tunnel in the Goldstein Laboratory at the University of Manchester. Applying suction to a fully developed turbulent attachment-line boundary layer, Danks found that suction could be used to relaminarise the boundary layer and that, for a constant suction coefficient, the longer the spanwise suction length the higher the $\overline{R}$ value at the onset of transition. Additionally, at large spanwise distances the suction required approached an asymptotic value, so there was a suction coefficient at which turbulent flow would not be possible and he proposed that it was approximately C_q=-0.0035. An empirical relation was presented[51] that allowed the effect of s/η to be removed by 'normalisation'. Using this, the suction coefficient results could be corrected to give the value that would have been required if s/η had been infinite This was done by defining a scaling parameter, w', such that the suction coefficient that would be required in the limit of s/η tending to infinity could be calculated from

$$\left(C_q\right)_{s/\eta\to\infty} = \frac{\left(C_q\right)_{s/\eta<\infty}}{w'}$$

where

$$w' = 1 + \exp\left(2.0 - 0.0025\, s/\eta\right)$$

for $500<s/\eta<\infty$

Danks[51] used his asymptotic suction coefficients to derive an empirical function relating $\overline{R}$ and C_q, in the limit of $s/\eta\to\infty$:

$$\overline{R} \approx 245\sqrt{(1.07(C_q\overline{R})^2 - 0.48(C_q\overline{R}) + 1)}$$

for $250<\overline{R}<600$

At ONERA, Arnal lead a team that often paralleled the work at Manchester. Part of that team, Reneaux[49] also looked at the effect of suction on the leading edge and demonstrated that suction was effective for relaminarising a turbulent attachment-line and that the boundary layer profiles following relaminarisation had characteristics typical of laminar boundary layers. Interestingly, the suction coefficients presented by Reneaux were higher than those given by Danks[5] for $\overline{R}$ values greater than 400. Reneaux also derived an empirical function relating $\overline{R}$ and C_q and his was

$$\overline{R} = 250 - 150K$$

where K was their suction parameter defined as

$$K \equiv \overline{R}.\left(\frac{w(0)}{Q_e}\right) = \overline{R}C_q$$

Arnal *et al*[81] presented a comparison between leading edge transpiration wind tunnel results (both suction and blowing) and a numerical study using non-linear parabolised stability equations (PSE). This gave data in broad agreement with the experimental results, although the numerically predicted transpiration coefficients were slightly lower than their experimental equivalents.

8.1.3 Experimental Method

The model was swept back in the wind tunnel, as shown in Figure 7. For these tests, a geometric sweep angle of 70.2° was used, giving an $\overline{R}$ range between 600 and approximately 950. Plenum chamber 14, at the bottom of the model, was used and the porous surface in this case extended to ±10° either side of the geometric centreline of the model. The state of the boundary layer was monitored at six locations on the suction

surface, using a constant temperature hot-wire anemometer placed on the attachment-line 495mm, 610mm, 710mm, 750mm, 810mm and 865mm downstream of the start of the suction surface (1845mm, 1960mm, 2060mm, 2100mm, 2160mm and 2215mm from the upstream tip). This gave an s/η range from 800 to 2650. The hot-wire element was placed within 1mm of the model surface using the reflection from the titanium surface as a guide.

A 4mm diameter trip wire was wrapped around the leading edge of the model 900mm from the upstream tip. At values of $\overline{R}$ in excess of 600, d/η was greater than 6.5 which, as shown by Poll[4], constituted a gross trip (ie turbulence was shed directly from the trip-wire and transition occurred at the trip location). Therefore, the attachment-line boundary layer was turbulent and fully developed at the start of the suction region.

At each test point, the freestream dynamic pressure was set and the suction rate increased until relaminarisation occurred.

8.1.4 Results and Discussion

Figures 59 and 60 show the effect of increasing s/η on the suction coefficient required to produce relaminarisation, at fixed values of $\overline{R}$. It can be seen that, as s/η increases, the suction coefficient required to cause relaminarisation, at a given $\overline{R}$, decreases and approaches a constant value asymptotically. From these results, and the data from Danks[51], the asymptotic value is reached at $s/\eta \geq 2000$. The asymptotic value of the suction coefficients at each $\overline{R}$ can, therefore, be found and these are given in Table 3 together with the maximum s/η tested at that value.

$\overline{R}$	Asymptotic Suction Coefficient ($x10^3$)	Maximum s/η
600	-3.42	1696
650	-3.4	1837
700	-3.33	2031
750	-3.33	2176
800	-3.31	2321
850	-3.25	2466
900	-3.23	2600
950	-3.2	2756

Table 3. Values of Suction Coefficient Required For Relaminarisation in the Limit as $s/\eta \rightarrow \infty$

Fitting a curve to these data gives an empirical relation between $\overline{R}$ and C_q, in the limit of $s/\eta \rightarrow \infty$. The relation given in Section 8.1.2, from Danks[51], is a curve fitted to their asymptotic suction coefficient data, and the two are compared in Figure 61, along with the asymptotic coefficients from Reneaux[49]. The Danks relation was obtained from results for $250 < \overline{R} < 550$, and they predicted that a suction coefficient existed at which it was impossible for the boundary layer to be turbulent, irrespective of $\overline{R}$, with the value

given C_q=-0.0039. The Danks relation has been extrapolated to $\overline{R}$ =950 for comparison with the current results. The data from Reneaux[49] was valid for 250<$\overline{R}$ <650 and these have also been extrapolated up to 950. The asymptotic suction coefficients obtained in the current experiments were lower than the values predicted by Danks, showing a suction coefficient of approximately -0.0033 for turbulent flow to be impossible (a difference of approximately 6%). Some kind of difference is not entirely surprising given that the values of $\overline{R}$ used in this work were almost double those used by Danks. However, the difference was small, indicating that the behaviour of the attachment-line boundary layer is nominally the same at $\overline{R}$ =950 as at $\overline{R}$ =500. Note that the maximum experimental s/η values for the 600 and 650 $\overline{R}$ data were less than the 2000 limit previously found by Danks for the asymptotic s/η value. Therefore, it is probable that these suction coefficients are not the asymptotic values, which would be slightly smaller. This would bring them more into agreement with the extrapolation of Danks empirical relation. The differences with Renaux's data were more pronounced, with Reneaux suggesting suction coefficients as much as 50% larger.

The w' values for the current data were evaluated and are compared with the Danks relation in Figure 62, with the scatter of the Danks data shown by error bars. The data show good agreement for s/η>1500, but at smaller s/η the w' values were smaller than Danks'. Given these differences and a discussion with Danks in 1996[82], it was decided to derive a revised relation for w' and it was found to be

$$w'=1+\exp(2.3-0.003s/\eta)$$

for 500<s/η<3000. Figure 63 shows the revised curve fit compared to the current experimental data and Danks' empirical curve fit. Error bars have been added to Danks' empirical curve to show the scatter band of Danks' experimental data. The revised curve still fits the data at large s/η; the only change is to reduce the w' values slightly for s/η values between 750 and 1750. To go with this, a new empirical formula for the asymptotic suction coefficient has been derived and the best fit was found to be

$$C_q=-0.0033+\exp(-3.5-0.0095\overline{R})$$

for 250<$\overline{R}$ <950. The agreement with the experimental data is ±6.5% at worst, but on average is less than ±3%. From the form of the formula, it can be seen that the suction coefficient at which no turbulence will be possible, as s/η tends to infinity, is C_q=-0.0033, which is slightly larger than the value of –0.0039 proposed by Danks.

8.1.5 Conclusions

Experiments have been conducted to find the suction coefficients required to relaminarise a fully developed turbulent attachment-line at large $\overline{R}$. The previous work of Danks[51] up to $\overline{R}$ values of 600 has been extended to $\overline{R}$ values of 950 and it has been found that the trends evident at low $\overline{R}$ values have continued up to $\overline{R}$ values of 950. The data now cover a range of $\overline{R}$ values that comfortably exceeds the flight conditions of current large transport aircraft.

In the limit of s/η tends to infinity, the suction coefficient required to relaminarise a turbulent attachment-line boundary layer asymptotes to a value of approximately -3.3×10^{-3} at which turbulent attachment-line flow is not possible, at any value of $\overline{R}$.

8.2 The Effects of Large Suction Levels on Transition in the Attachment-Line Boundary Layer

8.2.1 Introduction

During the last fifteen years, extensive research has moved laminar flow control closer to industrial application and commercial civil aircraft manufacturers are studying the practicalities of operating an HLFC aircraft. One of the things they are looking at is the distribution and magnitude of the suction that will be used for the planned flight profiles. Laminar flow will be employed to provide a cost saving for the operating airline, whether in DOC or payload for example, so it is not enough to switch the suction on as high as possible because suction over the minimum required will simply be a reduction in benefit. However, this is not the only reason that excessively high suction levels should be avoided. Previous work, see below, has indicated that high suction levels can cause the onset of transition to occur at lower Reynolds numbers than if suction had not been used at all. This is known as critical oversuction and the definition is quite specific: only when the transition $\overline{R}$ with suction is lower than the $\overline{R}$ at which transition would have occurred without the use of suction can it be said that critical oversuction has occurred.

The experiments described in this Section were designed to see whether very large suction rates would cause critical oversuction to occur. Additionally, previous oversuction results from Pfenninger were reassessed.

8.2.2 Previous Work

During flight trials with an Anson Mk 1 aircraft, Head[83] reported that at high suction rates laminar flow was lost. Without any suction the boundary layer was turbulent, so it is difficult to know whether this was critical oversuction.

Results commonly quoted as evidence for critical oversuction at an attachment-line were produced by Pfenninger[26]. Using a blunt-nosed wing, swept at 45°, he experimented with attachment-line transition control using suction through slots and perforations. With strong suction upstream of the test zone the attachment-line boundary layer was relaminarised so that the attachment-line was laminar at the start of the porous test surface. Pfenninger investigated how suction could be used to delay the transition of the laminar boundary layer and his results are given in Figure 64 for reference. The suction parameter v_o^* is equivalent to C_q using the terminology of this thesis. From Figure 65 it can be seen that, at large spanwise Reynolds numbers (Wz/ν), as the suction parameter v_o^* increases the effect of the suction decreases. At high suction rates, the laminar momentum thickness Reynolds number at transition is less than that for medium suction rates. Pfenninger attributed this reduction to the formation of

longitudinal disturbance vortices originating from the suction holes and triggering transition (ie critical oversuction). When suction is applied each of the holes in the porous surface becomes a sink. The sink effect causes the formation of a 'horse-shoe' vortex around the hole, which introduces a perturbation into the boundary layer. With sufficiently large suction coefficients, the combination of the effects of all the holes can produce a disturbance that causes transition to occur prematurely.

The effect of large suction levels on a two-dimensional, flat plate boundary layer has been studied previously[84] where it was found that, at sufficiently high suction coefficients, transition could occur at a lower Reynolds number than if no suction had been used.
A comprehensive experimental study of the problem in two-dimensional flow, carried out by Ellis[84], produced an empirical criterion for critical oversuction conditions,

$$\frac{w(0)_h d_h^2}{V_e \delta^{*2}} = A$$

where A is a constant. From Ellis's work, critical oversuction occurred for two-dimensional (flat plate) flow when A exceeded approximately 2.

8.2.3 Experimental Method

Running concurrently with the relaminarisation experiments (Section 8.1), tests were made to investigate the issue of critical oversuction. At each of the spanwise positions used in the relaminarisation tests, the largest suction rates possible (limited by experimental arrangement) were used. Measurements were made at values of $\overline{R}$ ranging from 156 to 954, and with suction coefficients ranging from -0.100 to -0.004. The maximum suction rate (approximately 4000 litres/minute) was limited by the available equipment so the suction coefficient was inversely proportional to the boundary layer edge velocity (from Section 4.3.5, $C_q=w(0)/V_e$ and the maximum suction rate, w(0), was limited to 4000 litres/min). Therefore, the largest suction coefficient was obtained at the smallest $\overline{R}$.

8.2.4 Results and Discussion

No sign of oversuction was found and the attachment-line remained laminar throughout the tests. This is, perhaps, not entirely surprising. As reported by Danks[5], when the model was made the suction surface was consciously designed to be resistant to oversuction. The entire drilling pattern is skewed relative to the axis of symmetry by 14°, leading to a streamwise hole separation of not less than 1600μm and, in general, an irregular pattern of holes along any flow streamline.

Since no evidence of critical oversuction was found, it was decided to revisit the data for an experiment popularly considered to show oversuction and reassess the data based on the parameters used in this thesis, for example $\overline{R}$ and C_q. The experiment was performed by Pfenninger[26] and is described in the Previous Work section above. Figure 62 shows Pfenninger's data in its original form. The data are plotted as the attachment-

line transition momentum thickness Reynolds number, $Re_{\theta_{alT}}$, against a non-dimensional suction velocity, v_0^*, and it can be seen that there are effectively two different types of data plotted on a single chart. The individual data points are for different spanwise positions, while the solid lines are lines of constant spanwise Reynolds number. The data has been replotted in terms of $\overline{R}$ and C_q in Figures 66 and 67 respectively – the method used to convert Pfenninger's data to $\overline{R}$ and C_q is given in Appendix F. This shows that, at each spanwise position, as the suction coefficient was increased the transition $\overline{R}$ increased. At no spanwise position did an increase in the suction coefficient cause a reduction in the transition $\overline{R}$, or cause transition to occur at an $\overline{R}$ lower than that with no suction. According to our definition, Pfenninger did not see critical oversuction and it was the way the data was plotted that gave the impression of an adverse suction effect.

However, replotting the data does raise one interesting point: as Pfenninger increased the suction the $\overline{R}$ increased by 23% but the suction coefficient increased by 350%. This is a large increase, especially considering that Pfenninger was starting with a laminar attachment-line and was simply delaying the transition to a turbulent state, not relaminarising a turbulent boundary layer. Although a leak in the suction system would cause a similar situation, where a disproportionately large increase in suction is required to produce a small increase in performance, this is unlikely given Pfenninger's many years experience with suction systems, so it is more likely to have been a function of the porous surface he was using.

Pfenninger's data and the current data were compared using Ellis's criterion and the Ellis parameters for all the data are shown in Figure 68. It was found that the largest value of the Ellis parameter from Pfenninger's data was only 0.05 (at an $\overline{R}$ of 841) while the current data had an Ellis parameter of 21 (at an $\overline{R}$ of 156). This also suggests that Pfenninger did not encounter oversuction. The largest suction coefficient achieved in the current tests was at an $\overline{R}$ of 156, with a sweep angle of 15°. A flow rate of 3000 litres/min was used, at a freestream velocity of approximately 7m/s. This gave a suction coefficient of -0.100, at a unit Reynolds number of 1.003×10^6 m^{-1}. This is one hundred times larger than the suction coefficient required to relaminarise a fully turbulent attachment-line. However, it should be remembered that Ellis used a two-dimensional flat plate so a quantitative assessment using his oversuction criterion is probably not valid for the three-dimensional leading edge situation.

One difference between this case and Pfenninger's work could be the receptivity of the attachment-line. Pfenninger's tests were conducted at large $\overline{R}$ ($650 < \overline{R} < 800$), when the attachment-line without suction was unstable, whereas the above example was at $\overline{R} = 156$, when the attachment-line was stable without suction. The receptivity of the boundary layer must play a part in the transition process, but the suction coefficients used in the present tests were so large that it seems unlikely that the receptivity was the dominant factor. It should be noted that the relaminarisation data, presented in Section 8, was taken at $560 < \overline{R} < 960$, which is similar to the range used by Pfenninger, and no retransition was observed up to the highest suction coefficients achievable.

The main difference seems to be which Reynolds number was used. $\overline{R}$ has been used here, and converting all the data to this form removes the oversuction. Pfenninger used the momentum thickness Reynolds number, and the same data appears to show oversuction plotted in this way. The difference between the two Reynolds numbers is the length scale, with η being independent of the suction rate while the momentum thickness reduces as the suction rate increases.

8.2.5 Conclusions

Wind tunnel experiments have been performed to investigate the stability of the porous surface to oversuction. No sign of oversuction was found, even at a suction coefficient of -0.100.

Comparing the current work with the results of Pfenninger[26] showed that he was using lower suction coefficients, and when his results were analysed using Ellis's two-dimensional oversuction parameter it was found that the oversuction parameter values for his test were lower than for the current tests.

Therefore, it can be concluded that oversuction can be a matter of the definition of the Reynolds number. The definition used here involved $\overline{R}$, and converting Pfenninger's data to this form removed any suggestion of oversuction. However, using the momentum thickness Reynolds number, Pfenninger's data did suggest oversuction.

9. An Investigation of the Transition That Occurs When a Relaminarised Attachment-Line Encounters a Non-Porous Surface

9.1 Introduction

It has been shown many times that a turbulent attachment-line boundary layer can be relaminarised using suction[5, 26, 31, 39]. However, there are penalties associated with using suction[2], so airlines will be looking for an optimised suction distribution that controls transition but is not overly penalising for things like engine bleed required to power suction pumps. One possible option is not to use suction along the entire leading edge but to have a combination of porous and non-porous regions. Also, it is simply not practical to have suction along the entire leading edge – other things need to go into the wing apart from plenum chambers and suction pipes. Therefore, it would be useful to know what happens when a relaminarised attachment-line boundary layer flows onto a non-porous attachment-line surface.

9.2 Previous Work

It is already known that to delay the onset of transition on the wing chord suction is not required across the entire chord. Bobbitt *et al*[85] reported experiments conducted between 1981 and 1988 using a slotted-suction model in the NASA Langley 8ft transonic pressure tunnel and investigated the effect on transition location of reducing the chordwise extent of the suction. The model used was a 12% thick aerofoil with a sweep angle of 23°, giving a chord Reynolds number of $20\text{x}10^6$ at Mach 0.82. Figure 69 shows the results and it can be seen that suction over the first 25% of the chord gave laminar flow up to about 60% chord for a chord Reynolds number of $15\text{x}10^6$. Interestingly, suction between approximately 12% and 20% chord increased the amount of chordwise laminar flow from 30 to 60% chord. This was presumably by damping the crossflow instability before it could develop meaning that the amplification available over the unsucked region was insufficient to cause transition. It is probable that at 60% chord a different transition mechanism is causing transition, possibly two-dimensional T-S disturbances, since the additional suction between 20% and 25% chord has no effect on the transition location. This fits with work by Danks[5] who conducted a qualitative investigation to find the optimum suction distribution using a swept cylinder model in the University of Manchester 9'x7' low speed wind tunnel. He found that, while no optimum suction distribution existed, the minimum total suction rate was achieved by applying large suction rates just upstream of the location that transition would have occurred at without suction. Reduced suction rates could then be applied downstream of that location and suction was not required across the whole chord. Figure 35 shows an example of Danks' suction distribution and shows that with suction up to 25% chord transition occurred at 35% chord. Flight tests on a Dassault Falcon 50[33] employed suction through a perforated stainless steel surface up to 10% chord. With the wing swept at 30° and for chord Reynolds number between $12\text{x}10^6$ and $20\text{x}10^6$ laminar flow was measured up to 30% chord. Tests were also conducted on a Boeing 757 aircraft[34]. Suction was provided up to the front spar, approximately 20% chord, and laminar flow was measured at up to 65% chord at Mach 0.8. The only data for the stability of the relaminarised attachment-line beyond the porous surface comes from Reneaux *et al*[49]

who used a constant chord swept wing model with a 0.2m leading edge radius in the ONERA F2 wind tunnel. They also carried out a computational analysis, using the e^n stability method, with infinite swept assumptions and the effective sweep angle calculated from the experimental pressure distributions around the model leading edge. Experimentally, they showed that a relaminarised attachment-line remained laminar beyond the suction region. Measurements from two hot-film sensors at two different spanwise positions are shown in Figure 70 for a sweep angle of 50°. On the chart, D is the leading edge diameter, z is the spanwise distance and the suction parameter, K, on the x-axis is defined as

$$K \equiv \overline{R}\frac{w(0)}{Q_e} = \overline{R}C_q$$

K can also be regarded as a suction Reynolds number, which can be demonstrated by expanding $\overline{R}$ and recognising that on the attachment-line $Q_e = V_e$.

$$K = \frac{V_e\eta}{\nu}.\frac{w(0)}{V_e} = \frac{w(0)\eta}{\nu}$$

Therefore, the suction Reynolds number is characterised by the suction flow velocity perpendicular to the wall, w(0), and the spanwise viscous length scale, η.

The hot-film sensor at z/D=4.47 was placed just before the end of the suction panel while the sensor at z/D=5.05 was outboard of the suction panel. The data clearly show that for values of K greater than approximately –1.9 transition occurs on the non-porous section at $\overline{R} \approx 535$ independent of the suction rate. In contrast, the suction rate affects the sensor on the porous surface up to $\overline{R} \approx 675$. Reneaux states that $\overline{R} = 535$ is roughly the natural transition value. The results of the computations showed that the n-factors for transition at the locations on the model were between 12 and 13, close to those corresponding to natural laminar boundary layer transition.

9.3 Experimental Method

For these tests the model was swept forward at 60° so that the suction surface was at the upstream end of the model, as shown in Figure 55. The question then arose as to whether the flow was infinite swept over chamber 14 in this configuration. The static pressure distribution around the face showed, as for the swept-back configuration, that conditions were infinite swept between the middle and downstream tappings but not at the upstream tappings. For these tests it was not particularly important whether the whole of the suction surface was infinite swept, because it was the boundary layer behaviour on the non-porous surface that was of interest. Therefore, the static pressure distributions alone showed that conditions were infinite swept over the test area. However, it may be of interest to know approximately where infinite conditions were attained, so this has been estimated. For the swept-back configuration, infinite swept conditions were obtained between 565mm and 663mm from the upstream tip. With the model forward swept there is a 420mm wooden fairing between the end of the model

and the start of the titanium surface and 100mm between the start of the titanium surface and the start of the porous section, giving a total distance between the upstream tip and the start of the porous surface of 520mm. Taking the worst case from the swept-back results, 663mm, and applying it to the forward swept case we find that infinite swept conditions would be attained 143mm onto the porous surface. This leaves a further 757mm before the actual test area begins, which would compensate for errors in the assumption that the distance taken to reach infinite swept conditions was the same forward swept as swept-back. Note that the total distance between the upstream tip and the start of the test area when swept forward is 1420mm, which is larger than the distance from the upstream tip to the middle static pressure tappings when the model is swept-back.

A 4mm diameter two-dimensional trip wire was wrapped around the leading edge of the model 475mm upstream of the start of the plenum chamber 14, the chamber used to provide the attachment-line suction. This ensured that the attachment-line was turbulent and fully developed when it encountered the suction surface. Suction was then used to relaminarise the attachment-line and the newly laminar boundary layer than flowed off the porous section and onto the solid surface. The state of the boundary layer was monitored on the solid surface using a hot-wire anemometer located at 0mm (the end of the suction surface), 80mm, 280mm, 490mm and 690mm downstream of the end of the suction surface. The end of the suction surface was monitored to show that the flow leaving the porous surface had been successfully relaminarised. A schematic view of the experimental arrangement is shown in Figure 71, and it should be noted that the spanwise distance, s, for these tests was the non-porous distance between the end of the suction surface and the measuring station. At each hot-wire position the suction rate was set and the freestream velocity was increased until the onset of transition, where the conditions were noted. The suction rate was then set at a slightly higher level and the process was repeated. This continued until the maximum speed of the tunnel was reached and then was repeated for each spanwise position. At several spanwise positions, the suction needed crossed over the range of two sets of flow meters, so tests were conducted using both sets of flowmeters to get a good range of $\overline{R}$ values. This means that data was obtained for the same spanwise position at nominally the same conditions, so there are pairs of data points in the results.

9.4 Results and Discussion

Data for the onset of transition on the non-porous surface are presented in Figure 72. It can be seen that up to suction Reynolds numbers of approximately –3.3 the results are independent of the spanwise distance. The data from the end of the suction surface show that transition on the non-porous surface occurs because, with those suction rates, transition actually occurs at the end of the porous surface (ie transition is caused by attachment-line contamination). Also plotted on Figure 70 are data calculated from Danks[5] asymptotic suction limits equation (see Section 8 for a description of this), which is valid up to $\overline{R}$ values of 600, and these agree well with the current data. For greater suction Reynolds numbers, the behaviour changes so that, at the 280mm, 490mm and 690mm spanwise positions, transition is independent of the spanwise position and $\overline{R}$, with a critical $\overline{R}$ of approximately 790. The data from the end of the suction surface (s=0) show that the boundary layer is laminar for these suction Reynolds

numbers, so transition is occurring because of conditions on the non-porous surface, not attachment-line contamination. The suction Reynolds value of –3.3 is higher than the value of –2.6 found in Section 8 for the suction Reynolds number at which turbulence would not be possible at the end of the suction surface for those $\overline{R}$ values. The reasons for this are not known at present.

The results from the 490mm and 690mm measuring positions show the clearest asymptotic trends, and the maximum s/η values obtained at these positions were 1690 and 2348 respectively. The critical $\overline{R}$ value of 790 seemed similar to the natural transition $\overline{R}$ obtained by Poll[4] for transition onset in the absence of a trip wire at small s/η. The present experiments were conducted at s/η values between 150 and 2400, putting them beyond the lower end of Poll's data, so his data were extrapolated by fitting a cubic polynomial trend using linear least-squares regression, which fitted the data to within ±2%. The cubic used is given below:

$$\overline{R} = 3.67\text{x}10^{-10}\left(\frac{s}{\eta}\right)^3 + 7.18\text{x}10^{-6}\left(\frac{s}{\eta}\right)^2 - 0.059\left(\frac{s}{\eta}\right) + 851$$

for $2500 < s/\eta < 10\,000$. The extrapolated data are compared to the experimental results in Figure 73, plotted as $\overline{R}$ against s/η. It can be seen that for s/η values greater than 1500 asymptotic $\overline{R}$ values are approached, shown by the clustering of the suction coefficient data. Poll's extrapolated data predicts that natural transition will occur at values of $\overline{R}$ between 740 and 780, in the s/η range 1713 to 2300 and this matches the experimental data quite well. This would suggest that, for large suction coefficients, what has been seen is 'natural' transition behaviour, so that the relaminarised attachment-line behaves as though it had never been turbulent. The boundary layer holds no 'memory' of what occurred upstream and behaves as though the surface began at the end of the porous surface.

This is not the same thing as using suction to reduce the effective trip size from 4mm to zero. If this were the case the boundary layer would behave as though it had originated at the start of the model, 1320mm upstream of the end of the suction surface. This would give s/η values of the order of 7000 and Poll showed that this would cause the onset of transition at $\overline{R} \approx 650$. What has actually happened is that the suction surface has removed everything upstream of the end of the suction surface so the boundary layer behaves as though the leading edge physically begins at the end of the suction surface. The obvious explanation is that the suction surface was actually removing the entire boundary layer, so it actually was a new boundary layer at the end of the suction surface. This was not the case because the suction rates simply were not large enough. To remove the entire boundary layer would have required approximately 50% more suction than was used.

9.5 Conclusions

Measurements have been made for the conditions at the onset of transition for a relaminarised attachment-line flowing onto a non-porous surface. It has been found that,

for suction Reynolds numbers less than approximately –3.3, the conditions at transition onset are independent of the spanwise distance downstream of the end of the suction surface and that this is due to attachment-line contamination. For suction Reynolds numbers larger than this, at sufficiently large s/η values the $\overline{R}$ value at transition onset is independent of the suction Reynolds number. It has been shown that for these cases transition is occurring because of conditions on the non-porous surface, and a comparison with an extrapolation of Poll's[4] natural transition data shows good agreement. Therefore, the relaminarised flow behaves like a new laminar boundary layer developing on a smooth surface.

This has important implications for the spanwise extent of suction required to maintain laminar flow on a swept wing, showing that large suction rates are not required in a continuous strip along the entire leading edge of a wing. The porous surface could be split into patches, with the first patch used to relaminarise the attachment-line and subsequent patches using lower suction rates to delay the onset of natural transition. Of course, each patch could still be used to relaminarise the attachment-line if a gross source of turbulence appeared, for example an insect strike.

Conclusions

Experiments have been performed to investigate the effect of surface transpiration at, and near, the leading edge of a swept wing. The effect of transpiration on attachment-line and cross-flow transition has been studied and a single, overall conclusion can be made: small amounts of surface transpiration can effectively modify the state of the boundary layer at the leading edge of a swept wing. This modification may be beneficial (suction) or detrimental (blowing) for drag reduction, but the transpiration coefficients required are sufficiently small that design studies are being undertaken to quantify what practical effects HLFC would have on DOC, payload or fuel use.

More specifically, transition due to cross-flow instability near a laminar attachment-line has been studied. The experimental results have confirmed work by Danks[5] that, for a non-porous surface, the conditions at transition onset can be described by $\overline{R}$ and Re_x. A simple power law relation was derived which describes the data well.

On a porous surface, with no transpiration, it was found that the onset of transition occurred at a lower value of $\overline{R}$ than on a non-porous surface at the same Re_x. It was also found that the magnitude of this porosity penalty increased with Re_x. The reasons for this have not been identified, but it seems reasonable to assume that the surface roughness caused by the presence of the drilled holes imposed a stability penalty. A mathematical expression for this penalty was found, but since the roughness effect is probably affected by the hole size and drilling pattern the quantitative results can only be applied to the model used.

A quantitative study of the use of uniform distributed suction to delay the onset of crossflow transition was made, and it has been shown that only moderate suction levels are required. With suction, conditions at the onset of transition are a function of $\overline{R}$, Re_x, and C_q and a simple expression has been derived, adequately representing the data over a wide range of conditions.

The effect of two-dimensional trips on cross-flow instability was investigated. It was found that these had no measurable effect on crossflow transition, except where the trip contaminated the attachment-line.

On the attachment-line, the effect of transpiration on the state of the spanwise boundary layer was studied. Suction was applied in the immediate vicinity of a wing-fuselage junction. It was found that, for the experimental arrangement used, the boundary layer could not be relaminarised, even using suction coefficients ten times larger than those required for infinite swept conditions. From this it can be implied that it is more efficient to use suction away from the wing-fuselage junction.
The conditions required to relaminarise a fully turbulent attachment-line have been investigated up to $\overline{R}$ values of 1000. It was found that, as s/η tends to infinity, at constant $\overline{R}$ the suction coefficient required for relaminarisation tends to an asymptotic value. Also, it was found that there exists a suction coefficient at which turbulent attachment-line flow is impossible, at all values of $\overline{R}$, and this is approximately -0.0033.

Critical oversuction, an effect caused by very large suction levels introducing large disturbances into the boundary layer and causing transition to occur at a lower $\overline{R}$ than without suction, has been investigated. It was found that even with a C_q of -0.100 no adverse effects were seen. Data from a previous investigation were re-examined and compared with an empirical criterion taken from two-dimensional work by Ellis[84]. It was found that the data did not exceed Ellis's criterion, whereas data from the current work did.

The transition that occurs when a relaminarised attachment-line flows onto a non-porous surface was studied. It was found that, at large s/η, the $\overline{R}$ for retransition onset approached an asymptotic value independent of the suction coefficient used for relaminarisation. Transition onset occurred at $\overline{R} \approx 760$ which, at $s/\eta \approx 2400$, agrees well with work by Poll[62], for transition in the absence of a trip wire. Therefore, it seems that a relaminarised attachment-line flowing onto a non-porous surface behaves as though it had never been turbulent and undergoes 'natural' transition behaviour.
Finally, attachment-line blowing has been investigated. The results agree well with previous work by Danks[5]. The laminar attachment-line is very sensitive to blowing and this highlights the danger of a fault occurring in the suction system during flight, causing a reversal in the transpired flow. The results indicate that, at small $\overline{R}$, an asymptotic $\overline{R}$ limit exists below which blowing can not cause transition. This limit is probably at an $\overline{R}$ between 150 and 200.

Recommendations For Further Work

The following areas are recommended for further investigations into crossflow transition:

- A study should be conducted to find which part of the crossflow instability (stationary, travelling or high frequency) actually causes transition on a swept cylinder. To allow direct comparisons to be made with the work reported in this thesis the same model should be used (Section 5.2.4.2).
- More data is required for values of Re_x between 400 000 and 700 000. Also, data at values of Re_x greater than 1 000 000 would show whether there was an asymptotic $\overline{R}$ value below which crossflow transition could not occur, for a given suction coefficient. This will require a model with a significantly larger diameter than the one used here, possibly as much as twice as large, which in turn will require a larger wind tunnel than the Cranfield 8'x6' to avoid unacceptable blockage effects. A wind tunnel with a higher top speed could be used to reduce the required model diameter, but care would have to be taken not to invalidate the incompressibility assumption.
- The effect of two-dimensional trip-wires on crossflow transition up to an s/η of approximately 8000 and a d/η of approximately 4.5 should be investigated using a non-porous model (Section 5.4.5).
- The capability of suction to damp the effects of three-dimensional trips on crossflow transition should be studied. This would, essentially, be a study of the capability of suction to control crossflow transition caused by discrete particles (eg insects, dirt) on the surface. Radeztsky *et al*[40] looked at the effect of three-dimensional trips on

the crossflow instability and suggested that the vorticity from the trip interacted strongly with the crossflow. Flynn[86] studied the effect of three-dimensional trips without suction, so there is already a good database for comparison.

- The effect of combining suction on and off the attachment-line should be studied. In the current work suction on and off the attachment-line were used independently. Danks[5] looked at the combination of attachment-line and chordwise suction but he used the lower part of the model where the porosity is in discrete strips separated by strips of non-porous surface. Due to equipment deficiencies Danks was only able to do a qualitative study of the effects of non-uniform suction distributions on controlling boundary layer transition near the leading edge, so a quantitative study would be useful for investigating the value of using an automatic suction control system that would give the optimum suction distribution around the leading edge for given flow conditions. One of the objectives would be to develop an automated system for identifying transition and implementing a positive feedback system so that a system could automatically maintain laminar flow.

References

1 Thibert, J J and Reneaux, J and Schmitt, R V: ***ONERA Activities On Drag Reduction***. ICAS-90-3.6.1, Proceedings Of The 17th Congress Of The International Council Of The Aeronautical Sciences, pp1053-1059, 1990

2 Wilson, R A L and Jones, R I: ***Project Design Studies On Aircraft Employing Natural And Assisted Laminar Flow Technologies***. SAE Technical Paper Series 952038, Aerotech 95, Los Angeles, California, September 1995

3 Nitsche, W and Szodruch, J: ***Concepts And Results For Laminar Flow Research In Wind Tunnel And Flight Experiments***. Conference Proceedings, International Council Of The Aeronautical Sciences, Stockholm Sweden, 1990

4 Poll, D I A: ***Some Aspects Of The Flow Near A Swept Attachment-Line With Particular Reference To Boundary Layer Transition***. PhD Thesis, Cranfield Institute Of Technology, 1978

5 Danks, M: ***Issues Relating To Laminar Flow Control On The Leading Edge Of Swept Wings***. PhD Thesis, The University Of Manchester, June 1995

6 Smith, A and Poll, D I A: ***Instability And Transition Of Flow At, And Near, An Attachment-Line – Including Control By surface Suction***. NASA CR-1998-208443, July 1998

7 Smith, A and Poll, D I A: ***Effect Of Surface Suction On Cross-Flow Instability And Transition Occurring Near A Swept Attachment-Line***. College of Aeronautics Report CoA 9802, Cranfield University, 1998

8 Jones, R T: ***Effects Of Sweepback On Boundary Layer Transition And Separation***. NACA Report 884, 1948

9 Sears, W R: **The Boundary Layer Of Yawed Cylinders**. *Journal of Aeronautical Sciences*, Vol 15, pp28-34, 1948

10 Gray, W E: ***Laminar Flow At High Reynolds Number***. RAE Technical Memo (Aero) No. 98, June 1950

11 Gray, W E: ***The Effect Of Wing Sweep On Laminar Flow***. RAE Technical Memo 255, February 1952

12 Gray, W E: ***The Nature Of The Boundary Layer At The Nose Of A Swept Wing***. RAE Technical Memo 256, June 1952

13 Gregory, N and Walker, W S: ***The Effect On Transition Of Isolated Surface Excrescences In The Boundary Layer***. ARC Report No. 13436, October 1950

14 Owen, P R and Randall, D G: ***Boundary Layer Transition On A Swept Back Wing***. RAE Technical Memo 277, 1952

15 Owen, P R And Randall, D G: ***Boundary Layer Transition On A Swept Back Wing: A Further Investigation***. RAE Technical Memo 330, 1953

16 Gregory, N and Stuart, J T and Walker, W S: ***On The Stability Of Three-Dimensional Boundary Layers With Application To The Flow Due To A Rotating Disk***. Philosophical Transactions Of The Royal Society, Series A, Vol. 248, 1955-56, Pp155-199

17 Tollmein, W: ***Ein Allgemeines Kriterium Der Instabilität Laminarer Geschwindigkeits-Verteilungen***. Nachr. Ges. Wiss. Göttingen, Math. Phys. Klasse, Fachgruppe I, 1, 79-114, 1935

18 Anscombe, A and Illingworth, L N: ***Wind-Tunnel Observations Of Boundary Layer Transition On A Wing At Various Angles Of Sweepback***. Aeronautical Research Council Reports And Memoranda No. 2968, May 1952

19 Head, M R and Johnson, D and Coxon, M: ***Flight Experiments On Boundary Layer Control For Low Drag***. ARC Report R&M 3025

20 Pfenninger, W: ***Recent Developments In The Field Of Low Drag Boundary Layer Suction Research***. Report 262, AGARD Fluid Dynamics Panel, London, April 1960

21 Allen, L D and Burrows, F M: ***Flight Experiments On The Boundary Layer Characteristics Of A Swept Back Wing***. College Of Aeronautics Report No. 104, Cranfield Institute Of Technology, 1956

22 Burrows, F M: ***A Theoretical And Experimental Study Of The Boundary Layer Flow On A 45° Swept Back Wing***. College Of Aeronautics Report No. 109, Cranfield Institute Of Technology, 1956

23 Boltz, F W and Kenyon, G C And Allen, C Q: ***Effects Of Sweep Angle On The Boundary Layer Stability Characteristics Of An Untapered Wing At Low Speeds***. NASA Technical Note D-338, 1960

24 Brown, W B: ***A Stability Criterion For Three-Dimensional Laminar Boundary Layers***. Boundary Layer And Flow Control (Edited By G V Lachmann), Vol. 2, 1961, Pp913-923. Pergamon Press Ltd

25 Lin, C C: **On The Stability Of Two-Dimensional Parallel Flows**. *Quarterly Of Applied Mathematics,* 177, 1945-46

[26] Pfenninger, W: ***Flow Problems Of Swept Low Drag Suction Wings Of Practical Construction At High Reynolds Numbers***. Lecture Presented At Subsonic Aeronautics Meeting, New York, April 1967

[27] AIAA Astronautics And Aeronautics, Volume 4, Number 7, 1966

[28] Pfenninger, W: ***Laminar Flow Control – Laminarization***. Special Course On Concepts For Drag Reduction, AGARD Report 654, March 1977

[29] Gaster, M: **On The Flow Along Swept Leading Edges**. *The Aeronautical Quarterly*, May 1967

[30] Fisher, D and Fischer, M: ***The Development Flight Tests Of The Jetstar LFC Leading-Edge Flight Experiment***. NASA Symposium On NLF And LFC Research, NASA CP-2487, 1987, Pp117-140

[31] Maddalon, D V and Braslow, A L: ***Simulated Airline Service Flight Tests Of Laminar Flow Control With Perforated Surface Suction System***. NASA Technical Paper 2966, 1990

[32] Wagner, R D and Maddalon, D V and Fisher, D F: ***Laminar Flow Control Leading Edge Systems In Simulated Airline Service***. 16th Congress Of The International Council Of The Aeronautical Sciences, Jerusalem, Israel, August 1988

[33] Courty, J C and Bulgubure, C and Arnal, D: ***Studies On Laminar Flow Conducted At Dassault Aviation; Calculations And Test Flights***. Recent Advances In Long Range And Long Endurance Operation Of Aircraft, AGARD CP-547, 1993

[34] Collier, F S: ***An Overview Of Recent Subsonic Laminar Flow Control Flight Experiments***. AIAA-93-2987, 1993

[35] Maddalon, D V: ***Hybrid Laminar Flow Control Flight Research***. NASA TM 4331, 1991

[36] Bippes, H and Müller, B: ***Disturbance Growth In An Unstable Three-Dimensional Boundary Layer***. Numerical And Physical Aspects Of Aerodynamic Flows, Vol. IV (Editor T. Cebeci), Springer-Verlag, 1990

[37] Bippes, H: ***Experiments On Transition In Three-Dimensional Accelerated Boundary Layer Flows***. Proceedings Of The Royal Aeronautical Society Boundary Layer And Transition Control Conference, Cambridge, 1991

[38] Kohama, Y and Saric, W S and Hoos, J A: ***A High Frequency Secondary Instability Of Cross-Flow Vortices That Leads To Transition***. Proceedings Of The Royal Aeronautical Society Boundary Layer And Transition Control Conference, Cambridge, 1991

[39] Saric, W S and Krutckoff, T K and Radeztsky, R H: ***Visualisation Of Low-Reynolds-Number Flow Fields Around Roughness Elements***. Bulletin Of The American Physics Society, Vol. 35, No. 2262, 1990

[40] Radeztsky, R H and Reibert, M S and Saric, W S: ***Effect Of Micron-Sized Roughness On Transition In Swept Wing Flows***. AIAA 93-0076, 31st Aerospace Sciences Meeting, Reno, 1993

[41] Malik, M R and Li, F and Chang, C-L: **Crossflow Disturbances In Three-Dimensional Boundary Layers: Non-Linear Development, Wave Interaction And Secondary Instability**. *Journal Of Fluid Mechanics*, Vol. 268, 1994, Pp1-36

[42] Radeztsky, R H and Reibert, M S and Saric, WS: ***Development Of Stationary Crossflow Vortices On A Swept Wing***. AIAA 94-2373, 25th AIAA Fluid Dynamics Conference, Colorado Springs, 1994

[43] Dagenhart, J R: ***Crossflow Disturbance Measurements On A 45-Degree Swept Wing***. NASA TM-108650, 1992

[44] Reibert, M S and Saric, W S and Carrillo Jr, R B: ***Experiments In Nonlinear Saturation Of Stationary Crossflow Vortices In A Swept-Wing Boundary Layer***. AIAA 96-0184, 34th Aerospace Sciences Meeting And Exhibit, Reno, 1996

[45] Mullender, A J and Bergin, A L and Poll, D I A: ***Application of Laminar Flow To Aero Engine Nacelles***. Boundary Layer Transition and Control Report PNR-90916, ETN-92-92205, 1991

[46] Mullender, A J: ***The Application of Laminar Flow To Aero-Engine Nacelles***. PhD Thesis, The University Of Manchester, 1995

[47] Robert, J P: ***Drag Reduction: An Industrial Challenge***. AGARD Report 786, Special Course On Skin Friction Drag Reduction, March 1992

[48] Arnal, D and Juillen, J C: ***The Experimental Study Of Transition And Leading Edge Contamination On Swept Wings***. AGARD CP-438, 1988

[49] Reneaux, J and Preist, J and Juillen, J C and Arnal, D: ***Control Of Attachment-Line Contamination***. Second European Forum On Laminar Flow Technology, Bordeaux, France, June 1996

[50] Arnal, D and Reneaux, J and Casalis, G: ***Numerical And Experimental Studies Related To Skin Friction Drag Reduction Problems***. Proceedings of the Colloquium on Transitional Boundary Layers In Aeronautics, Royal Netherlands Academy Of Arts and Science, 1996

[51] Poll, D I A and Danks, M: ***Relaminarisation Of The Swept Wing Attachment-Line By Surface Suction***. IUTAM Symposium On Laminar-Turbulent Transition, Sendai, Japan, 1995

[52] Poll, D I A and Danks, M and Davies, A J: ***The Effect Of Suction Near The Leading Edge Of A Swept-Back Wing***. First European forum On Laminar Flow Technology, Hamburg, Germany, 1992

[53] Yardley, M R: ***An Investigation Into The Mechanisms Of Turbulent Boundary Layer Relaminarisation On Swept Wing Leading Edges***. PhD Thesis, The University Of Manchester, November 1995

[54] Johnson, P L: ***Effects of Suction on Crossflow Disturbance Growth – NASA/BCAG Crossflow Experiment Results***. World Aviation Congress and Exposition, Los Angeles, 1996

[55] Bippes, H and Lerche, T: ***Transition Prediction In Three-Dimensional Boundary-Layer Flows Unstable To Crossflow Instability***. AIAA 97-1906, 1997

[56] Gregory, N and Stuart, J T and Walker, W S: ***On The Stability Of Three-Dimensional Boundary Layers With Application To The Flow Due To A Rotating Disc***. Philosophical Transactions Of The Royal Society Of London, Series A, Vol.248, 1955, Pp155-199

[57] Emmons, H W: **The Laminar-Turbulent Transition In A Boundary Layer, Part 1**. *Journal Of Aerospace Sciences*, Vol. 18, 1951, Pp490-498

[58] Poll, D I A: ***The Development Of Intermittent Turbulence On A Swept Attachment-Line Including The Effects Of Compressibility***. College Of Aeronautics Report No. 8108, Cranfield Institute Of Technology, 1981

[59] Morkovin, M V: ***On The Many Faces Of Transition***. Viscous Drag Reduction (Editor C S Wells), Plenum, 1969, Pp1-31

[60] Morkovin, M V: ***Instability, Transition To Turbulence And Predictability***. Agardograph No. 236, 1977

[61] Choudhari, M and Streett, C L: ***Boundary Layer Receptivity Phenomena In Three-Dimensional And High-Speed Boundary Layers***. AIAA 90-5258. AIAA Second International Aerospace Planes Conference, Orlando, 1990

[62] Poll, D I A: **Transition In The Infinite Swept Attachment-Line Boundary Layer**. *The Aeronautical Quarterly*, Vol. XXX, Pp607-629, November 1979

[63] Cumpsty, N A and Head, MR: **The Calculation Of Three-Dimensional Turbulent Boundary Layers. Part II Attachment-Line Flow On An Infinite Swept Wing**. *The Aeronautical Quarterly*, Vol. XVIII, May 1967, Pp150-164

[64] Poll, D I A and Danks, M and Humphreys, B E: ***The Aerodynamic Performance Of Laser Drilled Sheets***. First European Forum On Laminar Flow Technology, DGLR-Bericht, 1992

[65] Anderson, J D Jnr: ***Fundamentals of Aerodynamics***. International Edition, 1991. McGraw-Hill

[66] Poll, D I A: **Transition Process On The Windward Face Of A Yawed Cylinder**. *Journal Of Fluid Mechanics*, Vol 150, pp329-356, 1985

[67] Poll, D I A: ***Three Dimensional Boundary Layer Transition Via The Mechanisms of Attachment-Line Contamination and Cross Flow Instability***. IUTAM Symposium On Laminar-Turbulent Transition, Stuttgart, Germany, 1979

[68] Müller, B and Bippes, H: ***Experimental Study Of Instability Modes In A Three-Dimensional Boundary Layer***. AGARD Conference Proceedings No. 438, Fluid Dynamics Of Three-Dimensional Turbulent Shear Flows And Transition, 1988

[69] Banks-Davies, L: Private Communication. Aerodynamics Department, Cranfield University, 1998

[70] Poll, D I A: ***Leading Edge Transition On Swept Wings***. AGARD Conference Proceedings, Laminar-Turbulent Transition, AGARD CP 224, 1977

[71] Gibbings, J C: ***On Boundary-Layer Transition Wires***. ARC CP 462, December 1958

[72] Gibbings, J C and Goksel, O T and Hall, D J: **The Influence Of Roughness Trips Upon Boundary Layer Transition, Parts 1, 2 And 3**. *Aeronautical Journal*, 90 (898-900), Pp289-301, 357-367, 393-398, 1986

[73] Hall, D J: ***Boundary Layer Transition***. PhD Thesis, The University Of Liverpool, 1968

[74] Danks, M and Poll, D I A: ***Non-Linear Instability And Transition In Flow Near A Swept Leading Edge***. IUTAM Symposium On Nonlinear Instability And Transition In Three-Dimensional Boundary Layers, pp133-146, 1996

[75] Hall, P and Malik, M R and Poll, D I A: **On The Stability Of An Infinite Swept Attachment-Line Boundary Layer**. *Proceedings Of The Royal Society Of London*, A, 395, pp229-245

[76] Theofilis: Private Communication. DLR, 1997.

[77] Gaster, M: **A Simple Device For Preventing Contamination On Swept Leading Edges**. *Journal Of The Royal Aeronautical Society*, Volume 69, P788, November 1965

[78] Bergin, A: ***Transition Characteristics Of A Swept Cylinder In The Presence Of A Large Streamwise End-Plate***. ICAS-90-7.9.1, ICAS Conference Proceedings, 1990

[79] Philips, D B and Cimbala, J M and Treaster, A L: **Suppression Of The Wing-Body Junction Vortex By Body Surface Suction**. *Journal Of Aircraft*, pp 118-122, Vol 29, No. 1, 1992

[80] Barber, T J: **An Investigation Of Strut-Wall Intersection Losses**. *Journal Of Aircraft*, Volume 15, No. 10, 1968, Pp676-681

[81] Arnal, D and Juillen, J C and Reneaux, J And Gasparian, G: **Effect Of Wall Suction On Leading Edge Contamination**. *Aerospace Science And Technology*, No. 8, Pp505-517, 1997

[82] Danks, M: Private Communication. BAe Airbus, 1996

[83] Head, M R: The Boundary Layer With Distributed Suction. ARC R&M No. 2783, 1955

[84] Ellis, J: ***Laminar And Laminarising Boundary Layers By Suction Through Perforated Plates***. Second European Forum On Laminar Flow Technology, Bordeaux, June 1996

[85] Bobbitt, P J and Ferris, J C and Harvey, W C: ***Hybrid Laminar Flow Control Experiment Conducted In NASA Langley 8-Foot Transonic Pressure Tunnel.*** NASA TP-3549, 1996

[86] Flynn, G A: ***Experimental Investigation Of Attachment Line Transition On A Large Swept Cylinder***. PhD Thesis, Cranfield University, 1997

Appendix A. Work Proposal For NASA Research Contract

DIAP/KW/1/73

Instability and Transition of Flow at, and near, an Attachment Line - including Control by Surface Suction.

Introduction

In the previous programme of work, carried out under contract number NAGW-3871 and reported in Danks and Poll (reference 1), a considerable amount of progress was made in the understanding of the transition process at, and near, an infinite swept attachment line. The research was carried out using the unique, large scale, suction cylinder model available in the Goldstein Laboratory at the University of Manchester. Specifically the following actions were carried out -

a) Signal records and spectra were obtained in flows subjected to large cross-flow induced, instability.

b) The effect of attachment-line transpiration upon cross flow transition was determined.

c) For a fixed sweep angle (60°), a number of distributions of suction which produced transition at a fixed chordwise location were recorded and it is clear that optimum suction distributions exist.

d) The effect of transpiration on stability and transition at the attachment line were investigated.

e) Possible linkage between attachment-line disturbance frequencies and the frequency of vortex shedding at the trailing edge was investigated.

and

f) An investigation was conducted into the propagation of gross disturbances through the attachment-line flow in the immediate vicinity of a wing-fuselage function.

As a result of this work and detailed discussions with research staff from NASA Langley and from Boeing, a new list of issues and questions has arisen. The objective of the present proposal is to present a programme of work which address the most important items on this list.

Proposal

In the second round of tests, the following items will be addressed in priority order.

a) An investigation of turbulent-to-laminar (relaminarisation) by suction at the attachment-line when the value of $\bar{R}$ exceeds 600.

b) A study of attachment-line transition situated by two-dimensional and three-dimensional excrescences (trips) situated on the suction surface.

c) An assessment of the effects of large suction levels on transition in the attachment-line boundary layer, i.e. critical oversuction, at $\bar{R}$ values up to 600.

d) An investigation of the transition which occurs when a relaminarised, attachment-line encounters a non-porous surface.

and

e) A study of the effect of attachment line suction on the spanwise propogation of gross disturbance in the fuselage-wing junction region.

The work divides itself, quite naturally into two parts- Phase 1 and Phase 2. In Phase 1 items a, b and c will be addressed. The model will be used in its conventional configuration (figure 1) except that larger sweep angles will be used to achieve higher maximum values for $\bar{R}$. First tests will be conducted with a sweep angle of 65° which allows an $\bar{R}_{max}$ of 900 to be achieved. Provided that this configuration gives no problems, additional tests will be conducted at a sweep angle of 70° giving a $\bar{R}_{max}$ of 1100.

Work under item a) will be conducted in the same way as that reported in Poll and Danks (reference 2). With hot-wire anemometers and flattened, surface - Pitot tubes mounted at various distances from the onset of the attachment-line suction, the tunnel speed at which transition begins for a fixed surface suction velocity will be noted. The primary objective will be to establish the validity of the postulation that, beyond a certain suction level, turbulent attachment-line flow cannot be achieved. In the first instance, the attachment-line flow ahead of the suction surface will be tripped with a 4 mm diameter wire (as before). However, a test will also be performed in which the attachment line is contaminated with a streamwise, end-plate simulating a wing-body junction. The same experimental techniques will be used for item b). However, in this case, the attachment line will be laminar and the effect of 2-D trip wires and 3-D cylindrical trips (made up from disks of adhesive tape) will be investigated. Finally, with no artificial disturbances introduced into the attachment-line flow, the suction levels will be increased to their maximum values in order to determine whether, or not, critical suction levels exist.

The items d) and e) will be addressed in Phase 2 of the work. However, in order to achieve the necessary configuration of the suction surfaces relative to the upstream tip, the model has to be mounted upside down. This will necessitate some modification to the model - in particular a strengthening of the base section to allow it to take the full weight when the model is in its new position. The work will be carried out in our own workshops and only a relatively small amount of structural modification is required. With the model in its new position, the transition behaviour of a relaminarised attachment-line boundary layer as it encounters a solid surface can be determined. Finally, the end-plate system developed and used in the work described in reference 1 will be used to assess the ability of attachment-line (and off attachment-line) suction to suppress gross contamination emanating from a simulated wing-fuselage junction.

Workforce

It is proposed that the work be undertaken by a Research Assistant (to be appointed) and Professor D.I.A. Poll. The Research Assistant will be full time and Professor Poll would spend approximately ½ day per week on the project. A part time laboratory

technician will also be required. Direct involvement and interaction with NASA Langley personnel would be expected and welcomed.

Timescale

The project will run for 6 months and will start upon receipt of a contract. A meeting will be held at NASA Langley after three months. Data will be presented and progress reviewed. Modifications to the work programme may be considered at this stage. At the end of the contract a final meeting will be held where all the work will be presented.

Deliverables

One intermediate progress report (3 months) and a comprehensive final report will be produced. Conference and journal papers could be produced as deemed appropriate by NASA.

Appendix B Work Proposal For DRA Research Contract

DIAP/LJ/4530

Proposal for Programme of Research on the Instability and Transition of flow near an Attachment Line - including control by surface suction

Professor D.I.A. Poll

Department of Engineering

University of Manchester

Introduction

In recent years considerable interest has been shown in the problem of boundary layer transition in the leading edge region of a swept wing. The principal reason for this is that, at scales typical of those encountered in flight, transition to turbulent flow may occur there due to one of four reasons

1. Spanwise turbulent contamination of the attachment-line flow by disturbances emanating from the wing/fuselage junction or by roughness elements located on, or near, the attachment line.
2. "Natural" transition in the attachment-line flow due to a classical viscous instability.
3. "Natural" transition to turbulence near to the attachment line resulting from an inviscid instability of the cross-flow in the three-dimensional-boundary layer.
4. Transition due to the effect of surface roughness in the region of developing cross-flow.

If transition is promoted by any of the above, the flow over the wing is likely to be fully turbulent. Consequently, these are seen as barrier issues for the achievement low drag (laminar flow) aircraft and a more complete understanding of the various phenomena is a necessary prerequisite to successful design. Most important of all is the

understanding of the mechanisms which are available for control of the transition process - especially surface suction.

The transition research group at the University of Manchester has developed considerable expertise in the field of transition research especially in relation to the problems of transition on swept back wings. Of particular significance has been the design, building and testing of a large, swept-cylinder model. This comprises a 16" diameter circular cylinder which is faired from the maximum thickness positions to form an "aerofoil" with a thickness-to-chord ratio of 50% and a the design leading edge sweep angle of 60° - see figure 1. The cylinder itself was fabricated from a flat sheet of titanium 1.2mm thick. This was perforated, using the laser drilling technique, with holes 50μm in diameter. These were arranged with a "row to row" and "column to column" separation of 8 hole diameters (400μm). Moreover, in order to break up the spacing of those holes distributed along the attachment line, the rows were skewed by 14° relative to the plate centre line. Doing this guarantees that there is no spatial regularity of hole spacing along any flow streamline. The plate was drilled as shown in figure 2 allowing two separate areas for experimentation. At the upstream end, the drilled area does not extend to the attachment line and is intended, primarily, for the study of suction on cross flow instability. The hole pattern is uniform and the transpired air is gathered into eight plenum chambers. Walls between the chambers are very thin allowing a nearly continuous distribution of suction to be applied. At the downstream end, the suction is arranged in discrete strips separated by undrilled areas. There are four such strips with the first located under the attachment-line area. Each strip has two independently controlled plenum chambers and this allows different distributions of suction to be applied.

The model is mounted in a large, low-speed wind-tunnel with a cross section

measuring 2.77m x 2.13m and which is capable of free stream velocities of up to 65m/sec. The mean, unfiltered, free-stream turbulence level is approximately 0.1% over the whole speed range. Under normal conditions the model is mounted vertically with the upstream tip set approximately 0.3m below the tunnel roof. This ensures that there is no accidental contamination of the attachment-line flow by the turbulent boundary layer formed upon the tunnel roof. All the pipework for the suction system is fed out through the tunnel floor and is connected to a series of valves and flow meters (rotameters). Beyond the valves, all the pipes are connected to a single large plenum chamber which is linked to the laboratory vacuum tanks.

To date all the preliminary calibration measurements have been made e.g. surface pressure distribution, pressure drop versus mass flow rate for the plenum chambers, blockage correction as a function of sweep angle, etc. It has been demonstrated that on the blank parts of the model attachment-line instability and cross flow instability occur at the same conditions as those observed on the geometrically similar but half sized model previously used by Poll[1,3]. Moreover, preliminary tests with the suction system clearly indicate that suction can be used to control the instability and the transition process with great precision. In order to give an idea of the range of parameters which can be investigated with this model, we note that the attachment line similarity parameter $\bar{R}$ has a range

$$0 < \bar{R} < 1100$$

whilst the cross flow Reynolds number

$$0 < \chi < 450$$

These levels are much higher than those encountered near the leading edges of the current generation of civil transport aircraft but are typical of those anticipated on next generation Ultra High Capacity Aircraft. Therefore, this model has the potential for

investigating flows at a super flight scale.

In order to ascertain the relevance of the cylinder results in relation to flight we can make use of dimensional analysis. To begin with we note that, in general, the chordwise velocity distribution for a lifting aerofoil can be expressed as a power series

$$\frac{U_e}{V_\infty} = A\left(\frac{x}{C_o}\right) + B\left(\frac{x}{C_o}\right)^2 + C\left(\frac{x}{C_o}\right)^3 + \ldots$$

where x is the surface distance from the attachment line (x = 0) measured in a plane normal to the leading edge and C_o is the normal to leading edge chord. As the flight Reynolds number increases transition is expected to move closer and closer to the leading edge and, at some sufficiently large Reynolds number, transition will occur in a region of the aerofoil for which

$$\frac{U_e}{U_\infty} \simeq A\left(\frac{x}{C_o}\right)$$

If, in addition

a) the leading edge flow is infinite swept i.e. the mean boundary layer has no spanwise variations

b) the flow outside the boundary layer is isentropic

c) the flow outside the boundary layer is homenergic

d) the wall temperature is constant at Tw

and e) if surface suction, w(o), is applied, it is constant i.e. not a function of x

then any property of the boundary layer flow (including transition) can be expressed in terms of the parameters

V_Λ, T_Λ, ρ_Λ, μ_Λ, Cp, R, K, x, Tw and w(o)

where suffix A refers to conditions at the attachment line (i.e. V_Λ is the spanwise velocity), R is the gas constant and K is the chordwise velocity gradient -

$$K = \left(\frac{dU_e}{dx}\right)_{x=0}$$

This problem has 10 independent variables with 4 dimensions i.e. length, mass, time and temperature. It follows that it is governed by 6 non-dimensional groups. These are

$$\left(\frac{V_A^2}{\nu_A K}\right)^{1/2}, \left(\frac{x^2 K}{\nu_A}\right), M_A, \gamma, \frac{Tw}{T_A} \text{ and } \frac{w(o)}{V_A}$$

or

$$\bar{R}, \frac{U_e x}{\nu_A}, M_A, \gamma, \frac{Tw}{T_A} \text{ and } \frac{w(o)}{V_A}$$

If, in addition, we limit consideration to situations with no heat transfer at the surface and restrict the gas to air then the governing groups are

$$\bar{R}, \frac{U_e x}{\nu_A}, M_A \text{ and } \frac{w(o)}{V_A}$$

The important points to note from this result are that -

1. The flow is <u>not</u> aware of the wing sweep angle.
2. The relevant Mach number is the spanwise Mach number i.e. the flow is <u>not</u> aware of the free stream Mach number.

and 3. The flow is <u>not</u> aware of the geometry of the wing since the geometry dependent variable is K and it never appears alone.

It follows that, a cylinder tested at large angles of sweep in a conventional, low speed, wind tunnel is capable of producing data which are relevant to flight conditions for aerofoils of arbitrary geometry - provided that the flight conditions are such that transition is very close to the attachment line - a situation which will be relevant to all but the smallest civil transport aircraft.

To demonstrate the validity of the arguments the proposed scaling is applied to data obtained in previous tests. Figure 3 shows transition data for a range of free stream

Reynolds numbers, sweep angles and chordwise locations for a model which is half the size of the current suction model - see reference 1. Preliminary measurements with the suction model, reported in reference 2, show that, in this set of coordinates, the transition data for both models is the same, as shown in figure 4. The new scaling has been applied to all the data and the results are shown in figures 5 and 6. The impressive collapse validates the scaling arguments. However, it is also clear that the existing cross-flow transition data cover the region when $\bar{R}$ exceeds 400. In the flight case, typical $\bar{R}$ values for most aircraft are below 400 and, consequently there is a need to obtain information at lower values of $\bar{R}$ (but higher values of $(U_e x/\nu)$). The large suction model is well suited to this.

Figure 6 shows the region of primary interest for flight - indicated with a question mark - together with the line of maximum performance for the wind tunnel/model combination. It is clear that the region of interest can be covered comprehensively by varying the model sweep angle between 10° and 50° (in tests to date the sweep angle has been fixed at 60°). In terms of the chordwise Reynolds number ($(U_e x/\nu)$ this would extend the range investigated from 10^6 to 3×10^6. A complete figure 6 would allow designers to estimate the conditions necessary for transition to occur in the immediate vicinity of the leading edge with a high degree of certainty - much higher than is currently the case with stability methods.

Proposed Work Package

It is proposed that the suction cylinder be used to address the following problems.

1. For the case with smooth surface and zero suction, complete the picture indicated in figure 6 so that the existing cylinder data can be linked with the existing data for conventional aerofoils contained in references 4, 5 and 6.

2. To investigate the effect of surface suction by repeating the tests in (1) for a range of constant values of the suction parameter, $w(o)/W_A$. This will produce a family of curves in the coordinate system of figure 6.

and

3. To investigate the effects of isolated roughness both on the attachment line in the presence of surface suction and in the region of cross-flow instability both with and without suction.

In addition to the above, a complete review of all the available experimental data will be undertaken and a data base will be established. As well as providing information directly applicable to design i.e. information which enables design decisions to be taken, the exercise will provide a challenging test case for the transition prediction tools. Most importantly the experiments will produce a series of high quality results which will indicate parametric trends and, as such, will be much more valuable than "single point" experiments.

Workforce

It is proposed that the work be undertaken by a postgraduate research assistant under the direct supervision of Professor D.I.A. Poll. The research assistant would be full time and Professor Poll would spend approximately ½ day per week on the project. A laboratory technician would also be required on a part time basis.

Timescale

The project would run for 3 years in the first instance and would start upon receipt of a contract. Progress meetings will be held quarterly.

References

1. Poll D.I.A. Some observations of the transition process on the windward face of a long yawed cylinder. Journal of Fluid Mechanics vol 150 pp 329-356, 1985.

2. Poll D.I.A., Danks M. and Humphreys B.E. The aerodynamic performance of laser drilled sheets. Proceedings of the First European Forum on Laminar Flow Technology, March 1992. Hamburg FRG.

3. Poll D.I.A., Danks M. and Davies A.J. The effect of suction near the leading edge of a swept-back wing. Proceedings of the First European Forum on Laminar Flow Technology, March 1992, Hamburg FRG.

4. Anscombe, A. and Illingworth, L.N. "Wind-tunnel observations of boundary-layer transition on a wing at various angles of sweepback". ARC R & M 2968, May 1952. (RAE/TN/Aero - 2170)

5. Gregory, N. and Walker, W.S. "Brief wind tunnel tests on the effect of sweep on laminar flow".

6. Boltz, F.W., Kenyon, G.C. and Allen, C.Q. "Effect of sweep angle on the boundary layer stability characteristics of an untapered wing at low speeds". NACA TN-D 338, July 1960.

Figure 1 Schematic of the Swept Cylinder Model in the Goldstein Lab. 2.74m x 2.13m Low Speed Wind Tunnel

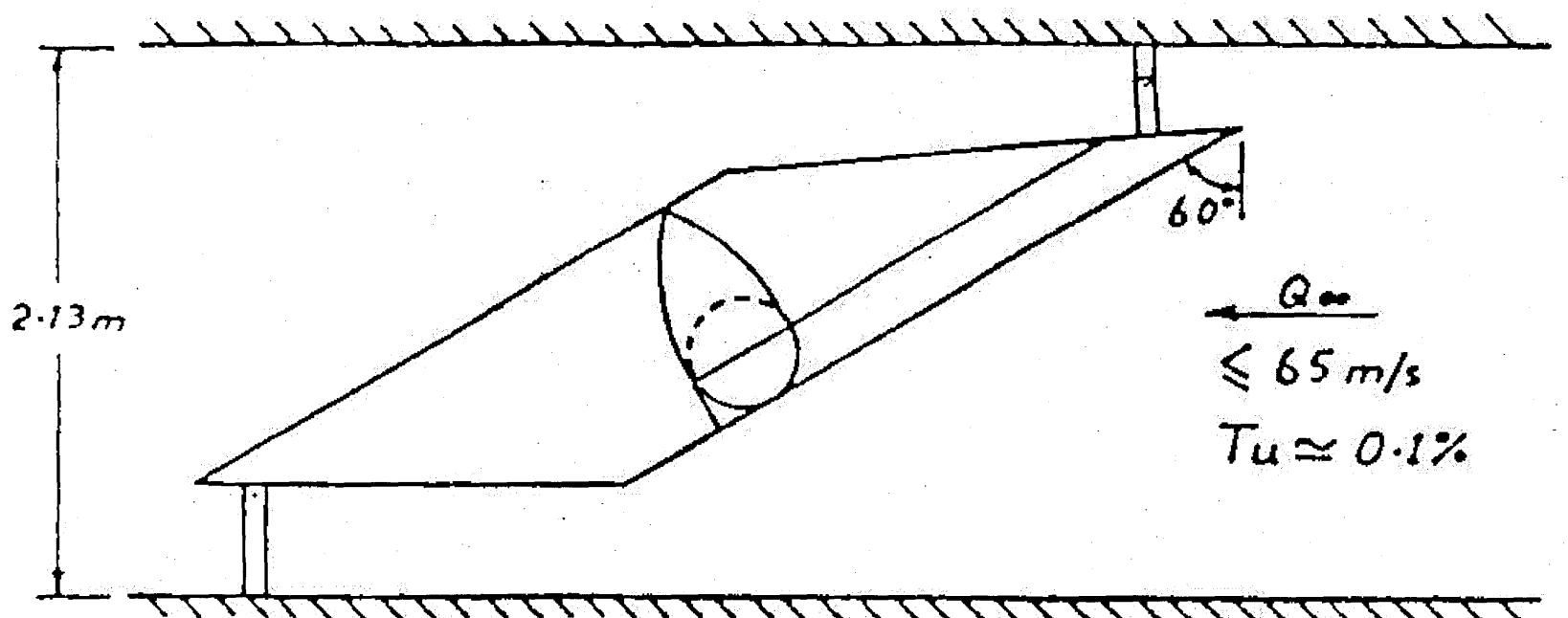

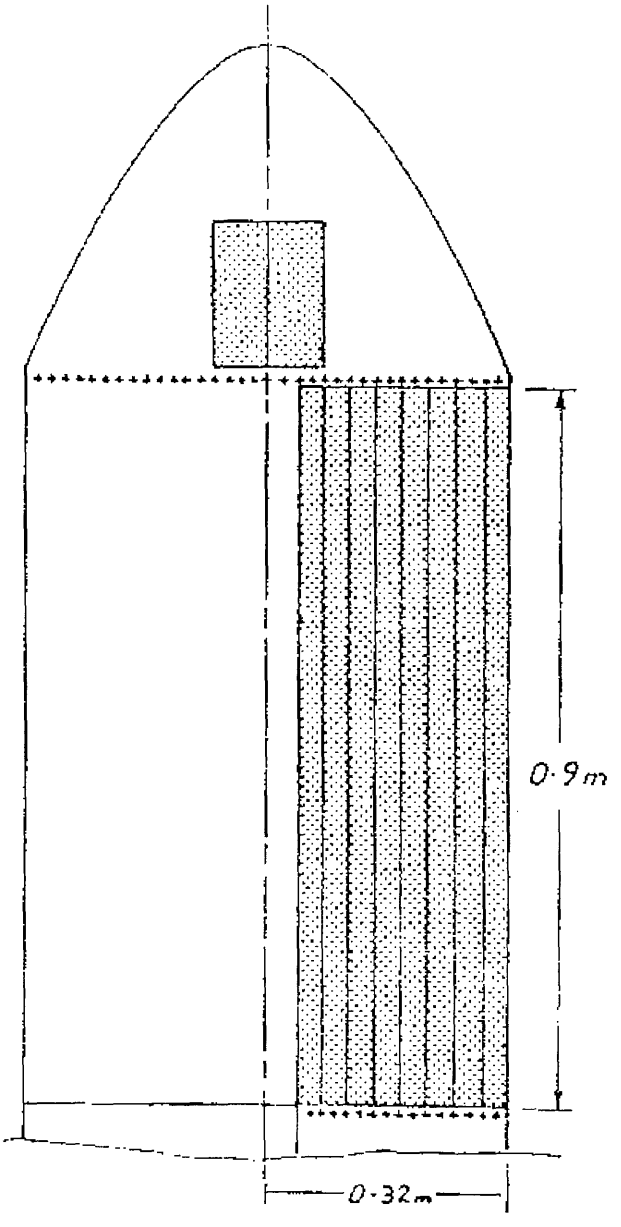

Hole Diameter = 50 μm
Hole Separation = 400 μm

Drilled Pattern Skewed at
14° to the Attachment Line.

Figure 2 Schematic View of the Titanium Surface.

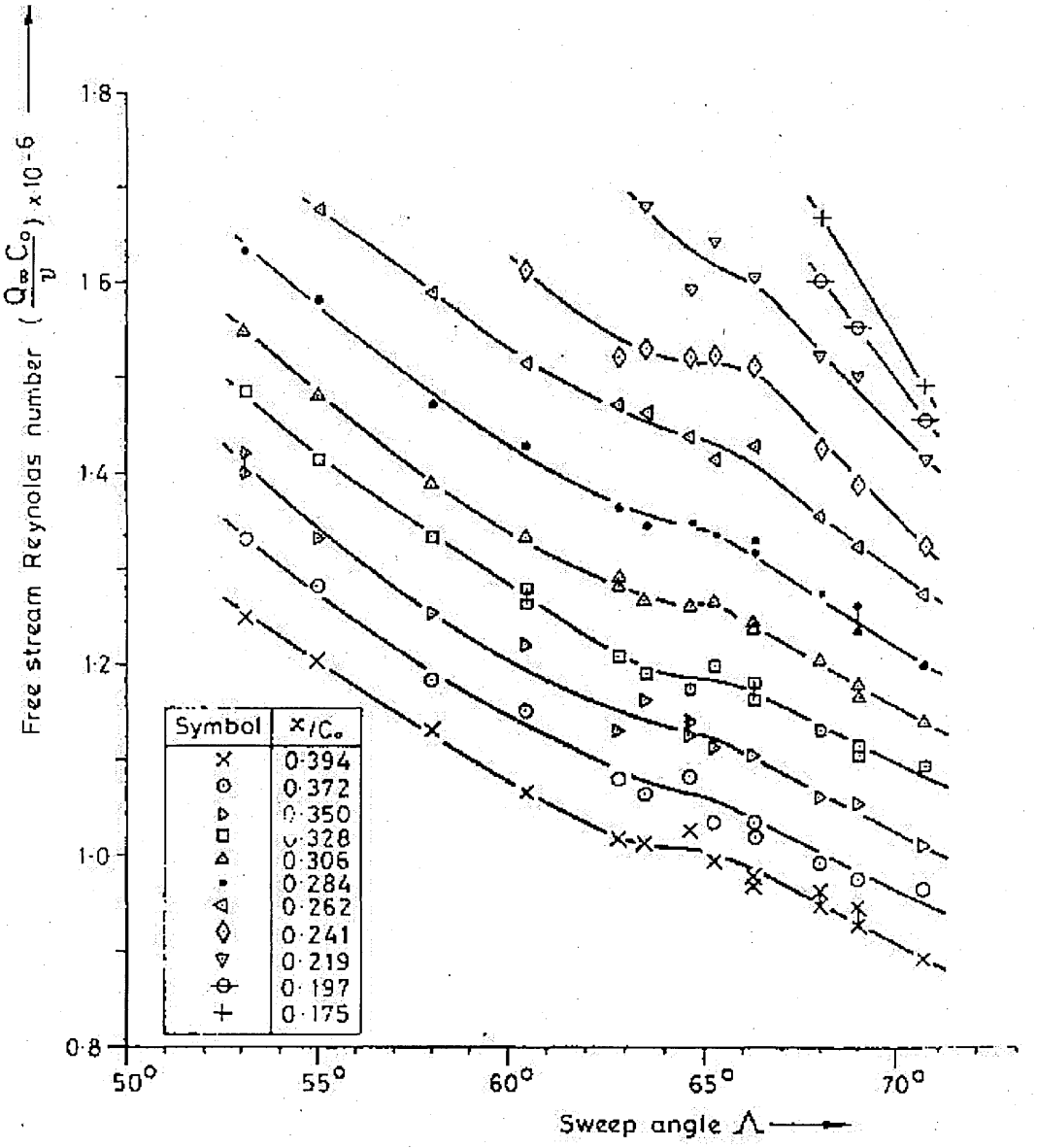

Fig. 7.3 Variation of free stream Reynolds number with chordwise position and sweep angle for the beginning of transition.

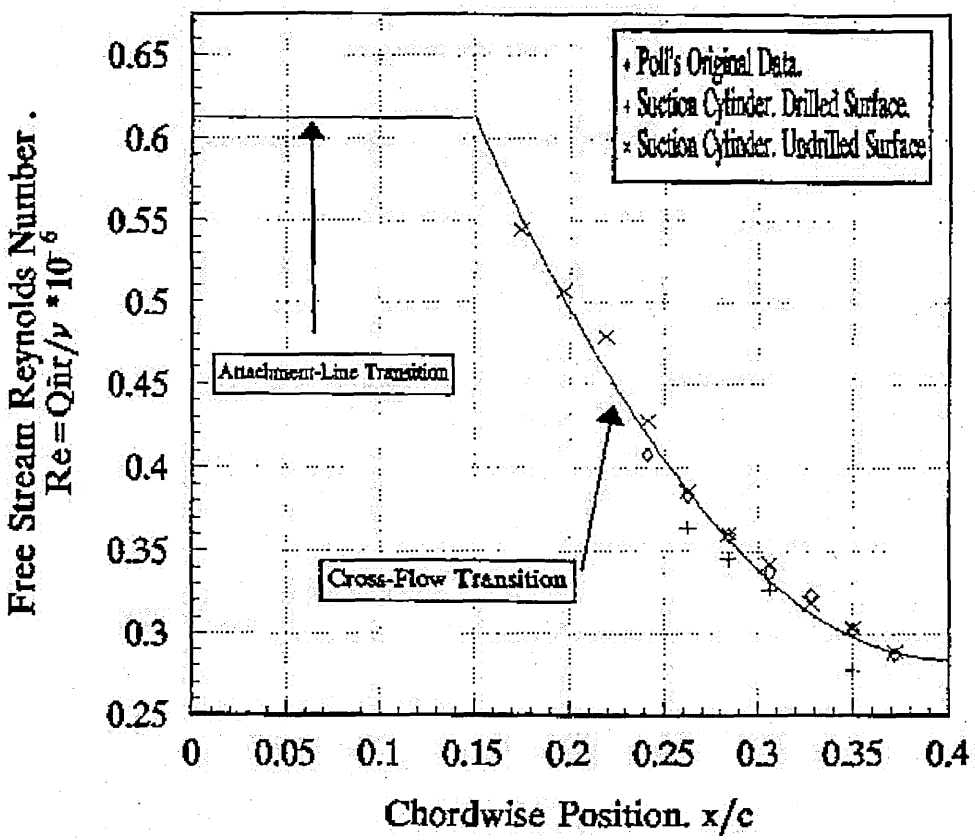

Figure # 4 Results for Transition via Cross-Flow Instability without Transpiration.

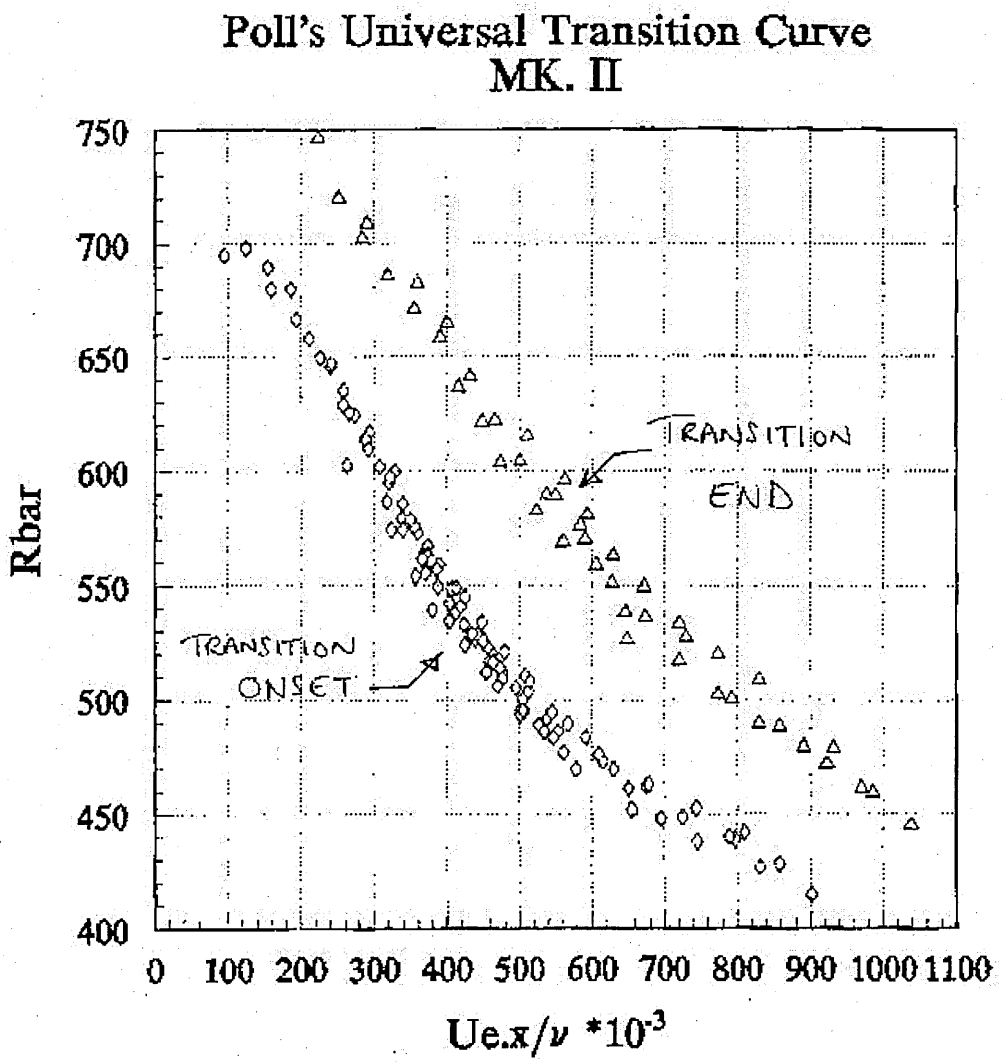

FIGURE 5 RESULTS FOR TRANSITION CAUSED BY CROSS-FLOW INSTABILITY.

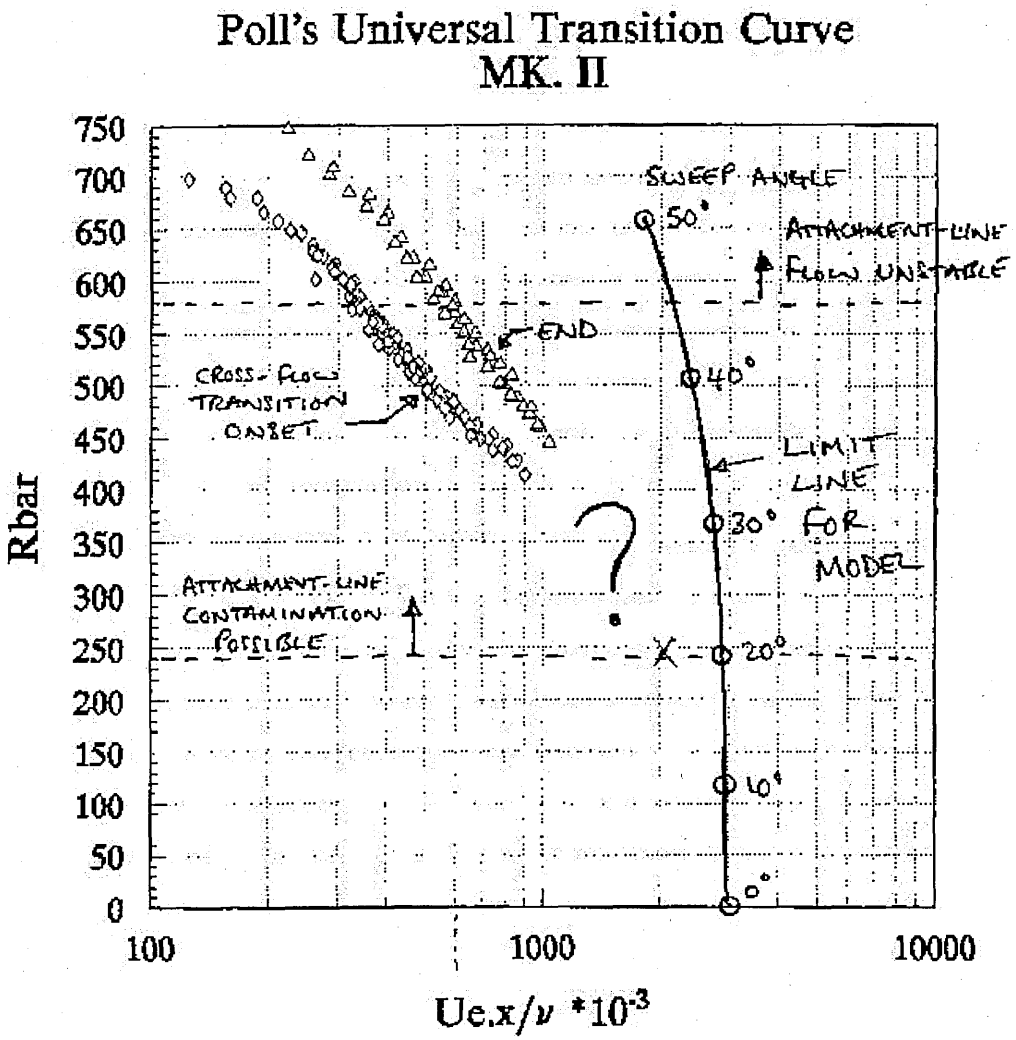
Poll's Universal Transition Curve
MK. II
Rbar
750
700
650
600
550
500
450
400
350
300
250
200
150
100
50
0
100
1000
10000
Ue.x/ν *10-3
SWEEP ANGLE
50°
40°
30°
20°
10°
0°
ATTACHMENT-LINE
FLOW UNSTABLE
END
CROSS-FLOW
TRANSITION
ONSET
LIMIT
LINE
FOR
MODEL
ATTACHMENT-LINE
CONTAMINATION
POSSIBLE
?

FIGURE 6

Appendix C. Calculation of Freestream Turbulence

Introduction

Receptivity, as discussed in Section 2.5, is the mechanism by which environmental disturbances enter a laminar boundary layer and interact with the flow to produce instability waves. The freestream flow can be a source of environmental disturbances so it is important to measure the freestream turbulence levels. The turbulence intensity, Tu, can be defined as

$$Tu \equiv \frac{\sqrt{\overline{Q'^2}}}{Q_\infty}$$

where Q' is the perturbation in the direction of the freestream flow vector. The resultant perturbation Q' is composed of three components: u', v' and w' which are the perturbations in the U, V and W velocity axes respectively. The u' component is commonly used to describe the turbulence characteristics of a wind tunnel because this is usually the largest component. It has been found previously[1] that freestream u' turbulence levels of less than 0.8% do not cause premature transition. However, low speed wind tunnels with turbulence reducing screens have much lower u' turbulence levels. The Cranfield 8'x6' wind tunnel had a nominal, quoted u' turbulence of approximately 0.1%[2] but it was decided to measure the u' turbulence levels throughout the dynamic pressure range, both with and without the model present, in case turbulence levels increase unacceptably at high freestream velocities. Because of the turbulence reduction screens in the wind tunnel it was expected that the turbulence level would be fairly uniform across the dynamic pressure range and that the presence of the model would have little, or no, effect.

Turbulence intensities were calculated for the empty working section and then with the model present (the model was swept at 60°, typical of experimental configurations).

Experimental Method

The same method was used for the empty working section and with the model in the working section. The hot-wire was secured, parallel to the floor, approximately at the vertical centre of the working section, just upstream of the model position and equidistant from the walls. When the model was present it was swept at 60°.

At each freestream dynamic pressure test point, the wind tunnel speed was set and allowed to stabilise and then the voltage output from the hot-wire was monitored for a total time of three minutes using a digital volt meter (DVM). The DVM allowed the measurement of AC and DC voltages, either instantaneous values or root mean square (RMS) values over a specified time period sampled at 50Hz. It would also measure the maximum and minimum values over a specified time period, again either instantaneous or RMS values. The RMS values were calculated by measuring the DC hot-wire output for a period of 30 seconds at a frequency of 50Hz, giving six RMS values over the three

minute test point. The maximum and minimum DC RMS voltages were then simply the maximum and minimum from these six values.

The DC hot-wire output was used to calibrate the output of the hot-wire to the wind tunnel dynamic pressure. The AC component of the hot-wire output was used to calculate the variation about the DC calibration value (ie the turbulence perturbation). For each test point, the ambient temperature and pressure were also measured.

From the RMS DC data, the hot-wire was calibrated against freestream dynamic pressure by plotting the square of the average DC RMS value over the three minute test period, $\overline{\text{RMS Volts}}^2$, against the dynamic pressure. The square of the average DC RMS value was calculated from

$$\overline{\text{RMS Volts}}^2 = \frac{\text{RMS Volts}^2_{max} + \text{RMS Volts}^2_{min}}{2}$$

Figure C1 shows the data for the empty working section. A quadratic polynomial curve fit was then applied to the data to give an expression relating dynamic pressure and the DC voltage output from the hot-wire, which is shown on the Figure. This curve fit matched the data to within ±0.1%. This curve fit was then differentiated with respect to $\overline{\text{Volts}}^2_{rms}$, to get the gradient of the hot-wire calibration curve.

The AC component of the hot-wire was the fluctuating variation in dynamic pressure, which was the u' perturbation, and the maximum and minimum AC voltages at each dynamic pressure test point gave the magnitude of the perturbation. The gradient of the hot-wire calibration curve was used with the maximum (most positive) and minimum (most negative) AC voltage data to find the variation in dynamic pressure about the freestream average by

$$\Delta q_{max} = \frac{d(q)}{d(\overline{\text{RMS Volts}}^2)} . \max V_{AC}$$

and

$$\Delta q_{min} = \frac{d(q)}{d(\overline{\text{RMS Volts}}^2)} . \min V_{AC}$$

Dividing these differences by the dynamic pressure at that test point and taking the square roots gives the maximum and minimum u' turbulence levels.

Results

The maximum and minimum turbulence levels are given for the empty working section and with the model in place in Figure C2. From these it can be seen that the maximum u' turbulence level is approximately 0.1%, the quoted nominal value for the Cranfield

8'x6' wind tunnel, and that, as expected, the presence of the model has little effect. It can also be seen that the u' turbulence level does not increase at large dynamic pressures so experiments can be conducted across the whole range of freestream velocities.

References

1 Schlichting, H: **A survey of some recent research investigations on boundary layers and heat transfer**. *Journal of Applied Mechanics*, June 1971, pp289-300

2 Banks-Davies, L: Private Communication. Aerodynamics Department, Cranfield University, 1998

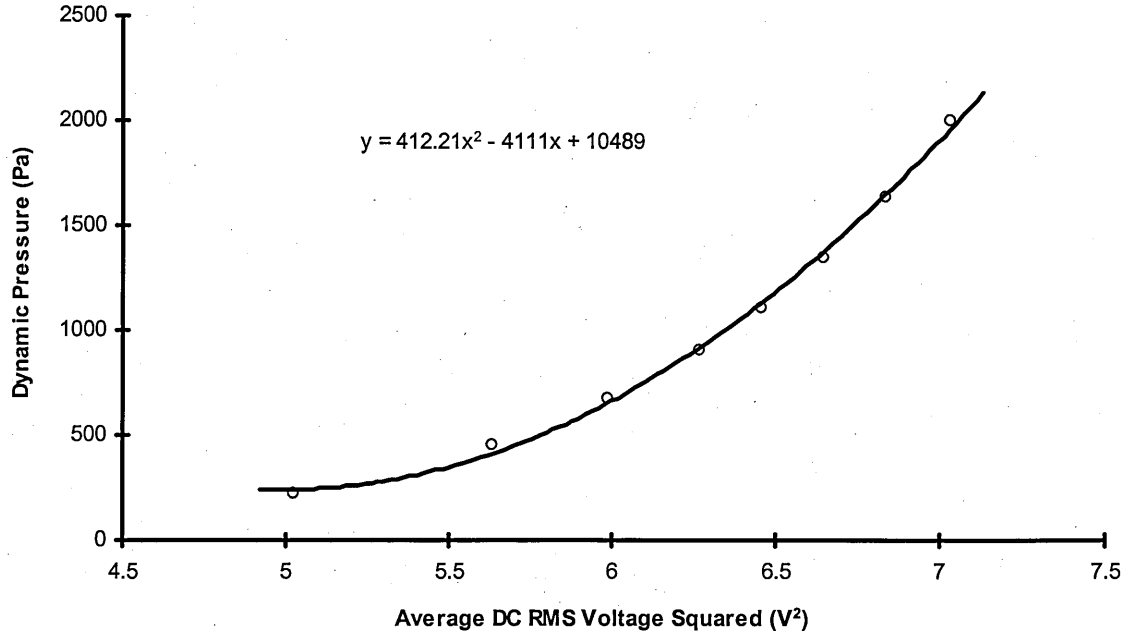

Figure C1. Calibration of Hot-Wire In Empty Working Section

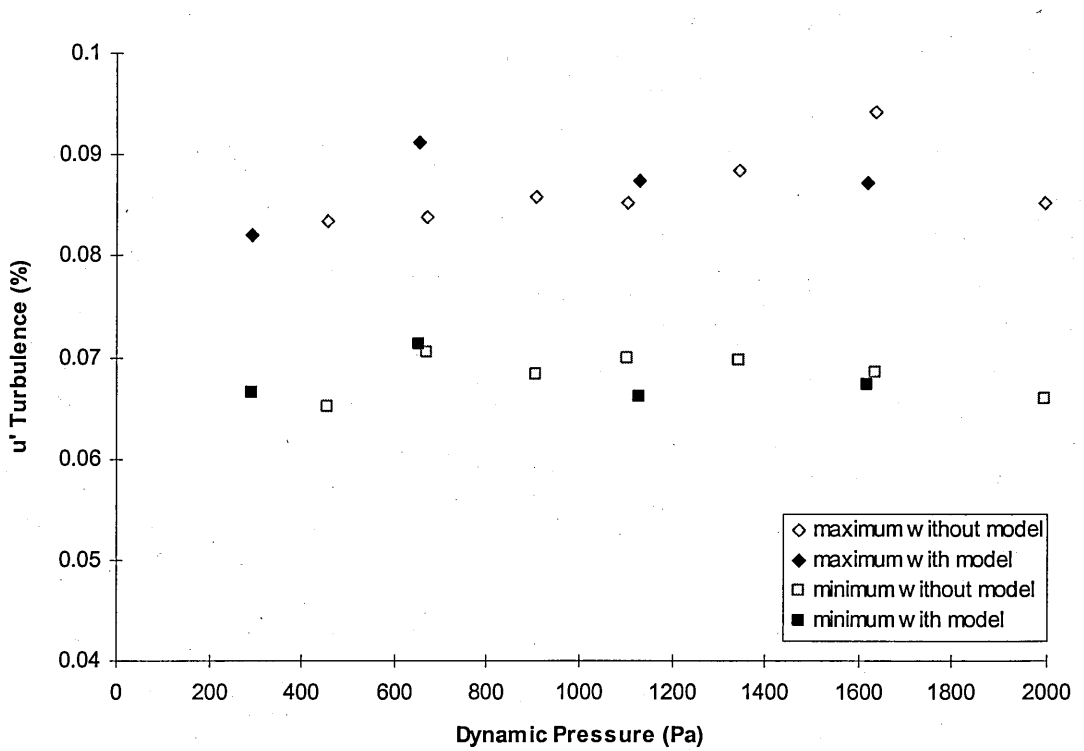

Figure C2. Maximum and Minimum u' Turbulence Levels With And Without Model

Appendix D. Wind Tunnel Calibration

The freestream velocity along the axis of the wind tunnel is required, so this must be measured somehow. One method sometimes used is to have a pitot-static tube in the wind tunnel during the tests and use this to measure the dynamic pressure. However, this is only possible if the pitot-static is outside the model's pressure field. The most common method is to calibrate the wind tunnel without the model present and then apply the calibration to the test results[1]. The wind tunnel was calibrated using a Pitot static tube, set up as shown in Figure D1. The Pitot-static probe was arranged on the centre-line of the wind tunnel and in the middle of the working section (approximately the position the model would occupy), so that the empty tunnel dynamic pressure at the model position could be measured. This dynamic pressure was then compared with the reduction in static pressures across the contraction cone. This method assumes that the total pressure is constant throughout the contraction cone and the working section and that Bernoulli's equation is valid, so the flow must be attached throughout the contraction. The dynamic pressure in the working section and the contraction cone static pressures are then related by

$$q_\infty = p_1 - p_2$$

where q_∞ is the dynamic pressure in the working section at the model position, p_1 is the static pressure at the start of the contraction cone and p_2 is the static pressure at the end of the contraction cone. Each static pressure was the average of five static pressure ports distributed equally around the circumference of the wind tunnel. The results of the calibration are shown in Figure D2, with a linear least-squares trendline fitted to the data, the calibration equation and the R^2 value showing how well the equation represents the data. $R^2 = 0.99987$ shows excellent agreement with the linear trendline. The calibration is

$$q_\infty = 1.1436 * \Delta p + 1.8$$

where Δp was the static pressure difference reading during the test, in mm H_2O.. The static pressure difference was displayed in the tunnel control room by a Furness differential pressure transducer, in units of mm H_2O. The experimental data was converted to dynamic pressure, in Nm^{-2}, using the formula

$$q_\infty (Nm^{-2}) = (1.9 - \Delta p_0) * (1.1436 * \Delta p) * 9.80665$$

where Δp_0 was the Furness reading without the tunnel running (the zero value), in mm H_2O.

The results from several previous calibrations are shown in Table D1, below. The calibrations by Bray and Broadley were done within a year of the current calibration, while Flynn's results were done 4 years before and Kanichi's approximately 3 years previous. All of the calibrations are similar, with Flynn's being slightly lower than the rest. However, the calibrations are all sufficiently similar to give confidence in the calibration obtained here.

Calibrator	Calibration Equation (neglecting offset)
Smith	$q = 11.219\Delta p$
Bray	$q = 11.572\Delta p$
Broadley	$q = 11.435\Delta p$
Kanichi	$q = 11.1244\Delta p$
Flynn	$q = 10.876\Delta p$

Table D1. Previous Calibration Equations

References

[1] Rae, W H and Pope, A: ***Low-Speed Wind Tunnel Testing***. 2nd Edition, 1984. John Wiley and Son

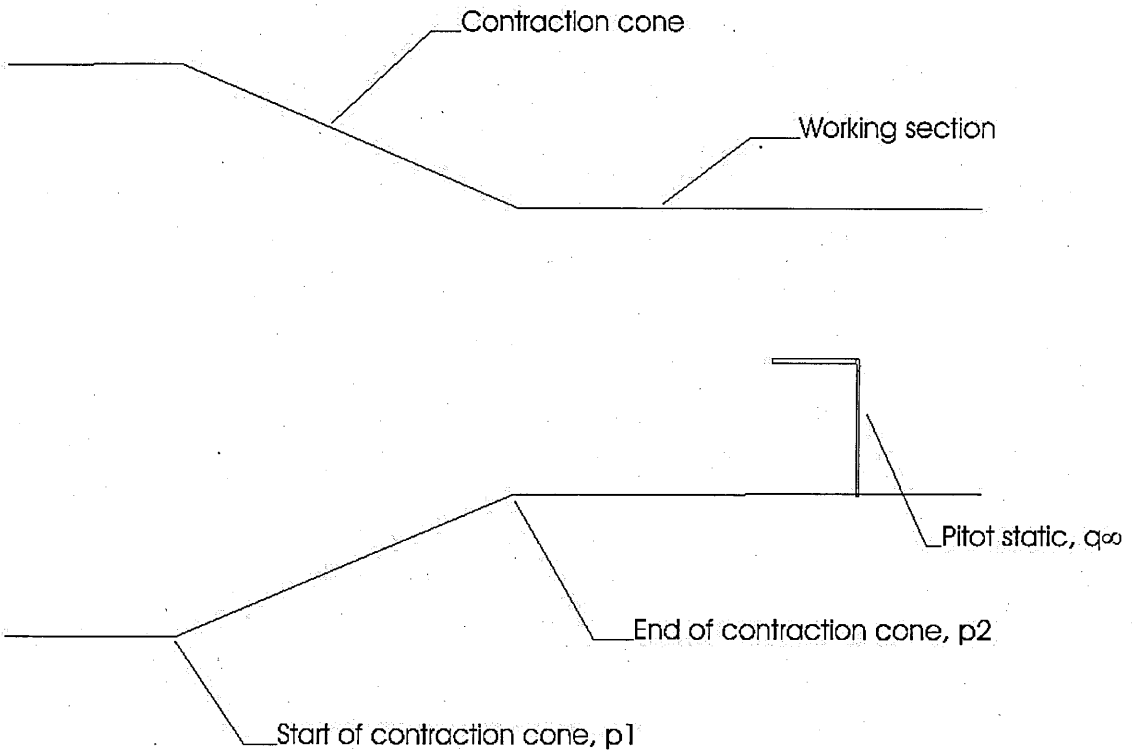

Figure D1. Wind Tunnel Arrangement for Calibration

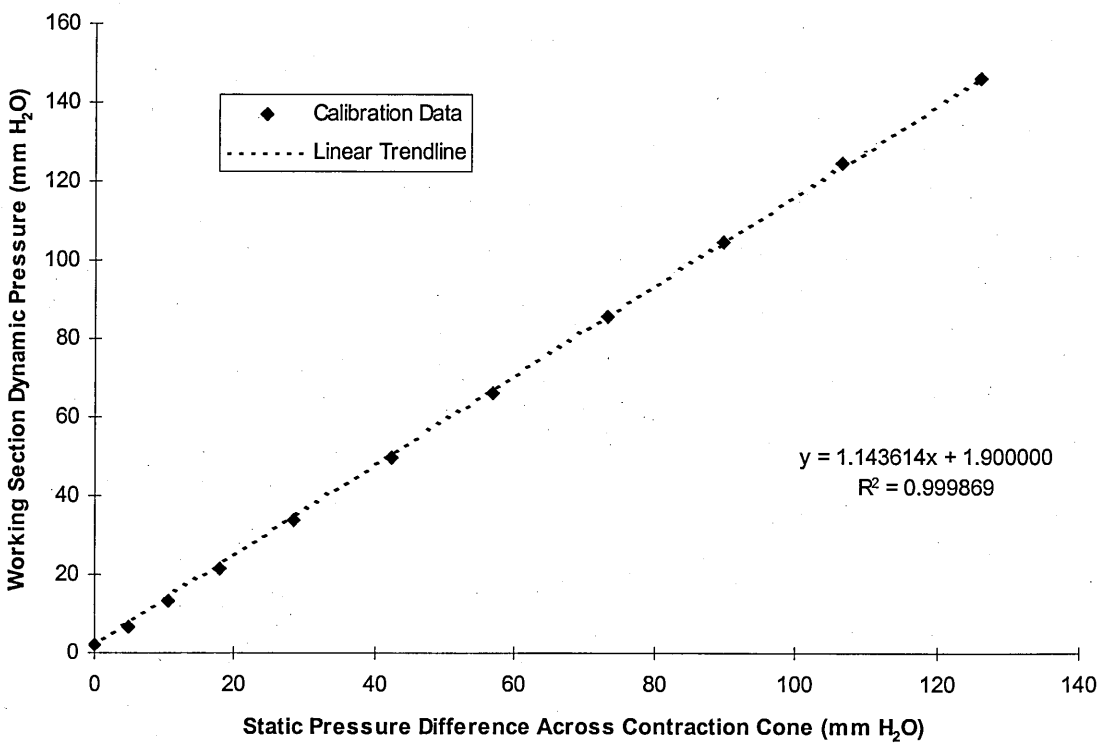

Figure D2. Cranfield 8'x6' Wind Tunnel Calibration Results

Appendix E. Experimental Data For The Effect Of Suction On Crossflow Transition

This Appendix contains the data that underlies Figure 30 from the main text. Plotting the data as $\overline{R}$ against Re_x, at constant C_q, is very useful but it does not give enough information to allow the experiments to be repeated, particularly computationally. The data in this Appendix, presented as graphs and tables, should give enough information to allow further analysis. The data is presented as a table of unit Reynolds number and x/C, and an associated graph, for suction coefficients of 0, -0.00006, -0.00012, -0.00018, -0.00024, -0.0003, and –0.00036.

Sweep Angle	Freestream Reynolds ($x10^{-6}$)								
	x/C								
	0.153	0.175	0.196	0.218	0.240	0.262	0.284	0.327	0.349
33.2					2.377	2.052			
40.1						1.787			
44.5			2.359	1.954		1.595			
45.7						1.690	1.572	1.372	1.263
55.1		1.917	1.775	1.614					
56.2		1.974	1.810						
58.6	2.163				1.355				
60.4					1.339	1.232	1.051		
63.8					1.327	1.200			
68				1.106	1.218	1.106			

Table E1. Unit Reynolds Number For The Onset of Crossflow Transition, C_q=0

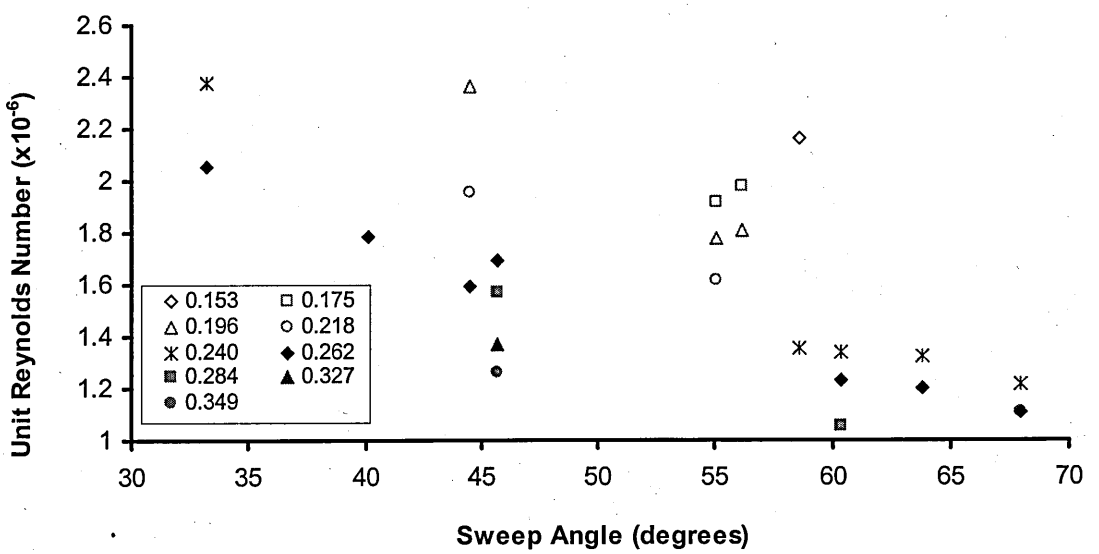

Figure E1. Unit Reynolds Number For The Onset of Crossflow Transition, C_q=0

Sweep Angle	Freestream Reynolds ($x10^{-6}$)								
	x/C								
	0.153	0.175	0.196	0.218	0.240	0.262	0.284	0.327	0.349
33.2									
40.1						1.956			
44.5				2.140					
45.7						1.791	1.674	1.456	1.367
55.1		2.111	1.917	1.758					
56.2		2.129	1.919						
58.6	2.251				1.506				
60.4					1.470	1.369	1.188		
63.8					1.428	1.287			
68									

Table E2. Unit Reynolds Number For The Onset of Crossflow Transition, C_q=-0.00006

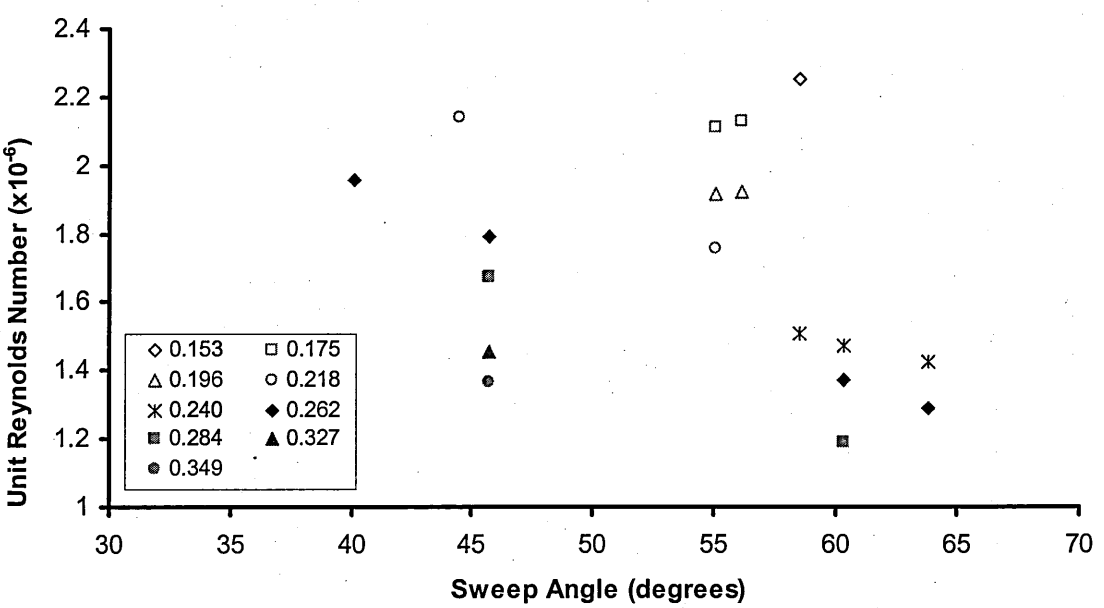

Figure E2. Unit Reynolds Number For The Onset of Crossflow Transition, C_q=-0.00006

Sweep Angle	Freestream Reynolds x10^{-6}) x/C								
	0.153	0.175	0.196	0.218	0.240	0.262	0.284	0.327	0.349
33.2									
40.1						2.126			
44.5				2.326					
45.7						1.891	1.776	1.539	1.470
55.1		2.304	2.059	1.902					
56.2		2.284	2.027						
58.6	2.340				1.657				
60.4					1.600	1.506	1.324		
63.8					1.529	1.374			
68									

Table E3. Unit Reynolds Number For The Onset of Crossflow Transition, C_q=-0.00012

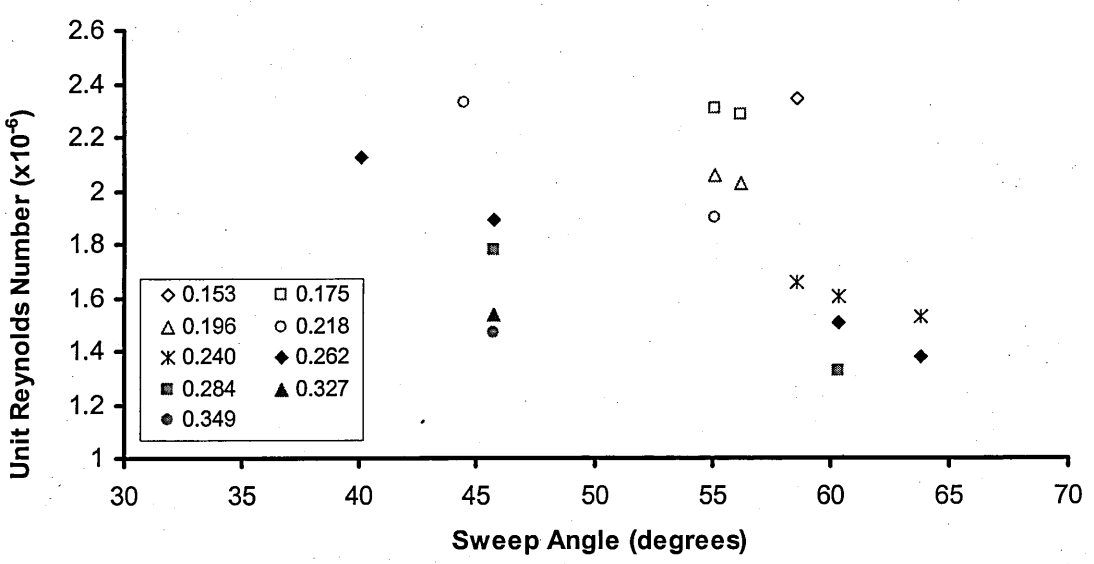

Figure E3. Unit Reynolds Number For The Onset of Crossflow Transition, C_q=-0.00012

Sweep Angle	Freestream Reynolds ($x10^{-6}$) x/C								
	0.153	0.175	0.196	0.218	0.240	0.262	0.284	0.327	0.349
33.2									
40.1						2.295			
44.5				2.512					
45.7						1.992	1.879	1.623	1.574
55.1			2.201	2.045					
56.2		2.440	2.136						
58.6					1.808				
60.4					1.731	1.643	1.461		
63.8					1.630	1.461			
68									

Table E4. Unit Reynolds Number For The Onset of Crossflow Transition, C_q=-0.00018

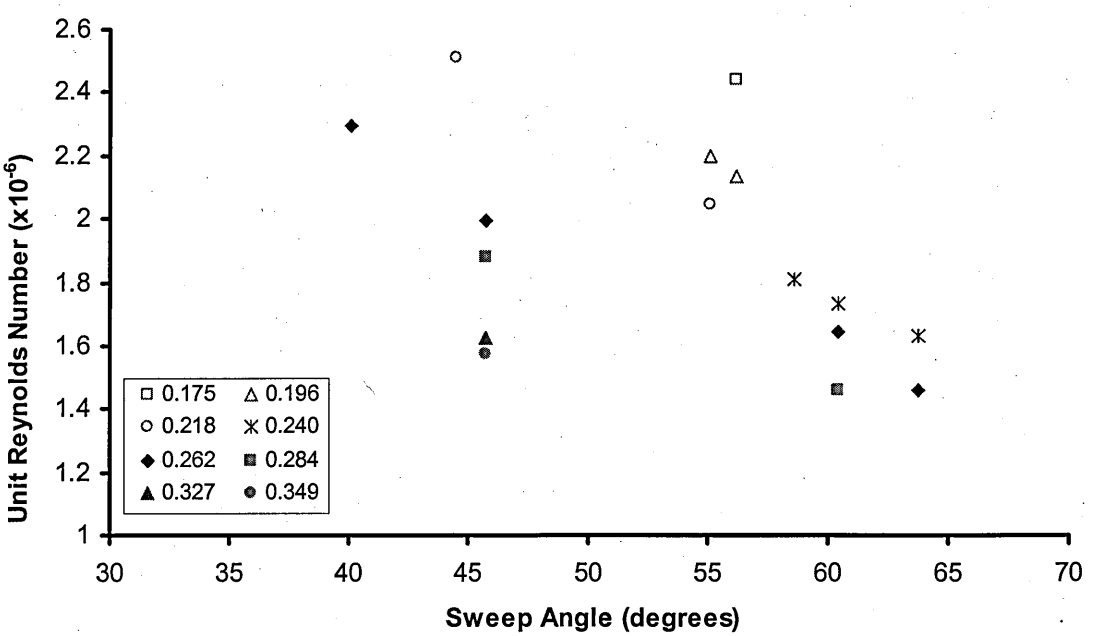

Figure E4. Unit Reynolds Number For The Onset of Crossflow Transition, C_q=-0.00018

Sweep Angle	Freestream Reynolds ($x10^{-6}$) x/C								
	0.153	0.175	0.196	0.218	0.240	0.262	0.284	0.327	0.349
33.2									
40.1						2.464			
44.5									
45.7						2.093	1.981	1.707	1.677
55.1			2.343	2.189					
56.2			2.244						
58.6					1.959				
60.4					1.861	1.780	1.597		
63.8						1.548			
68									

Table E5. Unit Reynolds Number For The Onset of Crossflow Transition, C_q=-0.00024

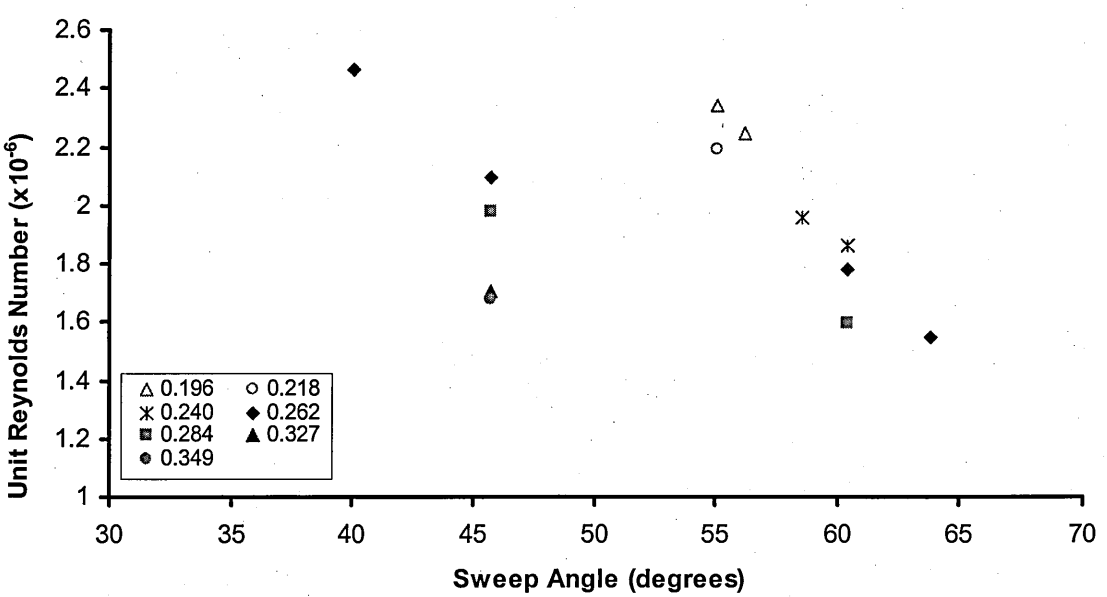

Figure E5. Unit Reynolds Number For The Onset of Crossflow Transition, C_q=-0.00024

Sweep Angle	Freestream Reynolds x10^-6 x/C								
	0.153	0.175	0.196	0.218	0.240	0.262	0.284	0.327	0.349
33.2									
40.1									
44.5									
45.7						2.194	2.083	1.790	1.781
55.1			2.485	2.333					
56.2			2.353						
58.6					2.110				
60.4					1.992	1.918	1.734		
63.8									
68									

Table E6. Unit Reynolds Number For The Onset of Crossflow Transition, C_q=-0.00030

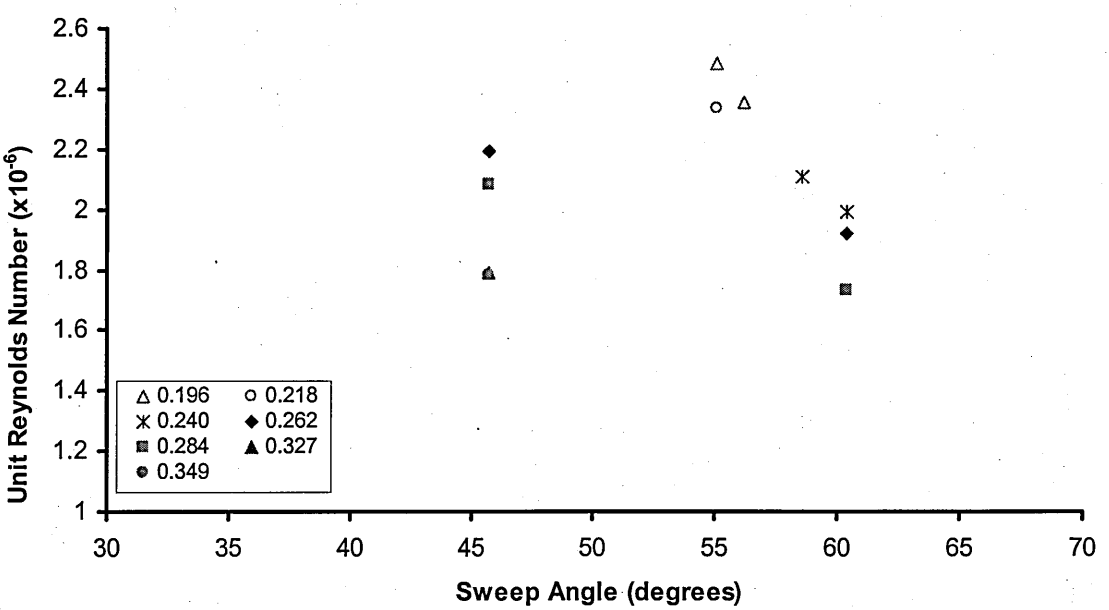

Figure E6. Unit Reynolds Number For The Onset of Crossflow Transition, C_q=-0.00030

Sweep Angle	Freestream Reynolds ($x10^{-6}$) x/C								
	0.153	0.175	0.196	0.218	0.240	0.262	0.284	0.327	0.349
33.2									
40.1									
44.5									
45.7							2.186	1.874	1.884
55.1									
56.2									
58.6					2.261				
60.4						2.055	1.870		
63.8									
68									

Table E7. Unit Reynolds Number For The Onset of Crossflow Transition, C_q=-0.00036

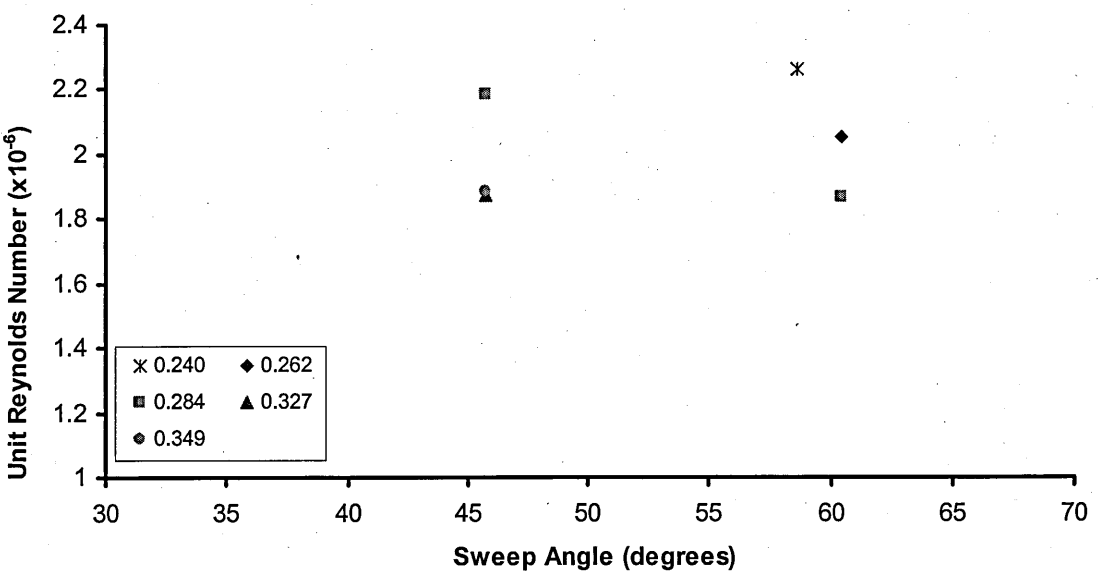

Figure E7. Unit Reynolds Number For The Onset of Crossflow Transition, C_q=-0.00036

Appendix F. Relation of Parameters Used by Pfenninger to Those Used Currently

Pfenninger used three parameters to describe the transpired attachment-line in his experiments[26]: a leading edge Reynolds number, a spanwise length Reynolds number and a suction parameter. Each of these can be expressed in terms of the parameters used in the current study and described in Section 3.6.

Leading Edge Reynolds Number

Pfenninger used the momentum thickness Reynolds number, Re_θ, for the attachment line. This was defined as

$$Re_{\theta_{al}} \equiv \frac{V\theta_{al}}{\nu} \quad \ldots(1)$$

where V is the velocity along the span, θ_{al} is the attachment-line momentum thickness, used as the spanwise length scale, and ν is the kinematic viscosity. Pfenninger then defined a non-dimensional momentum thickness, θ^*_{al}, as

$$\theta^*_{al} \equiv \theta_{al}\sqrt{\frac{1}{\nu}\left(\frac{\partial U}{\partial x}\right)_{al}} \quad \ldots(2)$$

Now, η is the spanwise length scale used in the current work and is defined as

$$\eta \equiv \sqrt{\frac{\nu}{\left(\partial U/\partial x\right)_{al}}} \quad \ldots(3)$$

so

$$\theta^*_{al} = \frac{\theta_{al}}{\eta} \quad \ldots(4)$$

The leading edge Reynolds number used in the current work is $\overline{R}$, which is defined as

$$\overline{R} \equiv \frac{V\eta}{\nu} \quad \ldots(5)$$

Substituting for η from equation D4 gives

$$Re_{\theta_{al}} = \theta^*_{al}\overline{R} \quad \ldots(6)$$

Pfenninger gave a chart of θ^*_{al} plotted against v^*_o, his non-dimensional suction coefficient, so the momentum thickness Reynolds number used by Pfenninger can be

converted to $\overline{R}$ easily. The chart of θ^*_{al} plotted against v^*_o has been reproduced as Figure F1.

Spanwise Length Reynolds Number

Pfenninger uses a spanwise length Reynolds number to non-dimensionalise his spanwise length. He doesn't give it a symbol, so Re_{span} will be used here. This Reynolds number was defined as

$$Re_{span} = \frac{Vs}{\nu} \quad \ldots(7)$$

where s is the length of the suction surface. This can be related to $\overline{R}$ (equation 5) by

$$\frac{Re_{span}}{\overline{R}} = \frac{s}{\eta} \quad \ldots(8)$$

which is the non-dimensional spanwise distance used in the current work.

Suction Parameter

Pfenninger used a suction coefficient, v^*_o, defined as

$$v^*_o \equiv \frac{v_{o_{al}}}{\sqrt{\nu\left(\partial U/\partial x\right)_{al}}} \quad \ldots(9)$$

where $v_{o_{al}}$ was the suction velocity at the attachment line. Substituting for η from equation 3 gives

$$v^*_o = \frac{v_{o_{al}}\eta}{\nu} \quad \ldots(10)$$

Multiplying by (V/V)

$$v^*_o = \frac{v_{o_{al}}}{V}\frac{V\eta}{\nu} = C_q\overline{R} \quad \ldots(11)$$

Conclusion

Pfenninger's data was presented as a chart of Re_θ plotted against v^*_o either at constant spanwise position or constant spanwise length Reynolds number (Figure 54). It has been shown that these data can be expressed in terms of $\overline{R}$, C_q and s/η.

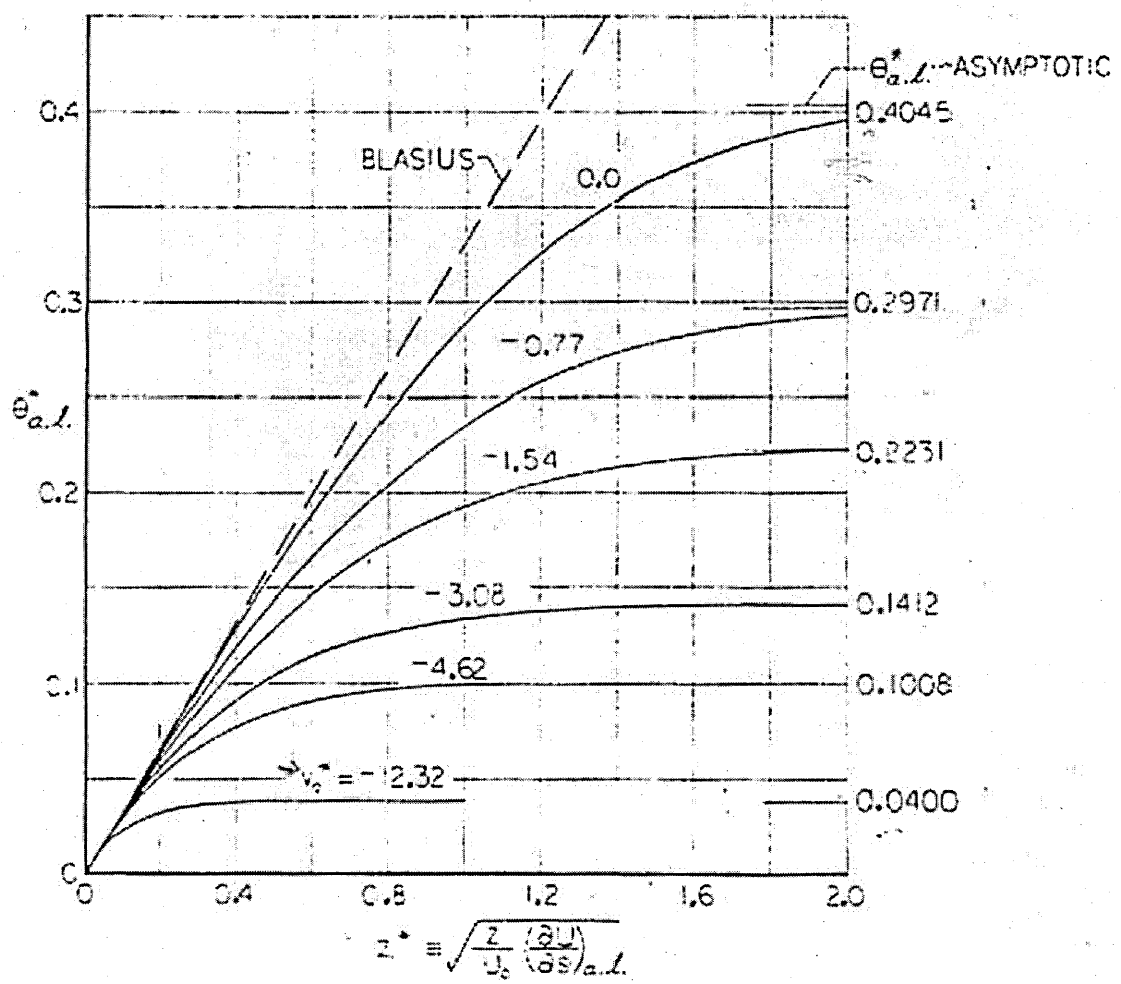

Figure F1. Spanwise Growth Of The Attachment-Line Boundary Layer Momentum Thickness, From Pfenninger[26]

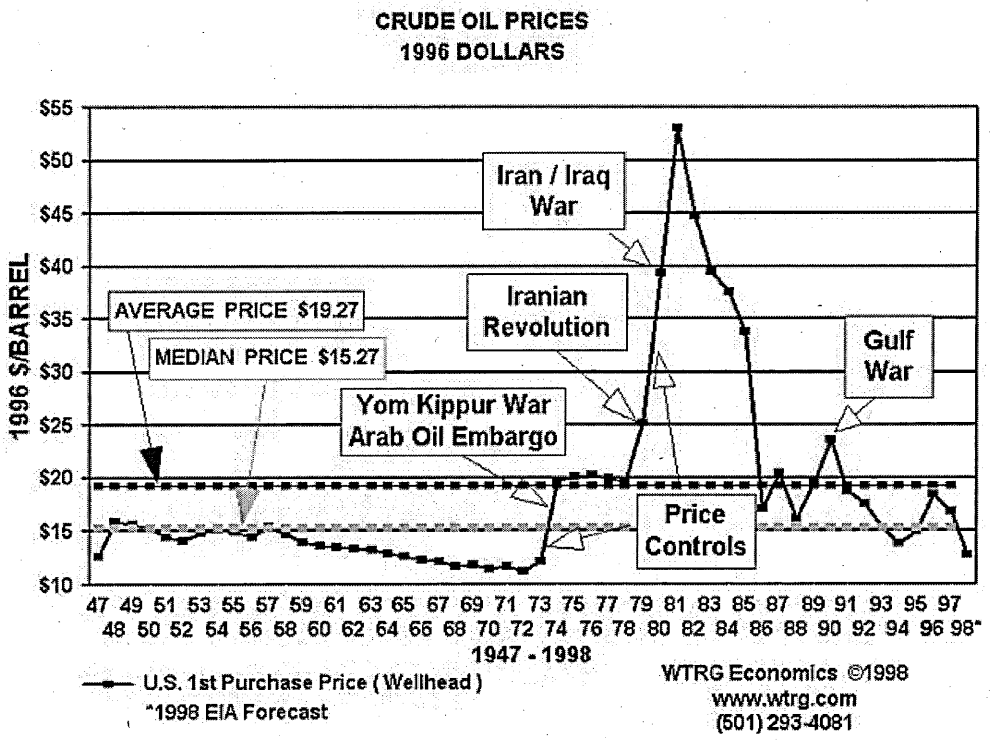

Figure 1. The Variation of Crude Oil Prices And The Correlation With World Events, from WTRG Economics 1998

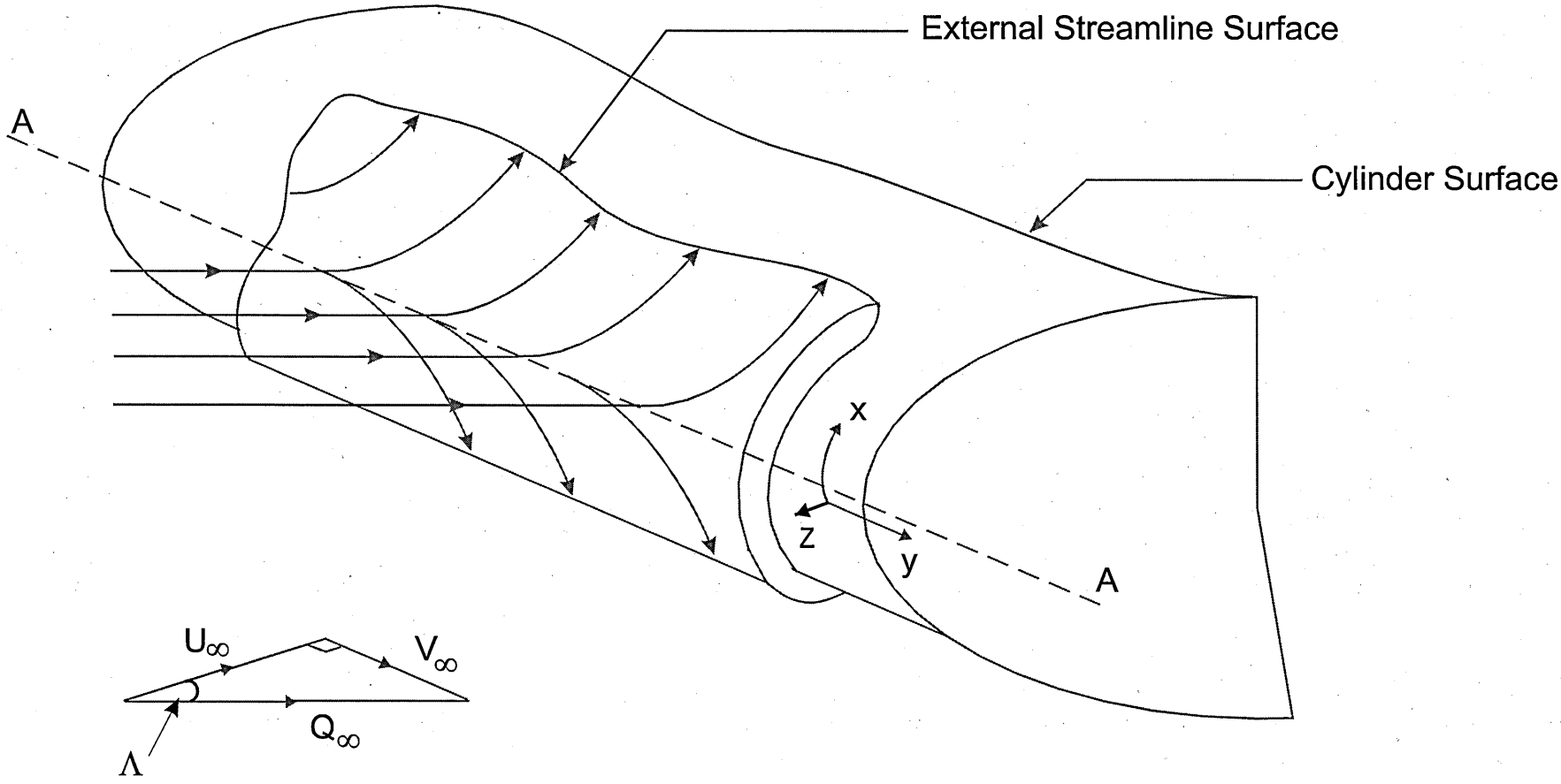

Figure 2. The Flow Near The Leading Edge of a Swept Wing

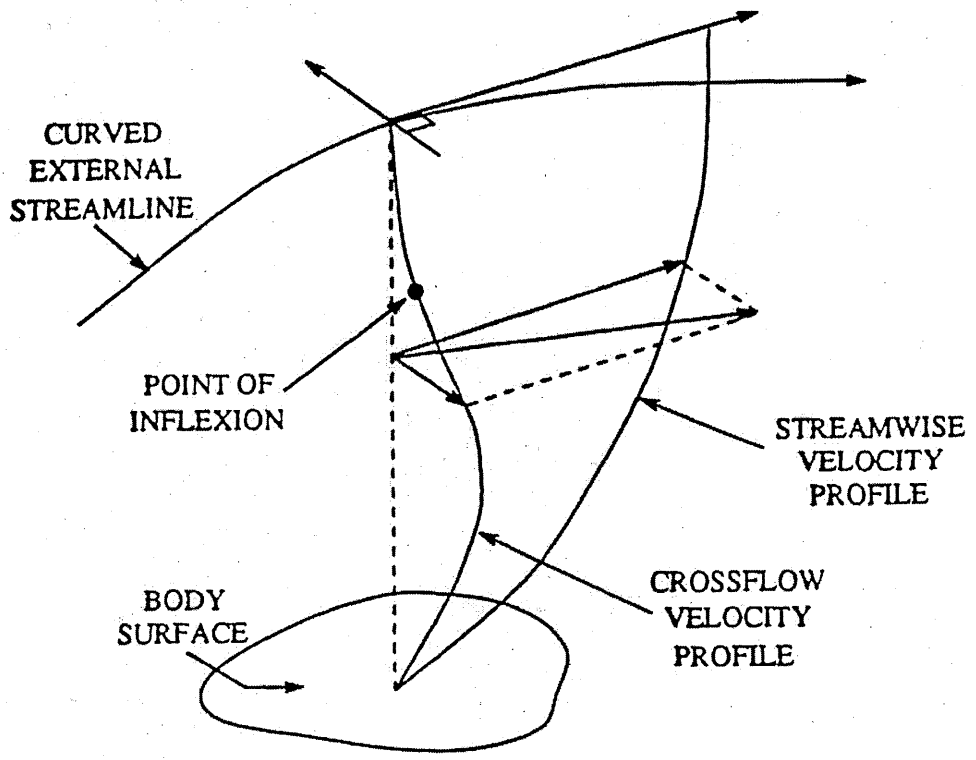

Figure 3. Typical Velocity Profile for a Three-Dimensional Boundary Layer, from Yardley[63]

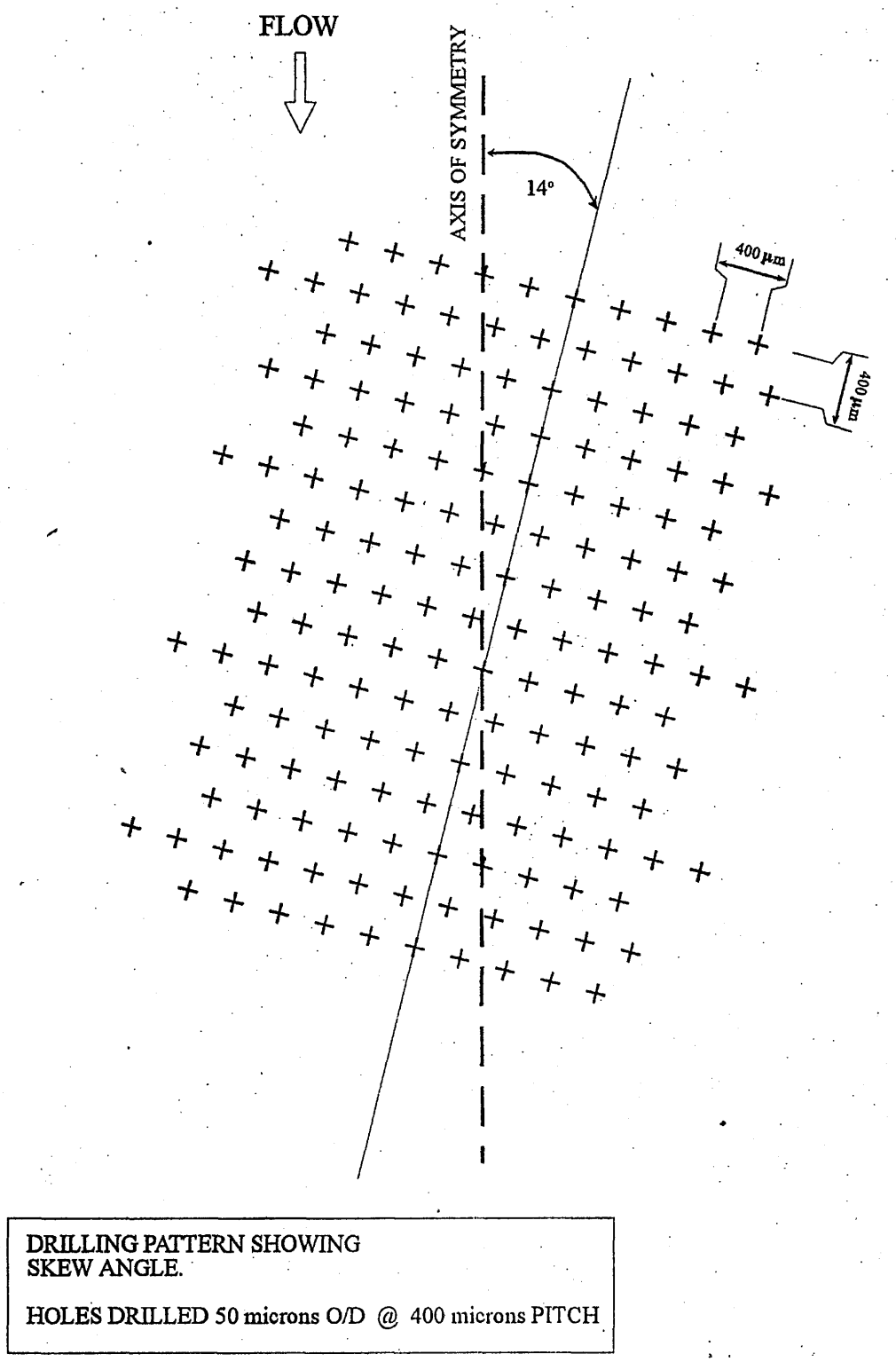

Figure 4. Leading Edge Perforation Pattern, From Danks[21]

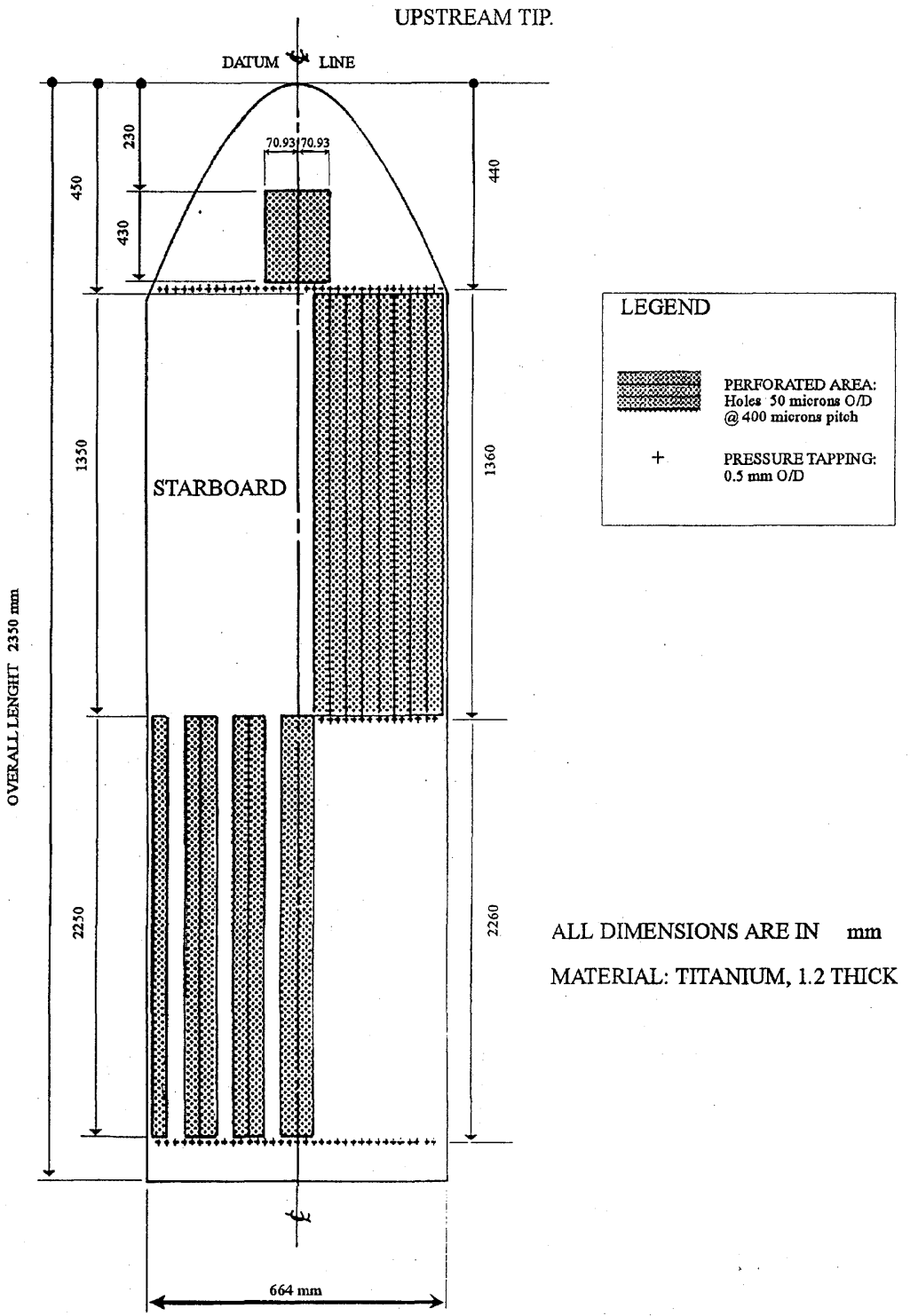

Figure 5. Distribution of Perforated Areas on Titanium Leading Edge, From Danks[21]

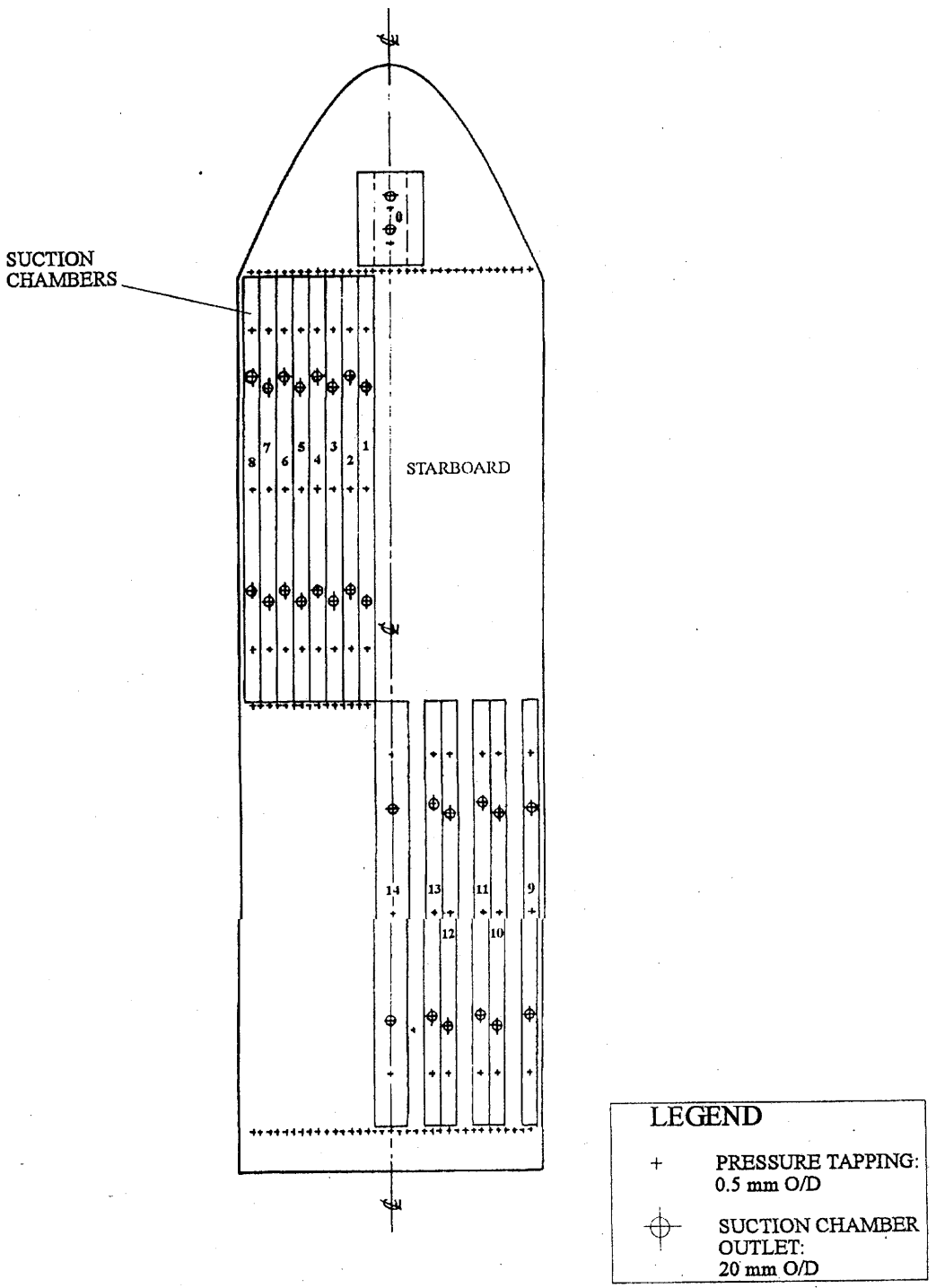

Figure 6. Distribution of Suction Chambers Within the Perforated Titanium Leading Edge Surface, From Danks[21]

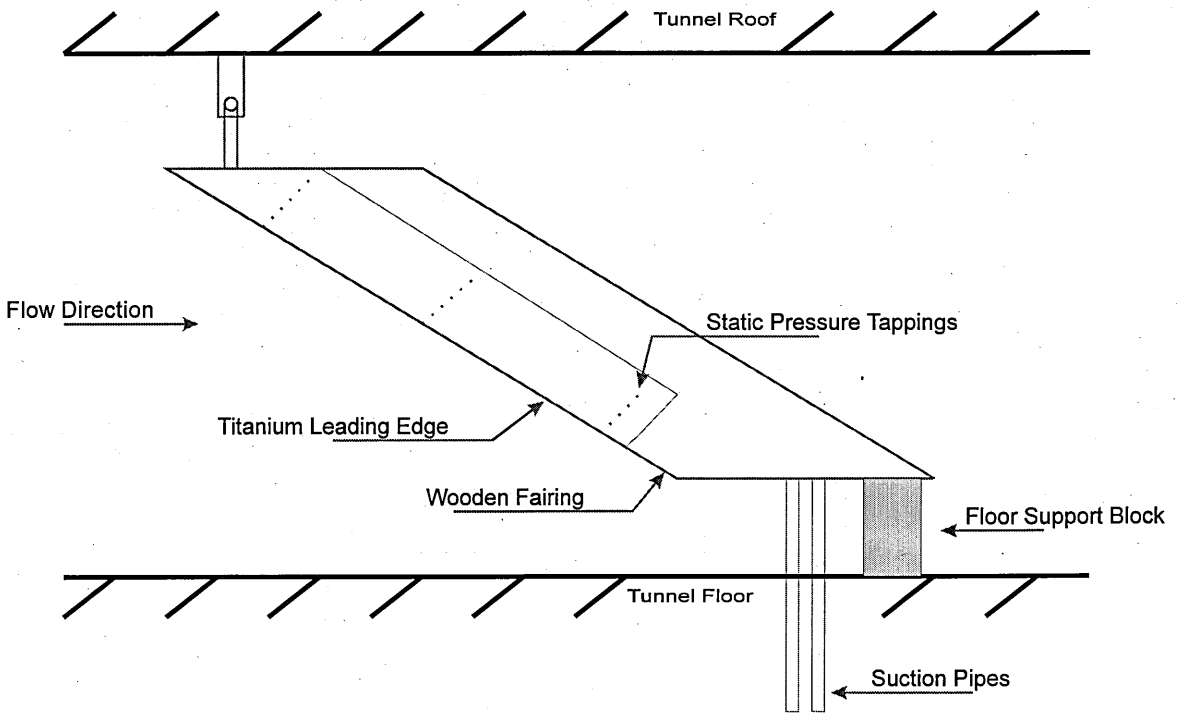

Figure 7. Arrangement of Model in 8'x6' Wind Tunnel

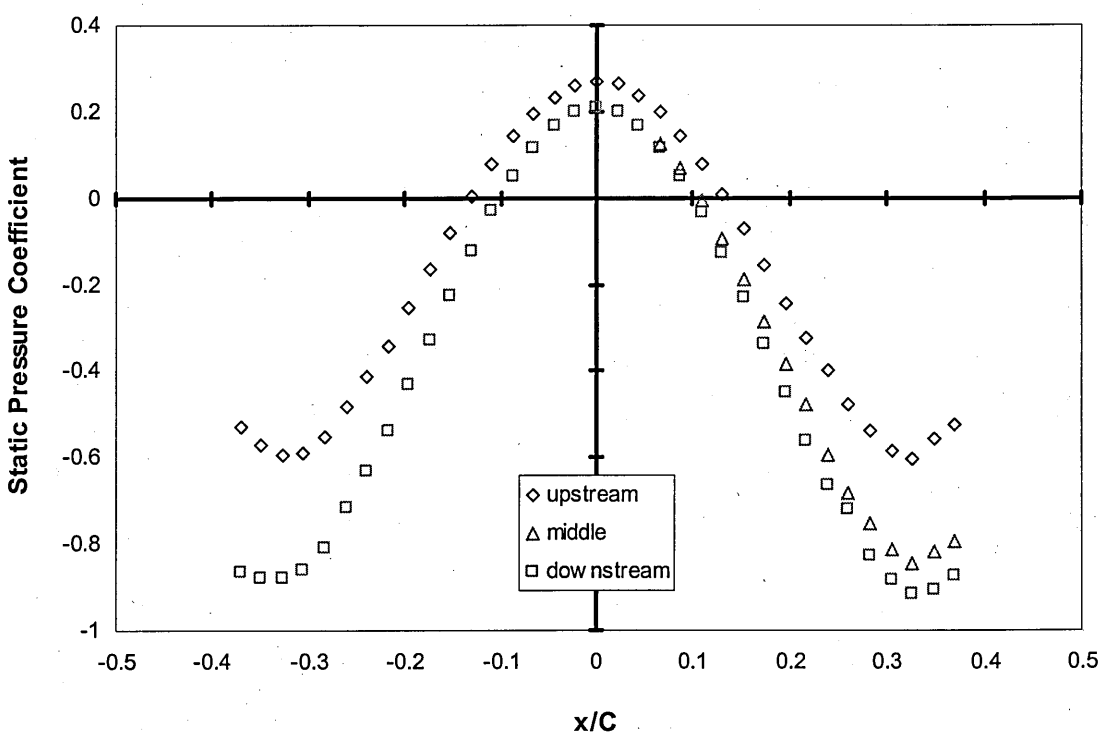

Figure 8. Example Static Pressure Coefficient Distribution Around Cylinder Leading Edge

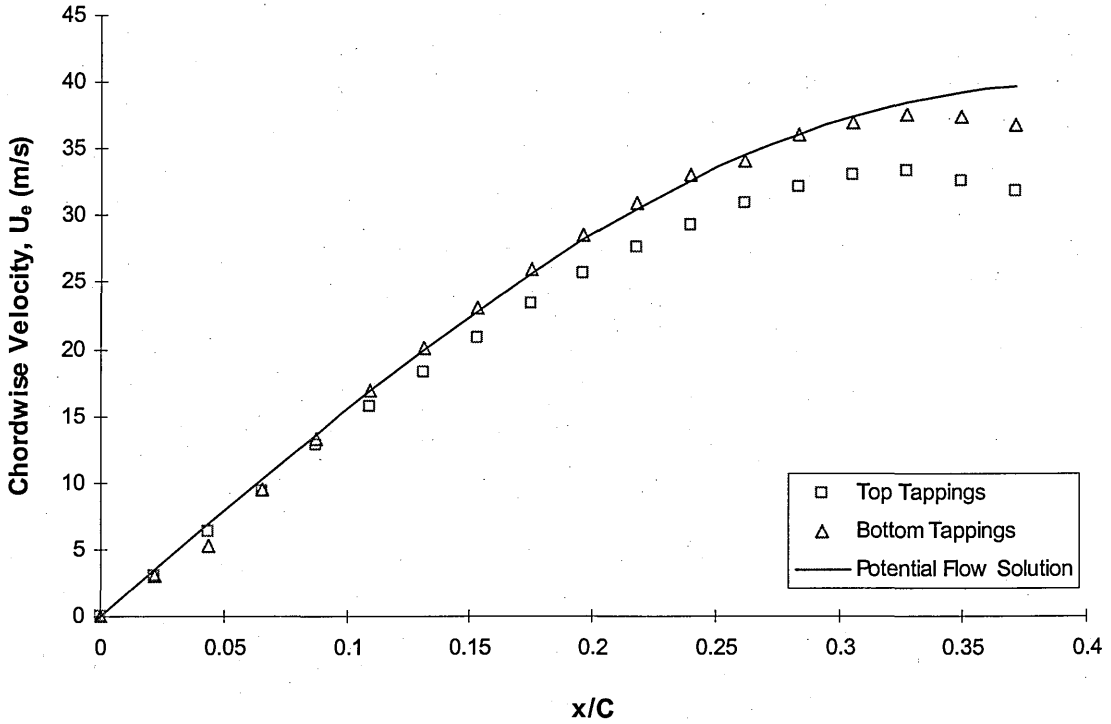

Figure 9. Chordwise Velocity Distribution and Comparison With Potential Flow Solution

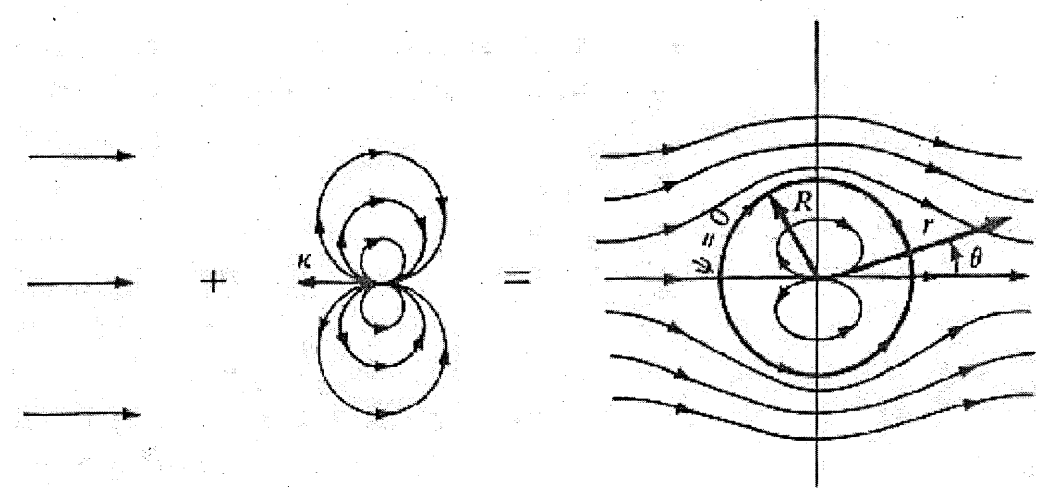

Figure 10. Diagram Showing The Addition Of A Uniform Flow And A Doublet To Represent The Potential Flow Over A Cylinder, From Anderson[65]

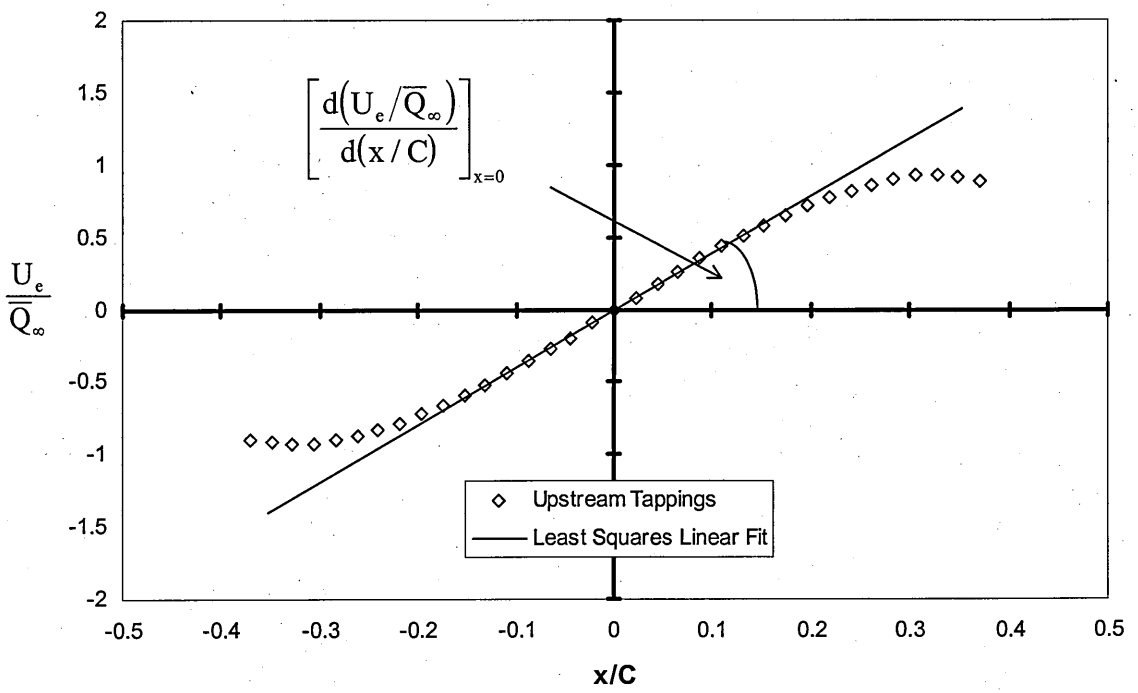

Figure 11. Typical Non-Dimensionalised Chordwise Velocity Distribution

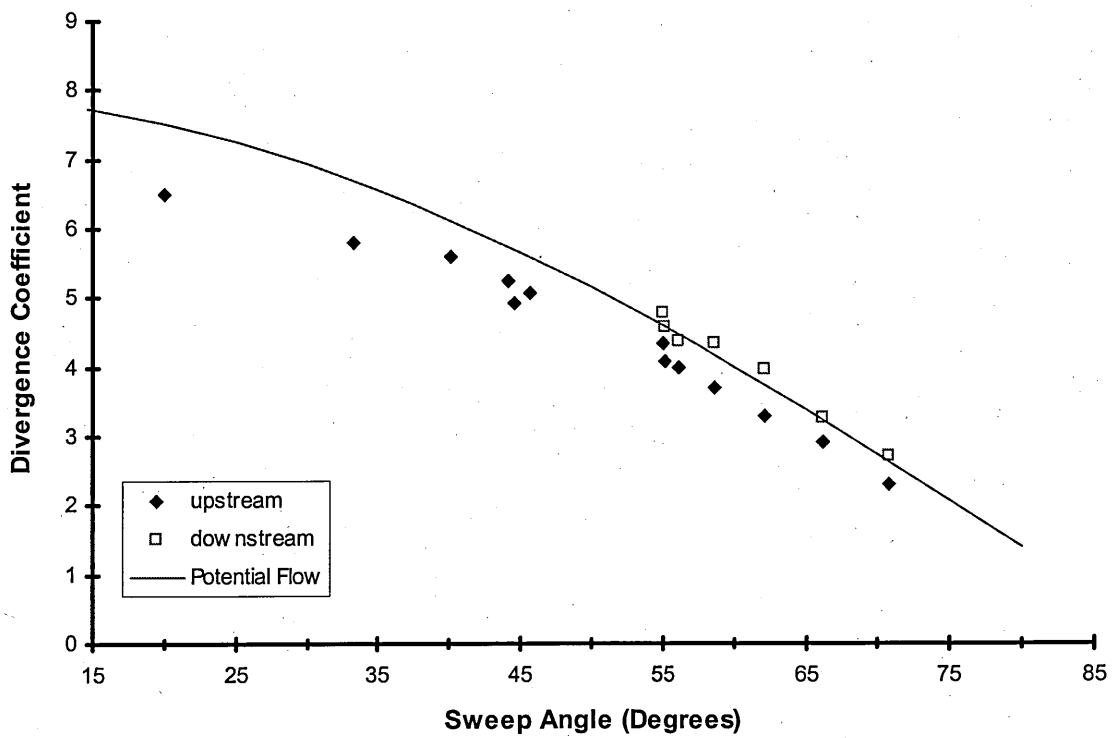

Figure 12. Comparison of Divergence Coefficients Obtained During Experimental Work and Potential Flow Solution

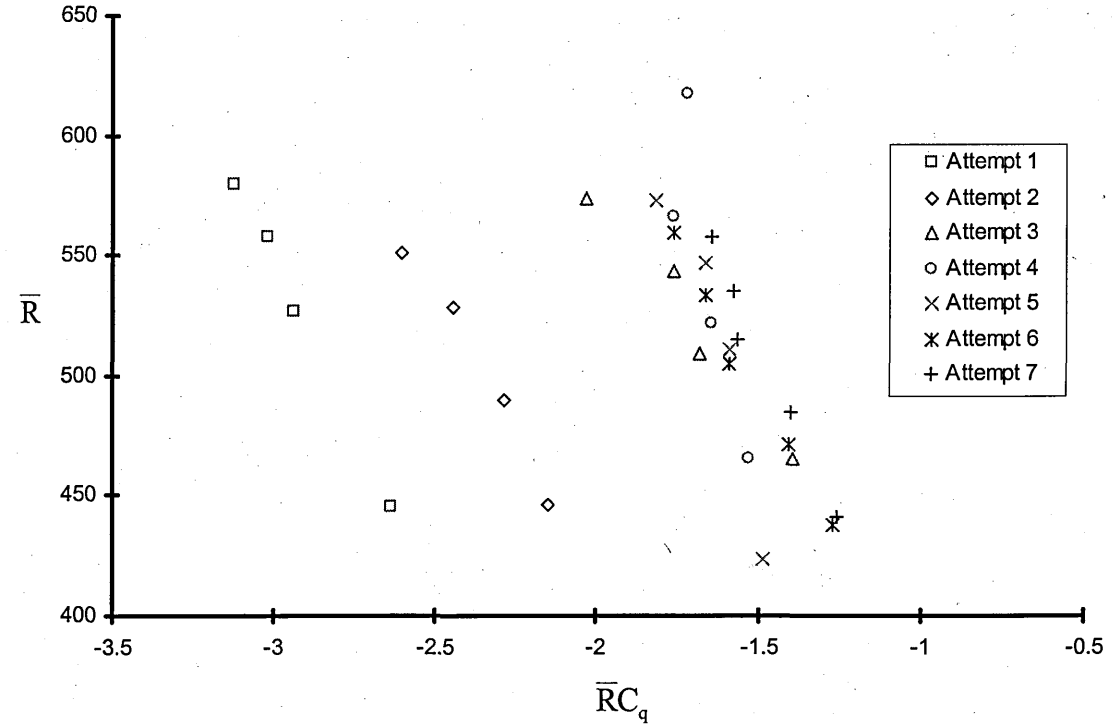

Figure 13. An Example of the Effect of Operator Experience When Using Hot-Wire Anemometry

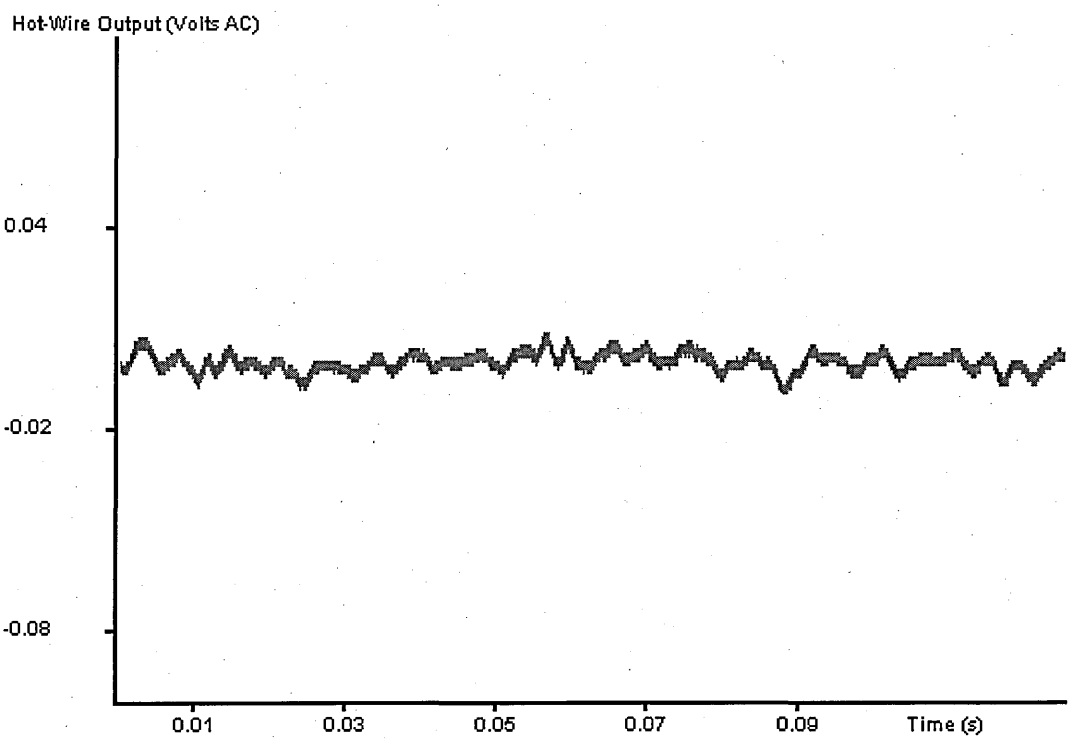

Figure 14. Typical Output from Hot-Wire For Laminar Boundary Layer

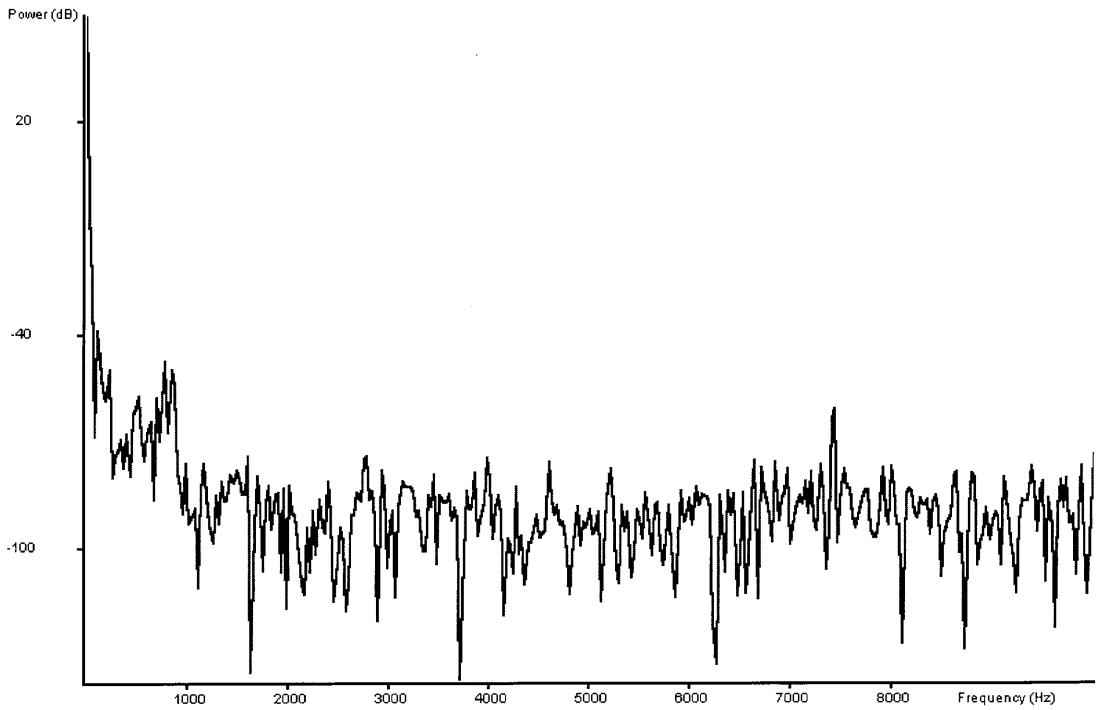

Figure 15. Power Spectrum of Laminar Boundary Layer Shown in Figure 14

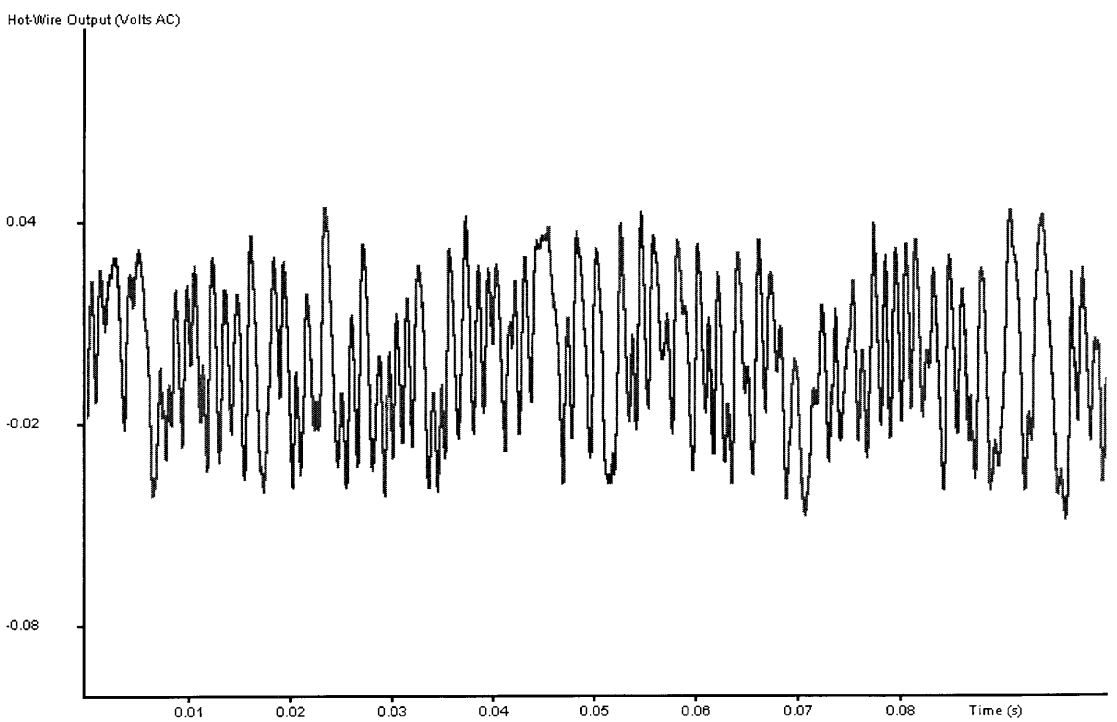

Figure 16. Typical Output from Hot-Wire For Laminar Boundary Layer With Laminar Disturbance

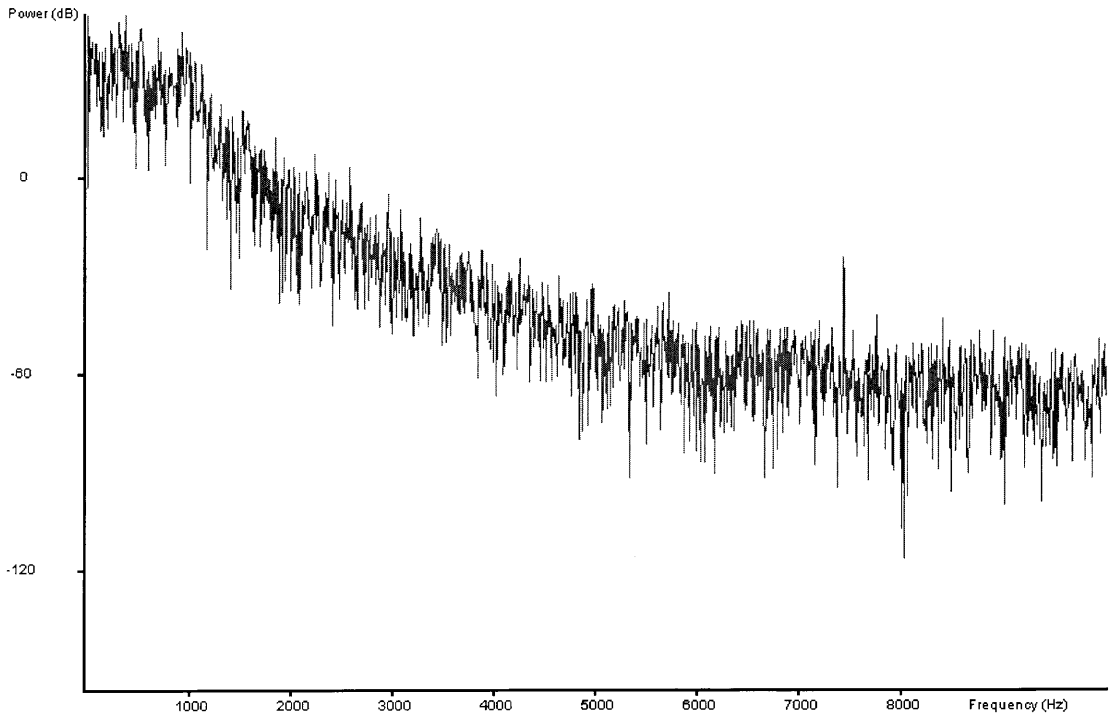

Figure 17. Power Spectrum of Laminar Boundary Layer With Laminar Disturbance Shown in Figure 16

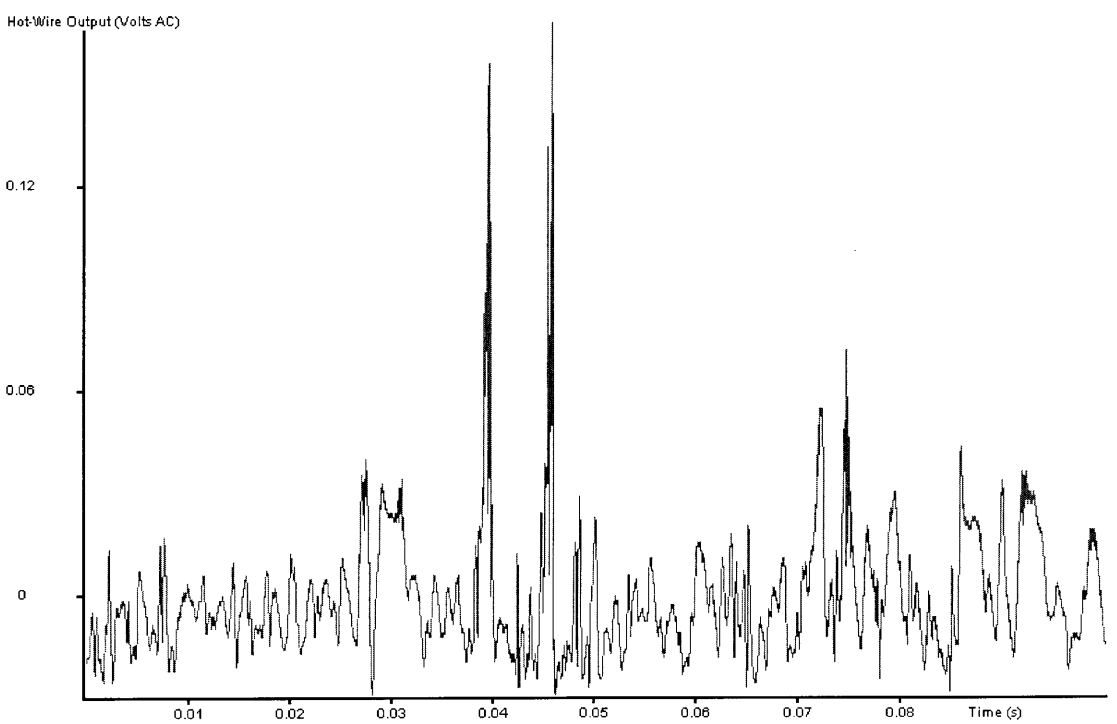

Figure 18. Typical Output from Hot-Wire For The Onset of Transition: Laminar Boundary Layer With Laminar Disturbance And Turbulent Bursts

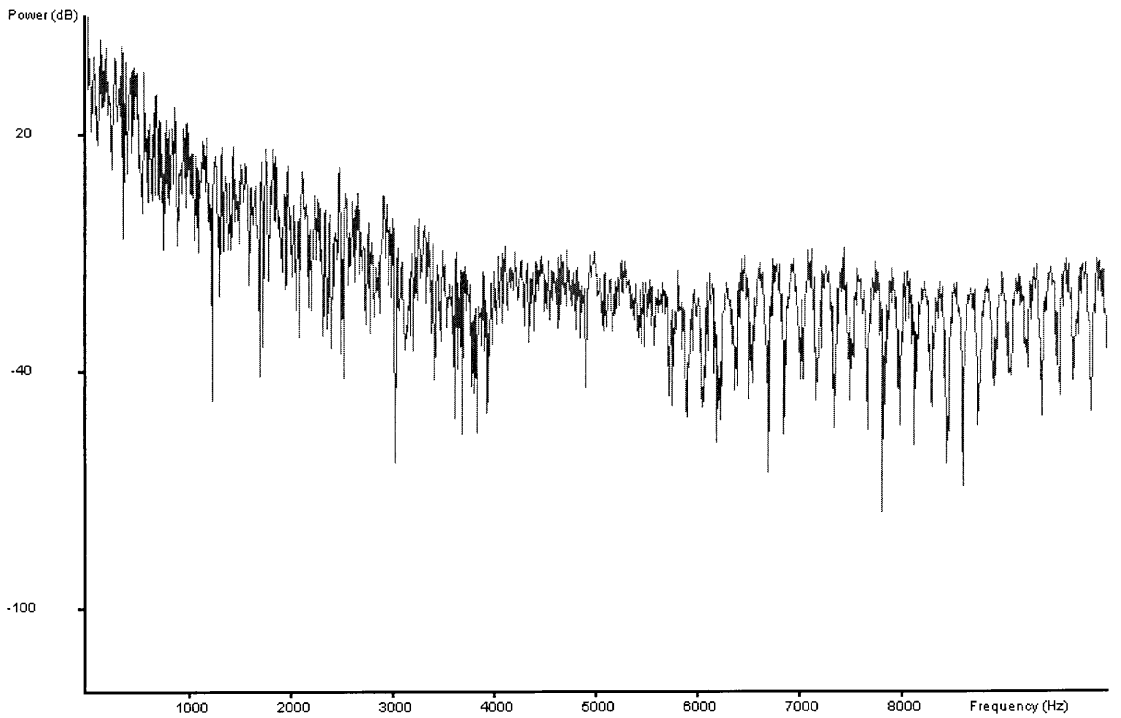

Figure 19. Power Spectrum of Laminar Boundary Layer With Laminar Disturbance and Turbulent Bursts Shown in Figure 18

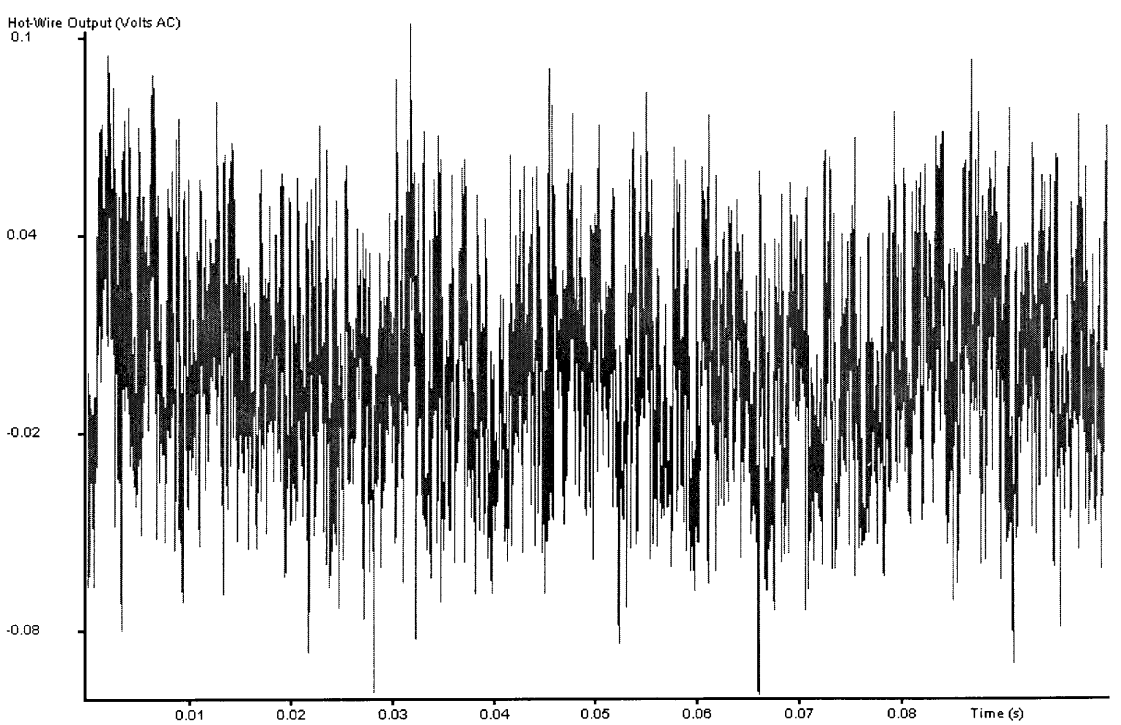

Figure 20. Typical Output From Hot-Wire For Turbulent Boundary Layer

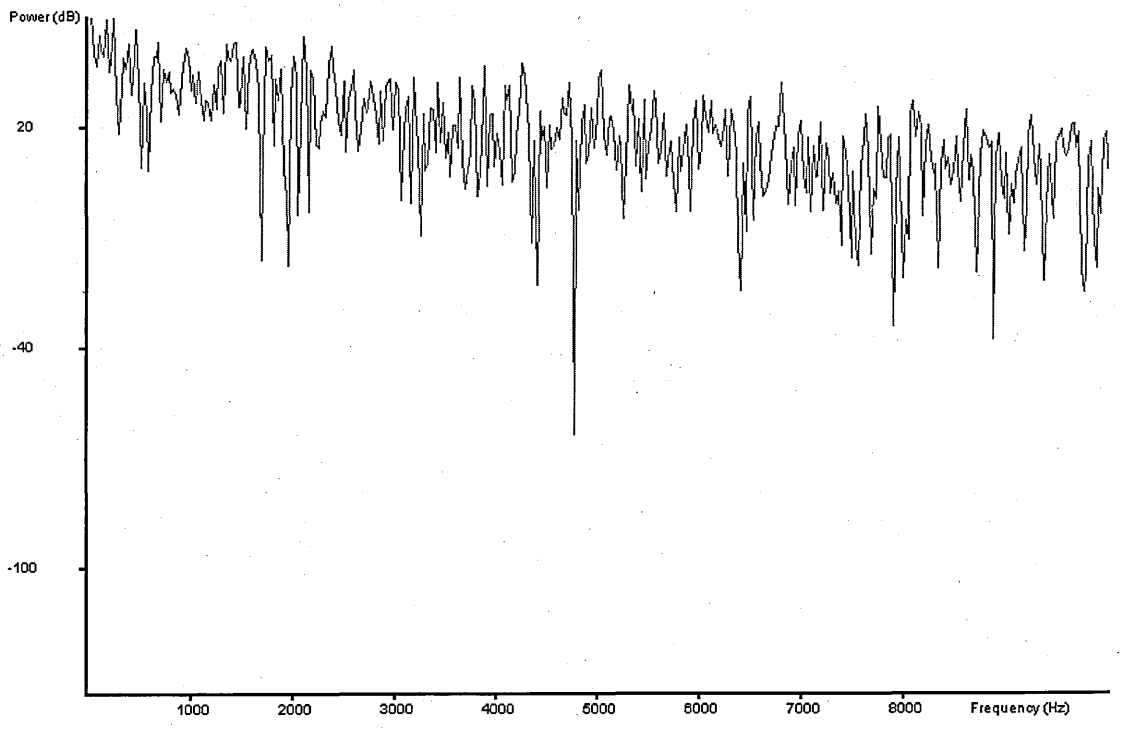

Figure 21. Power Spectrum of Turbulent Boundary Layer Shown in Figure 20

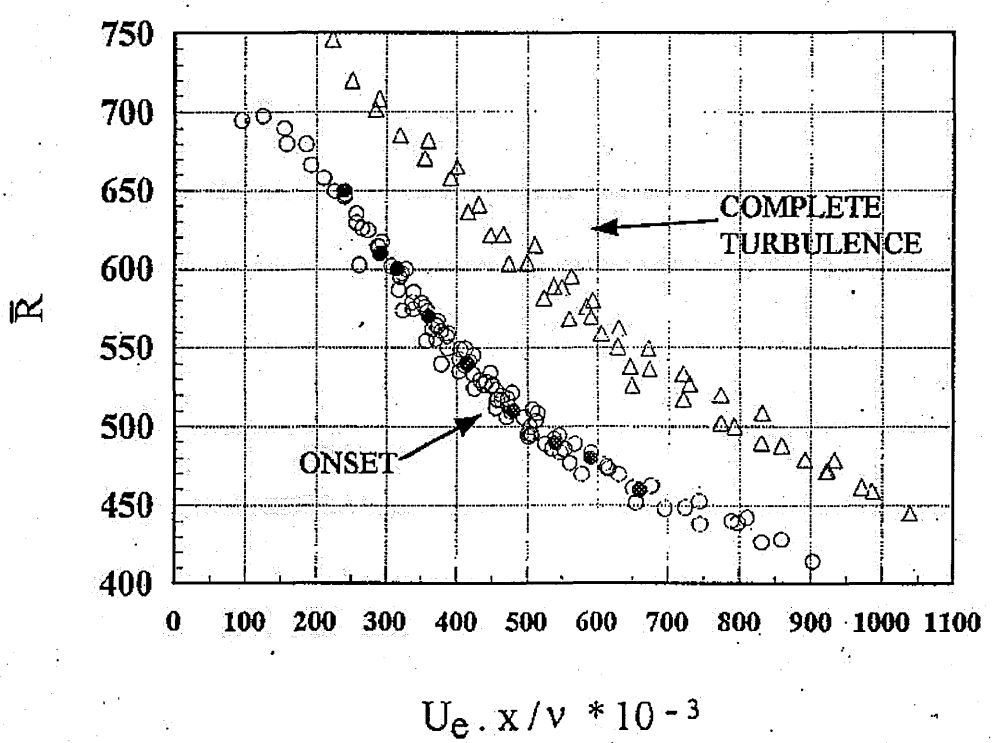

Figure 22. The Onset and End of Transition, Caused by Cross-Flow Instability, from Danks[21]

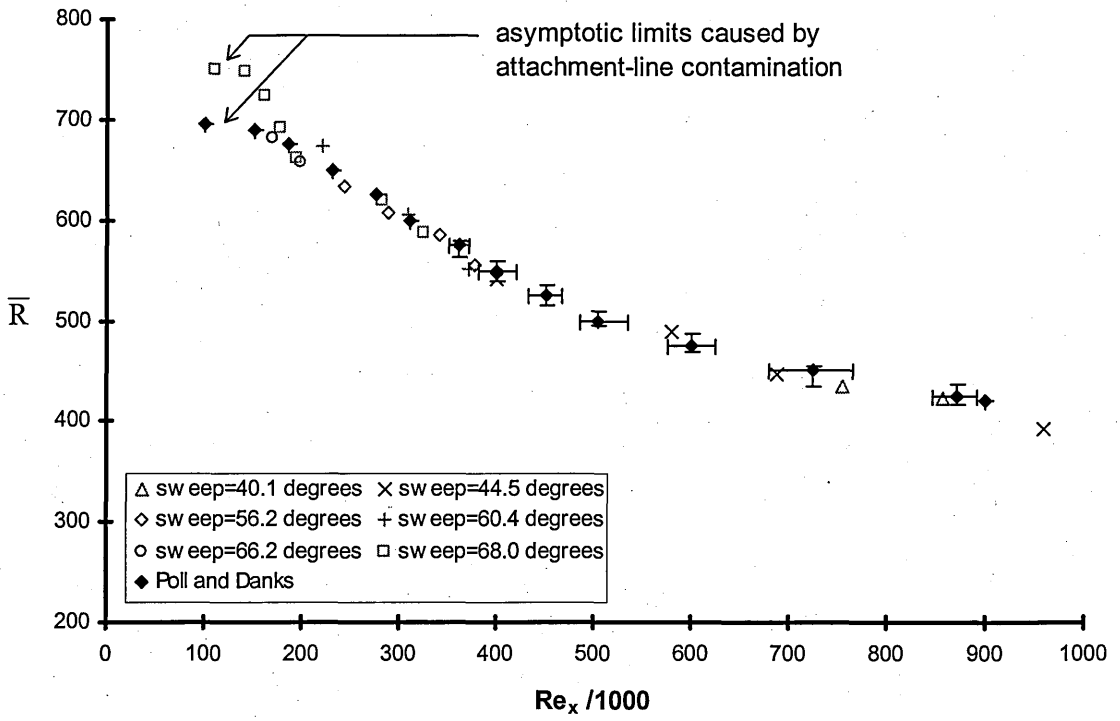

Figure 23. Natural Transition on a Non-Porous Surface and Comparison with Previous Work By Poll[4] and Danks[5]

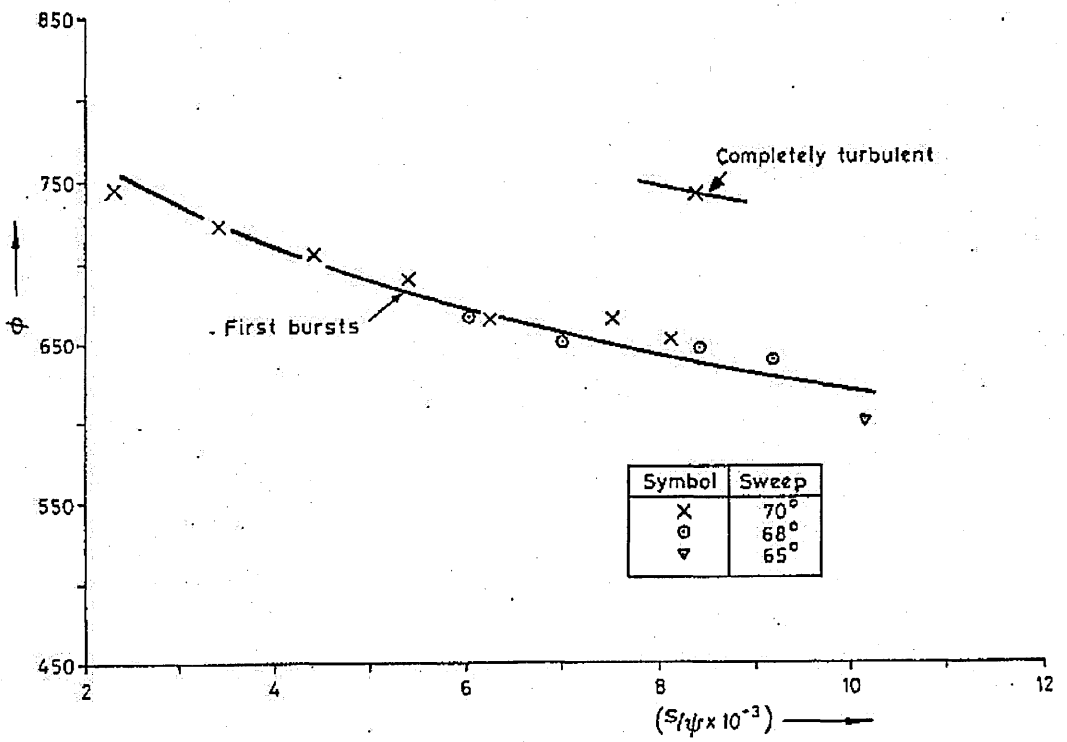

Figure 24. Transition Characteristics In The Absence Of A Trip-Wire, From Poll[62]

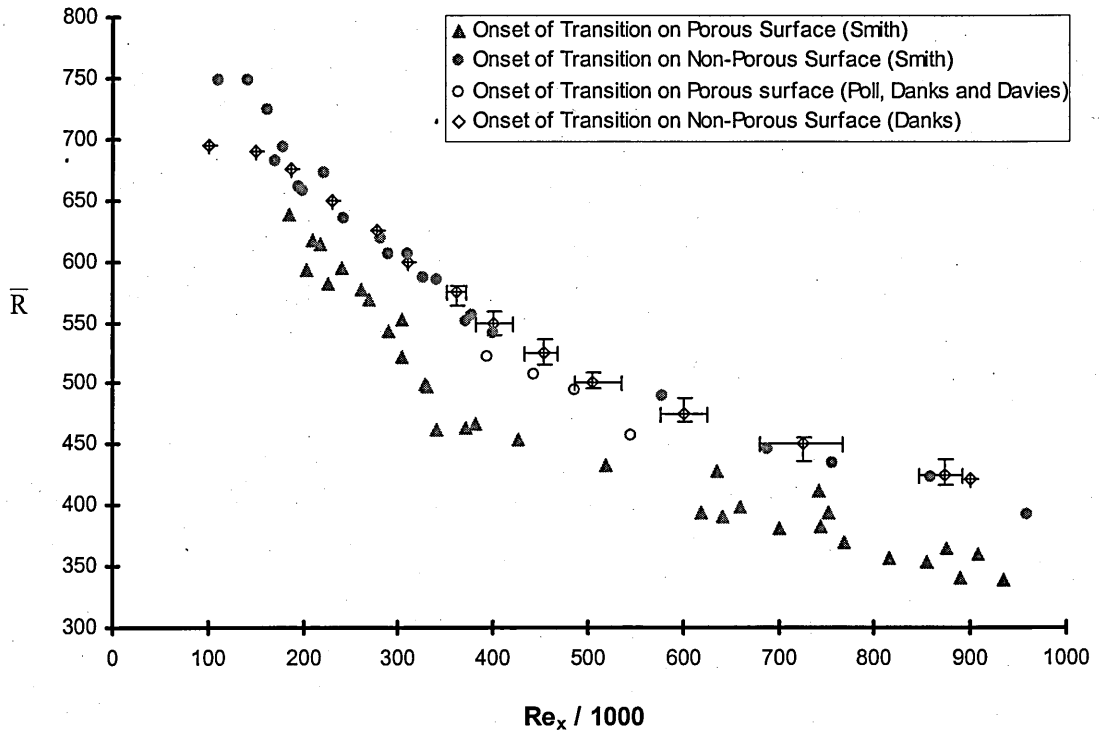

Figure 25. Comparison of the Onset of Transition on Porous and Non-Porous Surfaces, With Data From Poll *et al*[52] and Danks[5]

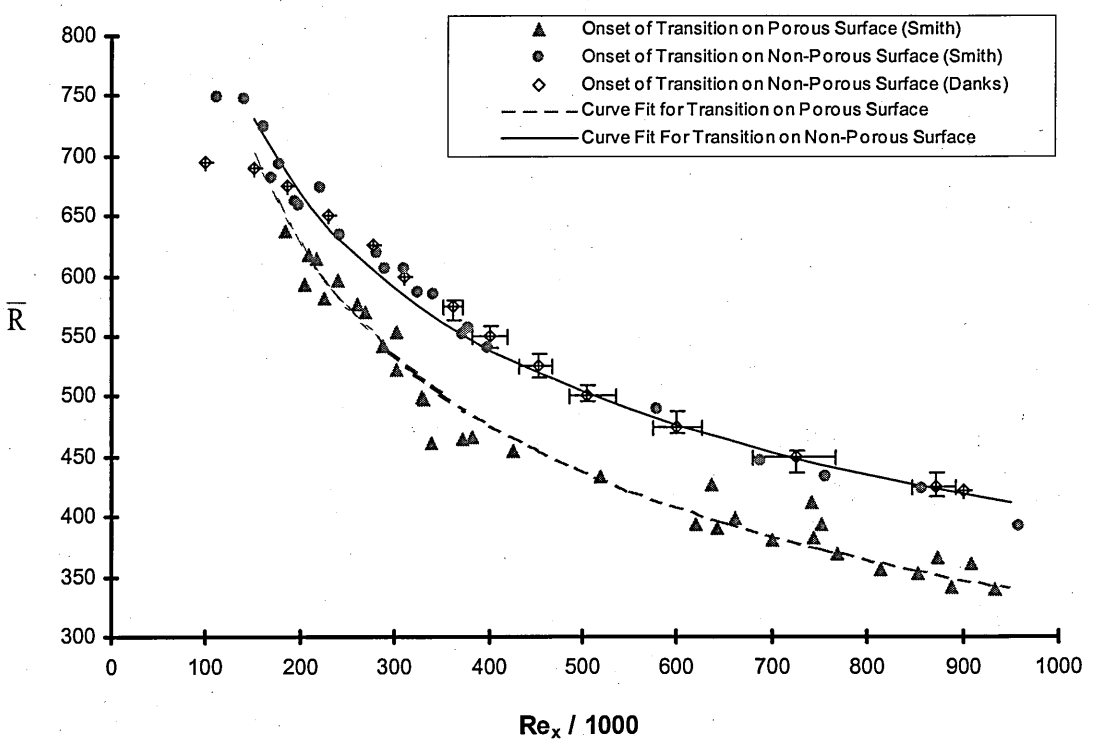

Figure 26. Comparison of Power Law Approximations with Experimental Data, With Data From Danks[5]

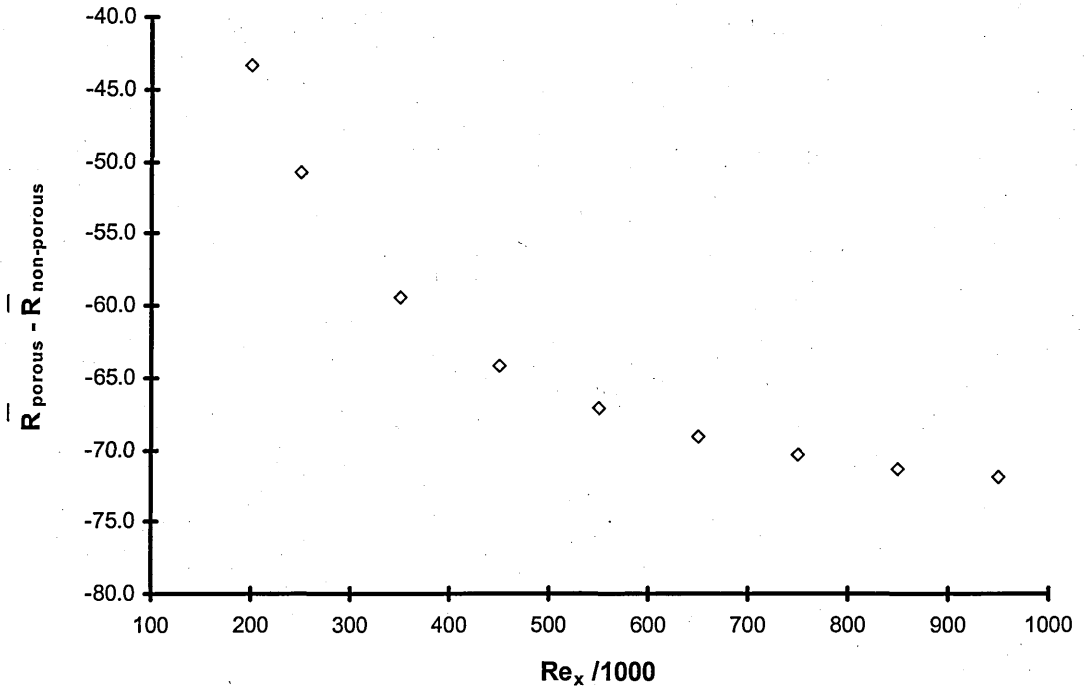

Figure 27. The Magnitude Of The $\overline{R}$ Reduction Due to the Porous Surface

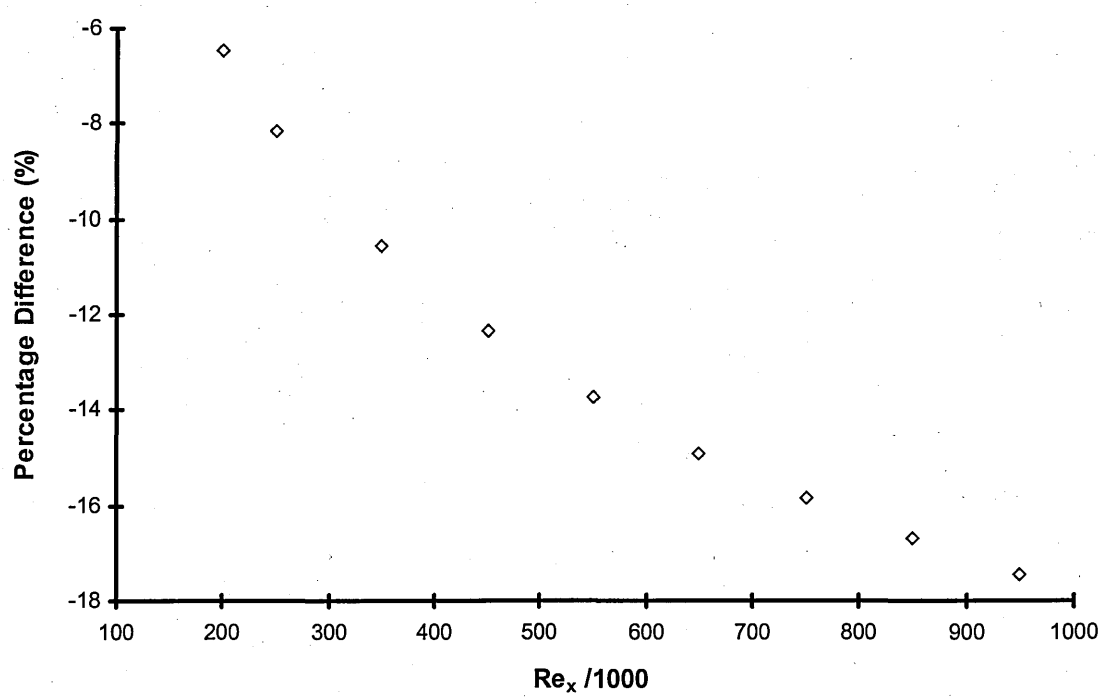

Figure 28. Percentage Reduction of $\overline{R}$ Due to the Porous Surface

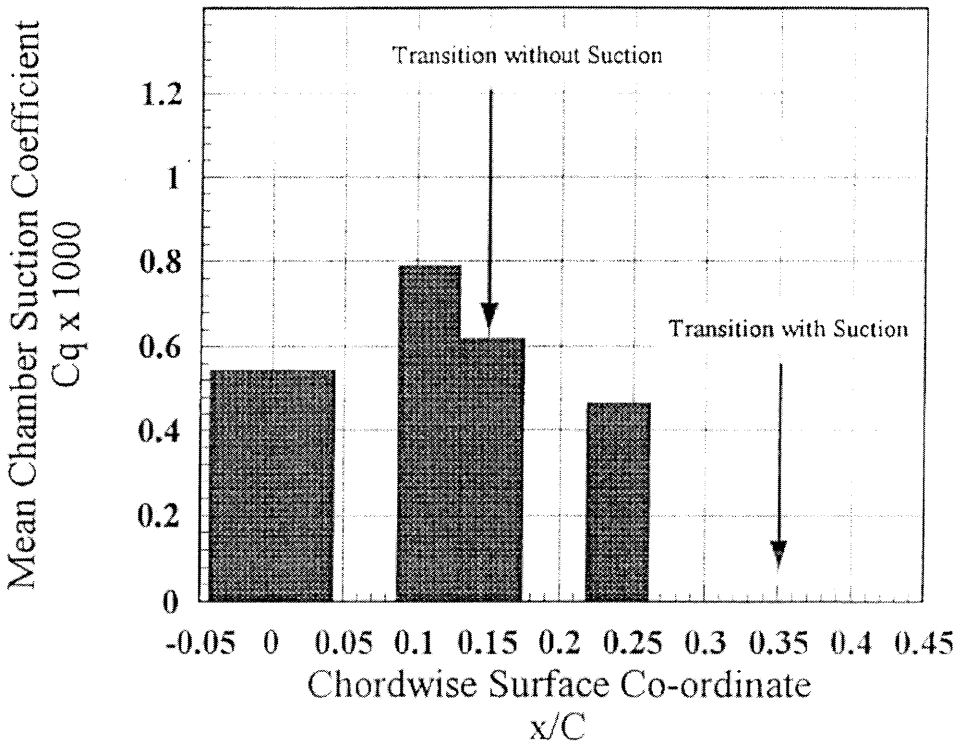

Figure 29. Example Suction Distribution, From Danks[5]

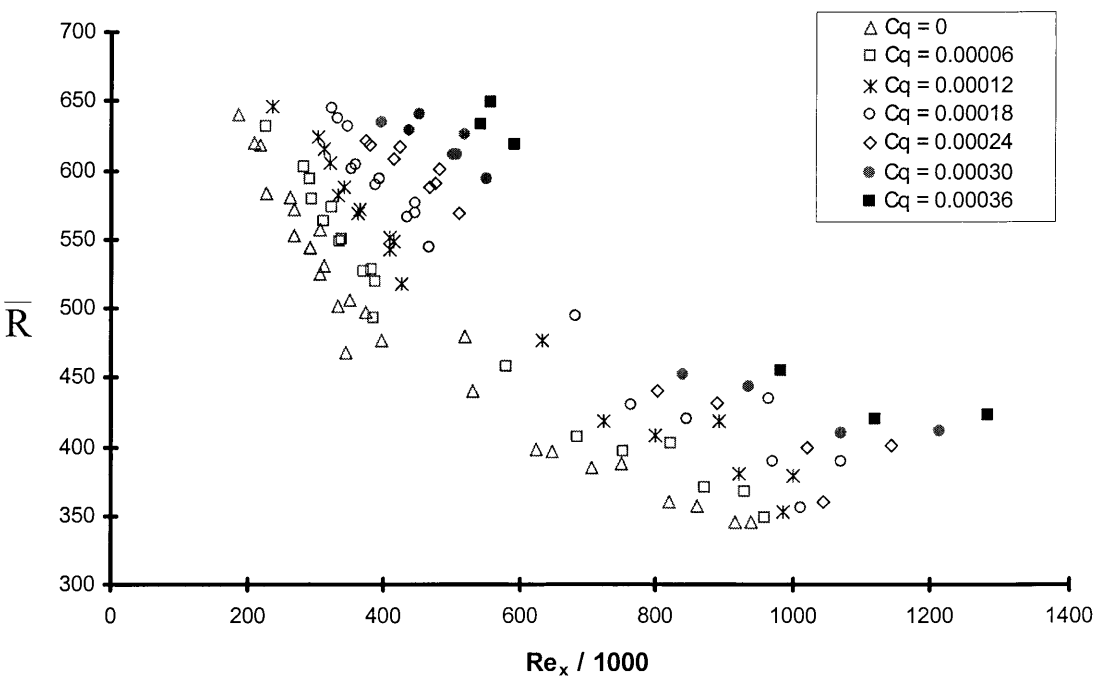

Figure 30. The Effect of Uniform, Distributed Suction on Cross-Flow Instability - The Onset of Transition

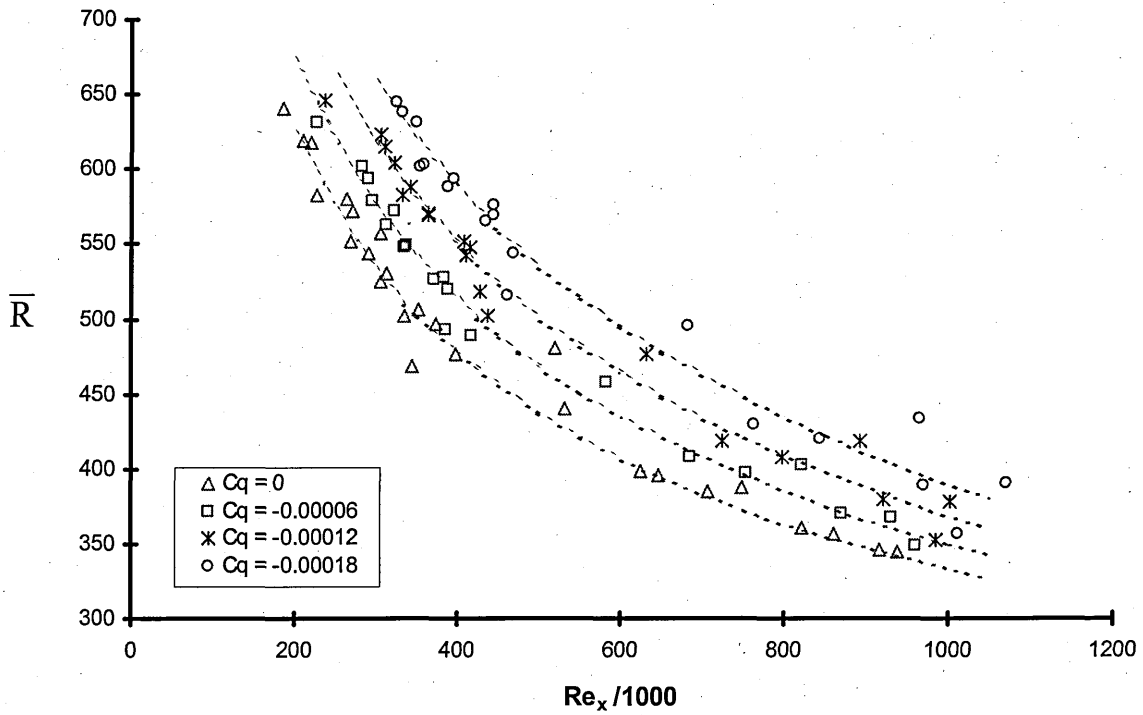

Figure 31. Comparison of Power Law Curve Fits with Experimental Data

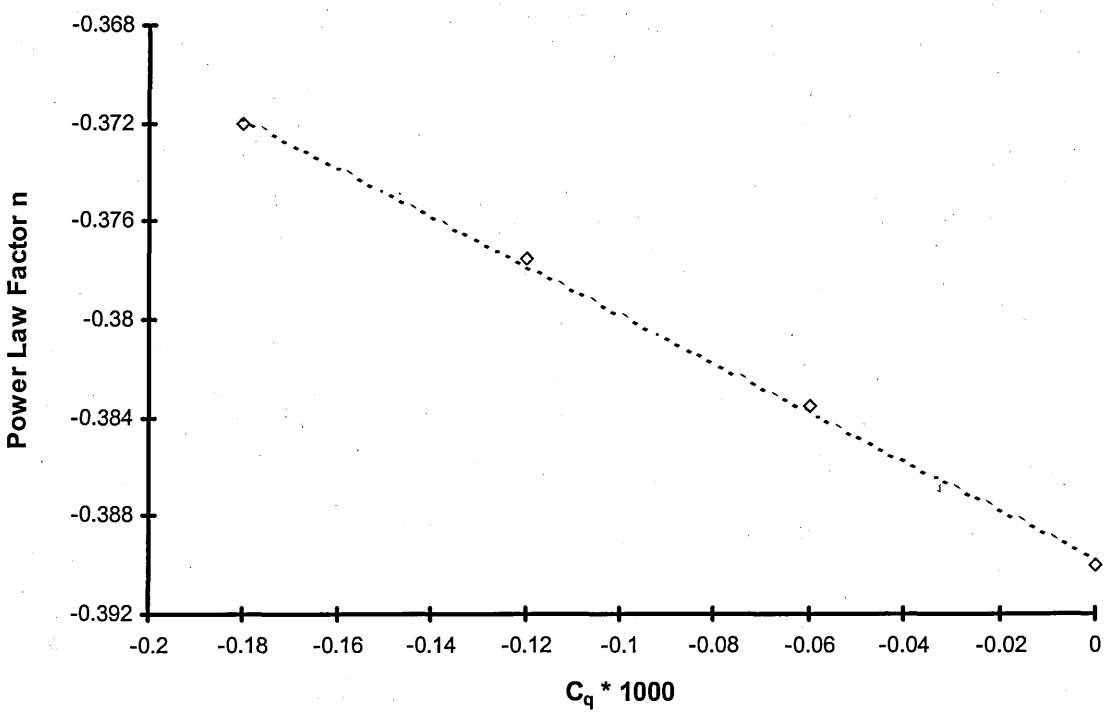

Figure 32. Variation of Empirical Relation Coefficient n With C_q and Linear Approximation

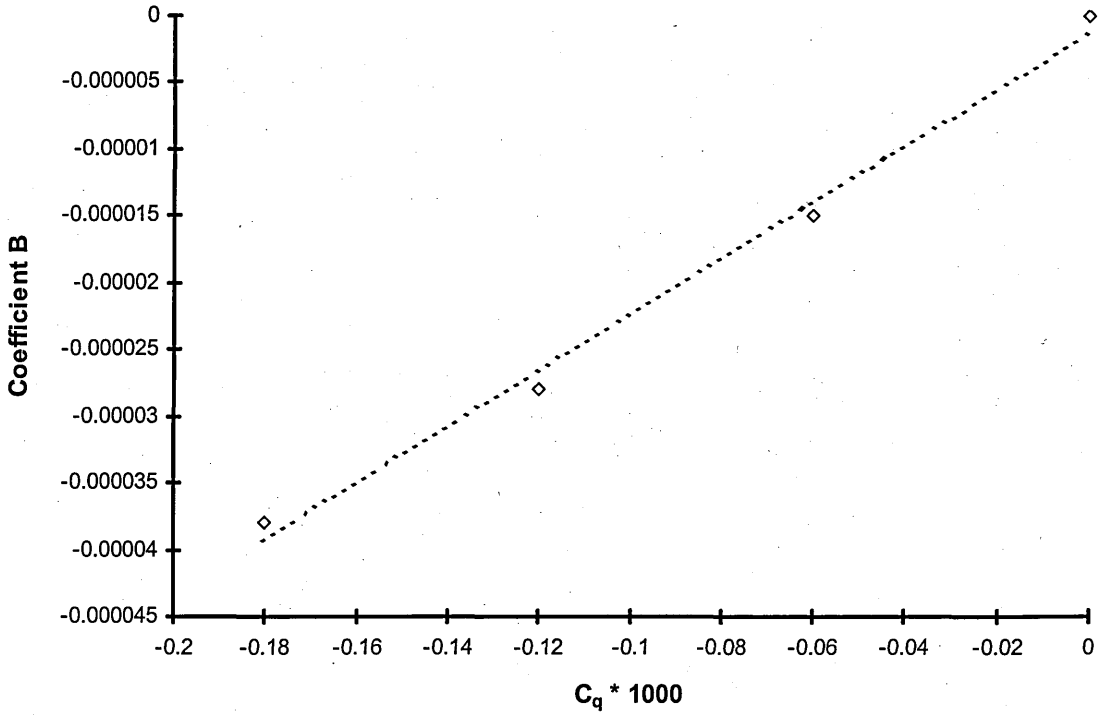

Figure 33. Variation of Empirical Relation Coefficient B with C_q and Linear Approximation

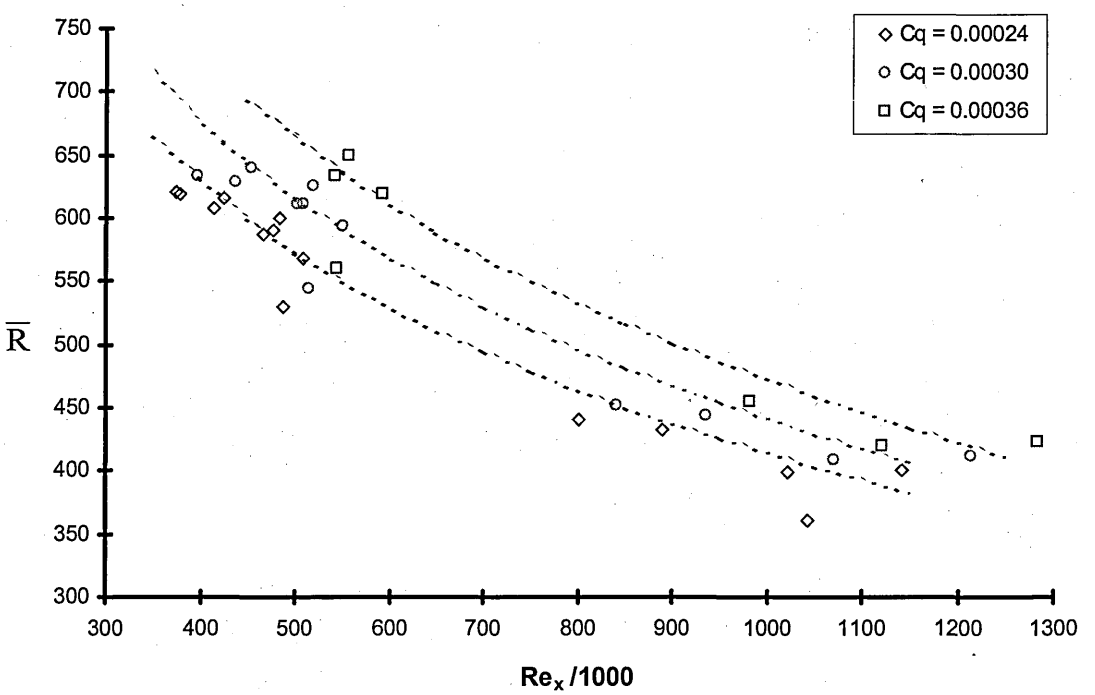

Figure 34. Curve Fits Calculated from Empirical Relation and Comparison with Experimental Data

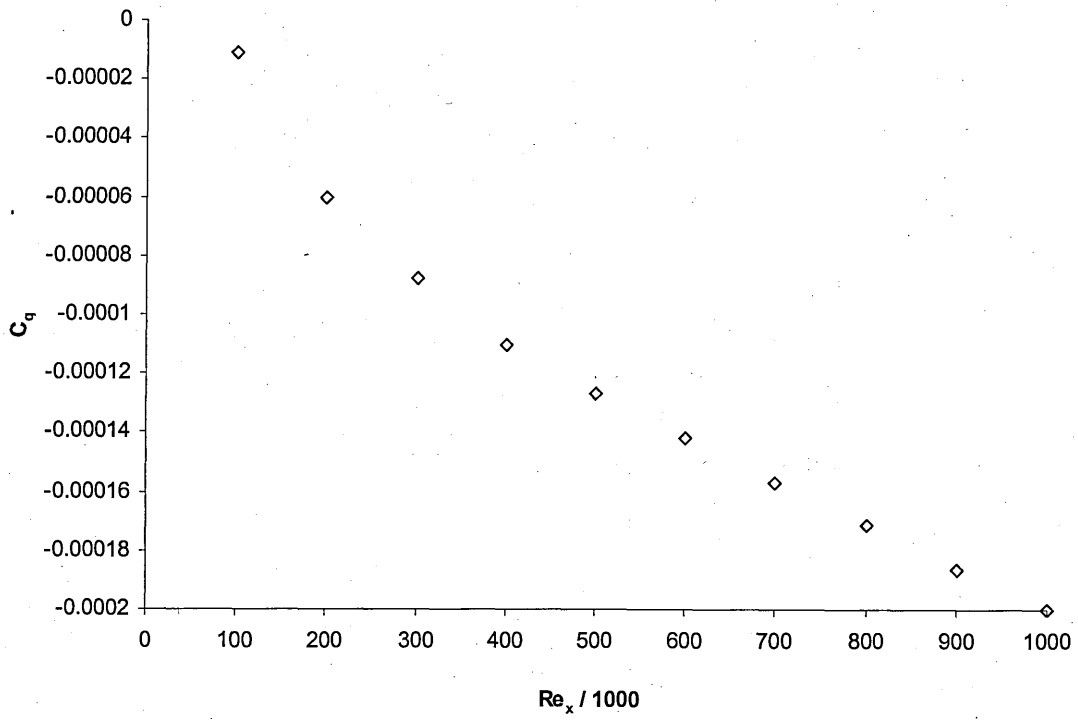

Figure 35. The Suction Required To Offset The Porous Surface Penalty

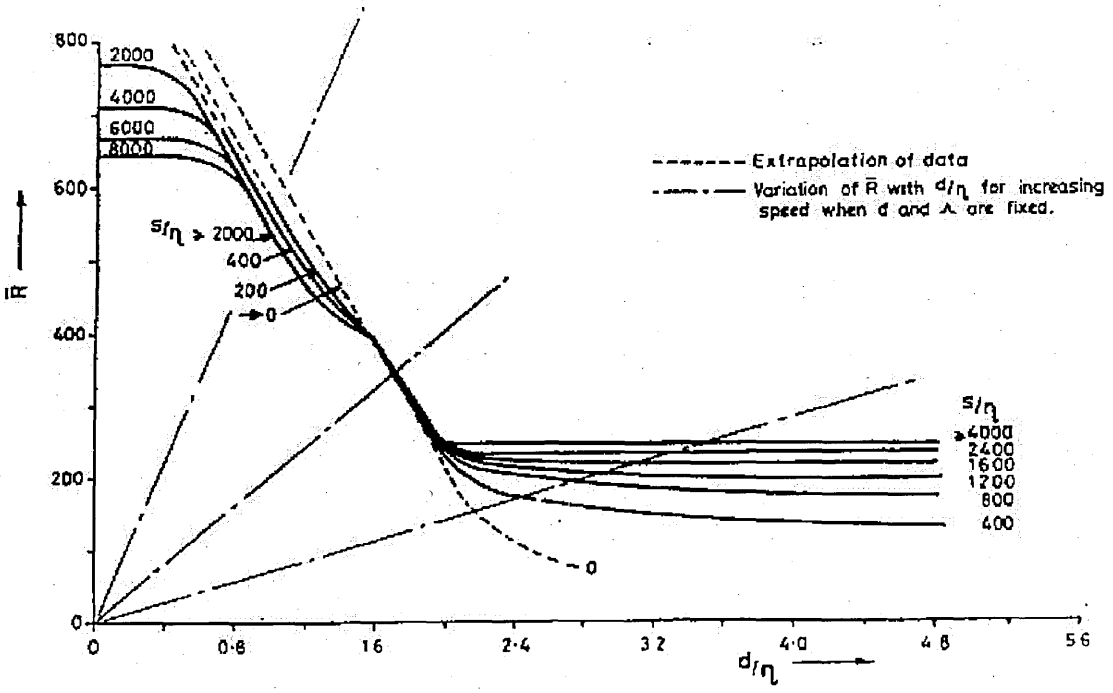

Figure 36. The Variation Of $\bar{R}$ With d/η And s/η For The Appearance Of First Bursts Of Turbulence, From Poll[4]

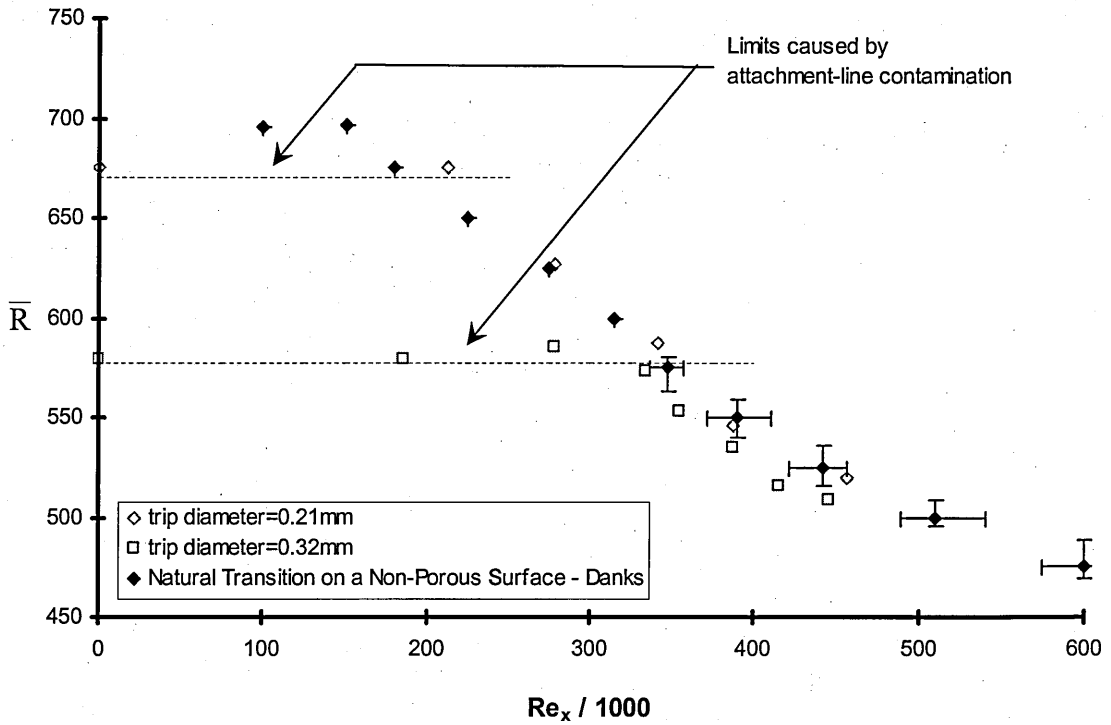

Figure 37. Transition Characteristics, On Non-Porous Surface, with Two-Dimensional Trip-Wires, And Comparison With Natural Transition Data From Danks[5]

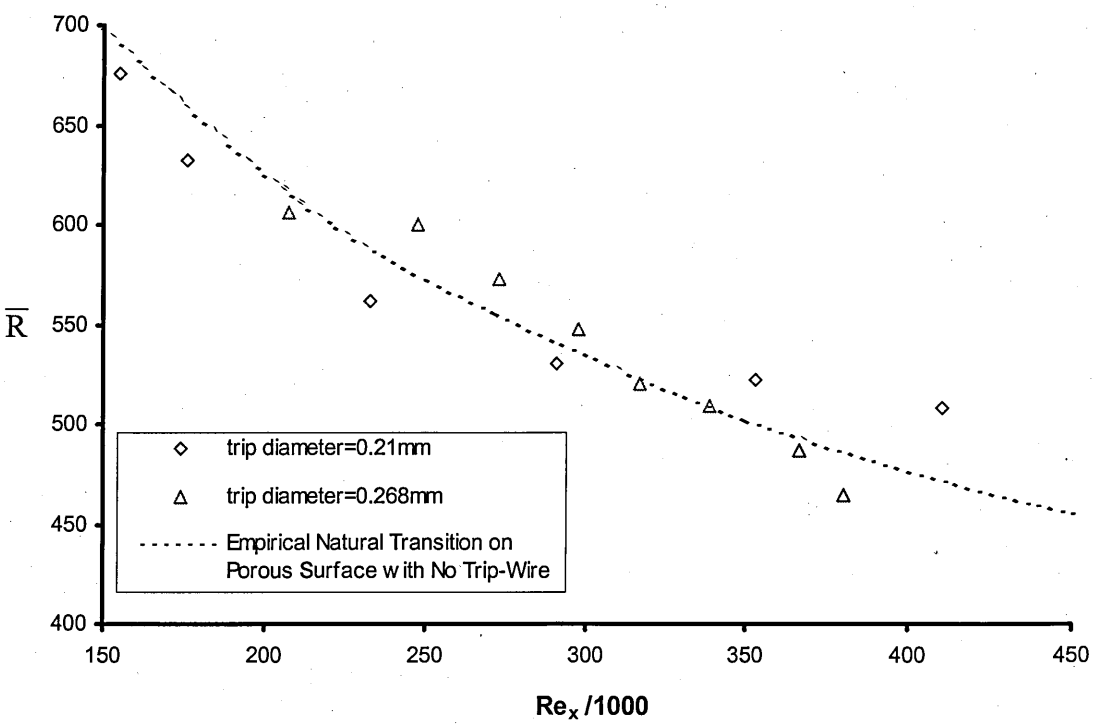

Figure 38. Transition Characteristics, On A Porous Surface, with Two-Dimensional Trip-Wires

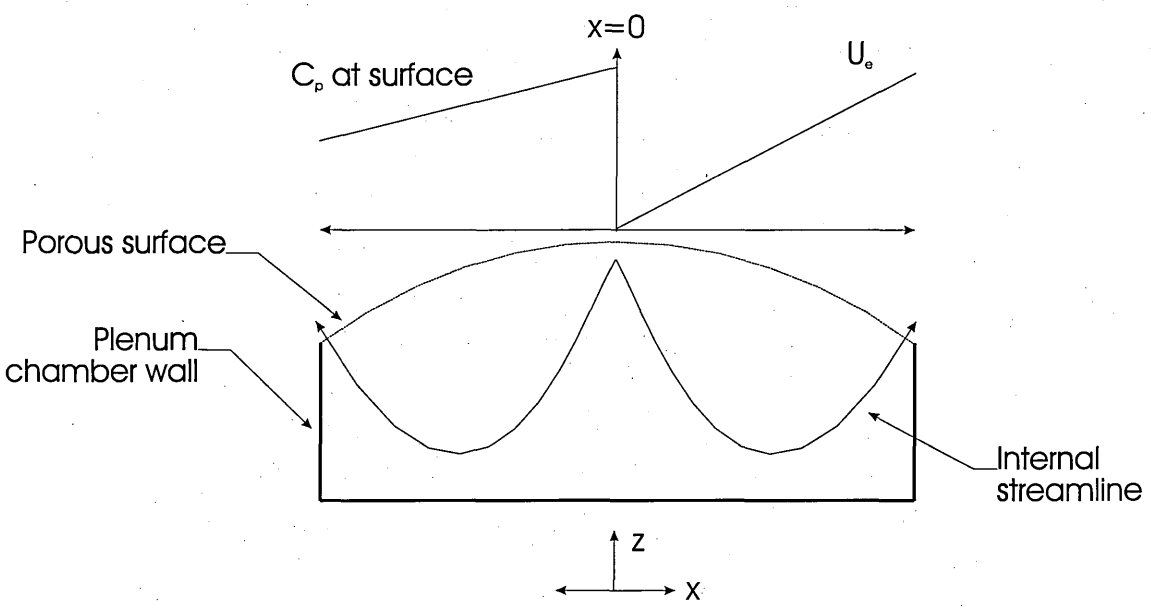

Figure 39. Schematic Diagram of Flow Pattern Leading To Attachment-Line Blowing

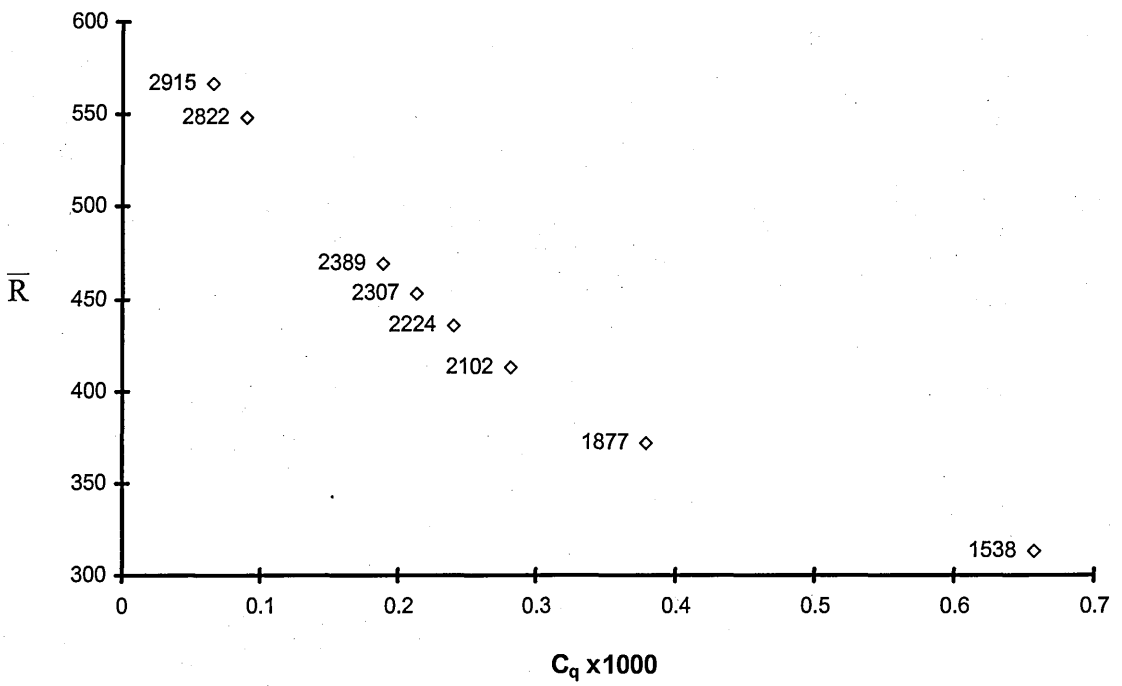

Figure 40. Attachment-Line Transition Characteristics Caused by Blowing, With s/η Values

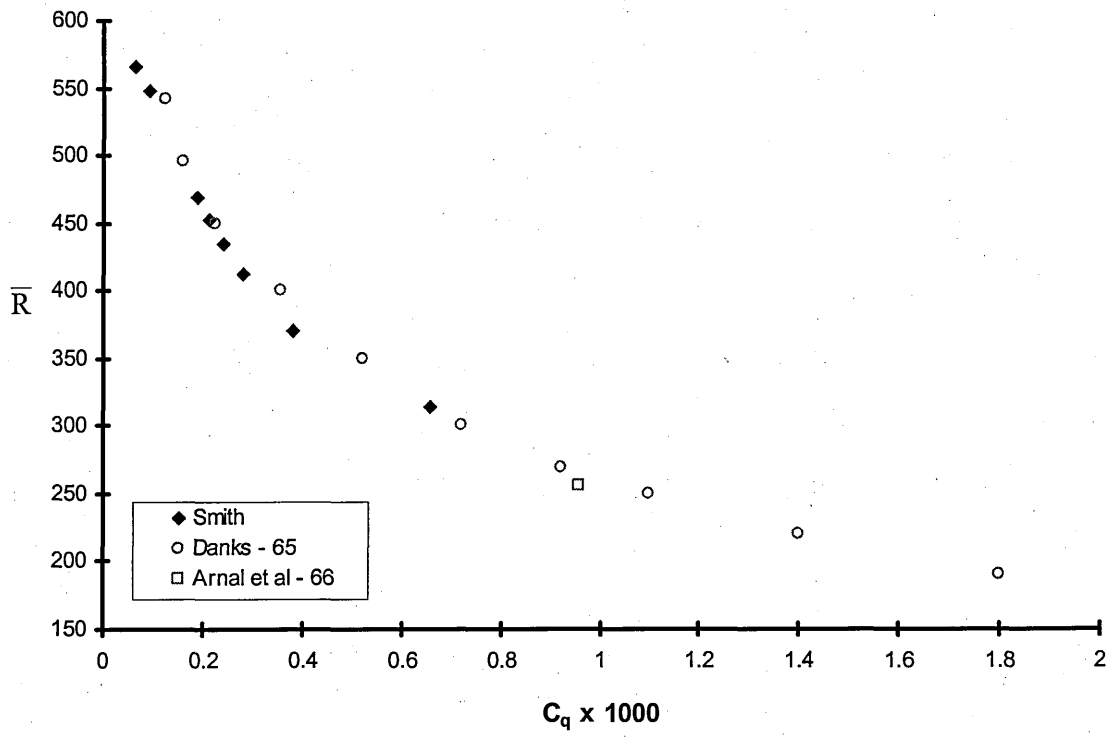

Figure 41. Comparison of Attachment-Line Transition Characteristics Caused by Blowing with Data from Danks[65] and Arnal[47]

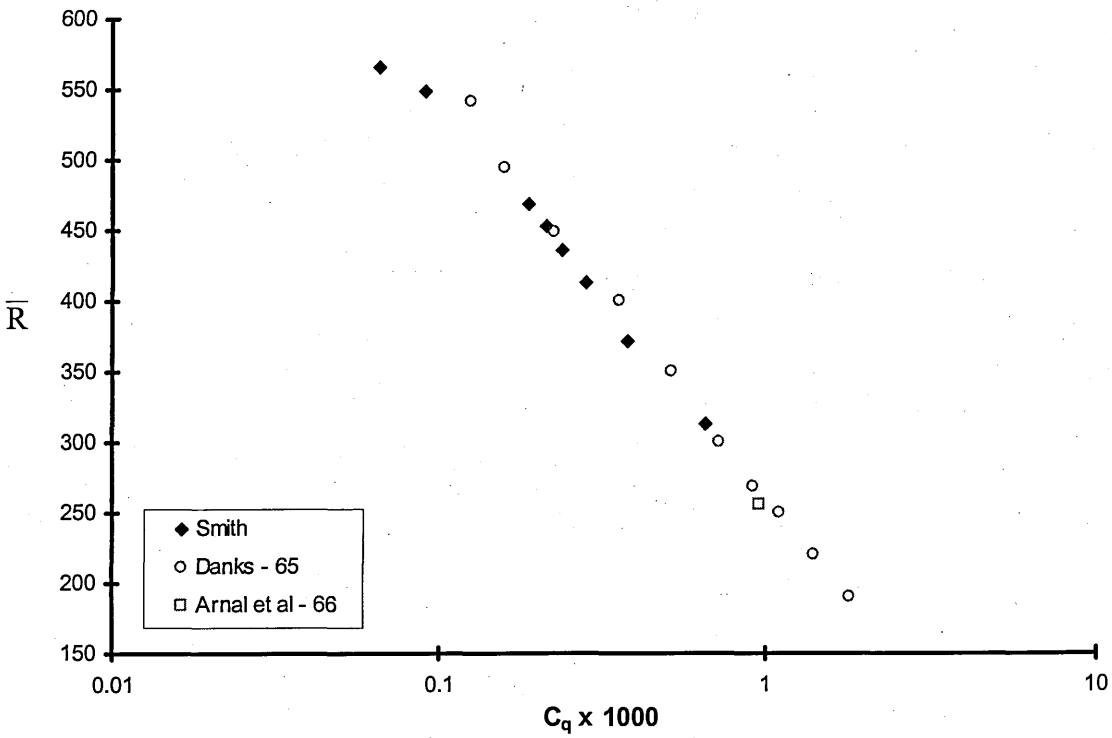

Figure 42. Attachment-Line Blowing Results Plotted on a Logarithmic Scale

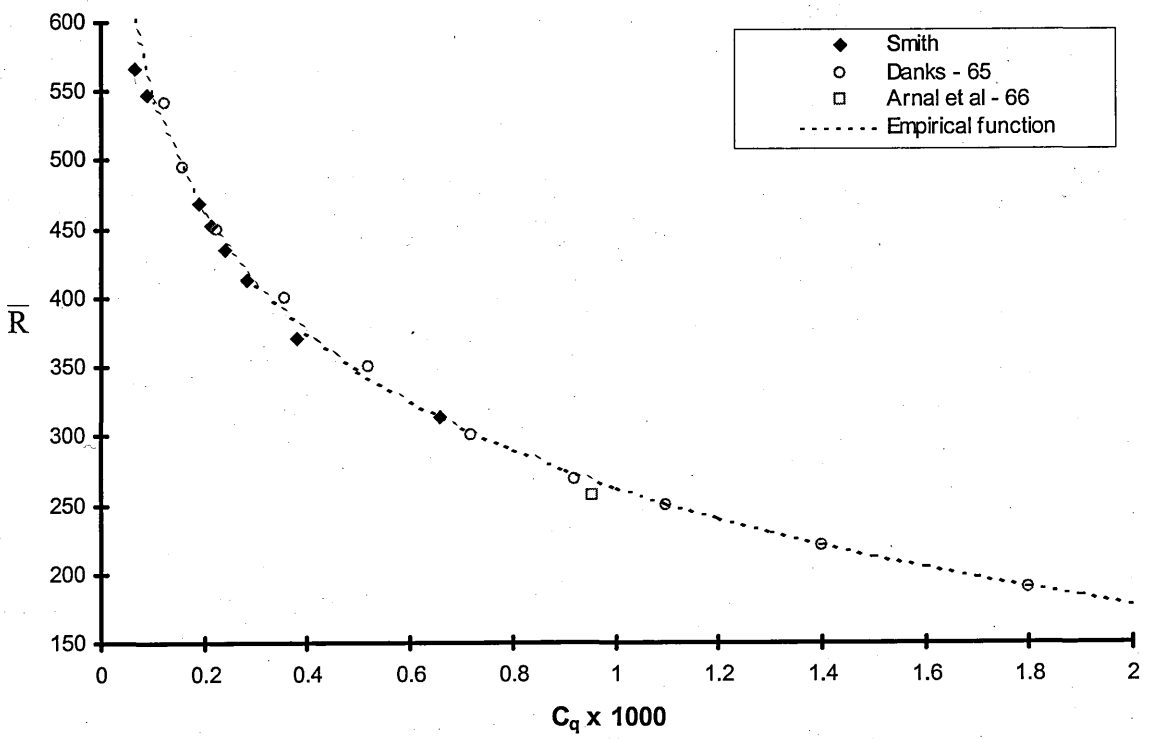

Figure 43. Comparison of Empirical Function with Experimental Blowing Results

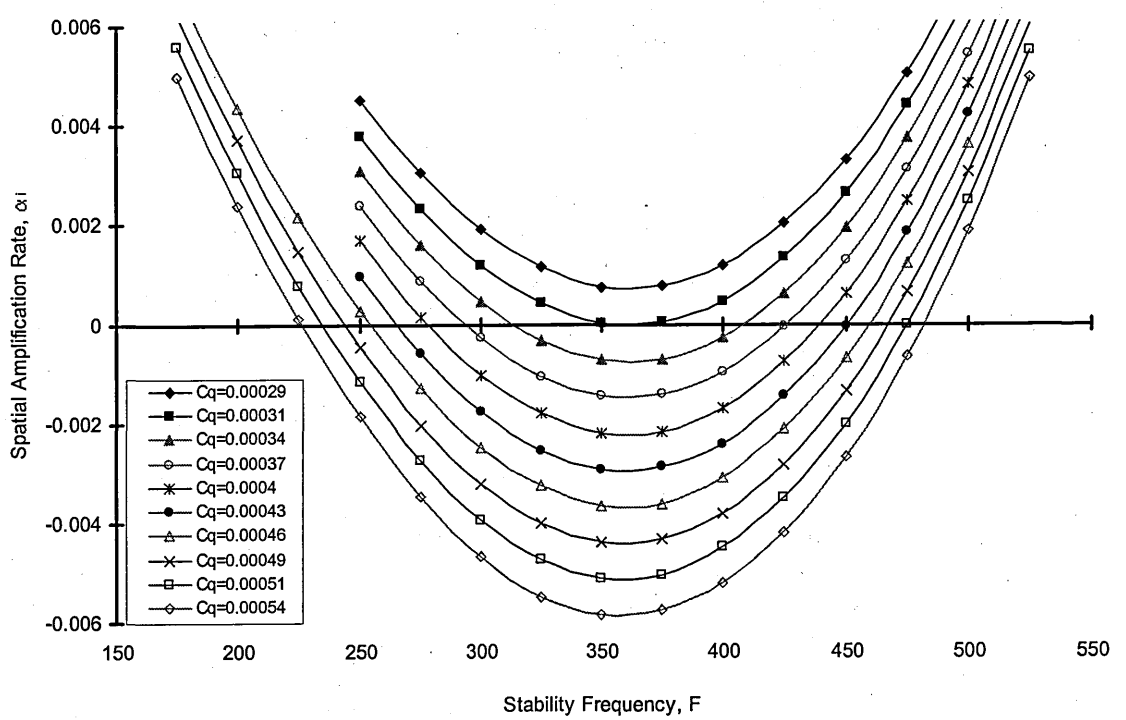

Figure 44. Linear Stability Envelope For $\bar{R}$=350, From Theofilis[48]

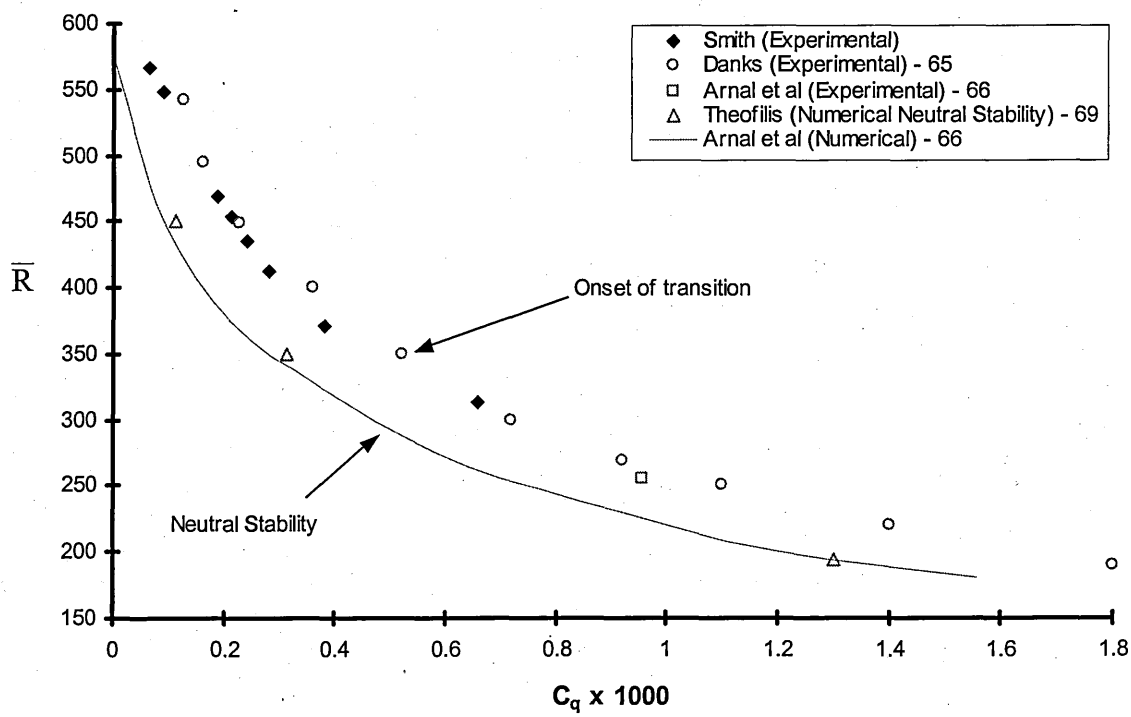

Figure 45. Comparison of Experimental and Numerical Blowing Results

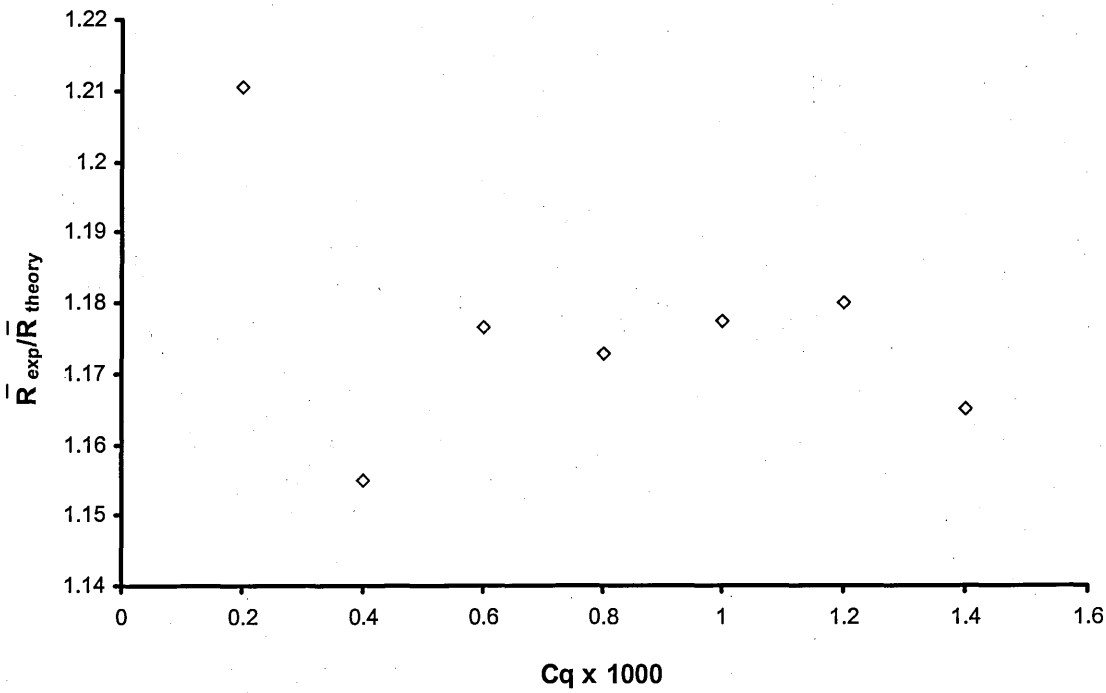

Figure 46. Difference Between Experimental and Theoretical Blowing Results

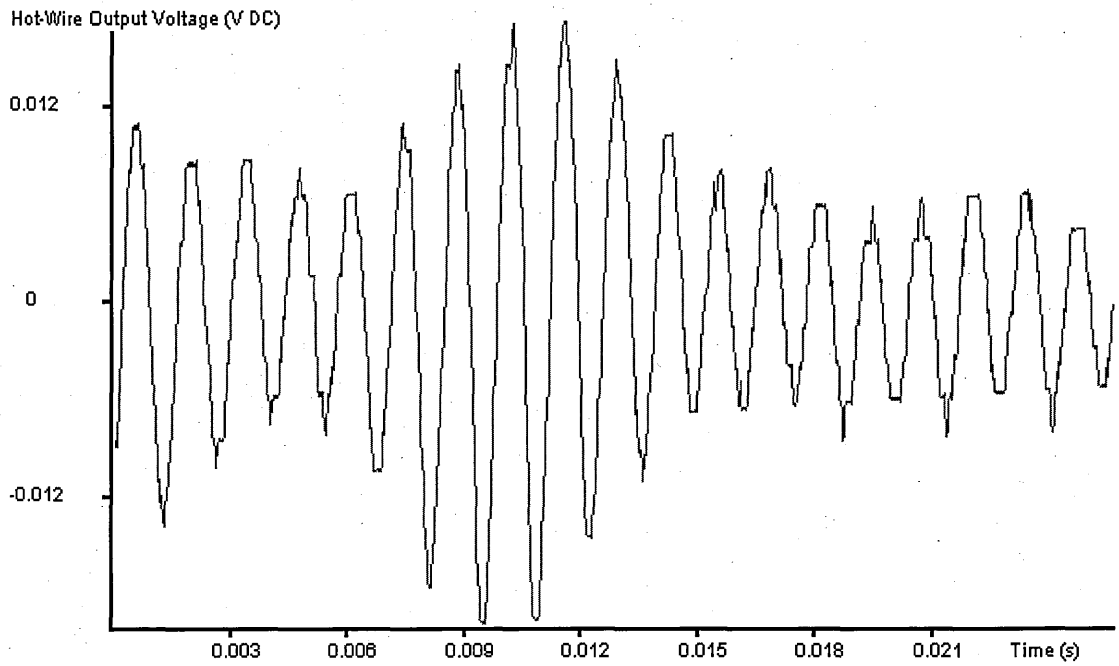

Figure 47. Example of Laminar Disturbance in an Attachment-Line With Blowing; $\overline{R}$ =372, C_q=0.000349, s/η=1900

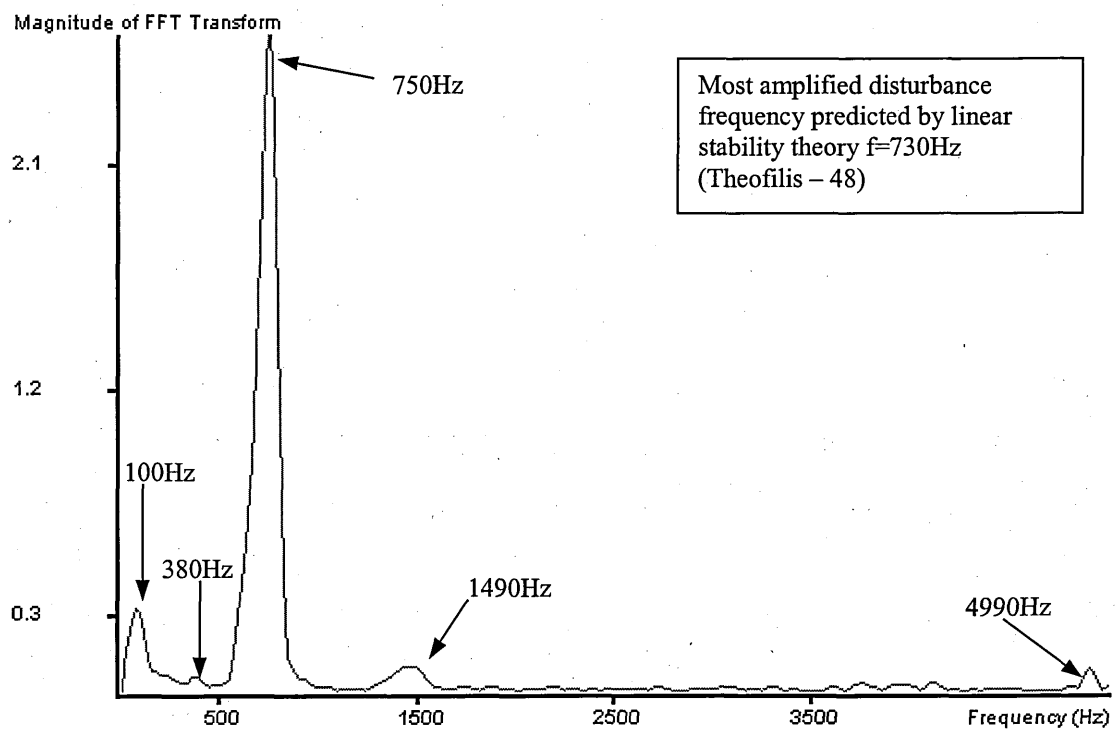

Figure 48. Amplitude Spectrum of Laminar Disturbance with Key Frequencies Marked; $\overline{R}$ =372, C_q=0.000349, s/η=1900

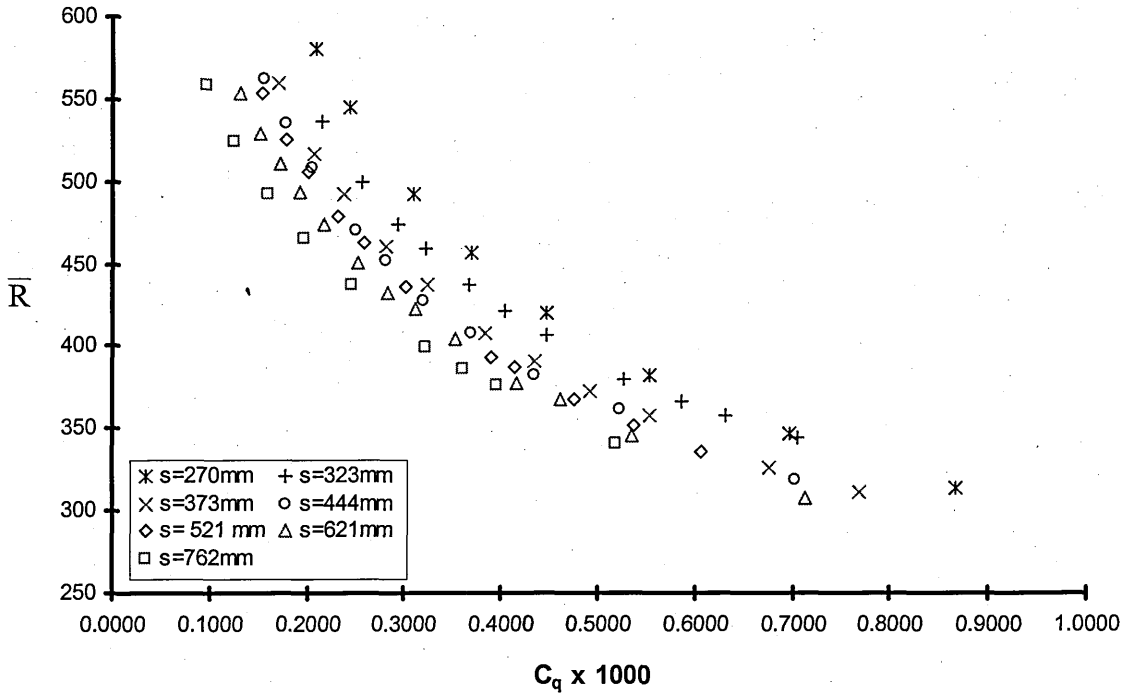

Figure 49. Effect of Spanwise Transpiration Length on Blowing Characteristics for a Sweep Angle of 55°

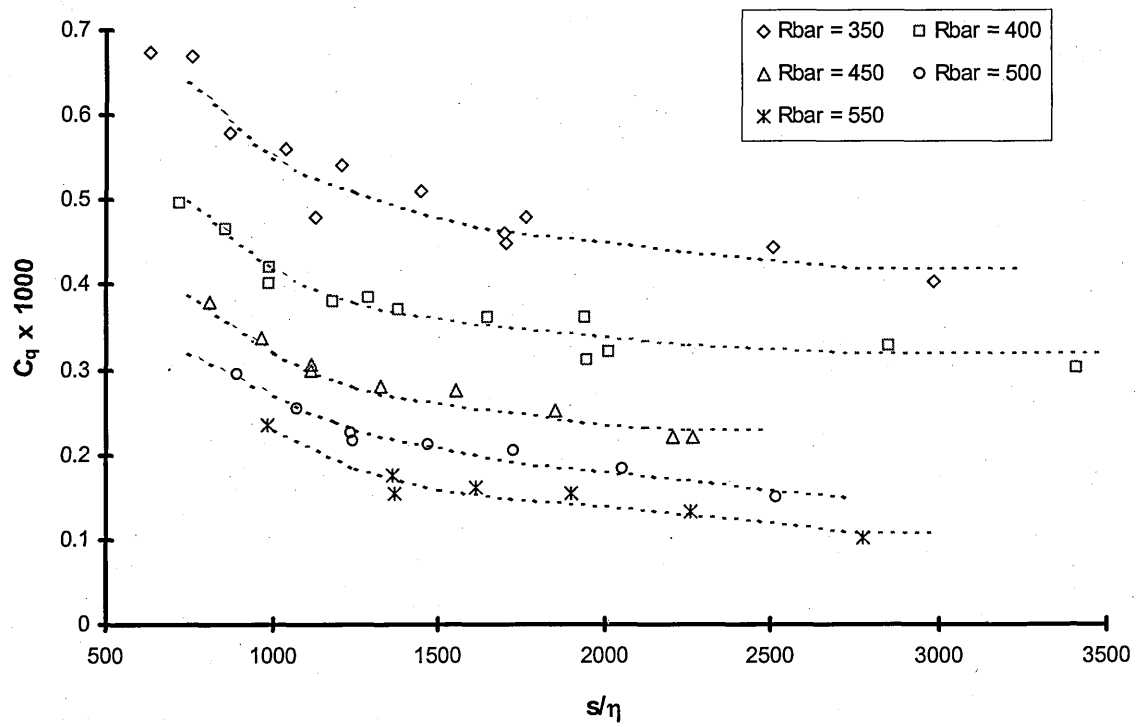

Figure 50. Effect of Non-Dimensional Spanwise Length on Blowing Characteristics at Constant $\overline{R}$

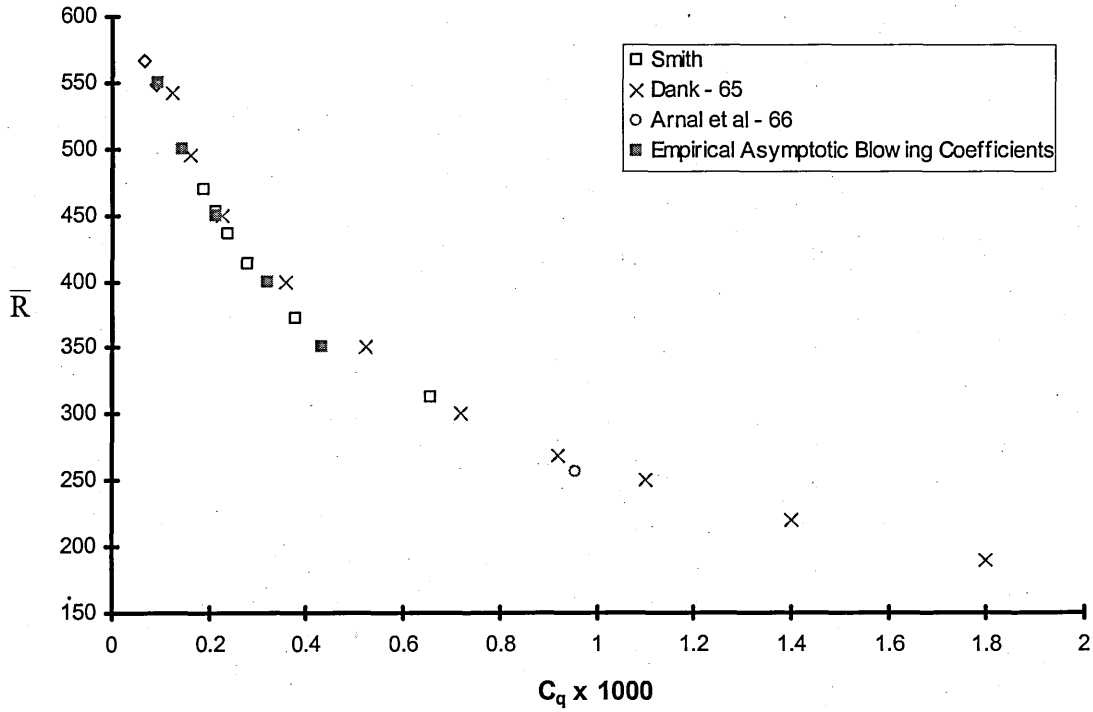

Figure 51. Comparison of Empirical Asymptotic Blowing Coefficients with Previous Experimental Results

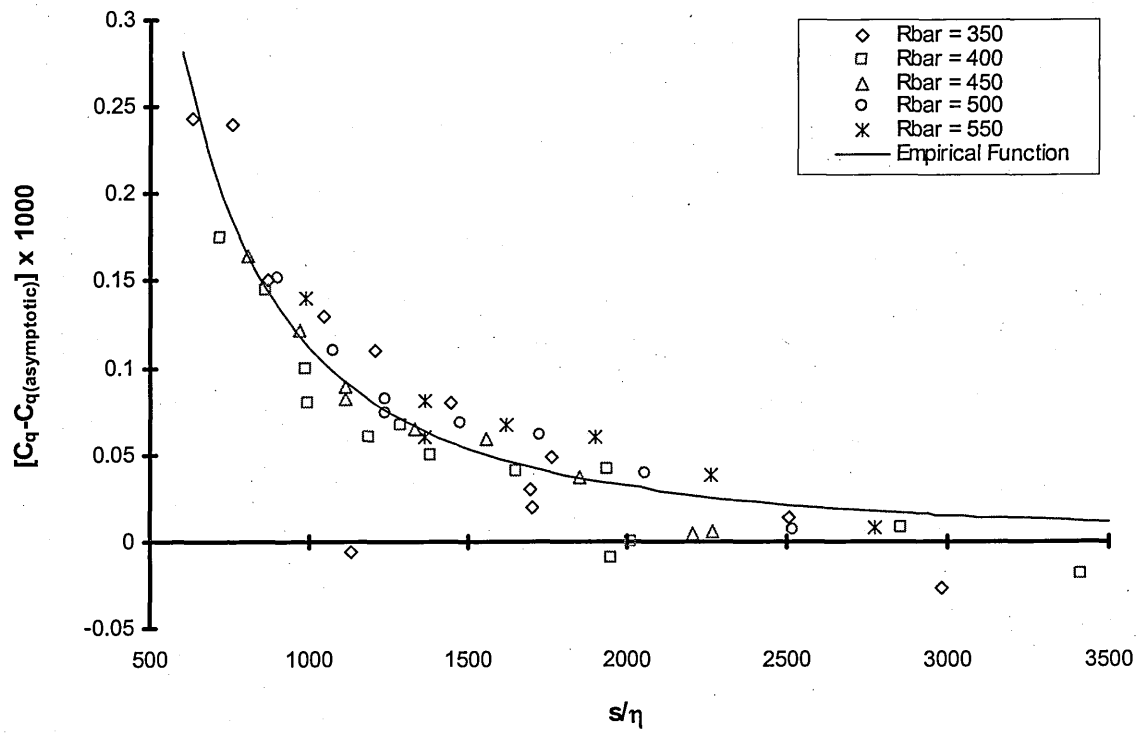

Figure 52. Collapsed Blowing Data and Comparison with Empirical Function

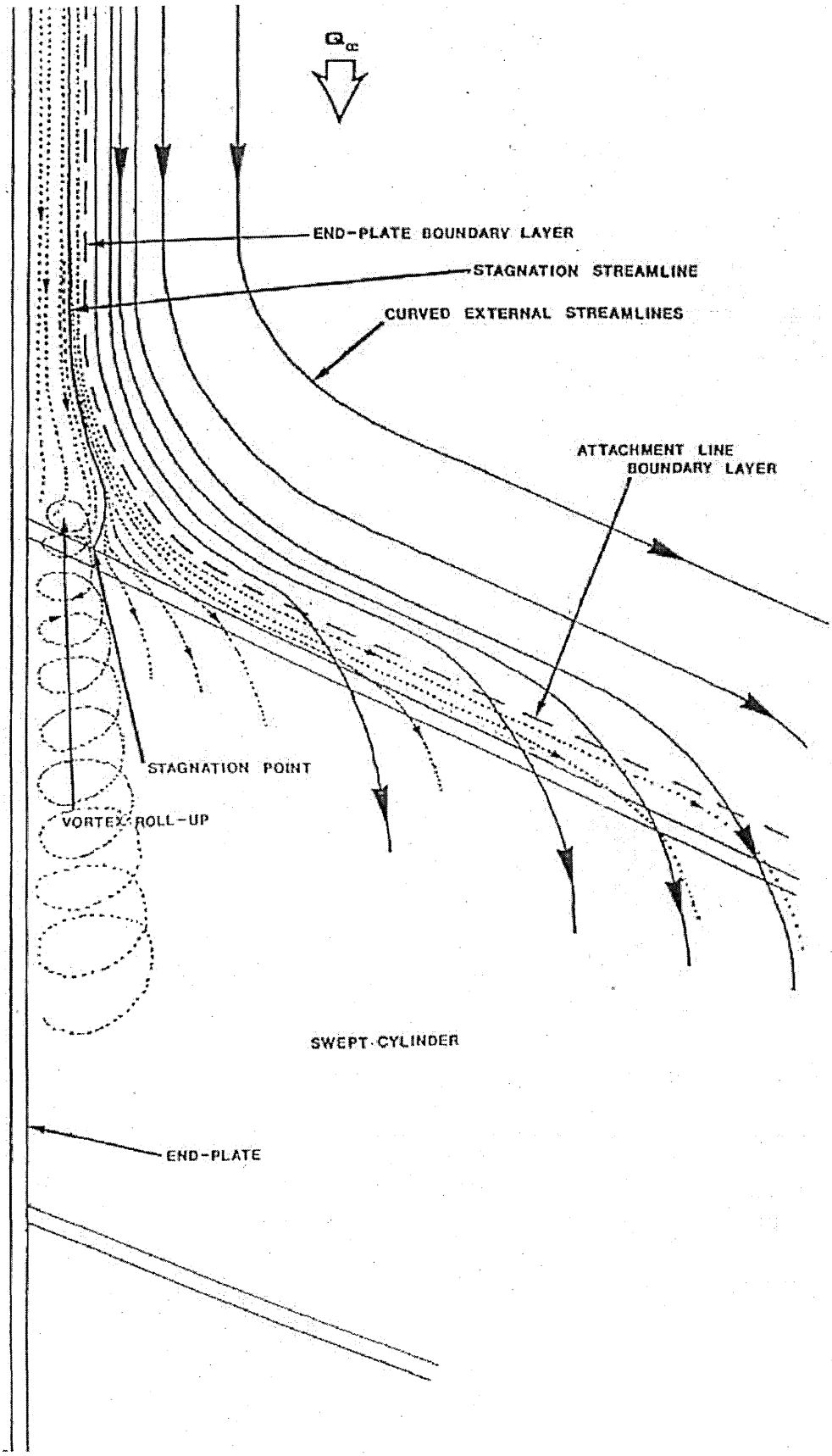

Figure 53. Schematic Representation Of The Likely Flow Characteristics In The Root Region, From Bergin[44]

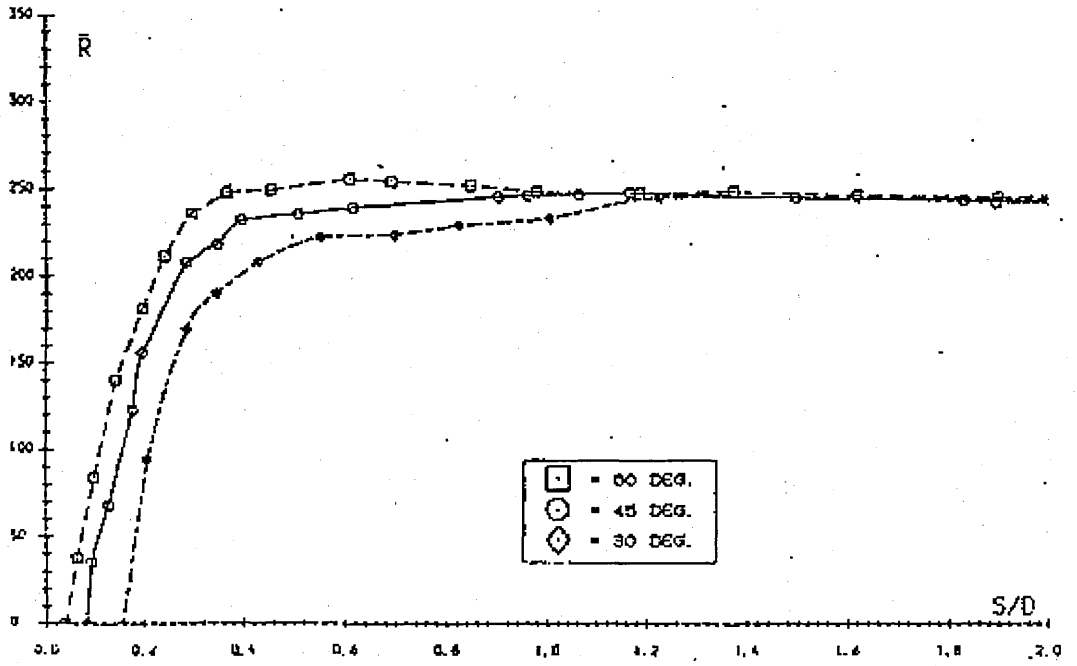

Figure 54. Variation of $\overline{R}$ in the Wing-Fuselage Junction, From Bergin[51]

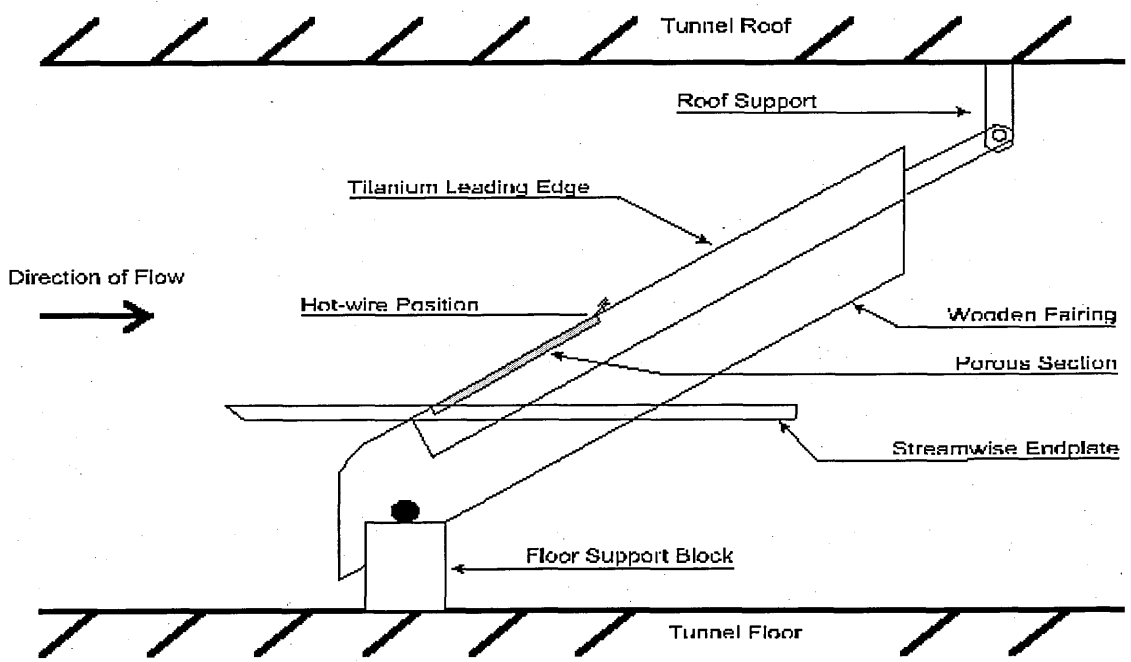

Figure 55. Arrangement of the Model in the Wind Tunnel during the Wing-Fuselage Junction Experiments

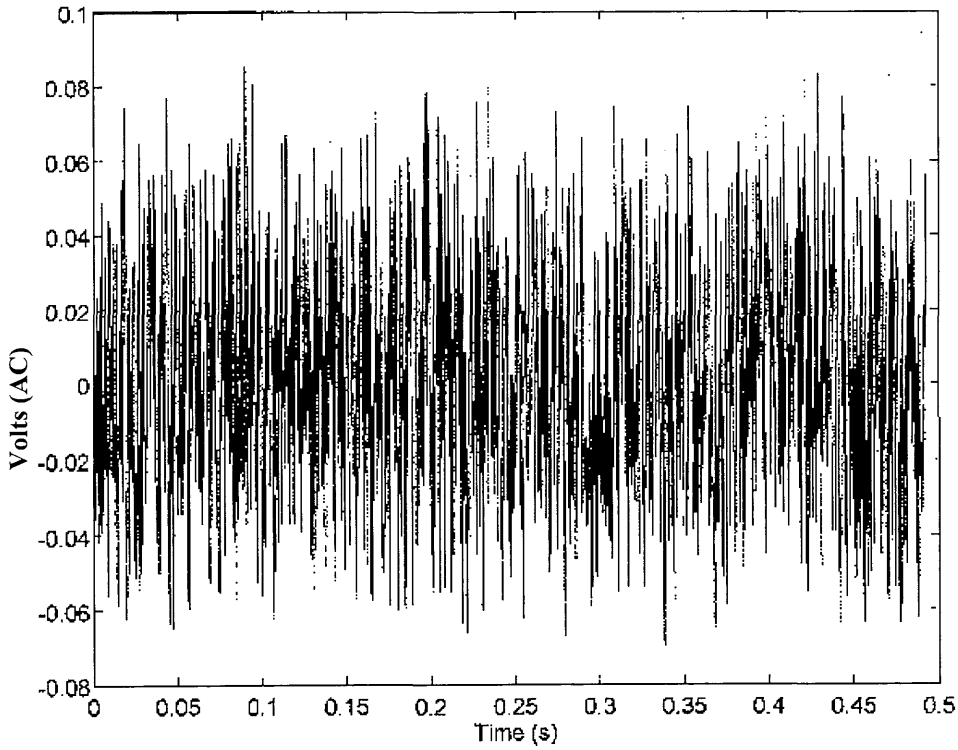

Figure 56(a). Hot-Wire Signal of Attachment-Line Downstream of Wing-Fuselage Junction - $\overline{R}$ =518, s/η=2492, s/D=2.2, C_q=0, Γ=1

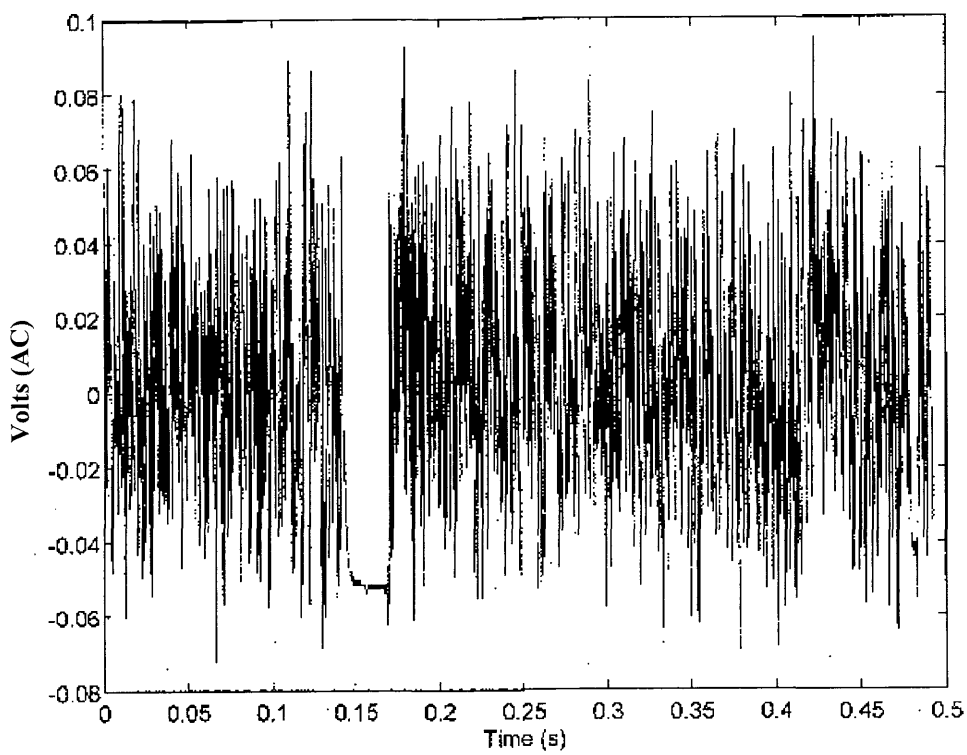

Figure 56(b). Hot-Wire Signal of Attachment-Line Downstream of Wing-Fuselage Junction - $\overline{R}$ =518, s/η=2492, s/D=2.2, C_q=-0.00465, Γ=0.94

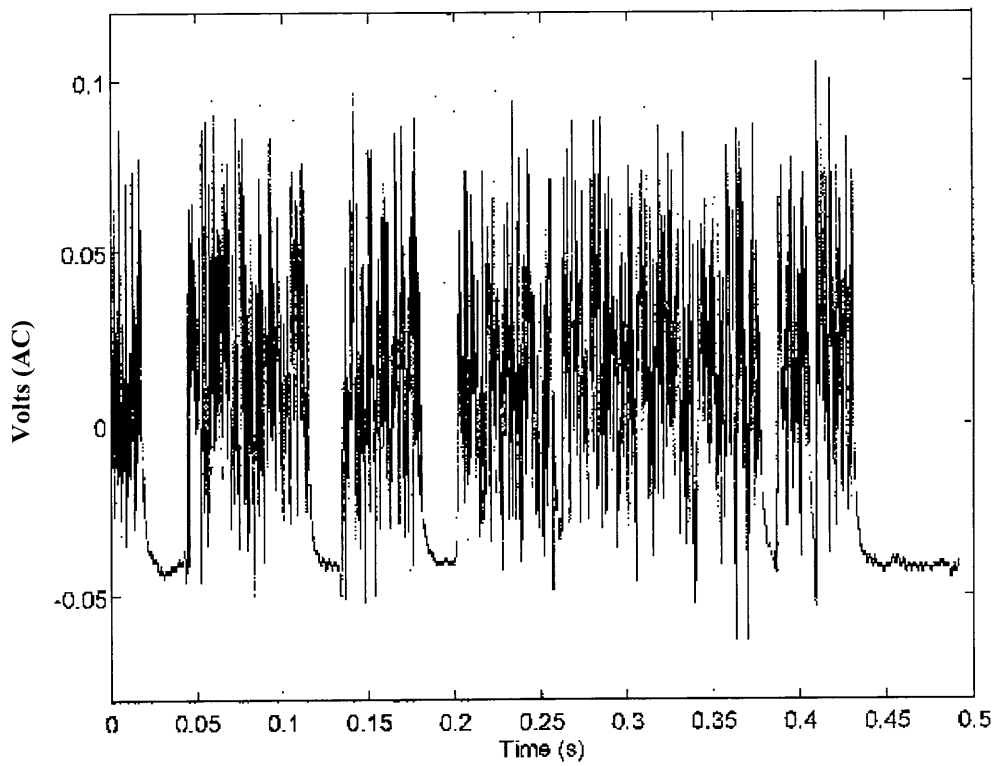

Figure 56(c). Hot-Wire Signal of Attachment-Line Downstream of Wing-Fuselage Junction - $\overline{R}$ =518, s/η=2492, s/D=2.2, C_q=-0.00623, Γ=0.79

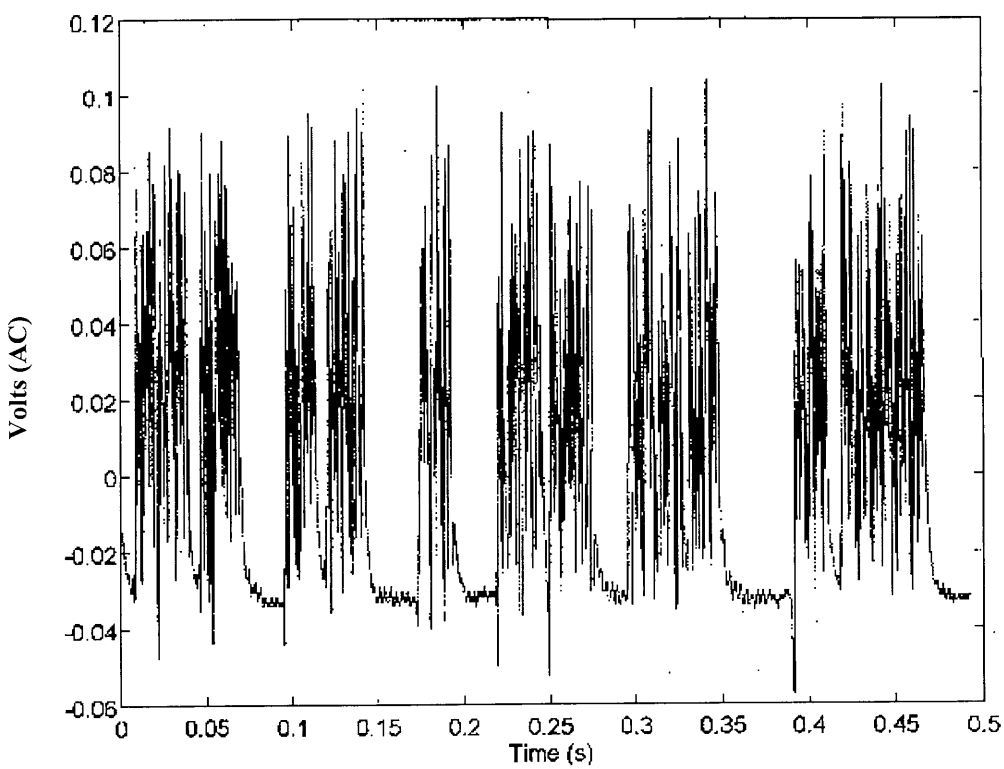

Figure 56(d). Hot-Wire Signal of Attachment-Line Downstream of Wing-Fuselage Junction - $\overline{R}$ =518, s/η=2492, s/D=2.2, C_q=-0.0151, Γ=0.72

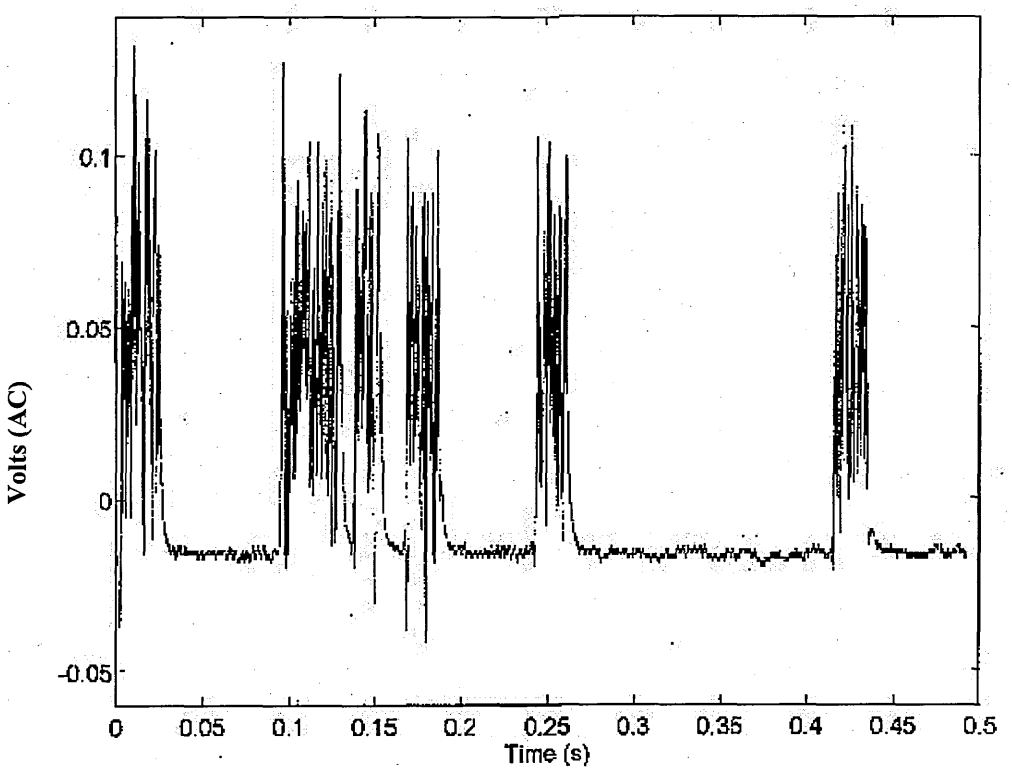

Figure 56(e). Sampled Hot-Wire Signal of Attachment-Line Downstream of Wing-Fuselage Junction - $\overline{R}$ =518, s/η=2492, s/D=2.2, C_q=-0.0339, Γ=0.33

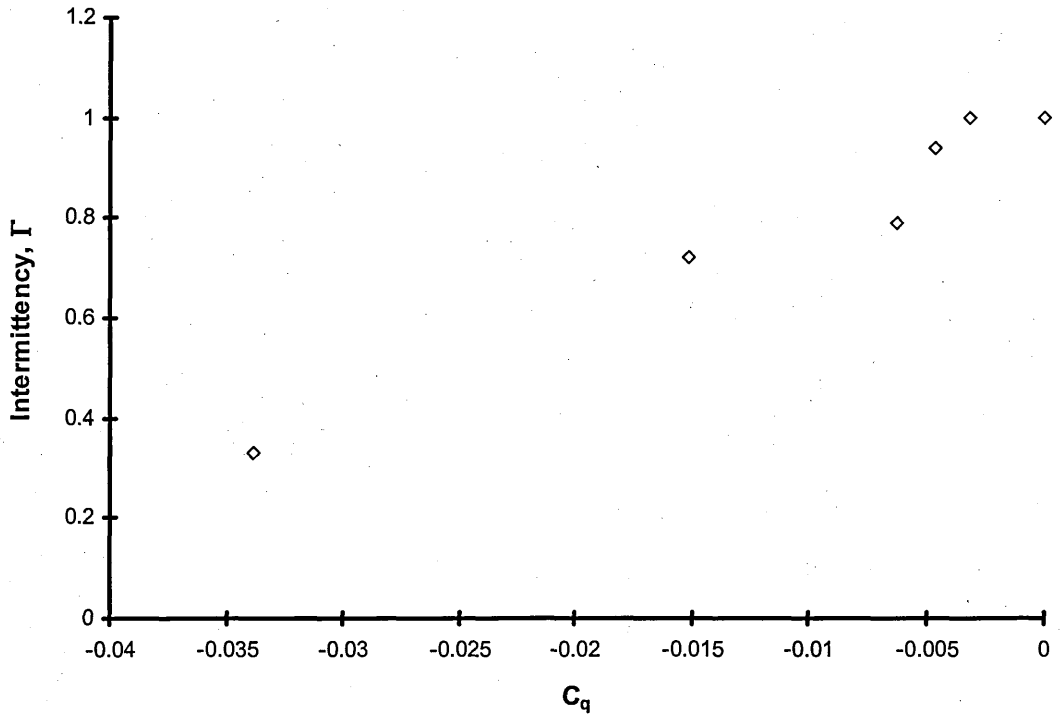

Figure 57. Variation of Intermittency With Suction Coefficient In The Wing-Fuselage Junction, $\overline{R}$ =518, s/η=2492, s/D=2.2

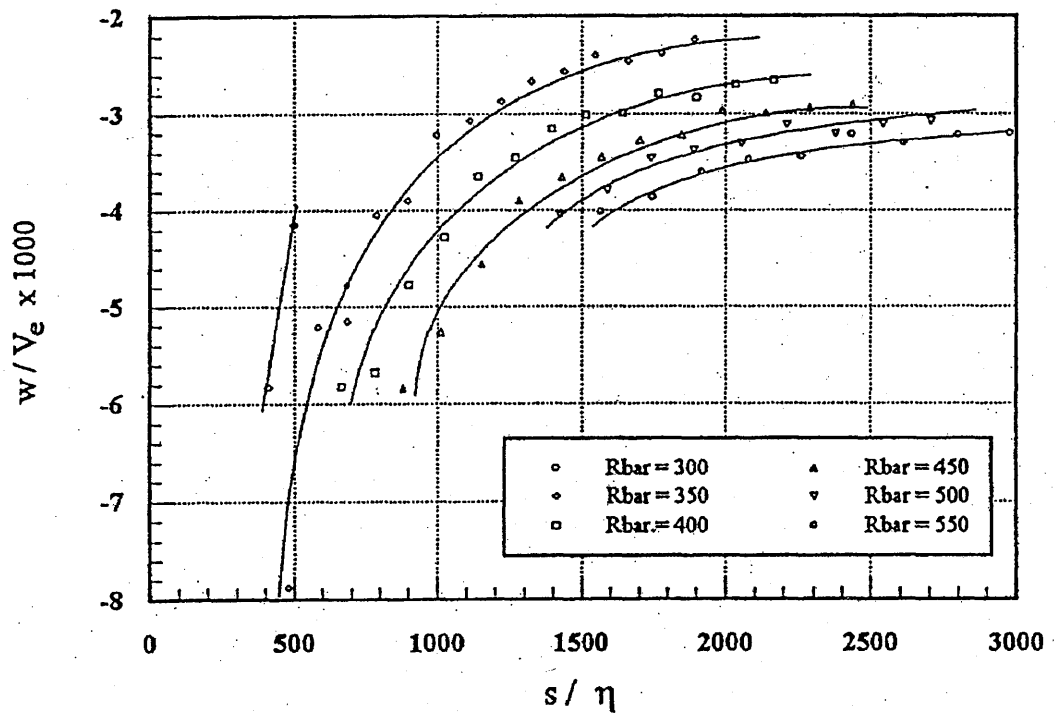

Figure 58. Results for the End of Attachment-Line Relaminarisation, From Danks[21]

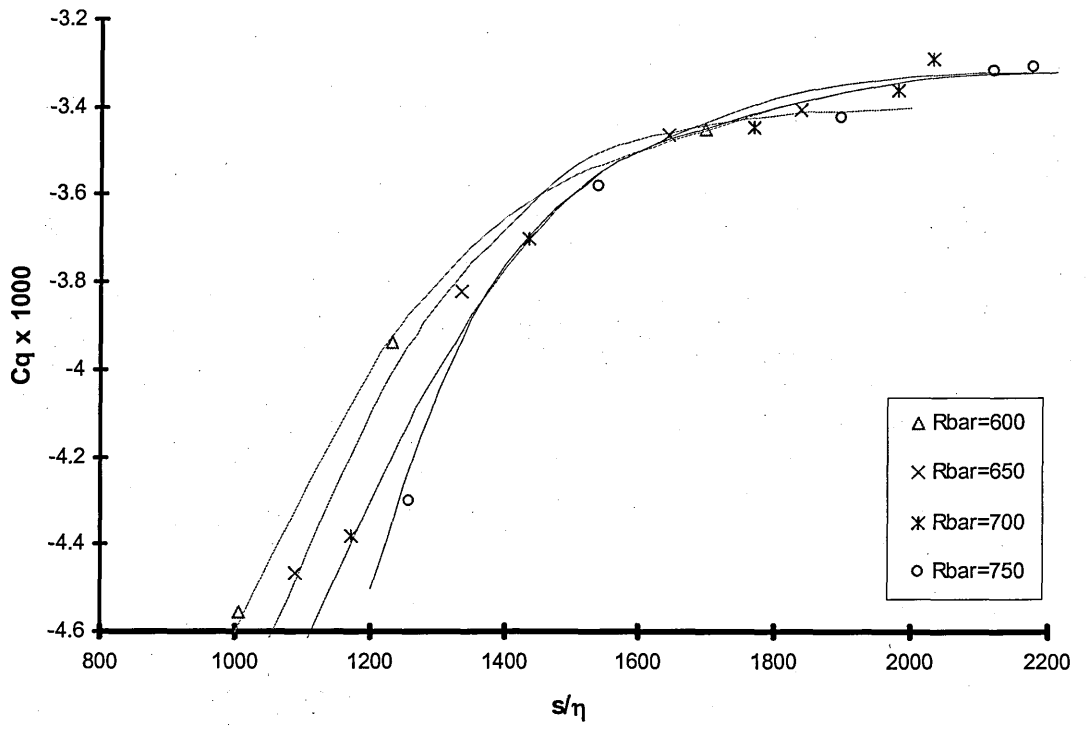

Figure 59. Critical Suction Rate For The End Of Relaminarisation (At Constant $\overline{R}$ Values Between 600 and 750)

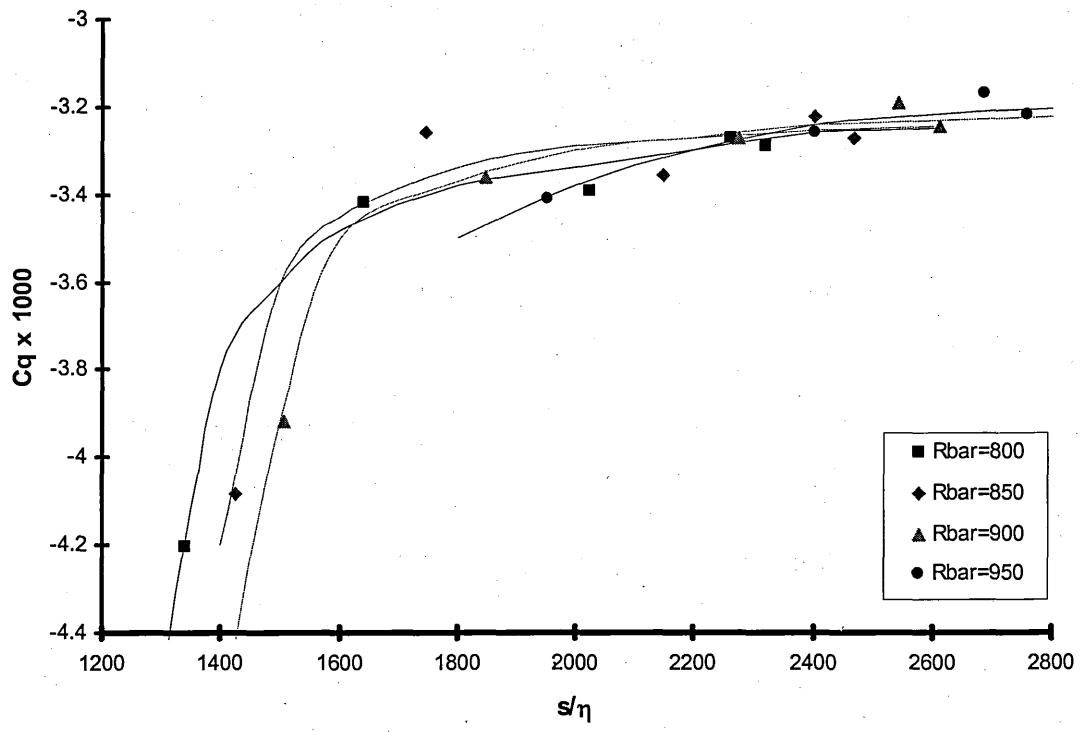

Figure 60. Critical Suction Rate For The End Of Relaminarisation (At Constant $\overline{R}$ Values Between 800 and 950)

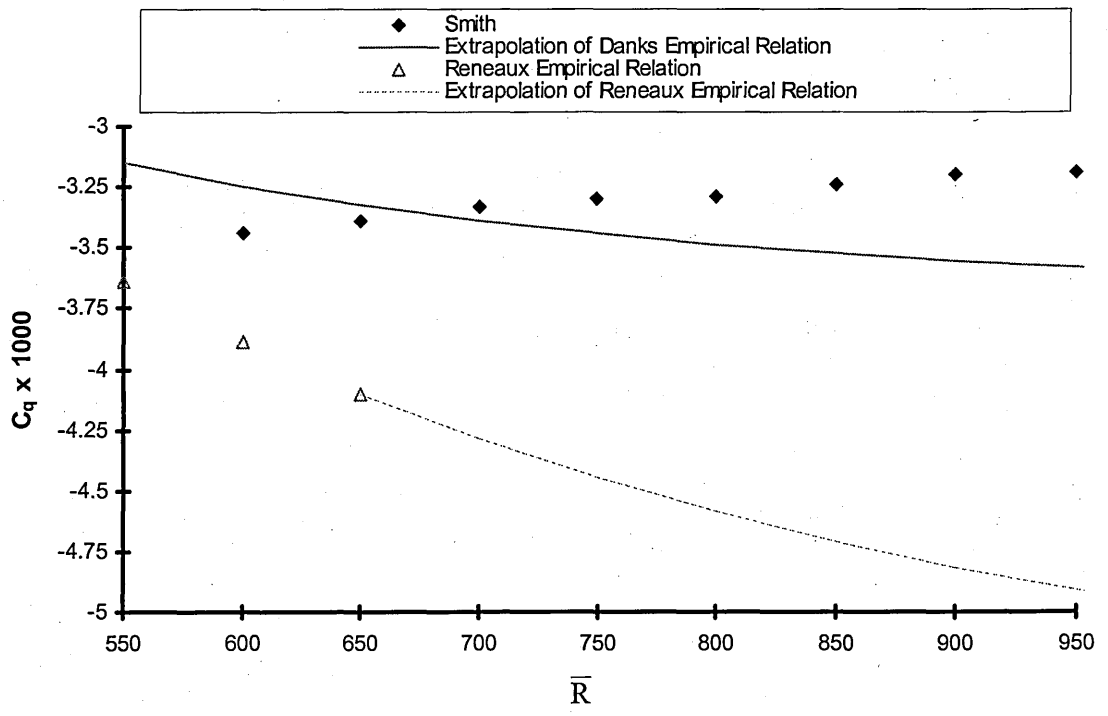

Figure 61. Comparison of Asymptotic Suction Coefficient Results with Danks[51] and Reneaux49

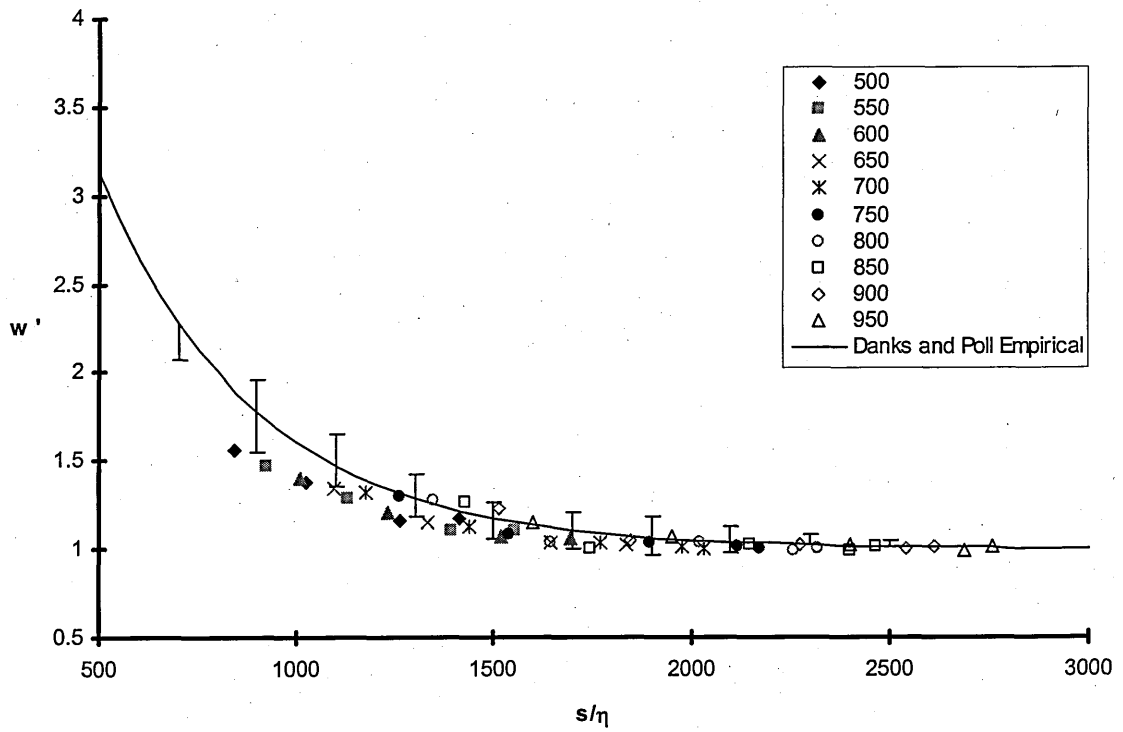

Figure 62. Normalised Suction Rate as A Function of Streamwise Distance (At Constant $\overline{R}$)

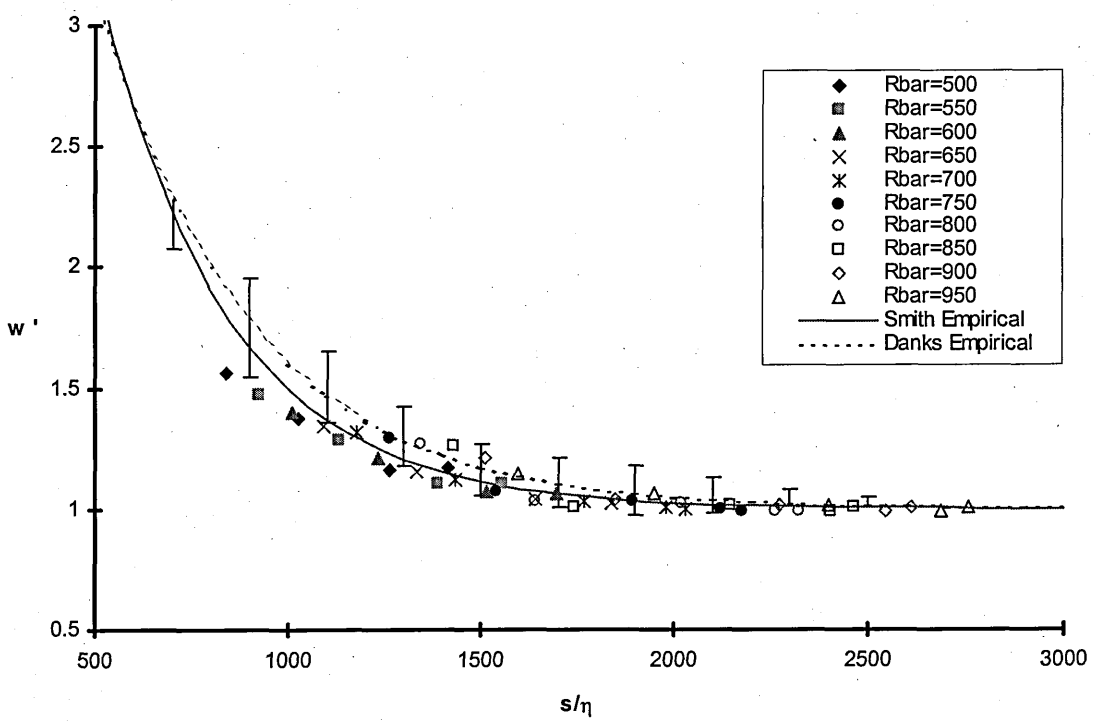

Figure 63. Revised Curve Fit For Normalised Suction Rate as A Function of Streamwise Distance (At Constant $\overline{R}$) And Comparison With Danks[51]

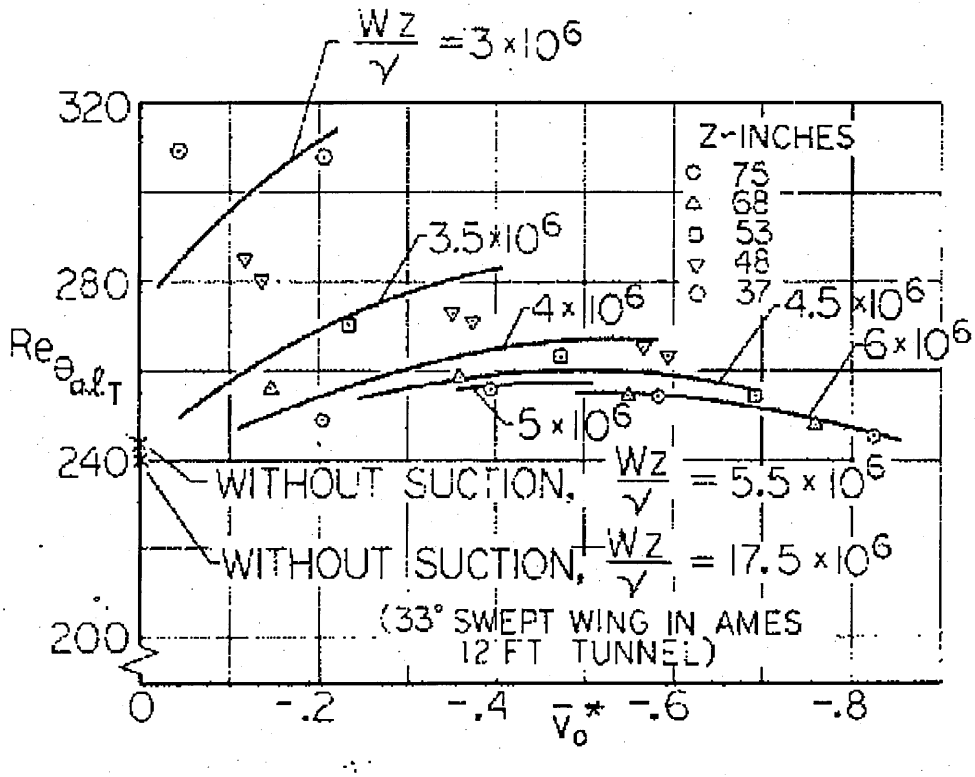

Figure 64. The Beginning Of Transition On A 45° Swept Blunt-Nosed Wing For Different Spanwise Length Reynolds Numbers, From Pfenninger[26]

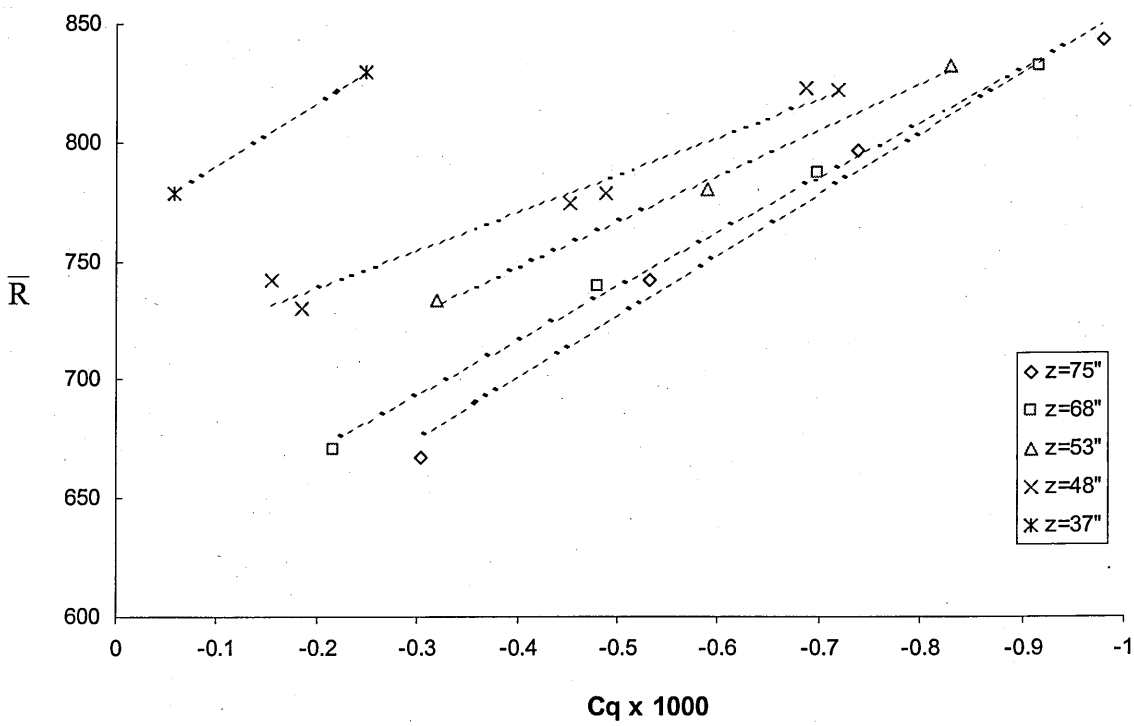

Figure 65. The Beginning of Transition at the Leading Edge of a 45° Swept Blunt-Nosed Wing for Different Spanwise Lengths, From Pfenninger[26]

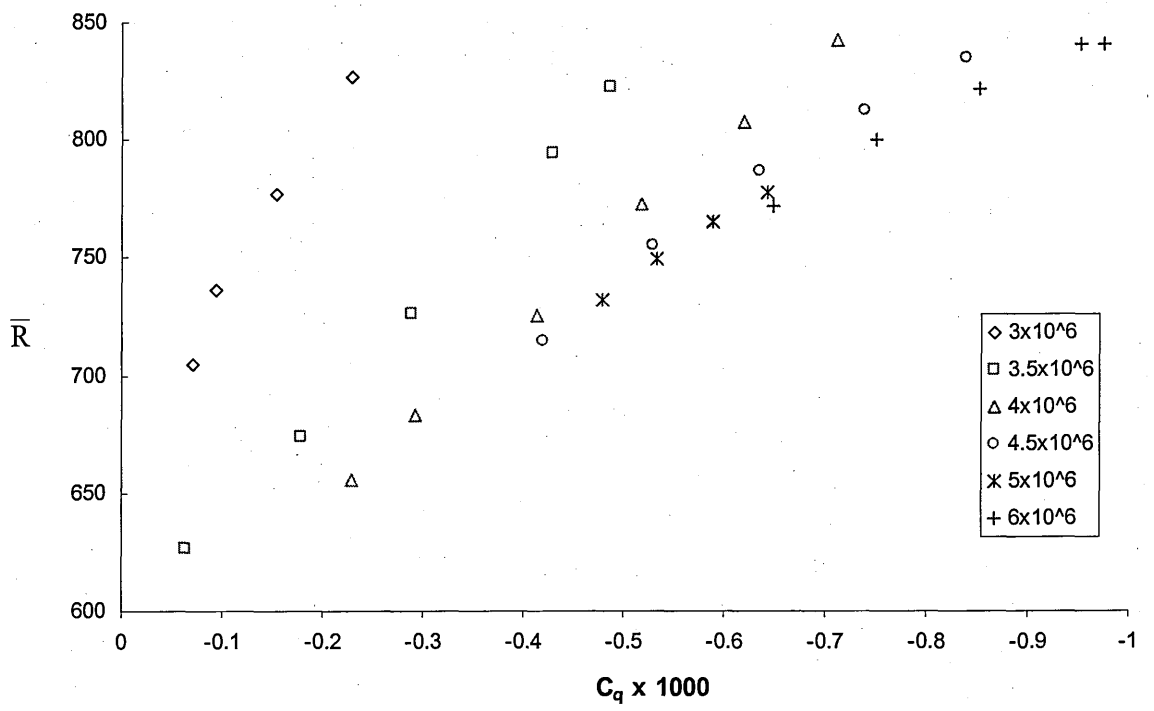

Figure 66. The Beginning of Transition at the Leading Edge of a 45° Swept Blunt-Nosed Wing for Different Spanwise Reynolds Numbers, From Pfenninger[26]

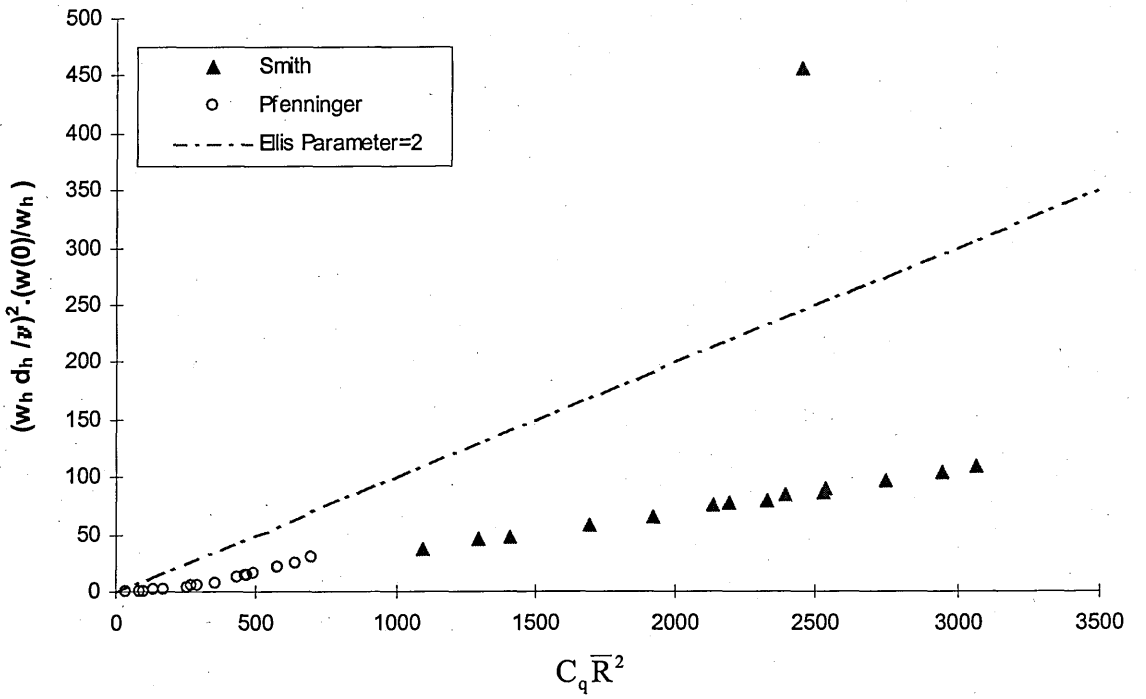

Figure 67. Comparison Of The Two-Dimensional Ellis Criterion Values For The Pfenninger[26] and The Current Data

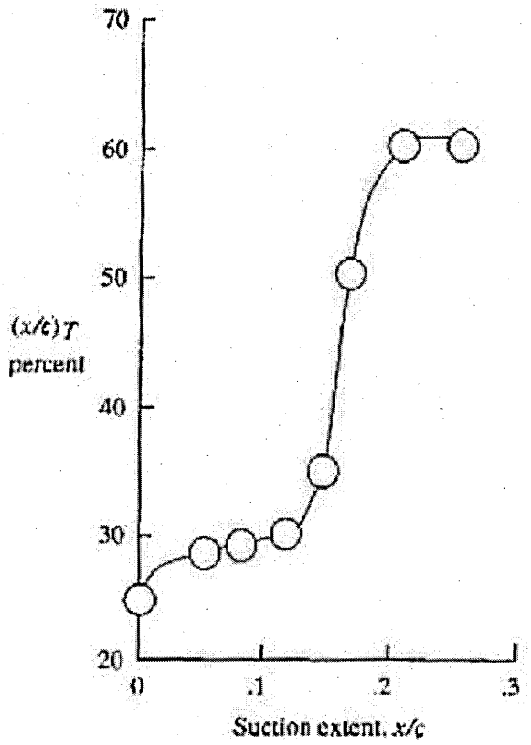

Figure 68. Variation of Transition Location With Chordwise Extent of Suction, From Bobbitt *et al*[77]

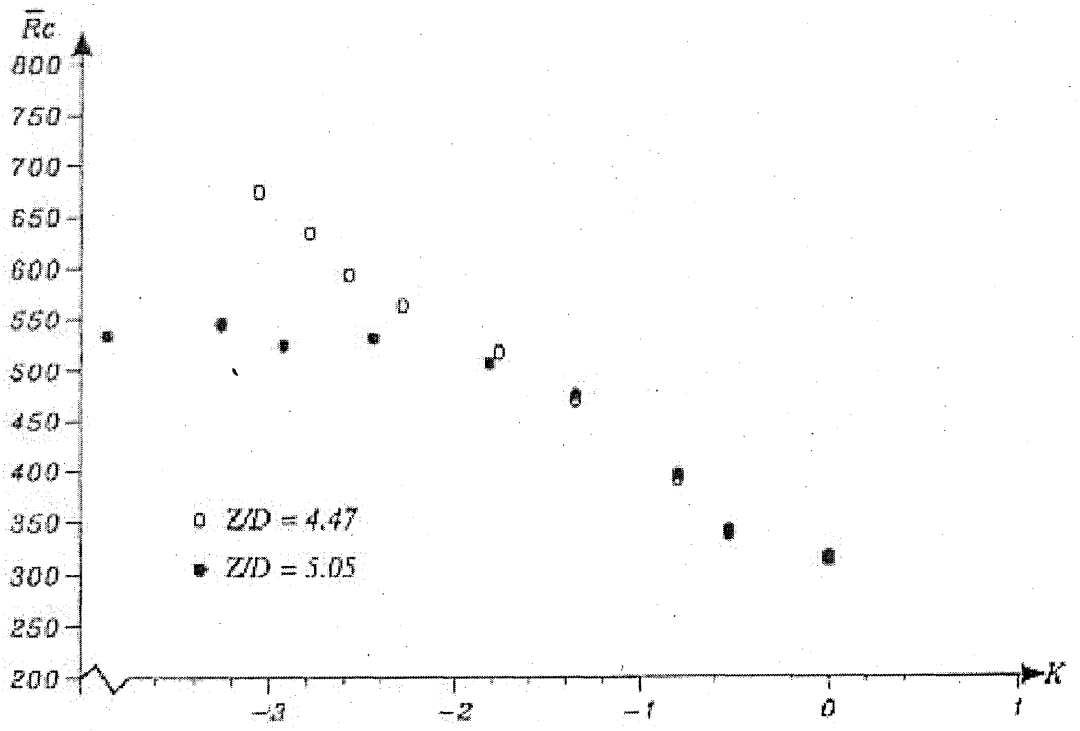

Figure 69. Transition Data For A Relaminarised Attachment-Line Flowing Onto A Non-Porous Surface, From Reneaux[48]

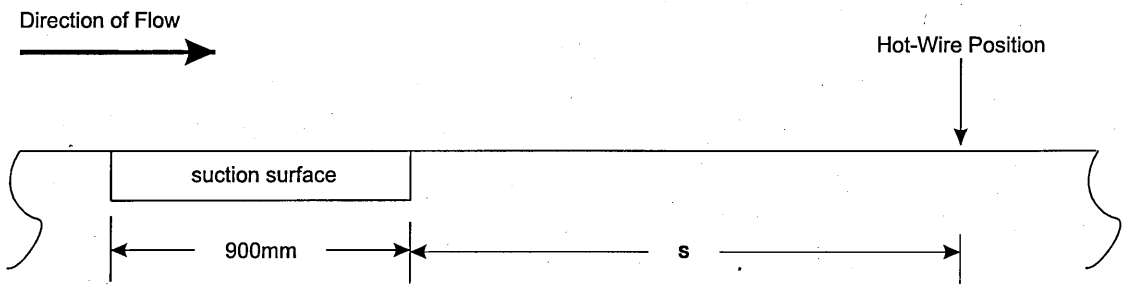

Figure 70. Schematic of Attachment-Line Arrangement During Non-Porous Surface Experiments

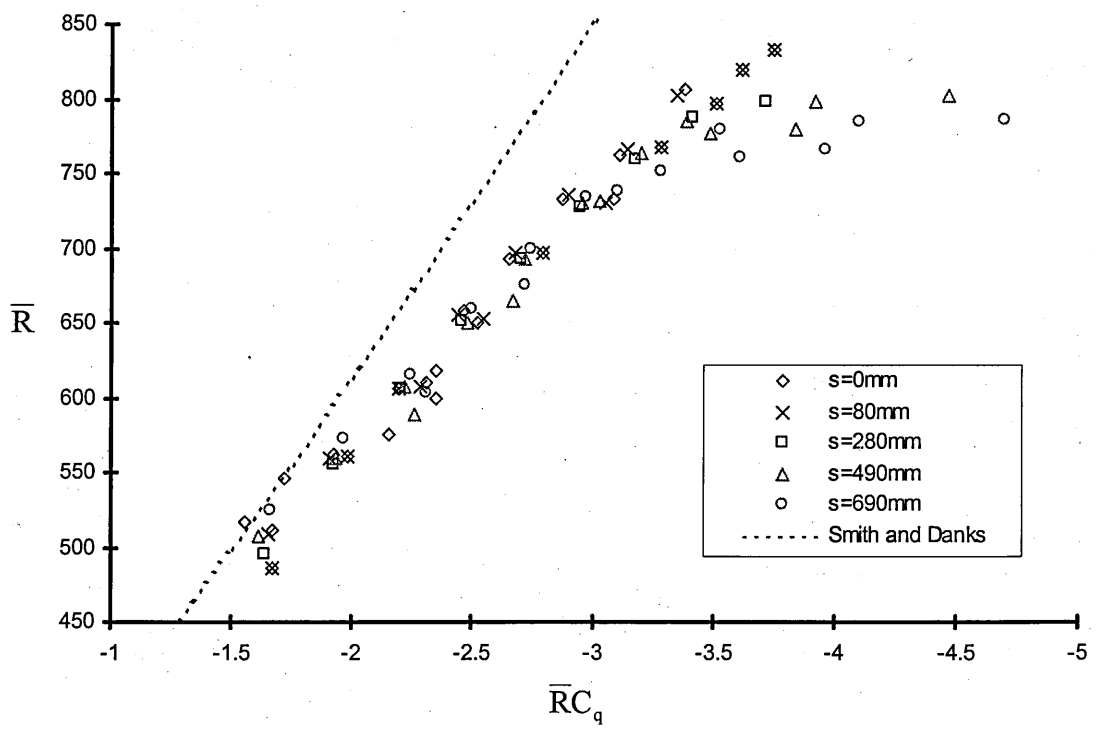

Figure 71. Transition Characteristics of A Relaminarised Attachment-Line Boundary Layer Flowing Onto A Non-Porous Surface

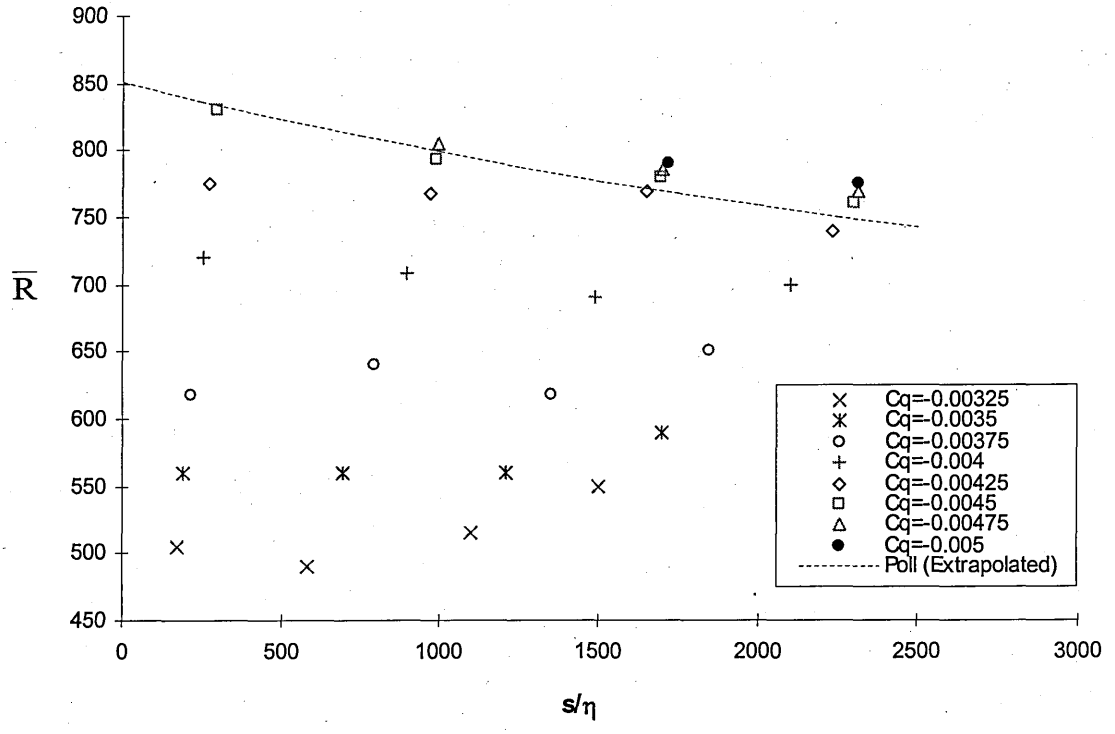

Figure 72. The Effect of Spanwise Distance on the Transition Characteristics of A Relaminarised Attachment-Line Boundary Layer That Flows Onto A Non-Porous Surface